Implications of Microorganisms in Future Crewed Missions to Mars

Leite, Mara

https://doi.org/10.34737/wx442

Implications of Microorganisms in Future Crewed Missions to Mars

Mara Leite

University of Westminster

A thesis submitted in candidature
for the award of the degree of

Doctor of Philosophy

November, 2023

This PhD thesis is dedicated to my late grandfather, Antonio F. G. Do Novo, who instilled in me his exemplary work ethic, strength, and immense courage.

Esta tese é dedicada ao meu falecido avô, Antonio F. G. Do Novo que me incutiu a sua exemplar ética de trabalho, força e coragem avassaladora.

Declaration

I declare that the present work is the author's own. I also declare that this thesis has not been submitted for any degree or qualification at another other university or institution.

Signed: Mara Leite

Date: July, 2023

Acknowledgements

I want to start by thanking my supervisor, Dr Lewis Dartnell, for this opportunity and guidance over the last few years and for the trust deposited in me.

Many thanks to Prof Saul Purton and Dr John Ward from the University College London, as well as Dr Karen Olsson-Francis from the Open University, for their willingness to collaborate.

I am incredibly grateful to Dr Pooja Basnett at the University of Westminster for her guidance and allowing me to work in her laboratory facilities.

I will forever be thankful to Dr Henry Taunt for his valuable time and for the several discussions regarding various aspects of microalgae.

I would also like to thank Dr Dragana Dobrijevic, Dr Michael Macey and Dr Jing Cui for training me.

A heartfelt thank you to all the technical staff from the University of Westminster, particularly Neville, for his assistance and knowledge of fermentation.

I am incredibly grateful to Vittoria Vecchiato for training me in polymer production and for her friendship, encouragement, and support during the last year of my PhD journey.

A big thank you to Marina Barcenilla for sharing her spectroscopy knowledge with me. I also want to thank Marian for being so supportive and my “partner-in-crime” during the ups and downs of the last few years.

I would also like to thank my friends in Seattle and Naomi, who, even miles apart, never stopped encouraging me in the pursuit of my dreams.

I want to thank my family, parents, sister and brother-in-law, who always supported and believed in me no matter how big the challenge was.

Lastly, I would like to thank my partner, Pedro, for his love and patience and for always being the light at the end of every tunnel.

Abstract

Crewed deep space missions will likely become a reality in the coming decades. One of the most challenging issues associated with Mars is the lack of resources for sustaining human life. Microbes can be used to help humans settle on Mars. However, they can also be problematic since terrestrial microorganisms carried by astronauts could contaminate the Martian landscape and be mistaken for Martian native life. Organic carbon is one of the resources limited on Mars. Microalgae, capable of producing organic carbon photoautotrophically, can provide various crucial products for human survival, such as oxygen and food. Moreover, due to their ability to accumulate lipids and starch, microalgae, such as *Chlamydomonas reinhardtii*, can be used as feedstock for heterotrophic bacteria that can produce products required for daily routine, such as plastics. In this work, a two-step system was developed to produce bioplastics by microbial culture. *C. reinhardtii* was cultured to create biomass, which was processed to produce 16.8 g/100g ± 0.67 of starch as feedstock with a productivity of 2.79 mg/L/h for a *Bacillus subtilis* culture yielding polyhydroxybutyrate (PHB) biopolymer. A photobioreactor capable of growing large volumes of *C. reinhardtii* biomass was developed, and different techniques evaluated to estimate the starch content during culture. An optimised protocol for collecting the microalgae cells by combination of coagulation and centrifugation was developed, and then for chemical hydrolysis of the harvested starch into fermentable sugars with acid under high temperatures. The successful cultivation of *B. subtilis* grown on *Chlamydomonas*-derived sugars was also demonstrated, producing a maximum of 23% ±1.45 of CDW or 0.18 ± 0.1 g/L of PHB with a productivity of 7.6 mg/L/h. Infrared spectroscopy was used to track the production of starch and PHB in the primary and secondary cultures, respectively. The PHB obtained was successfully used to produce a plastic film with improved flexibility. The use of such PHB in fused deposition modelling 3D printing to create tools was also demonstrated in principle by use of commercially available blends. An improvement to the starch harvesting and hydrolysis stage was attempted with novel genetic tools based on the Golden Gate assembly. An attempt was made to introduce a thermophilic external alpha-amylase with the objective of facilitating the separation and hydrolysis of starch. However, the work could not be completed within the allotted timeframe due to unforeseen challenges. To address the potential negative impact of human-associated microbes leaking out onto the Martian surface, a culture-independent study was conducted at the Mars Desert Research Station (MDRS). Despite its inherent bias, PCR amplification is a highly sensitive method, used here to evaluate the risk of contaminating Mars in future crewed missions to Mars. Microbial DNA extraction, 16s rRNA and ITS sequencing and identification from swab samples of the habitat interior were used to characterise the human-associated microbiome, along with a complementary analysis on soil samples from the immediate vicinity to test for evidence of contamination from the habitat. No contamination was observed, but even if present such habitat-associated microbes in the desert soil would be expected to be present in very low numbers that may have fallen below the detection threshold of this approach.

Table of Contents

List of Figures

List of Tables

Nomenclature

AACC	American Association of Cereal Chemists
AGPase	ADP-glucose pyrophosphorylase
AM	Additive Manufacturing
AMF	Additive Manufacturing Facility
AMG	Aminoglycoside
AOAC	Association of Official Analytical Chemists
ASVs	Amplicon sequence variants
ATP	Adenosine triphosphate
ATR-FTIR	Attenuated total reflectance Fourier transform infrared
Bes	Branching enzymes
BESs	Bioelectrochemical systems
BLSS	Bioregenerative life-support system
BPEC	Bio-photo electrochemical cells
CAES	Closed Aquatic Ecosystem
CBP	Consolidated bioprocessing
CDW	Cell dry weight
CEBAS	Closed Equilibrated Biological Aquatic System
CFUs	Colony-forming units
CoA	Coenzyme A
COSPAR	Committee on Space Research
DNA	Deoxyribonucleic acid
DOE	Design of experiment
DSC	Differential Scanning Calorimetry
ECLSS	Environmental Control and Life Support Systems
EDTA	Ethylenediaminetetraacetic acid
EPS	Extracellular polymeric substances

ESA	European Space Agency
Eu:CROPIS	*Euglena gracilis*: Combined Regenerative Organic-food Production In Space
EVA	Extravehicular activities
FDA	Food and Drug Administration
FDM	Fused deposition modelling
FFF	Fused filament fabrication
FTIR	Fourier-transform infrared spectroscopy
GBSS	Granule-bound starch synthases
GC-MS	Gas Chromatography/Mass Spectrometry
GOE	Great Oxidation Event
GOPOD	Glucose oxidase/peroxidase reagent
GRAS	Generally Recognized As Safe
GTP	Guanosine triphosphate
G3P	Glyceraldehyde-3-phosphate
G1P	Glucose-1-phosphate
HI-SEAS	Hawaii Space Exploration Analog and Simulation
HSM	Sueoka's high salt medium
ICP-OES	Inductively Coupled Plasma Optical Emission Spectroscopy
IR	Infrared
ISRU	In-situ resource utilization
ISS	International Space Station
ITS	Internal transcribed spacer
LED	Light emitting diode
LSS	Life Support Systems
MaDL	Maximum detection limit
Mcl-PHA	Medium chain length polyhydroxyalkanoate
MDRS	Mars Desert Research Station
MELiSSA	Micro-Ecological Life Support System Alternative
MELT	Manufacturing of Experimental Layer Technology
MF	Jurassic-aged Morrison formation
MFCs	Microbial fuel cells
MIS	Made In Space
MoClo	Modular cloning
MOXIE	Mars Oxygen ISRU Experiment

MRE	Molten Regolith Electrolysis
MW	Molecular weight
NADPH	Reduced nicotinamide adenine dinucleotide phospate
NASA	National Aeronautics and Space Administration
NB	Nutrient Broth
NGS	Next-generation sequencing
OD	Optical density
OGS	Oxygen Generation System
OM	Organic matter
OTUs	Operational Taxonomic Units
PBRs	Photobioreactors
PCR	Polymerase chain reaction
PE	Polythylene
PEF	Pulsed Electric Field
PHB	Polyhydroxybutyrate
P(3HB)	Poly(3-hydroxybutyrate)
PHBV	Poly(3-hydroxybutyrate-co-3-hydroxyvalerate)
PHAs	Polyhydroxyalkanoates
PLA	Polylactic acid
PUFAs	Polyunsaturated fatty acids
RAM	Repair and assembly module
RNA	Ribonucleic acid
RuBisCO	Ribulose-1,5-bisphosphate carboxylase/oxygenase
RuBP	Ribulose bisphosphate
SDRs	Short-dispersed repeats
SLS	Selective laser sintering
Srl-PHA	Short chain Polyhydroxyalkanoate
SSs	Starch synthases
SS4	Starch synthase 4
STA2	Starch synthase gene
STEP	Synthetic Toolkit for Engineering Plastids
TAG	Triacylglycerol
TAP	Tris-acetate-phosphate medium
Tc	Crystallization temperature

TCA	Tricarboxylic acid
Tg	Glass transition temperature
TGA	Thermogravimetric Analysis
Tm	Melting temperature
UV	Ultraviolet
VFAs	Volatile fatty acids
WCA	Water contact angle
WRS	Water Recovery System
WT	Wild type
E	Young's Modulus
ε	Elongation at break
Rm	Tensile strength
δ	Symmetric bending
ν	Symmetric stretching
νas	Asymmetric stretching
3D	Three dimensional

Chapter 1 General Introduction

Microbes are fundamental to life on Earth. They are directly associated with human, animal and plant health and are at the basis of our planet's biosphere. As the ancestors of all life forms, they are responsible for some of the most essential cycles on Earth and for supporting all other life forms.

As human missions to Mars start to be planned by different space agencies (Cockell, 2004; Nangle et al., 2020; Rapp, 2008), it is important to reflect and explore the roles that microbes can play in the upcoming Mars missions. Similar to Earth, they have the potential to positively or negatively impact human life. For instance, microbes can aid the exploration of Mars by producing several bioproducts. However, the appearance of maladies is a risk present in human missions everywhere.

One of the groups of microorganisms that can most significantly facilitate human exploration of deep space and Mars is microalgae. Green algae and cyanobacteria can offer an array of different products that are crucial to human survival. One of the products less investigated is starch which can serve as feedstock for heterotrophic organisms and can be used in the indirect production of other products, such as plastic. Microbe-produced polymers can be used to manufacture on-demand objects in deep space missions through techniques such as three-dimensional (3D) printing.

The present work explores both aspects of microbes, the good and bad. The dissertation, divided into six chapters, starts by offering a detailed review of algae products useful for human settlements on Mars, with a detailed focus on biopolymers and 3D printing in space presented in Chapter 1. The main objectives and aims of this work can also be found here.

The overall main objective is the production of malleable and printable plastic produced by using algal starch as a carbon source. The following chapters address different aspects of this process and are each organized by a general introduction, materials and methods, combined results and discussion, and a general conclusion.

Due to the biotechnological importance of microalgae to deep space exploration, Chapter 2 focuses on developing a bioreactor that can produce large quantities of algal biomass. Methods for converting biomass into starch are also discussed in this section.

Chapter 3 reviews biopolymer synthesis by Gram-positive bacteria and explores the potential of algal starch to serve as carbon feedstock in the production of biopolymers. An attempt to facilitate the separation of starch from other cell constituents and simplify the whole process is shown in Chapter 4.

One of the potential downsides of microbes during future missions to Mars is addressed in Chapter 5. In addition to diseases and infections, human-associated microbes can contaminate the Martian surface, which can negatively impact scientific research, as will be discussed later. Finally, the overall conclusions and future work suggested for each chapter is presented in the last section - Chapter 6.

1.1 Photosynthesis as the key for sustainable long-term missions

Sustainability is key to a scientifically and economically successful human settlement on Mars or other long-term crewed missions. Providing the necessary support and resources for a permanent human presence in the harsh Martian environment can be financially costly (Mapstone et al., 2022). However, prices are expected to decrease in the near future as technology continues to advance. A prime example is SpaceX's development of reusable rockets. Furthermore, reducing the onset payload, in both mass and volume, will help minimize mission cost. The first group of humans to set foot on Mars will require various valuable products, such as oxygen (O_2) and food. However, transporting 1 kg of materials to the Martian surface is estimated to cost upwards of $300,000 (Massa et al., 2006). It is therefore deemed

critical that we find solutions to reduce the amount of cargo to be transported during long-term missions.

In-Situ Resource Utilization (ISRU), which consists of extracting and utilizing the local resources already present at the exploration site, together with three-dimensional printing (3D printing), are innovative solutions that can reduce cargo-related costs. Apart from reducing payload costs, 3D printing will also save time should additional items become necessary throughout the mission. 3D printing is already being used aboard the International Space Station (ISS). Waste management via anaerobic digestion and recycling, which can be achieved through bioregenerative life-support systems (BLSS), will also play a central role in reducing mission expenses in deep space expeditions by reusing waste products.

The biggest challenge for a human settlement on Mars is the Martian environment, which significantly contrasts with that of the Earth, as seen in **Figure 1.1.** A few immediate threats to humans on Mars are the absence of surface liquid water, intense radiation, and an atmosphere mainly consisting of carbon dioxide (CO_2) with only small traces of oxygen (Lehto et al., 2006; Mapstone et al., 2022).

Despite the obstacles, human presence on Mars will be possible thanks to Closed-Loop Life Support-Systems, whose primary function is to support human life by providing a controlled environment capable of recycling valuable products such as oxygen and water. Regarding the biological components of the Life-support systems, photosynthetic organisms such as green algae and cyanobacteria will offer versatile solutions to the vast array of challenges presented by Mars, some of which include a non-breathable atmosphere and soil which is not optimized for agriculture (Alexandrov, 2016; Lehto et al., 2006; Saei et al., 2013).

A comprehensive review of the various applications proposed for cyanobacteria and algae on Mars was published by Mapstone et al. (2022). The author of the present thesis is also a co-first author of this publication and created many of the illustrations and tables, some of which are exhibited here.

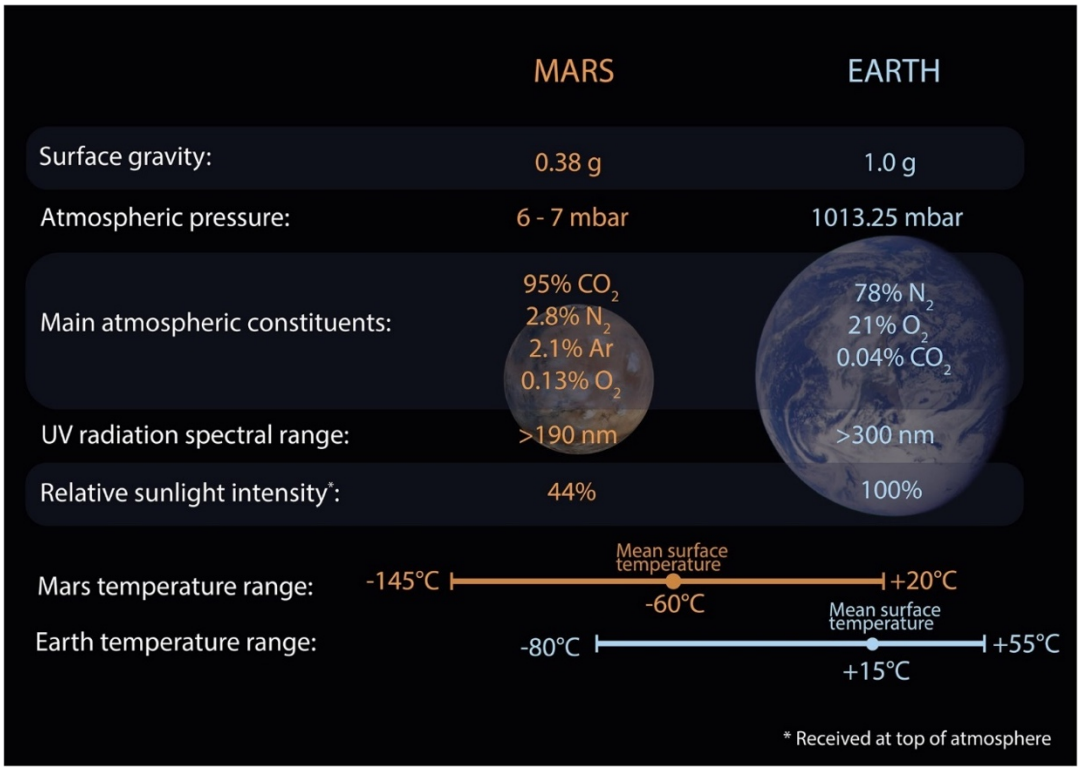

Figure 1.1 Average surface conditions on Mars and Earth. This image was co-produced by the author of the present work who is a co-first author of Mapstone *et al,* 2022. The figure is reproduced here under a Creative Commons license.

Oxygenic photosynthesis is perhaps the most important biochemical process on Earth. Simply stated, it is the process through which phototrophic organisms harness carbon dioxide and energy from the sunlight and convert it into oxygen and carbohydrates. Hence, in addition to O_2 production, photosynthesis can provide food for heterotrophic organisms. Through carbon fixation, CO_2, combined with water, is converted into carbohydrates, which are essential biomolecules for numerous life forms (Janssen et al., 2014).

On the Martian surface, sunlight and CO_2, the main ingredients of photosynthesis, are both available. Essential minerals, crucial to microbial growth, can also be obtained from the Martian regolith using ISRU. As a result, it is possible to grow and maintain photosynthetic organisms in pressurized facilities on Mars, with the goal of producing O_2 and organic food. Cyanobacterial biomass and algal starch are rich in lipids and carbohydrates and can be, therefore, also used to produce other valuable products such as bioplastics, as schematically shown in **Figure 1.2,** which can subsequently serve as raw

material for on-site 3D printing. Water, an essential component of this process, can be obtained on Mars from the Martian atmosphere, from subsurface permafrost, or recycled within closed facilities where plants, algae and others, will grow under controlled temperatures and a pressurized atmosphere (Lehto et al., 2006; Mapstone et al., 2022).

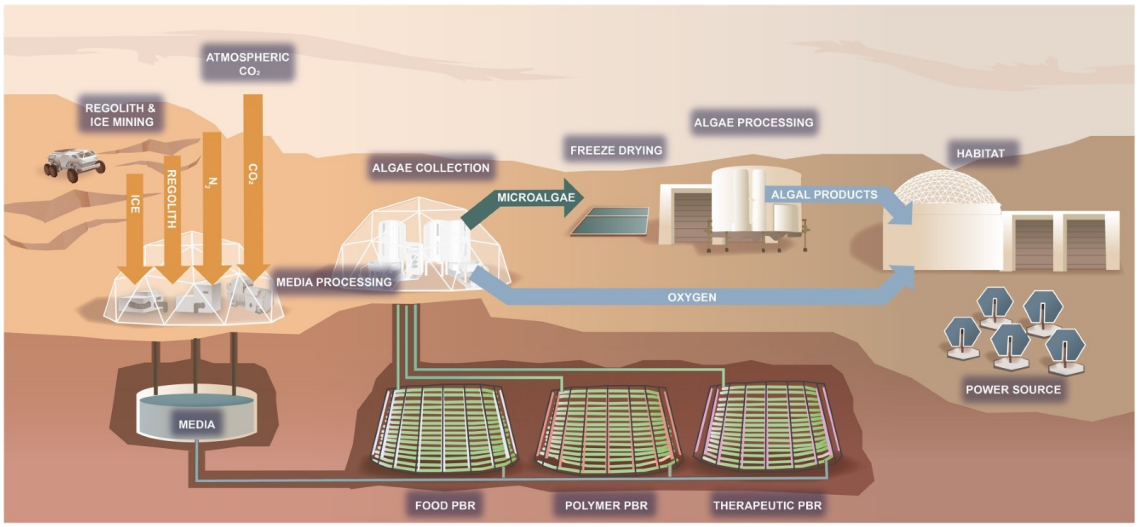

Figure 1.2 Schematic representation of a photoautotrophic microbial system for the production of valuable products solely using Martian resources. This image was co-produced by the author of the present work who is a co-first author of Mapstone et al, 022. The figure is reproduced here under a Creative Commons license.

On Earth, photosynthetic microorganisms, such as microalgae, are responsible for most of the oxygen we consume. Their CO_2 fixation rates reach higher photosynthetic efficiency (10-20 %) than terrestrial plants (1-2 %) (Singh and Ahluwalia, 2013). The use of these microorganisms, instead of higher plants, offers the following advantages: higher growth and biomass productivity, less water uptake, and undemanding maintenance (Singh & Olsen, 2011). Another impressive feature is the capability of some of these microbes to thrive in a wide range of environments, including tolerance to hostile conditions, similar to those on Mars (Dartnell, 2011). Moreover, fast growth rates and small sizes enable their growth in various physical spaces, ranging from large ponds to confined bioreactors (Saei et al., 2013). Additionally, their biomass can yield high-value products, such as oils and plastics, through diverse pathways (Brar et al., 2017; Saei et al., 2013). Lastly, photosynthetic-based support systems also facilitate the recycling of human waste into purified water and nutrients (Lehto et al., 2006).

Algae are a large and diverse group of photosynthetic eukaryotic organisms, while cyanobacteria, also known as Cyanophyta, are single-celled organisms and the only form of oxygenic photosynthetic bacteria. Cyanobacteria and their photosynthesis caused the Great Oxidation Event (GOE) over 2.4 billion years ago, which marked the first substantial increase in oxygen levels on Earth (Schirrmeister et al., 2015). Misappropriating the term "algae" to describe cyanobacteria (e.g., Spirulina) has created confusion. Hence, in this body of work, they will not be addressed as such. Furthermore, in the current thesis, the word "algae" will be used to address green algae (e.g., *Chlorella* and *Chlamydomonas* sp.) exclusively, even though the term comprises algae with other colourations such as red and brown.

As with higher plants, in algae photosynthesis is performed in photosynthetic compartments bounded by three membranes (outer, inner, and thylakoid membranes), known as chloroplasts. Cyanobacteria have no nucleolus or membrane-bound organelles (e.g., chloroplasts). Nonetheless, they also possess thylakoid envelopes (hypothesised ancestors of chloroplasts) which are interconnected membranes with photosynthetic pigments where photosynthesis occurs. Additional differences between the two organisms are depicted in **Figure 1.3**. Both microorganisms share an evolutionary history despite the differences; algal chloroplasts evolved from cyanobacteria through endosymbiosis. In algae cells, the membrane folds into a stacked oval-shaped structure (thylakoids) called granum. Several grana are connected by a thin layer of membrane (lamellae) that prevents them from cluttering together to ensure efficient light harvesting. Photosynthetic pigments embedded in this membrane strongly absorb energy from visible light (solar or artificial) during the “light reaction.” Reflected light differs in wavelength depending on the pigment. Chlorophyll a is the main pigment in photosynthesis; it reflects green light most strongly among all pigments. It is the molecule responsible for the characteristic green colour of green algae and plants. In the thylakoids, water molecules are oxidised during the “light reaction;” oxygen and electrons are released. The latter is transferred to adenosine triphosphate (ATP) and NADPH in the first “dark reaction” to produce energy. During the second light-independent reaction, CO_2 is fixed from its inorganic form in a colourless matrix (stroma) surrounding the grana. This fluid has a metabolic enzyme - ribulose-1,5-bisphosphate carboxylase/oxygenase (RuBisCO) - critical for the Calvin cycle and the organic molecule ribulose bisphosphate

(RuBP). At the beginning of the cycle, CO_2 binds to RuBP (carbon fixation) with the help of RuBisCo, forming an intermediate molecule that will be reduced to glyceraldehyde-3-phosphate (G3P). With the energy produced from the light reaction, G3P will be synthesised into organic molecules such as sugars, while RuBP will be regenerated in the last step to continue the cycle. G3P can be converted into different hexose phosphates, including glucose-1-phosphate (G1P), which is a known starch precursor (Cuesta-Seijo et al., 2017).

To efficiently grow photoautotrophic organisms on Mars, it is fundamental to understand how their metabolism is affected by Martian and space-like conditions since physical factors, such as microgravity and radiation, are known to influence the biology and physiology of microbes (Coil et al., 2016). Outer space and Martian conditions differ; therefore, both should be tested to further understand the growth changes microorganisms will undergo during interplanetary transfer and on the surface of Mars, respectively (Mapstone et al., 2022). For instance, space is characterized by microgravity. Mars, on the other hand, has a partial gravity of 0.38 g (**Figure 1.1**), and while the response of photosynthesizers to microgravity has been the subject of several studies (Cockell, 2010; Horneck et al., 2010; Mapstone et al., 2022; Niederwieser et al., 2018), findings regarding the effect of fractional gravity are still scarce in the literature (Mapstone et al., 2022; Santomartino et al., 2020). The impact of microgravity on microalgae growth rate seems to be species-dependent. For instance, *Chlorella Pyrenoidosa* exhibited slower growth in simulated microgravity than in normal gravity conditions (Mills, 2003). On the other hand, a species of *Nostoc* sp. has shown an increased growth rate under microgravity when flown aboard the SHENZHOU-2 spacecraft (Wang et al., 2004).

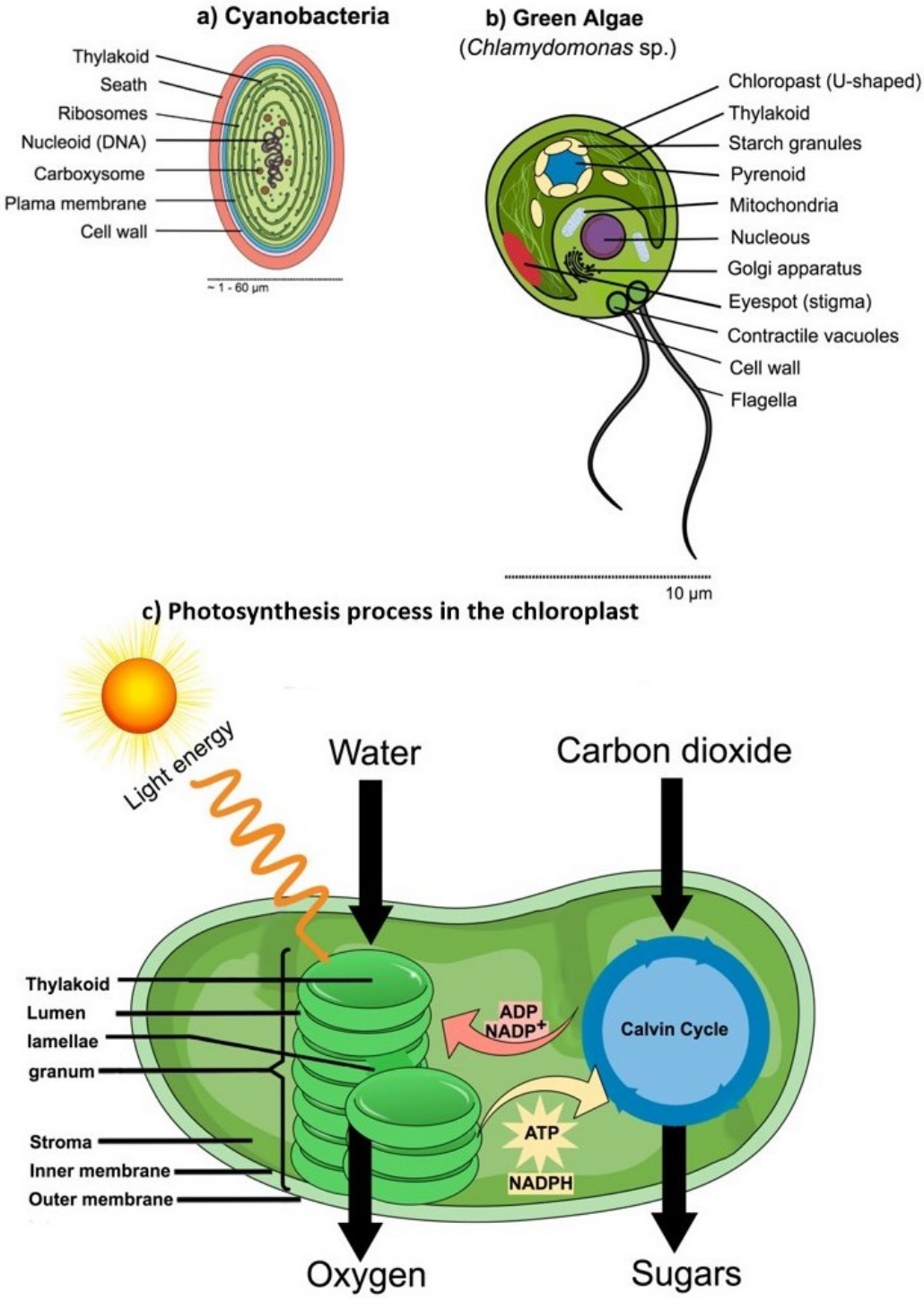

Figure 1.3 **S**chematic illustration of relevant features and differences between (a) cyanobacteria and (b) green algae. *Chlamydomonas reinhardtii* was chosen to represent green algae due to its significance for the present body of work and as a model organism in algal research. (c) Schematic representation of photosynthesis' light and dark reactions inside chloroplasts. All three image were produced in accordance with depictions found in the literature.

Since the 1960s, various space agencies have been using Earth-based simulators, internal and external facilities on the ISS, space shuttles and recoverable satellites (Billi et al., 2013; Cockell, 2010) to test microbial biological responses to the environmental factors mentioned above. Reviews with compiled information regarding the list of autotrophs tested and findings collected over the years were published by Niederwierser et al. (2018), Mapstone et al. (2022), and Fahrion et al. (2021). This chapter and the upcoming sections provide details regarding past experiments studying growth and survival rates in space, but overall, microalgae have been shown to be able to grow and adapt to microgravity, as shown above. Moreover, microalgae have also been tested as viable components for future biological life support systems. Although research is ongoing to optimize performance, various microalgae species hold promise for utilizing human waste products like urine, contributing to both water and air recycling in BLSS studies designed for space applications (**Table 1.1**).

The first algae/cyanobacteria flown in space was a green algae species from the *Chlorella* genus in 1960 (Alexandrov, 2016; Niederwieser et al., 2018). Various other photoautotrophic species have been tested in space since, including *Chlamydomonas* sp. and Spirulina, as shown in **Figure 1.4.** Spirulina's scientific name has recently been changed from *Arthrospira platensis* to *Limnospira fusiformis* due to reclassification of some species from the *Arthrospira* genus to the newly established *Limnospira* clade (Hicks et al., 2021; Nowicka-Krawczyk et al., 2019). To avoid confusion, the cyanobacterium will always be addressed as Spirulina in the current body of work. Details regarding past experiments are shown in this chapter in the upcoming sections, but overall, microalgae have been shown to have the ability to grow and adapt to space-like conditions and microgravity (Niederwieser, 2018). Additionally, various microalgae species hold promise for utilizing human waste products like urine, contributing to both water and air recycling in BLSS studies designed for space applications (**Figure 1.1**).

Figure 1.4 shows a timeline depicting the most significant achievements in algae research (e.g., genetic transformation and inclusion in a BLSS) and space exploration

relevant to this thesis. It includes the first and latest Mars missions from which we learnt more about Mars' geology (Viking program) and ISRU capabilities (Mars 2020 Perseverance Rover), respectively. The launch of the first crewed space station (Salyut programme) and the ISS - crucial precursors of future missions to Mars are also included. Milestones in the BLSS research, such as the beginning of the MELiSSA project (detailed in the following section) and the first genome (*Chlamydomonas* sp.) submission to the National Aeronautics and Space Administration (NASA)'s GeneLab – the first open repository and database for space-related biology, are shown as well.

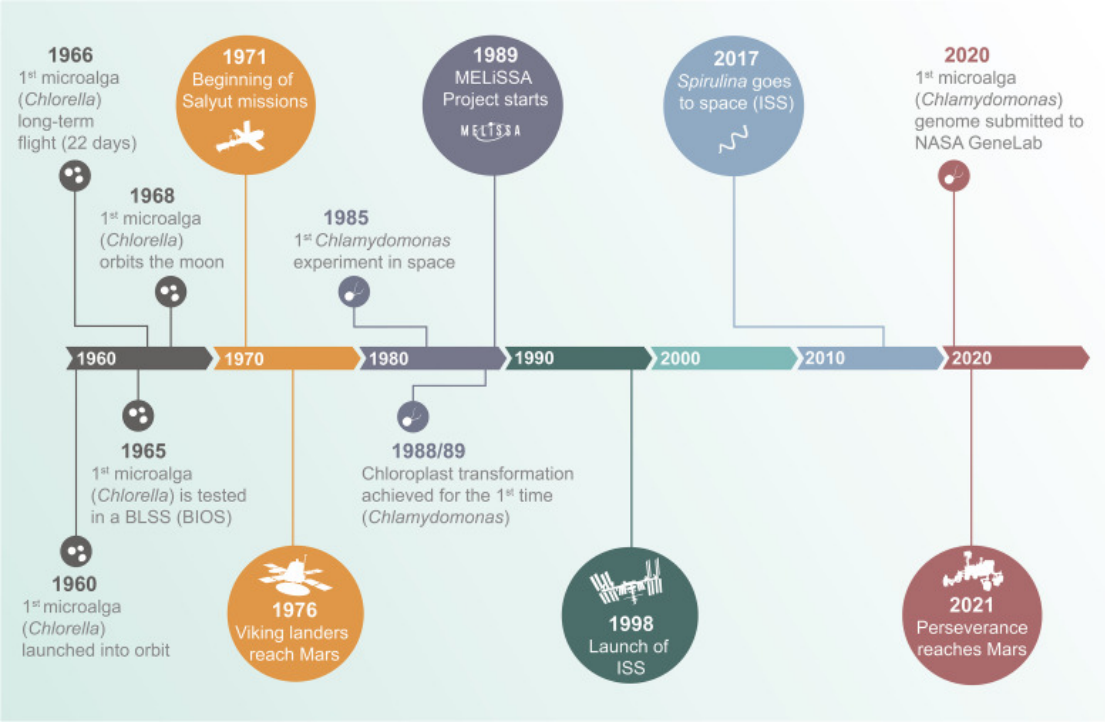

Figure 1.4 Chronological timeline of major scientific achievements in algal space research and in space and Mars exploration.

The following subsections will include an overview of the different potential applications of microalgae and cyanobacteria in supporting human space exploration and habitation on Mars. The list of applications covers various research areas, including the medical field. The review concludes with a summary and an overview of synthetic biology since the latter can be used to enhance all the areas discussed in this chapter.

1.1.1 BLSS – Biological Life Support Systems

A Life Support System (LSS) is a set of hardware that can help sustain human presence in space by providing valuable resources crucial to human survival, including oxygen, water and a pressurized atmosphere. One example is The Environmental Control and Life Support Systems (ECLSS) aboard the ISS. This regenerative system allows the recycling of waste into oxygen and purified water. Urine and air humidity are processed into drinkable water through the Water Recovery System (WRS). Subsequently, water can be split through electrolysis into hydrogen and oxygen in the Oxygen Generation System (OGS) to meet oxygen demands (Carter et al., 2011). However, despite decades of technological advances, the ISS still relies on frequent payloads from Earth. Unlike missions to the ISS, deep space missions will require life support technology with a significantly reduced resupply dependence (Berliner et al., 2021; Mapstone et al., 2022; Mitchell, 1994; Nelson et al., 2010). Increased system closure that could result in a circular system with near-100% recycling rate would be ideal.

Mars habitats will be equipped with bioregenerative life support systems (BLSS) systems designed for recycling waste into valuable products like water, food, gases, and propellant through the help of biological components such as microbes and plants, as represented schematically in **Figure 1.5**. BLSSs are self-sustaining artificial ecosystems developed to simulate Earth's biosphere through symbiotic relationships among the crew, plants, and microorganisms (de Micco et al., 2009; Lehto et al., 2006; Mitchell, 1994; Nelson et al., 2010).

Several space agencies have been active in developing artificial closed ecological systems. One prominent design is the European Space Agency's MELiSSA (Micro Ecological Life Support System Alternative). The artificial aquatic ecosystem loop has four interconnected biological compartments, all containing various organisms. Compartment IV is the photosynthetic compartment, and it is divided into two sections. The microbiological section (Compartment IVa) contains cyanobacteria, while Compartment IVb comprises higher plants. Some of the higher plant crops that have already been tested are wheat, tomato, potato, soybean, rice, and lettuce (Gòdia et al., 2002). However, rather than using a single, fixed organism to perform certain tasks (e.g., nitrification of vegetable waste), the system could benefit from a

mixture of microbes. Thanks to their diversity in terms of metabolic pathways, microbial consortia can perform specific tasks more efficiently and with less complex substrates (Ben Said and Or, 2017; Fu et al., 2009).

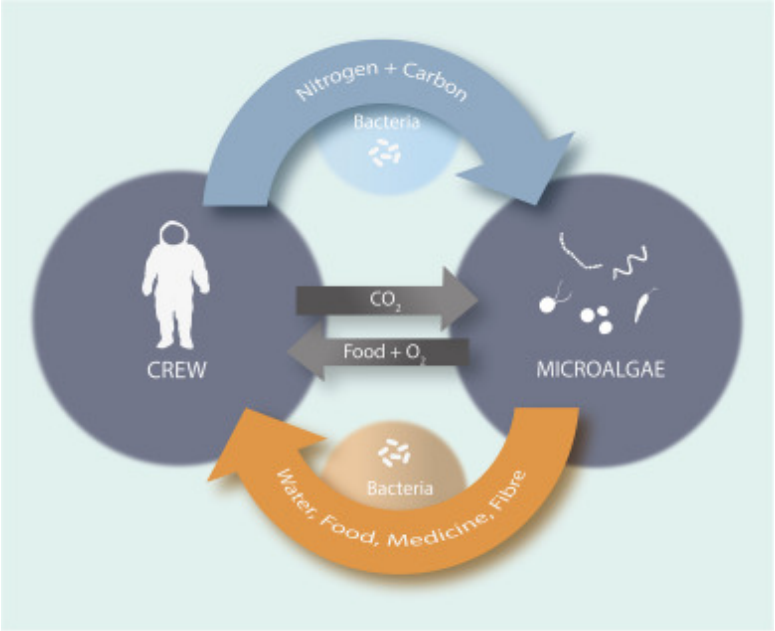

Figure 1.5 Simplified schematic representation of a closed-loop biological life support system involving microalgae as a main component. The image includes the products that humans can obtain directly from microalgae (e.g., food and oxygen) and indirectly through other microorganisms. This image was co-produced by the author of the present work who is a co-first author of Mapstone *et al,* 2022. The figure is reproduced here under a Creative Commons license.

BIOS–3 was Russia's venture into bioregenerative life support systems. In short, it is an underground, isolated facility built underneath the Siberian city of Krasnoyarsk. The facility still exists and has been recently used in partnership with the European Space Agency. During initial experiments, a three-person crew successfully lived in a closed system, using an atmosphere recycled by algal cultivators. *Chlorella* was the initial algae choice for air regeneration (Salisbury et al., 1997). Although the overall system was capable of sustaining life, its recycling capability was not 100% since it was not efficient in recycling all human waste (e.g., human solid waste) (Salisbury et al., 1997).

A parallel project was conducted at the University of Arizona. Biosphere 2 was an atmosphere-controlled facility featuring different artificial climates, from a desert to a rainforest. Even though Biosphere 2 was home to different projects, the facility had to be terminated in the early 1990s due to low oxygen levels. Vascular plants, responsible for providing a breathable atmosphere, could not produce enough oxygen because the concrete absorbed the CO_2 required for photosynthesis (Severinghaus et al., 1994). The University of Arizona is now home to NASA's Lunar Martian Greenhouse prototype. This five-and-a-half-meter-long inflatable cylindrical structure will test how to sustainably cultivate vegetables on the Moon and Mars using recycled O_2. The greenhouse(s) will be buried underneath the surface to address the radiation challenge, while LED lights and other artificial lighting will provide the necessary energy for photosynthesis (Granath, 2017).

A list of the photosynthetic microorganisms chosen by each BLSS can be found in **Table** 1.1. Another novel project is the Cyanobacterium-Based Life Support System (CyBLiSS). In a collaborative effort, NASA, the German Aerospace Center, and the Italian Space Agency plan to use cyanobacteria to process in-situ resources on Mars, which would then feed a biological support system, thereby expanding the applications of the bacterium on Mars (Verseux and Baqué, 2014).

Additionally, keeping the concentration balance of both CO_2 and O_2 inside Mars habitats and spacecrafts will be crucial for the survival of humans, plants, and crops. Compensatory systems should be in place to be used in emergencies when the CO_2-O_2 balance gets disrupted. *Chlorella vulgaris* has already been tested as a CO_2 regulator in a closed life support system and was shown to recover the balance in 3-5 days (Li et al., 2013).

Table 1.1 Microalgae tested in Biological Life Support Systems. This table was co-produced by the author of the present work who is a co-first author of Mapstone et al, 2022. The table is reproduced here under Creative Common license.

BLSS	Contributors	Microalgal species	Objective(s)	Reference(s)
BIOS (BIOlogical closed life support System)[a]	Russia	*Chlorella vulgaris*	Air revitalization/ Water recycling	(Gitelson et al., 1989; Salisbury et al., 1997)
MELiSSA (Micro-Ecological Life Support System Alternative)[b]	Belgium/ France/ Spain/ Canada	*Limnospira fusiformis (Spirulina)*	Air revitalization/ Food production/ Water recycling	(Hendrickx et al., 2006)
EU:CROPIS (Euglena and Combined Regenerative Organic food Production on Space)[b]	Germany/ Russia	*Euglena gracilis*	Air revitalization/ Water (urine recycling)	(Hauslage et al., 2018)
AQUACELLS[b]	Germany/ Russia	*E. gracilis*	Air revitalization	(Häder et al., 2006; Porst et al., 1997)
CAES (Closed Aquatic Ecosystem)[b]	China	*Chlorella pyrenoidosa*	Air revitalization/ Food production	(Wang et al., 2008)
OMEGAHAB (*Oreochromis Mossambicus-Euglena Gracilis*-Aquatic HABitat[b]	Germany/ Russia	*E. gracilis*	Air revitalization	(Strauch et al., 2008)
CERAS (Closed Ecological Recirculating Aquaculture System)[a]	Japan	*C. vulgaris*/ *L. fusiformis*/ *Scenedesmus quadricauda*	Air revitalization/ Water recycling	(Endo et al., 1999; Omori et al., 2001; Takeuchi and Endo, 2004)
CyBLiSS (Cyanobacterium-Based Life Support Systems)[a]	Germany/ USA/ Italy	*Anabaena* PCC 7938	Substrate for other BLSSS organisms	(Billi et al., 2021; Verseux et al., 2021)
SIMBOX (Science in Microgravity Box)[b]	China/ Germany	*E. gracilis*/ *C. pyrenoidosa*	Air revitalization/ Food production/ Water recycling	(Li et al., 2017; Preu and Braun, 2014)
PBR@LSR (Photobioreactor at the Life Support Rack)[b]	Germany/ Russia	*C. vulgaris*	Air revitalization/ Food production	(Detrell et al., 2019)

[a] *Earth-based simulations.*
[b] Tested in space.

1.1.2 On-site Production of Oxygen

The Martian atmosphere is inhospitable to humans, with not only very low atmospheric pressure but also virtually no oxygen. Therefore, oxygen production is one of the most essential necessities of a BLSS. Each crew member will need at least 1 kg of O_2 daily, an estimate that already includes the required time of intense physical activity (Horneck et al., 2003).

O_2 can be produced on Mars through several different processes. MOXIE (Mars Oxygen ISRU Experiment), an instrument carried aboard NASA's Mars 2020 Perseverance rover was tested on Mars and converted CO_2 into molecular oxygen with the help of solid oxide electrolysis cells that can split atmospheric CO_2 into O_2 and CO (Hecht et al., 2021; Meyen et al., 2016). Moreover, similar to the ISS, on the Martian surface, O_2 can also be produced through water electrolysis.

While oxygen can be obtained through solid oxide electrolysis of the CO_2 in the Martian atmosphere, in-situ O_2 recovery from Martian regolith is also possible. On Mars and other celestial bodies, oxygen is bound within minerals as oxides of many metals. The extraction of oxygen from rocks is challenging and requires chemical or physical methods that require a lot of energy and can be costly. Among the methods being explored, Molten Regolith Electrolysis (MRE) displays initial potential (Sibille and Dominguez, 2012).

On-site production of O_2 can also be achieved through photoautotrophic organisms. In addition to producing O_2, they will simultaneously reduce CO_2 levels produced by crew members. As one of the most efficient natural O_2 producers, cyanobacteria can be considered a highly cost-effective solution since they produce oxygen at a much higher rate than plants. Spirulina alone can produce 16.8 tons of oxygen per hectare per year, while, in comparison, trees only produce between 2.5 and 11 tons of oxygen per hectare per year (Verseux et al., 2016). Spirulina is most popular in the food industry, but on the MELiSSA loop, together with higher plants, it is also responsible for recycling CO_2 into O_2.

Algae have also been well-studied for O_2 production in BLSS environments. A prime example occurred during the initial stages of Russia's BIOS facility, where an 18 L algal

cultivator with *Chlorella vulgaris* was used to recycle air and water and was responsible for 20% of the system closure, which later was improved to up to 80-85% (Salisbury et al., 1997). Furthermore, *Chlorella pyrenoidosa* is the O_2-producing organism of choice in China's Closed Aquatic Ecosystem (CAES) (Wang et al., 2008). In addition to *Chlorella* and *Spirulina*, *Chlamydomonas reinhardtii* has been the subject of experiments aboard the ISS. Zhang and team (2020) cultivated this species inside commercial tissue bags placed in the station's Veggie plant growth chamber to determine its potential applicability in life space support systems. The results revealed that this microalgae species grew but suffered genetic changes to adapt to the unique space environmental conditions (Zhang et al., 2020).

In the long run, photosynthesizers have also been suggested for terraforming Mars. Terraforming is the process that, through planetary engineering, transforms the environment from hostile to hospitable by altering the planet's atmospheric and surface composition. In this instance, terraforming can make the Martian atmosphere breathable and O_2-rich by introducing photosynthetic microbes to the Martian surface, which will aid in the planet's habitability. Microbes will assist in making the Martian atmosphere breathable while also making the terrain more suitable for the growth of crops and other plants. Nitrogen-fixing cyanobacteria (e.g., *Nostoc*, *Anabaena*) can aid in this process by optimizing the composition of Martian soil. This topic will be discussed in the section entitled "Food Production" in further detail.

1.1.3 Food Production

On-site food production can help reduce missions' costs by lessening food-related payload and decreasing energy consumption associated with food preservation (Grossi et al., 2013). Photoautotrophic microorganisms have simple growth requirements and have long been suggested as direct and indirect food providers for long-term missions (Mapstone et al., 2022; Santomartino et al., 2023).

On Earth, photosynthesis is at the front line of a secure and sustainable food supply (Janssen et al., 2014). Photoautotrophic organisms could also be the primary source of food on Mars since sunlight and carbon dioxide - the prerequisites of photosynthesis - are both present in high quantities on Mars. Vegetables were already grown and consumed aboard the ISS,

proving they can resist microgravity (Sychev et al., 2007). Nevertheless, besides higher plants, some algae and cyanobacteria are edible and contain an impressive high nutritional value, rich in various compounds, such as antioxidants (Lehto et al., 2006; Mapstone et al., 2022; Verseux et al., 2016).

The most well-known cyanobacteria and algae in the food industry are Spirulina (*Limnospira fusiformis*) and *Chlorella*, respectively. They have a plethora of advantages and are almost complete, nutritionally speaking. As seen in **Figure 1.6**, they contain higher quantities of each essential amino acid when compared to cereal wheat, sweet potato, and insects, which have all been considered or even tested for space travel and Martian farming (Mapstone et al., 2022). **Figure 1.6** also shows their high levels of protein, polyunsaturated fatty acids (PUFAs), and mineral content (ash percentage) in comparison to more conventional food crops.

Furthermore, both Spirulina and Chlorella have been given the GRAS (Generally Recognized As Safe) status by the U.S. Food and Drug Administration (FDA, 2018) and have already been approved as a food supplement (Mapstone et al., 2022; Masojídek & Torzillo, 2008). Moreover, Spirulina is the only cyanobacteria that can be produced at industrial scales, while *Chlorella* is the most cultivated algae (Masojídek & Torzillo, 2014). Based on current ISS observations, each crew member requires 1.83 kg of food daily (Menezes et al., 2015). An estimated 2000 litre bioreactor can produce 5.272 kg of Spirulina per day (Menezes et al., 2015). One of its disadvantages is its flavour, but genetic modifications can be used to attempt to create versions of this species with an improved taste for the human palate (Mapstone et al., 2022).

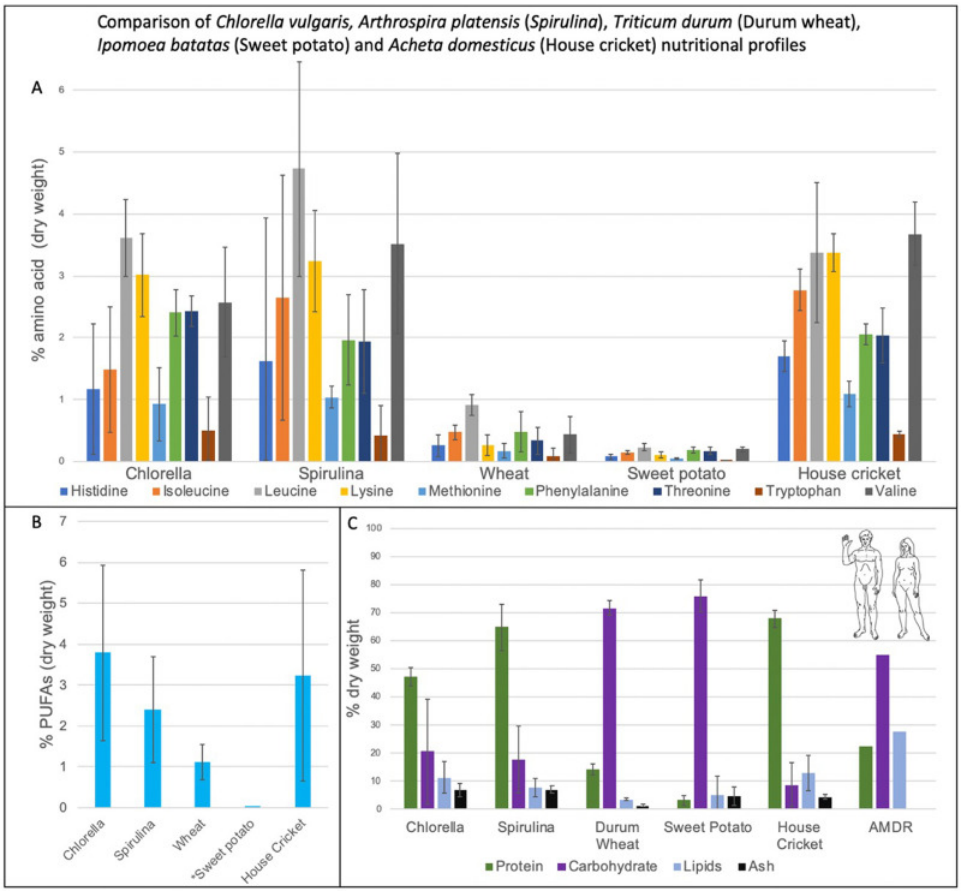

Figure 1.6 Nutrient composition of five species, which include (a) essential amino acid distribution; (b) Polyunsaturated fatty acids; and (c) Macronutrient content distribution. The AMDR (Acceptable Macronutrient Distribution Range) indicates the recommended proportion of a person's daily calories. This mage was produced by Mapstone et al, 2022 and reproduced under a Creative Commons license.

Moreover, some species such as *Chlorella pyrenoidosa* have lutein, carotenoids and other colour pigments that can be used to dye food, making it more visually appealing (Mezzomo & Ferreira, 2016). Outside the *Limnospira* genus, other cyanobacteria should also be investigated as a food source. Species from the *Nostoc* sp. and *Anabaema* sp., which are less demanding than Spirulina and can withstand more hostile conditions,, could be potential candidates for Mars (Verseux et al., 2016). As previously discussed, both cyanobacterial and algal biomass provide plentiful carbohydrates and proteins and can feed aquacultures with shellfish, crustaceans, and perhaps even fish in the later stages of Martian settlements (Masojídek & Torzillo, 2014).

Other indirect applications of microbial photosynthesizers in food production are their applicability in the growth of higher plants as fertilizers and bio-control agents. A biofertilizer consists of a solution of microorganisms whose function is to promote plant growth and crop productivity. Microbes from biofertilizers form symbiotic relationships with plants and assist them in synthesizing growth-promoting nutrients through natural processes such as nitrogen fixation. Nitrogen is an essential compound to all life forms; nitrogen-fixing cyanobacteria (and other N-fixing microbes) convert atmospheric nitrogen to ammonia and then glutamate, making it available to plants (Speer, 2006). Cyanobacterial species such as *Anabaena variabilis*, *Nostoc muscorum*, and *Tolypothrix tenuis* have already been proven effective biofertilizers (Singh et al., 2016).

Furthermore, cyanobacteria can also produce a variety of secondary metabolites with antibacterial and antifungal properties (discussed next in more detail) that suppress the growth of pathogens, potentially interfering with the healthy growth of plants and vegetables (Sign et al., 2016). For a review of the antagonistic effects of this bacterium against plant diseases and their applicability as a biofertilizer see Sigh et al. (2016).

1.1.4 Medical applications

A vast array of pharmaceuticals will be needed on Mars. Painkillers, sleeping pills and antihistamines are some of the most common medications astronauts take on the ISS (Kast et al., 2017). Space is known for increasing bacterial pathogenicity and weakening the human immune system (Schwendner et al., 2017), which, combined with the higher risk of microbial transmission under confinement, can pose severe threats to humans (Schwendner et al., 2017). Space can also negatively affect the stability and effectiveness of pharmaceuticals (Du et al., 2011; Kast et al., 2017).

The in-situ production of pharmaceuticals (e.g., through bacteria and plant-based systems) can help reduce mission costs. Cyanobacteria have long been known for their environmental and agricultural impact. However, recently, they have also been the focus of interest from the pharmaceutical industry (Singh et al., 2011) due to the many nutraceutical properties they possess in addition to the overall nutrient benefit. Spirulina, in particular, has been associated with an impressive list of health benefits that include reduced risk of metabolic diseases (i.g., diabetes) and improved immune response such as reduction of inflammation (Mapstone et al., 2022). They produce various secondary metabolites with significant pharmaceutical properties, such as antiviral, antibacterial, and immunomodulatory (Singh et al., 2011). Due to high doses of cosmic solar radiation on the surface of Mars, their anticancer activity is of extreme relevance. Compounds like cryptophycins, curacin A, and dolastin 10 are a few examples of promising anticancer agents produced by this bacterium (Singh et al., 2011; Mapestone et al., 2022). For instance, C-phycocyanin from Spirulina has triggered apoptosis in cells within breast and cervical cancer (Li et al., 2006). Furthermore, future research in this field can lead to the discovery of additional compounds with anticancer properties.

1.1.5 Waste Management and Bioremediation

While providing the necessary supplies for the success of future missions is crucial, finding suitable ways to process and manage biological matter (e.g., human liquid waste and solid matter) is of equal importance (Linne et al., 2014). Dealing with considerable amounts of waste produced by future human settlements will undoubtedly be a challenge. Waste management aboard the ISS is performed by its disposal via airlock to be burned in the Earth's atmosphere inside an emptied supply vehicle. This technique is not feasible on distant planets; alternative waste management methods that can eliminate or reduce pollutants and biological waste in long-term missions are under investigation (Linne et al., 2014). Bioremediation, the elimination of pollutants through plants or microbes is an eco-friendly approach that has given excellent results here on Earth (Cohen, 2002). Phytoremediation is a new branch of bioremediation that uses algae and cyanobacteria (Jassen et al., 2014). Due to their biological diversity, these organisms can neutralize a broad spectrum of organic and inorganic contaminants (Jassen et al., 2014). Examples of algal and cyanobacterial genera explored in bioremediation include *Chlorella, Phormidium, Chlamydomonas, Oscillatoria, Arthrospira,*

Nostoc, Cyanothece, and *Dunaliella* (Brar et al., 2017). Some of the benefits that phytoremediation offers over plant-based systems are as follows: high biomass productivity, a simple set-up and maintenance, easy monitoring, scalability, and resulting biomass with a high nutrient value that can be used as food supplement through nutrient recycling, and as fuel and others after proper bioprocessing (Brar et al., 2017).

Compared to conventional methods, algal and cyanobacterial bioremediation systems still need to be more cost-effective. Nonetheless, if we expand and combine their applications (e.g., CO_2 mitigation, biomass processing for value-added products, like bioplastics), the costs will decrease (Janssen et al., 2014; Brar et al., 2017), particularly in a place like Mars. Bioremediation on Earth is also used to restore soil to a healthy state (Luiz et al., 2018). Microbial bioremediation could aid the transformation of Martian regolith into a fertile soil (Mapstone et al., 2022).

Urine will pose another challenge during long-term space missions (Salisbury *et al*., 1997). Eu:CROPIS (*Euglena gracilis*: Combined Regenerative Organic-food Production In Space) is a system under development by the German Aerospace Center that uses *Euglena gracili*s to convert urine into a fertilizer solution in a two-step process (Hauslage et al., 2018). In the first step, a filter made from lava rocks with bacteria responsible for nitrification converts ammonia into nitrates. The latter and the remaining ammonia are utilized by *E. gracili*s and converted into biomass and a fertilizer liquid solution, rich in nutrients to support the growth of fruits and vegetables (Hauslage et al., 2018).

1.1.6 Biofuel and Bioenergy Biofuel and Bioenergy

During the last few decades, the world has seen increased interest in the biological production of fuel as a response to fossil fuel shortage, high prices, and negative environmental impact. Depending on the source of biomass, food crops (e.g., vegetable and sugar), non-edible biomass (e.g., waste), and microorganisms, biofuels are classified as 1st, 2nd and 3rd generation, respectively. Cyanophyta are particularly relevant as third-generation biofuels due to their higher biomass productivity and lipid content compared to other organisms and crops (Nguyen and Hoang, 2016).

Various methods can generate biofuels from algal and cyanobacterial biomass (e.g., *Synechococcus*, *Nostoc*, and *Chlorella*). The most well-known cases of cyanobacteria-produced fuels are biodiesel and biobutanol, which hold promise as a substitute for gasoline (Nozzi et al., 2013). Depending on the strain and process, the cost of converting the cyanobacteria into biofuel varies (Janssen et al., 2014). The production of biofuel through cyanobacteria has yet to be commercialized, but studies on this topic have been encouraging, especially those that have involved synthetic biology. Genetic modifications to cyanobacteria are easily accomplished; a prime example is the genetic engineering of the promising strain, *Synechocystis* sp. PCC 6803. Further information on genetically engineered cyanobacteria strains and their production of biofuels can be seen in the upcoming "Synthetic Biology" portion of this chapter.

Although lately, there has been substantial interest in algae-based biofuels for sustainability purposes on Earth, using such biofuels as the primary energy source on Mars is not feasible since these are currently far less efficient than other energy sources (Mapstone et al., 2022). On Mars, alternative power sources (e.g., photovoltaics and nuclear power) are preferable (Mapstone et al., 2022).

Alternatively, algae can help facilitate the decomposition of human waste produced by Martian crews, which can be used to generate biofuels and further help reduce the load mass of fuel during long-term missions (Verseux et al., 2016). Decomposed organic waste can be used to produce methane. Methane is the main ingredient found in natural gas, and on Earth, it is used to produce electricity and heat. Methane can also be used as a rocket fuel after combining with liquid oxygen. Even though a considerable amount of research has centred around producing methane from CO_2, methane can also be produced from algal and cyanobacteria biomass by anaerobic digestion through four consecutive stages: hydrolysis, fermentation or acidogenesis, acetogenesis, and methanogenesis (Singh et al., 2016). Several strains have already been studied in biogas production, including *Chlorella vulgaris*, *Arthrospira platensis/Limnospira fusiformis*, and *Spirulina maxima* (Samson et al., 1982; Doğan-Subaşı & Demirer, 2016; Varol & Ugurlu, 2016). Consequently, anaerobic digestion can be used in Martian wastewater treatment facilities to produce biogas and increase the

number of energy sources. Compared to the output of other alternative power sources (e.g., green diesel, biodiesel, bioethanol, hydrogen), biogas production from algal biomass has a much greater potential energy output (Bohutskyi & Bouwer, 2012).

Another hypothetical key source of alternative energy on Mars is hydrogen (Dutta et al., 2005). Hydrogen energy's conversion efficiency is far superior to conventional energy sources (e.g., petroleum), three times more potent than fossil-based fuel, and has a minimal environmental impact since it does not release greenhouse gases (Ali & Basit, 1993; Singh et al., 2019). Methods capable of producing hydrogen are abundant and include production by algae and cyanobacteria through photolytic water splitting. Due to the low investment cost associated with this technique and the fact that this is the cleanest process for producing hydrogen, this method is preferable over others (Dutta et al., 2005). H_2 can be used to produce methane (CH_4) and water (H_2O) on Mars if necessary (Verseux et al., 2016). Furthermore, detailed next, bioelectricity could serve as an additional energy source on Mars.

1.1.7 Bioelectricity

Electricity is produced by electron transfer from one chemical species (the reductant or donor of electrons) that gets oxidised to another compound (the oxidant or electron acceptor) which gets reduced, in a process known as an oxidation-reduction ("redox") reaction (Grossi et al., 2013). Redox reactions are commonly carried out in apparatus called electrochemical cells (e.g., voltaic/galvanic cells), which consist of a non-metallic substance placed in contact with two electrodes.

Microbial fuel cells (MFCs) are a new type of apparatus used in bioelectrochemical systems (BESs). MFCs consist of dual-chamber systems with anode and cathode half-cells separated by a proton exchange membrane (Grossi et al., 2013; Vishwanathan, 2021). In these hybrid systems, at least one of the electrode reactions is carried out by microorganisms, where organic energy is converted into electricity commonly under strictly anaerobic conditions.

MFCs are a renewable energy alternative since they can generate power through various wastes (Vishwanathan, 2021), including astronauts' urine, as suggested by Grossi et al., (2013).

One drawback of this system is the energy consumption required for aeration since the cathode chamber requires a constant oxygen supply (Gajda et al., 2015). Further developments of MFCs that can overcome such pitfalls are bio-photo electrochemical cells (BPEC). BPECs use oxygenic biomass, such as green algae and cyanobacteria, as biological components to convert solar energy into electrical power (Shlosberg et al., 2022).

In the photosynthetic apparatus's anodic chamber, the resulting electrons from water photolysis are transferred to the anode, producing electricity (Tschörtner et al., 2019). Oxygen is produced when photosynthetic cultures are used, resulting in lower running costs (Gajda et al., 2015; Liu et al., 2015). Moreover, BPECs allow the simultaneous generation of electricity and wastewater treatment (Gajda et al., 2015; Grossi et al., 2013).

The most commonly studied photosynthetic microorganisms in BPECs are *Dunaliella salina* and species from the *Chlorella* genus (Shlosberg et al., 2022). *Chlorella ohadii*, in particular, has added value since it can withstand extremely high light intensities (Shlosberg et al., 2022).

1.1.8 ISRU and Biomining

As mentioned previously, an additional avenue to reduce long-term mission expenditure is In-Situ Resource Utilization (ISRU). Methods for in-situ extraction of water and O_2 have already been successfully demonstrated on Mars, including the solid oxide electrolysis in the MOXIE (Mars Oxygen ISRU Experiment) instrument carried to Mars aboard NASA's Mars 2020 'Perseverance' rover (Hecht et al., 2021; Meyen et al., 2016).

Mission expenditure can also be reduced by extracting metals and minerals from the Martian regolith (Cockell, 2010) and Martian topsoil can provide important trace elements needed for the growth of algae and cyanobacteria in life support systems. Moreover, traditional techniques in the mining industry require high energy input, toxic substances, like cyanide, and/or large hardware, which may not be the most feasible solution on Mars. Biomining, extracting specific elements from their ores through living organisms, is an attractive alternative. Microbes like cyanobacteria can aid in this process since they can accelerate rock

weathering by attaching themselves and leaching rocky surfaces, similar in composition to those on Mars (Cockell, 2010). For example, the biomining of iron from lunar and Martian stimulants was achieved with the bacteria *Shewanella oneidensis*. Of particular interest are extremophilic cyanobacteria that resist extreme space conditions, such as the desiccation tolerant *Chroococcidiopsis* sp. (Cockell, 2010).

1.1.9 Summary and Synthetic Biology

As introduced above, photosynthetic microorganisms can produce a large array of products. However, their applications extend beyond the production of food, water, oxygen, fuel, and pharmaceuticals. Outlined in **Table 1.2** is the summary of phototrophic microorganisms relevant to future settlements on Mars, alongside their most advantageous features.

All of the above-described applications of algae and cyanobacteria to space exploration can be significantly expanded with synthetic biology. Molecular techniques can help improve existing strains' efficiency in specific roles (Verseux et al., 2016). Some of the most urgent are species with increased photosynthetic activity, biomass productivity (Menezes et al., 2015), and bioleaching activity (Cockell, 2010). Engineering microorganisms with higher resistance to extreme conditions is also pivotal to Mars (Verseux et al., 2016). In molecular biology, the modification of metabolic biological pathways and transformation with genes among different organisms have become standard practices. Cyanobacteria are regarded as promising 'low-cost' cell factory systems (Ferreira et al., 2018) - *Synechocysti*s sp. PCC 6803 is a photosynthetic model strain with an increasingly powerful genetic engineering toolbox, giving it its 'green' *Escherichia coli* nickname. (Ferreira et al., 2018). This cyanobacterium has been widely genetically engineered to produce higher quantities of bioplastics (please refer to the "Bioplastics and 3D Printing" section) and medical-related compounds (Singh et al., 2017; Ferreira et al., 2018). Other algal model systems are *Phaeodactylum tricronutum* and *Chlamydomonas reinhardtii* (Mapstone et al., 2022). The latter is probably the most versatile host due to the possibility of genetic manipulation of both the nuclear and chloroplast genomes (Mapstone et al., 2022). The applications of *C. reinhardtii* and its genetic toolkit are further discussed in Chapter 4.

Genetic engineering has been broadly used for the production of biofuels such as ethanol, butanol, isobutanol, and others. In this area of research, synthetic biology is used to maximize biomass yields and fatty acid biosynthesis and to optimize the physical and chemical structure of fatty acids, to produce biofuels with increased stability (Gimpel et al., 2013).

Moreover, mass cultivation of algae and cyanobacteria can be achieved in large ponds or closed photobioreactors. The second is a more attractive approach since it offers a controlled environment resulting in a lower risk of contamination and water loss (Huang et al., 2017; Voloshin et al., 2019). Considering the fact that bioreactors will be critical components of a Martian settlement, their optimization should be extensively explored. Factors such as light intensity, CO_2 flux, and temperature need to be optimised for (Verseux et al., 2016; Huang et al., 2017; Mapstone et al., 2022). Earth surface ponds need minimal operating costs in the form of financial investment and energy but require large land surfaces in order to scale up and these systems are susceptible to microbial contamination (Narala et al., 2016). On Mars, surface ponds would need to be pressurised which requires large surface structures and would also be subjected to transient fluxes of radiation and solar flare.

In summary, algae and cyanobacteria provide many in-situ solutions to most of the difficulties that humans will face on Mars. A few of the most discussed are summarized below.

- O_2 production;
- Dietary supplements, biomass for other food sources, and fertilizers;
- Pharmaceuticals, drug- delivery systems, and an array of medical items;
- Waste processing coupled with the simultaneous production of biofuel, water purification, and bioelectricity;
- Minerals, essential metals, and fertile soils;

Table 1.2 List of promising microalgae for space exploration and their most attractive features. This table was co-produced by the author of the present work who is a co-first author of Mapstone *et al,* 2022. The table reproduced here under a Creative Commons license.

Microalgae	Type of microalgae	Most relevant features	References
Anabaena/Nostoc	Filamentous cyanobacterium	Extremophile; genetic tools available; edible species; can use very high concentrations of carbon dioxide and Martian regolith simulant; biomining potential; capable of nitrogen fixation	(Arai et al., 2008; Bothe et al., 2010; Cockell et al., 2011; Murukesan et al., 2016; Olsson-Francis et al., 2012; Olsson-Francis and Cockell, 2010; Verseux et al., 2021)
Limnospira fusiformis (Spirulina)	Filamentous cyanobacterium	Edible with excellent nutritional and nutraceutical properties	(Rumpold and Schlüter, 2013; Wells et al., 2017)
Chlamydomonas reinhardtii	Green microalgae	Great set of genetic tools available (e.g., for production of pharmaceuticals)	(Dyo and Purton, 2018; Taunt et al., 2018)
Chlorella vulgaris	Green microalgae	Edible; air revitalization; well-characterized; most studied under spaceflight conditions	(Niederwieser et al., 2018; Wang et al., 2008; Wells et al., 2017)
Chroococcidiopsis	Unicellular cyanobacterium	Extremophile (including desiccation and radiation tolerance)	(Billi et al., 2000; Cockell et al., 2011; Olsson-Francis and Cockell, 2010; Verseux et al., 2016)
Euglena gracilis	Green microalgae	Edible with excellent nutritional properties; air revitalization; model organism in gravitational research; extremophile	(Gissibl et al., 2019; Hauslage et al., 2018; Martínez et al., 2017; Richter et al., 2014; Strauch et al., 2008; Suzuki, 2017)
Synechocystis/ Synechococcus	Unicellular cyanobacterium	Well-studied metabolism; vast array of genetic tools (e.g., boost biopolymer content); survival in very high concentrations of carbon dioxide	(Carpine et al., 2017; Murukesan et al., 2016)

Furthermore, it is important to keep in mind that sustainable approaches on Mars can also be utilized on Earth to combat environmental challenges.

Lastly, photoautotrophic organisms have also been gaining increasing attention as bioplastics producers. The production of bioplastics by photoautotrophic microbes is the focus of this thesis; therefore, this topic will be discussed in more detail in the next section.

1.2 Bioplastics and 3D printing

1.2.1 The Global interest in biopolymers

Biopolymers are biologically produced polymers, a promising alternative to conventional oil-derived plastics and their associated problems. Concerns regarding the negative environmental impact and limited availability of crude oil as well as problems of non-degradable waste of conventional plastics have increased the efforts to find a substitute. Fortunately, some biological (produced or derived from living organisms) thermoplastics such as polyhydroxyalkanoates (PHAs) have similar properties to conventional plastics, and they offer a set of advantages, such as being biodegradable and recyclable (Bussa et al., 2019; Pagliano et al., 2020) . Consequently, the global bioplastic market is expanding (Ashter, 2016). Their use is growing in various sectors like packaging and the medical industry (Keshavarz and Roy, 2010). Some organisms can synthesise adhesive biofilms that can be glued onto biological tissues, such as tissue sealants (Grossi et al., 2013) and bioplastics, as discussed in this chapter. Biopolymers can be 3D printed into medical utensils and devices. Indeed, one of the most promising applications of microbial-produced plastics on Earth is in the medical industry, where they proved their usefulness in wound management, bone and tissue engineering, drug delivery, and others, thanks to their biodegradability, encapsulation capability, and lack of toxicity (Asther, 2016).

Regarding biodegradability, PHAs can be degraded by depolymerases found in an array of microorganisms, from bacteria to fungi, occupying both aerobic (e.g., soil and marine) and anaerobic environments such as sewage. Carbon conversion to carbon dioxide during aerobic

composting must exceed 90% within 180 days for a bioplastic to be considered biodegradable (Brodhagen et al., 2014). For instance, over 90% of a well-known PHA – polyhydroxybutyrate - was effectively depolymerized anaerobically under mesophilic conditions for ten days. In contrast, polylactic acid (PLA) was only 7% biodegraded over 90 days (Yagi et al., 2014). PHA degradation can also be facilitated by a mixture of processes, including chemical and thermal degradation (Samori et al., 2022).

1.2.2 Polyhydroxyalkanoates and poly-B-hydroxybutyrate: structure, classification, and biosynthesis

Polyhydroxyalkanoates (PHAs) are mainly composed of linear polyesters. They vary in chain length, as seen in the general structure shown in **Figure 1.7**. These structural differences result in various physical and chemical properties with a broad spectrum of applications (Madison & Huisman, 1999).

Depending on the length of their chains, PHAs can be divided into three main groups: short-chain (scl), medium-chain (mcl) and long-chain (lcl) (Keshavarz and Roy, 2010; Troschl et al., 2017). Shorter polymers (3-5 monomers), characterized by increased stiffness, are the most common (Singh & Mallick, 2017). A well-known example of an scl-PHA is poly-B-hydroxybutyrate (PHB). In addition to being the most characterized polyhydroxyalkanoate, P3(HB) is the only PHA produced under photoautotrophic conditions (Troschl et al., 2017). PHB is stiff and brittle due to its semicrystalline structure (Turco et al., 2020). Its biocompatibility and biodegradability make it suitable for medical purposes, such as artificial tissues and implants (Kök and Hasirci, 2004).

The chemical synthesis of these polymers is complex and economically disadvantageous; therefore, they are solely produced by microorganisms (Valappil et al., 2007). Bacteria produce biopolymers like P3(HB) to act as carbon storage when subjected to stressful conditions, such as nutrient deficiency (Damrow et al., 2016). The most important trigger is nitrogen limitation, under which conditions several microbes accumulate and store PHAs in cytoplasmatic granules, which will later be used as energy source material (Keshavarz & Roy, 2010; Troschl et al., 2017). When nitrogen or other essential nutrient depletion occurs, the cells

enter the stationary phase and the carbon flux is then redirected into storage of carbon compounds in granules, such as PHB, and elimination of intermediary metabolites (Devadas et al., 2021).

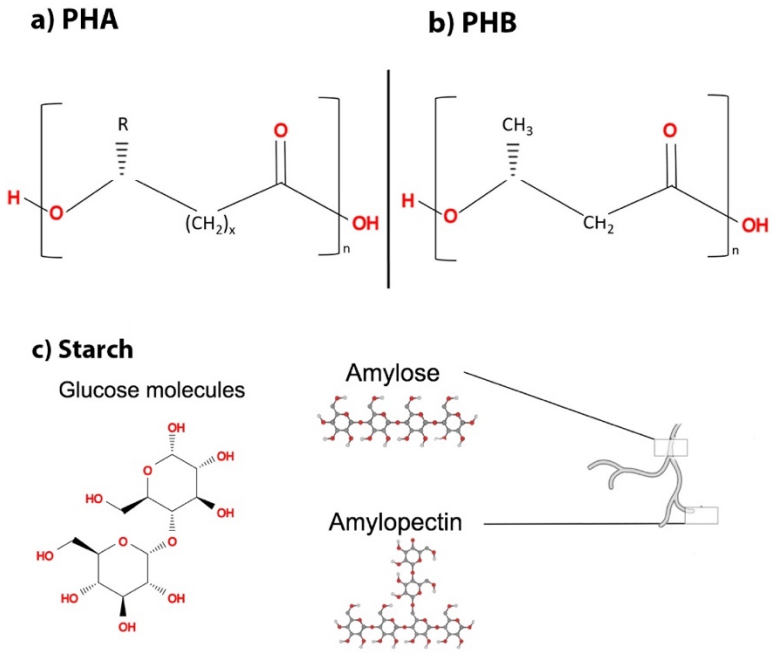

Figure 1.7 General chemical structures of (a) PHAs and (b) PHB in comparison with (c) starch $(C_6H_{10}O_5)_n$) which is one of the most abundant reserve polymers on Earth (R = alkyl chains (C_1 to C_{13}), x= 1–4, n = 1000–10000).

Among all known PHAs producers, bacteria are the most efficient. Over 300 bacterial species have been reported to synthesize PHAs (Keshavarz & Roy, 2010), and species from the genus *Bacillus* sp. and *Ralstonia eutropha* have been reported to accumulate an impressive 90% (w/w) PHAs of dry cells (Madison and Huisman, 1999).

PHB synthesis is directly linked to the Krebs cycle, also referred to as citric acid cycle or tricarboxylic acid (TCA) cycle (Monshupanee et al., 2019). The cycle is the primary source of cellular energy, in the form of ATP or guanosine triphosphate (GTP), during aerobic respiration. PHA synthesis is reduced under normal growth conditions since most carbon is consumed during glycolysis (Monshupanee et al., 2019). During cellular growth, the synthesis pathway of PHA is blocked due to the formation of high quantities of coenzyme A (CoA) obtained from the Krebs cycle (Marcello, 2020). CoA inhibits β-ketothiolase, which can not

cleave acetyl coenzyme A (Acetyl-CoA). The latter becomes available to other enzymes (e.g., citrate synthase) participating in other metabolic pathways, such as protein and lipid metabolism (Mothes et al., 1996; Oeding and Schlegel, 1973).

Complete inhibition of the TCA cycle is deleterious to cell growth, but a partial block has no significant adverse effects; it can reduce the TCA cycle carbon consumption, re-directing carbon flux towards the biosynthesis of carbon reserves, thus increasing their accumulation in the cells (Monshupanee et al., 2019). Due to changes in cellular priorities, unbalanced nutrient conditions decrease carbon consumption by the TCA cycle, resulting in reduced CoA levels that no longer inhibit the activity of β- ketothiolase (Marcello, 2020). Acetyl-CoA is now broken down by β- ketothiolase to acetoacetyl-CoA in the first step of PHA synthesis (Koch & Forchhammer, 2021).

PHAs can be produced by several metabolic pathways dependent on the organism and the carbon source used (Tan et al., 2014). **Figure 1.8** shows all 13 pathways described in detail by Tan and colleagues. The majority of the pathways (A-J) are responsible for the production of scl-PHAs. The remaining are involved in the synthesis of mcl-PHAs. Overall, all biochemical pathways involve two main phases starting with the synthesis of a precursor, which is often acetyl-CoA, followed by the polymerization of d-3-hydroxyacyl-CoA (3-HA-CoA) into the biopolymers (Marcello, 2020).

The three pathways most commonly described in the literature are B, J and K (Marcello, 2020). Pathway B, which is the one that uses glucose, is the one of interest in this body of work. In this pathway, P3(HB) synthesis from the intermediate acetyl-CoA occurs via three main enzymatic steps. Initially, acetoacetyl-CoA is converted from acetyl-CoA by β-ketothiolase, as mentioned earlier, to be reduced to d-3-hydroxybutyryl-CoA (3-HB-CoA) in the second step by acetoacetyl-CoA reductase, a NADPH dependent enzyme. Finally, P3(HB) and other scl-PHA are formed by PHA synthase (PhaC), which catalyses the polymerisation of 3-HB-CoA units (Balaji et al., 2013; Troschl et al., 2017). PHA synthases are classified into four classes based on their subunit composition (one or two submits) and substrate specificity; scl-PHAs are polymerised by Class I, III and I, while mcl-PHAs production is catalysed by class II

enzymes (Marcello, 2020). Some organisms have genes encoding several PHA synthases. The synthases of PHB from species belonging to the genus *Bacillus* the genus that will further be investigated here, belong to Class IV, which is characterised by the presence of two subunits. PhaC is a large (41 kDA) catalytic subunit, while the function of the smaller PhaR unit remains unknown (Neoh et al., 2022).

As seen in **Figure 1.8**, PHAs can also be synthesized by using lipids (e.g., fatty acids or oils) as feedstock through pathways I, J and K. Reports from the literature showed that PHAs have already been successfully produced using pure vegetable and waste oils such as frying oil and oil mill effluents (Mozejko-Ciesielska et al., 2017; Talan et al., 2020; Verlinden et al., 2011). Similar to carbohydrates, lipids are macromolecules that are also present in microalgae. However, this body of work focuses on carbohydrates rather than lipids as a raw material since most PHB work and adopted methodology worldwide uses excess of a carbon source, usually glucose, combined with limiting nitrogen conditions (L. Zhang et al., 2022). Moreover, *Chlamydomonas reinhardtii*, the microalgae strain selected for this work has a higher percentage of carbohydrates content than lipids, as shown in **Table 1.3**. Moreover, starch can be readily hydrolysed into glucose and used as feedstock, a key feedstock in the production of PHB, as mentioned above.

PHAs, and PHB, in particular, are currently manufactured by many companies worldwide. Unfortunately, the current commercial production costs of PHAs are around £2 to £5 per kg, which are not competitive with synthetic plastics (around £1.0 per kg) (Tan et al., 2022). The higher costs are associated with low productivity, pure bacterial cultures growing under optimal sterile conditions, and raw materials which employ expensive refined sugars. These expensive carbon sources account for 30-50% of the overall biopolymer production cost (Keshavarz & Roy, 2010; Tan et al., 2022; Możejko-Ciesielska et al., 2023). Photoautotrophic microorganisms, which do not require organic feedstock to grow, thanks to their natural photosynthetic capabilities, can help reduce the overall costs of PHB production if used as biopolymers producers or as a carbon source for the fermentation of other PHB-producing bacteria.

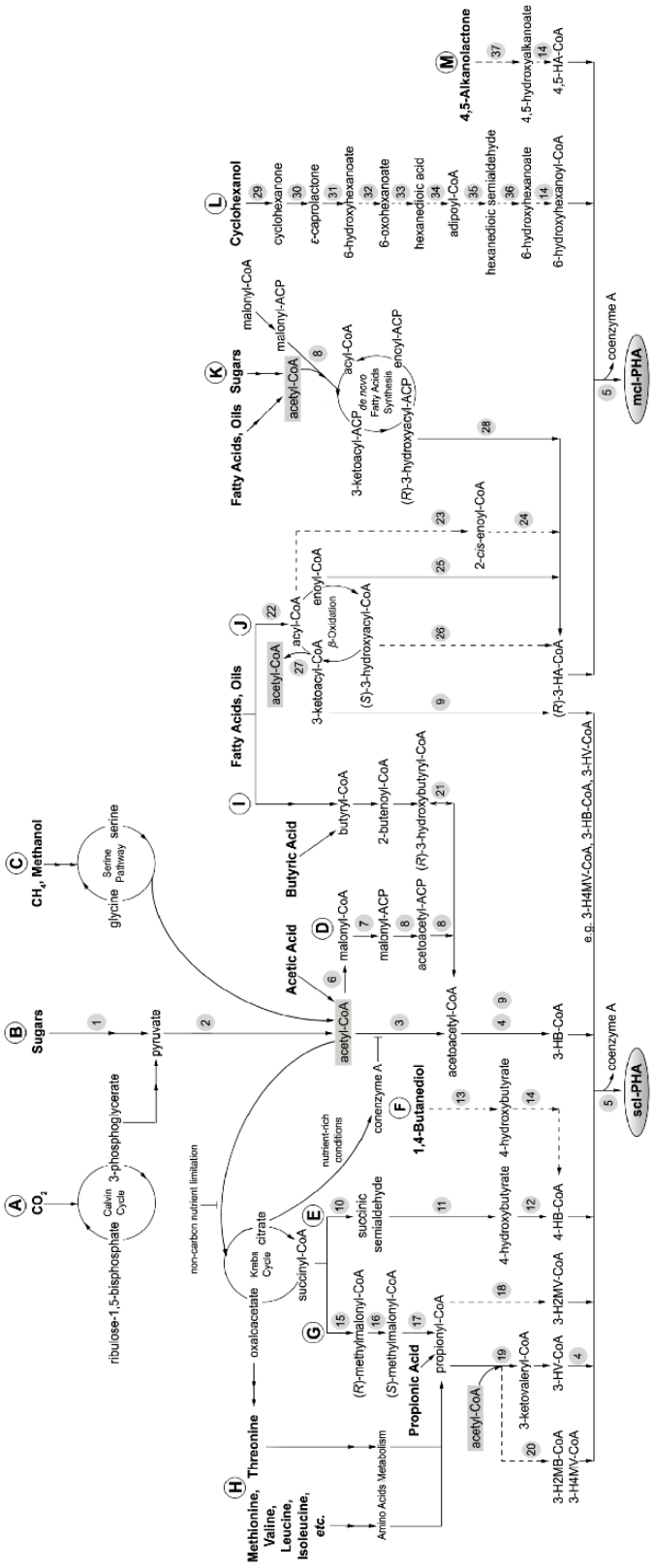

Figure 1.8 Main metabolic pathways for PHA production. The dotted lines represent putative pathways. The image was produced by Tan *et al*., 2014 and reproduced under Creative Commons license.

1.2.3 PHB production by cyanobacteria and algae

PHB can also be synthesized by cyanobacteria for energy storage under stressful conditions, although PHB content produced photosynthetically is much lower than that obtained from heterotrophic organisms (Koch et al., 2020). Similar to other prokaryotes, cyanobacteria, such as *Nostoc, Spirulina, Synechocystis and Synechococcus,* accumulate PHAs inside lipid granules or carbonosomes (**Figure 1.7**) in response to environmental or nutrient stimuli (Hirai et al., 2019).

Synechocystis sp. is the photoautotrophic genus most frequently studied in PHB research - the non-nitrogen fixing *Synechocystis* sp. PCC 6803 is a natural PHB producer and was the first phototroph to be fully sequenced, becoming a model organism for studying PHB production and its metabolic pathways (Afreen et al., 2021; Carpine et al., 2018; Troschl et al., 2017). This genus holds the record for the highest rates of photosynthetically produced PHB reported in the literature and only produces PHB under nutrient-limiting conditions (Koch et al., 2021). The highest yield was 55% of CDW (cell dry weight) in *Synechococcus* sp. MA19 under phosphate starvation (Nishioka et al., 2001), followed by 37% of Dry Cell Weight (CDW) when a mutant generated by random mutagenesis via ultraviolet (UV) radiation (*Synechocystis* sp. PCC 6714) grew in media with combined nitrogen and phosphorus deficiency (Kamravamanesh et al., 2018). Isotopic studies show that the majority (74%) of the carbon present in PHB comes from intracellular metabolites. As a result of a fully sequenced genome, several attempts have been made to reroute the metabolic flux of other organic compounds towards PHB synthesis. These attempts include overexpressing native PHB biosynthetic genes and blocking the pathway for biosynthesis of polyamine (Utharn et al., 2021) by deleting their biosynthetic genes and culturing the mutants under nutrient modified media. As a survival response to limiting nitrogen conditions, *Synechocystis* sp. has a resting phase known as chlorosis characterized by degradation of photosynthetic apparatus and syntheses of glycogen as a transit carbon-source. Later, still under nitrogen starvation, the cells start to convert glycogen into PHB. Genetic disruption of both pathways has been attempted but no major correlation between PHB and glycogen synthesis has been observed yet (Damrow *et al*., 2016; Koch et al., 2020). For instance, disruption to the PHB pathway results in increased

production of glycogen; however, blocking or overproduction of glycogen pathway does not increase PHB yields; and no growth differences or glycogen accumulation dissimilarities were observed in PHB-free mutant versus wild type (WT) (Damrow et al., 2016; Koch et al., 2020).

As mentioned earlier, Spirulina is a versatile cyanobacterium due to the variety of commercial compounds that it is capable of producing. Unfortunately, its PHB content is very low (less than 5%) (Troschl et al., 2017). Moreover, in view of the fact that strong cytoplasmatic endonucleases make genetic transformation difficult (Dehghani et al., 2018), it is not an ideal candidate for PHB production. Nonetheless, Spirulina and *Chlorella* sp. biomass have been tested in algae-polymer blends. Alga biomass is blended with bio or synthetic polymers as reinforcement material to improve plastic properties such as the tensile strength. Plastic properties will be introduced in further detail in Chapter 4. Hybrids of algae-polymer blends have been comprehensively reviewed by Cinar et al. (2020) and colleagues.

In contrast to cyanobacteria, the PHB synthesis pathway is not well-documented in green algae (Moah et al., 2022). Still, 29.5% of CDW of PHB has been produced in *Chlorella sorokiniana* SVMIICT8 in nitrogen-deficient media and under mixotrophic conditions using acetate as a carbon source (Kumari et al., 2022). Additionally, non-naturally producing PHB autotrophs can also be genetically engineered to produce PHB granules, as observed by transmission electron microscopy in transgenic cells of *Chlamydomonas reinhardtii* by Chaogang and colleagues after the incorporation of two PHA synthetases (phbB and phbC) from *Cupriavidus necator* (Chaogang et al., 2010). Moreover, Hempel and team introduced a complete pathway from *R. eutropha* H16 into *Phaeodactylum tricornutum* which resulted in PHB yields of up to 10.6% of dry algal weight (Hempel et al., 2011).

In summary, algae and cyanobacteria can be exploited in the production of plastics through three different scenarios (1) production of PHB (or other polymers) internally by naturally producing strains or genetically engineered mutants; (2) blending of algal or cyanobacterial biomass or polymers with other bio or conventional polymers (not discussed here in detail); and (3) by using whole biomass or intercellular components rich in

carbohydrates as feedstock for PHA-producing heterotrophic bacteria (Kumari et al., 2022; Cinar et al., 2020). The latter will be introduced next.

1.2.4 Algal biomass and carbohydrates as feedstock in bioplastic production

Ultimately, due to its rich content of starch, lipids and proteins **(Table 1.3**), both cyanobacterial and algal biomass have immense potential to be exploited as feedstock for heterotrophic biopolymer-producing bacteria (Averesch et al., 2023; Mapstone et al., 2022; Tan et al., 2022); either through direct biomass or pre-treatment and release of intercellular glucose-rich compounds (e.g., starch) from the organic material. Moreover, algal and cyanobacterial material contain trace elements necessary for microbial growth, such as calcium, magnesium, phosphorous, and potassium, as described in detailed by Cinar et al. (2020).

Table 1.3 Approximate macronutrient content of *Chlamydomonas reinhardtii* calculated as a percentage as a of dry weight.

Macromolecules	Content (%)	References
Proteins	47%	Darwish et al., 2020
Lipids	25%	Darwish et al., 2020
Polysaccharides	45-60%	Chen et al., 2013
Starch	53%	Kim et al., 2006

Chlamydomonas sp., for instance, is a robust producer of polysaccharides with quantities in the range of 45-60% (Chen *et al*., 2013). Kim *et al.* (2006) recorded that in batch culture the strain *C. reinhardtii* UTEX 90 can achieve a biomass concentration and starch content of 1.45 g CDW/L and 53%, respectively, after three days of culture (Kim *et al*., 2006; Chen *et al*., 2013). In the past few decades, the screening of high starch-producing algae strains has attracted researchers' attention (Ji *et al*., 2014; Gifuni *et al.*, 2017). Still, barely any emphasis has been given to the potential of algae starch to serve as feedstock for biopolymer production (Gifuni et al., 2017). The production rates of starch and other carbon-rich molecules

in algae varies considerably from species to species (Chen *et al*., 2013; Tang *et al.,* 2015). The carbohydrate content can be as little as 5% or reach as high as 80% depending on the microalgal species (Siddiki et al., 20202).

Even though cyanobacterial and algal biomasses have not been extensively explored as a feedstock in PHB synthesis via heterotrophic organisms, they have already shown to be a promising feedstock alternative in biofuels research leading to increased interest in algal biomass and lipids (Aikawa et al., 2013; Karatay, 2016; Sarsekeyeva et al., 2015; Abdallah et al., 2016). In bioplastic research, enhanced PHA yields have been reported in genetically engineered *Escherichia coli* using *Scenedesmus obliquus* biomass as a substrate (Rahman et al., 2013). Sathish et al. (2014) also demonstrated the production of PHB with 34 % of CDW by recombinant *E. coli* using algae-derived wastewater as the growth medium and sole carbon source in which the sucrose produced and released into media by the algae during photosynthesis was used to feed the heterotroph (Rahman et al., 2013; Sathish et al., 2014). A synthetic co-culture with *Synechococcus elongatus* as sucrose provider and a PHB-producing *Pseudomonas* strain achieved a maximum rate of PHA production of 23.8 mg/L per day under nitrogen limiting conditions (Löwe et al., 2017). Co-cultures, in which different microorganisms are cultivated together in the same medium, offer economic advantages since the step involving carbohydrates recovery from the phototrophic phase is removed (Löwe et al., 2017). Additionally, eliminating this step reduces quantity-related sugar losses and the risk of feedstock contamination (Löwe et al., 2017).

Another approach for coupling autotrophs and PHB-producing heterotrophs are biphasic systems. These systems involve two separate modules in which algae or cyanobacteria grow autotrophically in the first stage, followed by biomass harvesting, which is treated or directly fed to PHB-producing heterotrophic bacteria in the second stage. Even though biphasic systems reintroduce the sugar recovery step, they still offer advantages over microbial consortia, such as those mentioned earlier, in the previous paragraph. In terms of advantages, in a biphasic system, both cultures can be adjusted separately for maximum growth and carbohydrates/PHB productivity. Moreover, the biomass/sugar originating from the first step is not limited to bioplastic production. In a Martian scenario, where the availability of some

products is crucial for human survival, a biphasic bioreactor offers flexibility in terms of the type of products that are captured in the first stage (e.g., biomass, sugars, and lipids) and the end product that can be obtained in the second phase (e.g., bioplastic, food, and biofuel). For instance, in emergency cases, bioplastic production could be switched off, and the bioreactor can be repurposed to produce higher-value products such as food. For these reasons, a biphasic system was selected for this work.

Sucrose is not the only algal carbohydrate that can be used in PHB production. Other carbohydrates can also be found in algae as soluble sugars, as part of the cell envelope structure, and as extracellular polysaccharides (Tang *et al*., 2015). Starch is a naturally occurring polymer internally produced by microorganisms, which will be the focus here.

1.2.5 Starch: an abundant source of glucose

Starch is one of the most abundant carbohydrates on the planet, with numerous applications in our everyday lives (e.g., food, paper, adhesives, textiles, cosmetics, and pharmaceuticals) (Ji et al., 2014; Gifuni et al., 2017). As well as in higher plants, starch, is also the most widely distributed polysaccharide in algal species, including Chlorophyta, such as the *Chlamydomonas* genus (Chen et al., 2013; Gifuni et al., 2017; Koo et al., 2017; Mathiot et al., 2019; Velazquez et al., 2018).

The synthesis of plant-like starch in algae is an additional advantage of using algae as a feedstock since algae starch can be easily processed by using the same infrastructure developed for the treatment of starches produced by terrestrial plants, such as corn (Tang et al., 2016). Currently, potatoes, wheat, sorghum, and maize are the primary sources of this polysaccharide (Gifuni *et al*., 2017). The starch found in these higher plants is structurally and functionally identical to algae-based starch (Choi *et al*., 2010). Since microalgal cultures provide additional benefits over agriculture, algae could offer an excellent alternative for the sustainable production of starch (Gifuni *et al*., 2017). Such benefits include a faster growth rate, no competition for arable land, and a broader list of industrial applications, compared to terrestrial plants (Gifuni *et al.*, 2017).

Starch comprises two glucose polymers, amylose and amylopectin, composed of α-1,4 linked by linear α-1,6 chains (Bertoft, 2017; Pfister et al., 2014) and organised in insoluble semicrystalline granules of various shapes and sizes (Plancke et al., 2008). The sizes range from 0.1 to 100 μm in diameter (Findinier et al., 2019) and can be visualised in detail by electron microscopy, as shown in Figure 1.9.

While carbohydrate metabolism in algae is not entirely understood (Tang et al., 2016), starch biosynthesis has been studied in *Chlamydomonas* sp. (Busi et al., 2014; Koo et al., 2017). In fact, *Chlamydomonas* sp. has become a model organism in studying starch biosynthesis and regulation (Ball & Deschamps, 2009).

Starch is a product of photosynthesis and the Calvin cycle, where ATP/NADPH converts inorganic CO_2 into glucose and other sugars (Chen et al., 2013). Under optimal growth conditions, *Chlamydomonas* produces carbohydrates mainly as a cell wall component, while under stressful circumstances, starch is synthesized as an energy storage compound (Chen et al., 2010; Ji et al., 2014). In the presence of light, during diurnal growth rhythms, starch is deposited around the pyrenoid to be later utilized during the dark phase (Harris, 2009; Gifuni et al., 2017).

In *Chlamydomonas*, starch grains are concentrated around a proteinaceous microcompartment called the pyrenoid that enhances carbon dioxide fixation. Pyrenoids are responsible for approximately 30% of the globe's carbon fixation (Barrett et al., 2021). The pyrenoids in the chloroplast are where RuBisCO assembles and are involved in polymerising sugars into starch as a transient reserve compound during photosynthesis (Velásquez-Mejía et al., 2018). Furthermore, starch granules might also serve as a barrier to prevent CO_2 leakage from the pyrenoid (Wang et al., 2020).

Starch biosynthesis from CO_2 is under tight environmental regulation, is highly conserved (Gámez-Arjona et al., 2011; Geigenberger, 2011), and it starts with the conversion of G1P and ATP into ADPglucose by ADP-glucose pyrophosphorylase (AGPase) (Li et al., 2017). The enzymes involved in starch biosynthesis belong to different enzymatic classes, such

as branching enzymes (BEs) and debranching enzymes and starch synthases (SSs) (Gámez-Arjona et al., 2011).

Soluble starch synthases (SSs) and granule-bound starch synthases (GBSS) are the enzymes responsible for elongating amylopectin and amylose chains, respectively (Malinova et al., 2018). Previous publications show that SS4 (starch synthase 4) seems to be the most important for the formation of starch granules; for instance, overexpression of SS4 in *Arabidopsis* increased starch content (Gámez-Arjona et al., 2011).

Synthases are aided by branching and debranching enzymes (isoamylases). BEs cleave existing α-1,4-linked chains of donor glucans and transfer the cleaved segments to an acceptor chain by creating an α-1,6 linkage (Hussain e al., 2003; Ran et al., 2019; Seung & Smith, 2018). Debranching enzymes cleave α-1,6 linkages, catalysing the trimming of misplaced branches and irregular structures (Hussain e al., 2003; Ran et al., 2019; Seung & Smith, 2018).

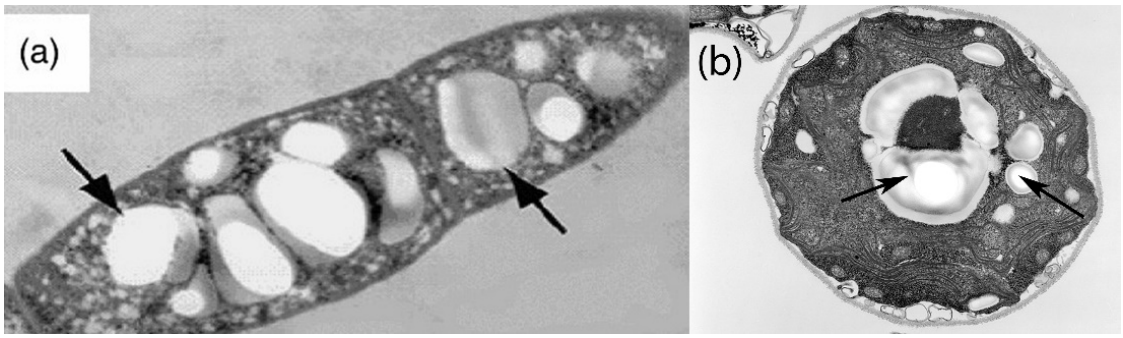

Figure 1.9 Transmission electron micrograph of (a) *Bacillus* strain CL1 cells with PHB-containing granules (indicated by arrows) and (b) an individual *Chlamydomonas reinhardtii* cell exhibiting the pyrenoid surrounded by a starch sheath (indicated by arrows). Image (a) was produced by Muhammadi et al., 2015 and reproduced under the terms of Creative Commons license from Taylor & Francis. Figure (b) has been available to the public domain by Dartmouth Electron Microscope Facility, Dartmouth College (New Hampshire, United States).

Various growth parameters can be tuned to enhance starch production in algae (Ho *et al.*, 2012). Starch accumulation increases under depletion of certain nutrients (Ivanov et al., 2021; Mathiot et al., 2019). The most effective strategy, similar to PHB-production, is nitrogen stress (Yang *et al.*, 2018). For instance, green algae *Tetraselmis subcordiformis* accumulated 54.3% of starch when submitted to limited nitrogen or sulfur conditions coupled with low light irradiance (Yao et al., 2012); starch content of *Chlorella vulgaris* P12 reached 41% of dry algae

weight on nitrogen depleted media (Maia et al., 2020); and *Chlamydomonas reinhardtii* 11-32A produced a 49% w/w starch-to-biomass ratio on medium with a reduced amount of sulphur (Mathiot et al., 2019). Although nutrient depletion effectively increases the starch content of *C. reinhardtii* to almost 49% (w/w), the overall productivity is reduced due to the amount of time (several weeks) it takes to reach maximum starch concentration under nutrient-limiting conditions (Ivanov et al., 2021). Moreover, while nutrient depletion inhibits cell growth, it also promotes lipid accumulation after the first phase of starvation, when starch biosynthesis occurs (Yang et al., 2018).

In addition to nutrient deprivation, enhanced starch accumulation has been achieved through temperature change. A 3-fold increase of starch was observed in *Chlamydomonas reinhardtii* grown under supraoptimal temperature (39 °C) in just 1-2 days compared with the five days of the control culture (Zachleder et al., 2021).

Upon nutrient deficiency, the cells switch off photosynthesis and start accumulating starch via metabolic pathways that are still unclear (Findinier et al., 2019). Here, starch accumulates in large insoluble granules distributed throughout the chloroplast's stroma, which can almost fill an entire cell in just a few days of continuous nutrient depletion (Giffuni *et al.*, 2017; Findinier et al., 2019). In addition to the chloroplasts - inside granules or around the pyrenoid – starch can also be produced in the cytosol by red algae (Placket et al., 2008; Ran et al., 2019).

Similar to PHB, microalgal starch can be used to produce biocomposites or various blends with other biodegradable polymers (e.g., PLA), as reviewed by Jiang et al., 2020 and Moah et al., 2022. Unfortunately, starch-based polymers offer low tensile strength and water resistance, making them unfavourable for many commercial uses (Moha et al., 2022). Alternatively, as discussed in the following chapters, algae-derived starch can be used as feedstock for polymer-producing heterotrophic bacteria.

Starch can be divided into three main categories, as described by (Bashir and Aggarwal, 2019). Native starch has not been submitted to any treatment. When the original characteristics

of starch are modified by a combination of treatments (e.g., chemical, or physical), the starch is addressed as modified starch. Lastly, and significant to this thesis, hydrolysed starch is starch in which the polymeric chains have been broken into simpler sugars (e.g., glucose). The treatments most involved in starch hydrolysis will be addressed in Chapter 2.

1.2.6 Three-dimensional printing in space

Additive manufacturing or 3D printing offers great promise for building on-demand infrastructure and other objects in support of space exploration. 3D printing with biologically produced polymers can provide a locally produced and sustainable solution for habitation on Mars. Due to their biodegradability, PHAs can be readily recycled.

In additive manufacturing, layers are progressively deposited on top of one another to create 3D solid structures from a digital model controlled by computerized systems (Tofail et al., 2018). The first steps to demonstrate the feasibility of 3D printing in space have already been achieved. Using parabolic flights to simulate a zero-gravity environment, Made in Space Inc., a 3D printing California-based company, was able to test its technology. The three flights were successful and gave no indication of a strong microgravity effect on the printers (Snyder et al., 2013). In 2014, Made In Space (MIS), in a partnership with NASA, launched a 566.5 x 460.4 x 273.2 mm printer to the ISS to evaluate the impact of microgravity on the material and to test remote commanding (Additive Manufacturing Facility (AMF) User Guide, 2016). Capable of processing acrylonitrile – butadiene – styrene (ABS) plastics, the printer was installed onboard the ISS on the Microgravity Science Glovebox. The machine used filament deposition modelling, also known as fused filament fabrication (FFF), to create print-on-demand objects for the crew. FFF is a printing technique whereby a thermoplastic material undergoes melt extrusion. The filament is heated, increasing its malleability. Because the filament is easy to manipulate in low gravity, this process was chosen, as opposed to using powder sintering or wire-based systems. Powder is challenging to work in microgravity, and wire-based systems are difficult to scale compared to the chosen technique (Prater et al., 2017). (Prater et al., 2019).

A faceplate was the first item to be 3D printed in space, which was followed by a ratchet wrench. The wrench was the first object 3D printed to meet astronauts' needs. **Figure 1.10** shows commander Barry Wilmore holding the object, which was transmitted remotely from Earth and produced by an MIS printer in 2014 (Buck et al., 2017). Twenty-five pieces in total were made aboard the ISS and returned to Earth to have their material properties analysed and compared to 22 pieces that were made using the same printer prior to being taken to the ISS. Even though some differences were seen (one example being that flight samples were stiffer than ground analogues), overall, no major differences in their properties were observed (Prater et al., 2017).

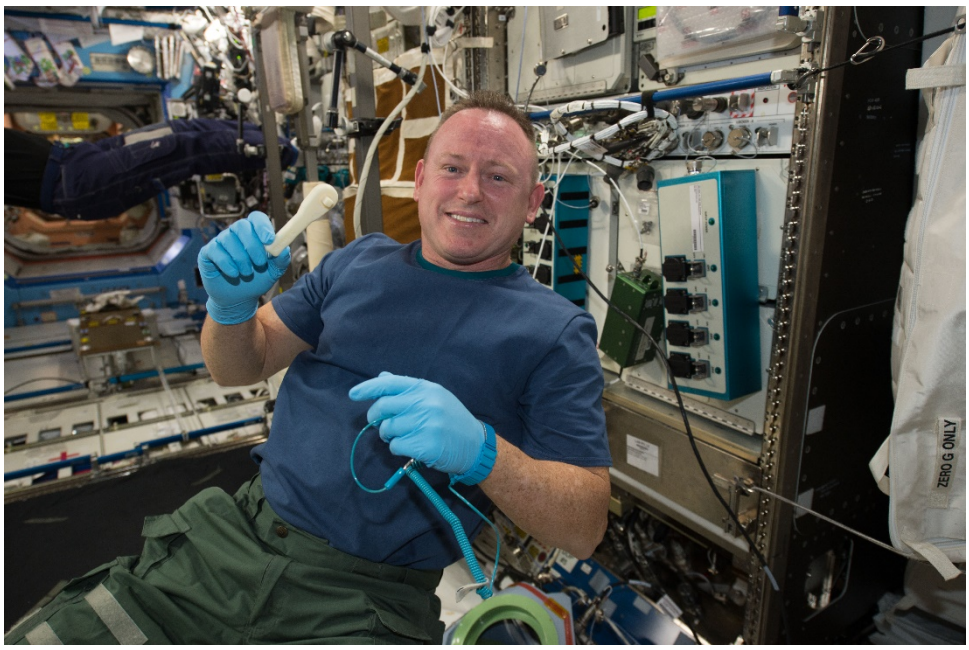

Figure 1.10 The first object 3D-printed in Space and designed and transmitted from Earth. ISS commander Barry Wilmore holding a 3D-printed wrench. The image was produced by NASA. The image is in the public domain and not subject to copyright.

Due to the potential of this technology, the European Space Agency has also invested in its own 3D printer prototype. The Manufacturing of Experimental Layer Technology (MELT) can operate in various orientations, including upturned, negating any microgravity restriction. It is also based on FFF and can print a variety of thermoplastics (European Space Agency, 2018).

Concerning PHB production for in-space manufacturing, Astroplastic, a Canadian company, has established an end-to-end process for polyhydroxybutyrate production using genetically engineered *Escherichia coli* (*E. coli*) and volatile fatty acids (VFAs) from solid human waste as feedstock. After collection, the waste is transferred to a tank and undergoes a three-day fermentation process with the resident gut microbiota, which increases the concentration of VFAs. Finally, a VFA-enriched stream is continuously fermented with genetically modified *E. coli* that produces PHB under anaerobic conditions (Chen et al., 2018). For the printer, the team uses selective laser sintering as a technique and PHB powder as feedstock. Future research for Astroplastics includes processing the system's safety in terms of flammability and off-gassing and optimizing the system for microgravity to produce PHB *en-route* to Mars (Chen et al., 2018).

Another private company, Mango Materials, is also working on the production of PHAs. The team aims to scale up the production of PHA using methane as feedstock. The company was awarded capital from NASA to continue developing its membrane bioreactor system and has been exploring the efficiency of its system in a microgravity environment (Morse, 2016).

In support of Martian habitation, NASA conducted a multi-year contest to design 3D-printable Mars habitats. The material used in the full-scale prototype of the winning project included regolith and renewable polymer (Anderson et al., 2018; Schuldt et al., 2021).

Since microgravity has been shown to affect bacterial growth and secondary metabolism (Demain and Fang, 2000; Huang et al., 2018), Thiruvenkatam and Scholz investigated how microgravity influences bacterial polyester synthesis in *Azotobacter vinelandii* UWD under simulated microgravity. The results showed that bacterial cells skipped the lag phase and started producing polymer immediately after exposure to simulated microgravity. This study reported a production threefold higher within 24 h of fermentation when compared to conventional growth in shake flasks (Thiruvenkatam & Scholz, 2000).

In-space manufacturing must also expand the types of materials that can be processed and 3D printed in microgravity, including recyclable feedstock. For instance, the Refabricator printer aboard the ISS was installed in 2019 due to its capability to recycle plastic (Srinivasan et al., 2018). High-strength polymers, such as PHB, locally synthesized polymers, and bioplastics produced within closed-loop systems should be further considered and tested (Mapstone et al., 2022).

1.3 Aims and objectives

This body of work has four main aims. The first three are associated with the potential applications microbes, specifically photosynthetic organisms, can offer during deep-space missions and how they can support human settlements on Mars. The fourth aim is related to the negative impact that microorganisms can have on future crewed missions to Mars.

1.3.1 Developing a large-scale bioreactor for batch cultivation of algae

The first aim involves the development of a low-tech bioreactor that can produce large quantities of photosynthetic algae biomass suitable to be converted into carbon feedstock in future missions to Mars. The objectives to accomplish this aim were the following: (1) design and construct a suitable photobioreactor with appropriate structural framework for supporting large scale-up culture volumes (15 L), lighting source and aeration; (2) evaluate different media composition, cultivation systems and microalgae strains; (3) develop a methodology for determining maximum starch accumulation and thus optimal harvesting time; (4) develop a protocol that can decrease biomass harvesting times; and (5) compare the efficiency of different methods for hydrolysing microalgal starch into simple sugars suitable for feedstock for subsequent heterotrophic culture.

1.3.2 Production of PHB by heterotrophic bacteria using algae-based feedstock

The second aim involves developing a two-phase system for producing biopolymer to be used in three-dimensional printing. The objectives outlined for this aim were (1) choice of the most appropriate PHB-producing strain; (2) validate fermentation and evaluate polymer production by the strain of choice with algae-derived biomass and sugars; (3) evaluate different protocols for identification of harvesting time for maximum biopolymer yield; (4) produce and characterize biopolymer using algae hydrolised biomass as sole feedstock; and (5) evaluate the practicality of using PLA/PHA blends to 3D print an object relevant to the routine life of astronauts in space.

1.3.3 Genetically engineer a microalgae mutant to facilitate separation and self- hydrolysis of its own starch

The third aim focuses on simplifying the starch harvesting process by genetically inserting a starch-degrading enzyme into the chloroplast of a microalga strain, which will facilitate starch separation and its degradation into simple sugars. The objectives required to reach this aim were: (1) choose a convenient cloning technique; (2) determine the most appropriate insertion region in the chloroplast and the most suitable algae recipient strain; (3) select a starch-degrading enzyme compatible with the selected hydrolysis conditions (4) design the cloning pipeline and plasmid constructs; (5) verify correct genetic assembly; (6) visualize enzyme localization inside the chloroplast and (7) test enzyme activity and efficiency in hydrolysing starch.

1.3.4 Analysis of microbial dispersal at a Mars analogue habitat

This body of work has four main aims. The first three are associated with the potential applications microbes, specifically photosynthetic organisms, can offer during deep-space missions and how they can support human settlements on Mars. The final aim is to understand

the risk of contamination of the Martian pristine soil by human-associated microbes carried by astronauts during future space missions to Mars. The specific objectives to accomplish this goal were: (1) characterise the microbial composition inside a Mars analogue habitat by swabbing and DNA analysis; (2) analyse the soil microbiome of a soil sample collected close to the habitat's airlock (3); investigate the occurrence of microbial dispersal from inside the habitat into the environment; and (4) characterise the elemental composition, physical properties and DNA recovery of a Mars analogue soil.

Chapter 2 Large-scale Cultivation and Treatment of Algae Biomass

I want to acknowledge Dr Henry Taunt's valuable contributions and feedback in selecting a microalgae species and the type of bioreactor.

2.1 Introduction

Green algae and cyanobacteria are attractive photosynthetic groups of organisms to culture to produce nutrient media for subsequent heterotrophic growth. Besides carbon dioxide and light source, green algae and cyanobacteria growth requires a container, and media composed of water with trace elements, salts, and nutrients such as nitrogen and phosphorus (Tan et al., 2022). Various aspects of algae growth will be introduced and discussed to develop a low complexity Mars-adaptable large-scale bioreactor. Analytic procedures will also be addressed in further detail in this chapter.

2.1.1 *Chlamydomonas reinhardtii* as a model organism

Current feedstock, such as sugarcane and corn, present many challenges, as acknowledged earlier. The objections raised against first-generation raw material refer to the demand for arable lands, potable water, and the risk of interference with the food supply (Chen et al., 2013). These problems will be intensified on Mars due to the lack of readily available liquid water and toxic perchlorates in the Martian regolith. Algae have been recognized as an

attractive alternative as a consequence of faster growth rates, higher growth yields, simple growth and maintenance conditions, and the ability to grow in non-potable water sources (Chen et al., 2013; Dassey and Theegala, 2013).

Within algal species, the unicellular *Chlamydomonas reinhardtii* is among the most well-known and studied, as it is metabolically well-characterized, has a fully sequenced genome, and has a growing array of genetic tools (Gifuni et al., 2017; Scholz et al., 2011). Moreover, as seen in **Table 1.1,** *Chlamydomonas reinhardtii* has not been widely studied in a BLSS context; choosing this microalgae species might therefore result in novel contributions to the field. In addition to being photoautotrophic, the fact that it can also display relative rapid growth in the laboratory under non-photosynthetic conditions is also of great interest to researchers (Harris, 2009). *Chlamydomonas* was first mentioned and discovered in the 1930s by German naturalist Christian Ehrenberg (Salomé and Merchant, 2019) and established as a model organism in the '50s (Sasso et al., 2018). Ever since, it has contributed significantly to our understanding of flagellar motility, metabolism regulation, and photosynthesis (Sasso *et al*., 2018; Salome & Merchant, 2019).

The absence of lignin in the cell wall of most algae is an additional attribute relevant to second-generation feedstocks. The presence of this complex polymer in the cell walls of terrestrial plants makes it difficult to degrade this physical barrier in order to release lipids and carbohydrates from the cell's interior. The lack of lignin in algae facilitates the disruption of cell walls, thereby resulting in cheaper biomass pre-treatments over lignocellulosic biomass (Velazquez et al., 2018). Moreover, algae also possess advantageous assets over cyanobacteria. These benefits include the amassing of high quantities of lipids and the synthesis and storage of starch structurally identical to that produced by vascular plants (Abdullah et al., 2018; Radakovits et al., 2010).

Most *C. reinhardtii* cells are oval-shaped and about 10 µm in diameter (Harris, 2009). These algae are predominantly found in soil but also capable of occupying aquatic environments, from fresh to seawater (Harris, 2009). The genus' most prominent features include two flagella and a single cup-shaped chloroplast where the pyrenoid - a key organelle

for CO_2 fixation and starch production - can be found (Harris, 2009; Sasso *et al*., 2018). Most species of *Chlamydomonas*, including *C. reinhardtii*, have a distinctive red or orange light-sensing eyespot, responsible for detecting directional light (Harris, 2009). Other features include a centrally positioned nucleus and a protein-rich cell wall (Sasso *et al.*, 2018).

Chlamydomonas and other algae have been long known for accumulating energy-rich compounds such as lipids and carbohydrates, including triacylglycerol and starch (Valazquez-Lucio et al., 2018). Owing to their ability to accumulate high quantities of starch, some strains can be a rich source of glucose and, thus, a promising feedstock for a variety of microorganisms (Choi et al., 2010; Velazquez et al., 2018). Although algal starch and biomass have been contemplated as a prospective emerging feedstock, most studies to date have been focussed on the biofuel industry (Tang et al., 2016; Bhalamurugan et al., 2018) as further detailed in Chapter 1.

C. reinhardtii was one of the first algal species to be studied and engineered for commercial purposes (Scranton et al., 2015). This strain can, therefore, aid researchers to better understand how to transfer transgenic laboratory algae into profitable and commercially viable systems (Scranton *et al.*, 2015). Genetic tools are also being used to help maximize the yield of biomass, biofuels, and other valuable compounds such as biopolymers (Radakovits et al., 2010; Scaife et al., 2015; Scranton et al., 2015). It is for these reasons that *C. reinhardtii* was selected in this project to provide feedstock in the production of biopolymer. The use of *C. reinhardti*i starch as the raw material in PHB synthesis by *Bacillus subtilis* will require a series of steps, as represented in the **Figure 2.1**, and discussed in detail in the following sections.

In summary, the whole process starts with culturing *C. reinhardtii* in liquid media until the maximum biomass yield is reached. The succeeding steps are the separation of the biomass from the liquid medium and subsequent pre-treatment of the biomass to rupture the cell walls and release the starch granules. Starch hydrolysis will then be undertaken to release sugars that will be fed to *Bacillus subtilis,* which will grow under nutrient stress in medium with low nitrogen content, will produce PHB as a fermentation by-product.

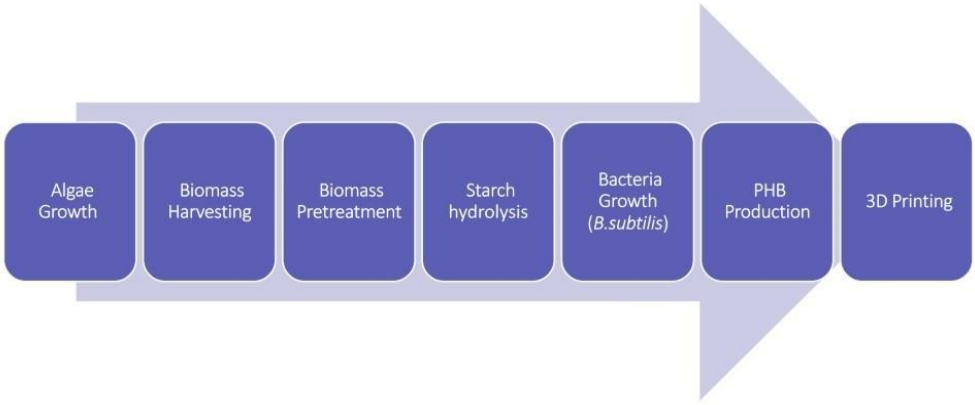

Figure 2.1 Schematic representation of the overall process. Algal biomass will be used as a carbon source to grow PHB-producing *Bacillus*. *Chlamydomonas reinhardtii* will be grown in liquid media until the end of the exponential phase or beginning of the stationary phase. Both centrifugation and flocculation will be tested and improved to develop an efficient technique to harvest the algal biomass. Enzymatic pretreatment will also be examined to evaluate its efficiency in hydrolysing starch granules that will be fed as a carbon source to *Bacillus subtilis. B. subtilis* will produce the biopolymer PHB which will be used in three-dimensional printing applications.

2.1.2 Growth Conditions and Life cycle

Chlamydomonas reinhardtii is a facultative heterotroph and possesses a versatile metabolism (Huang et al., 2017). Autotrophic growth occurs in the presence of light, using CO_2 as sole carbon source. In the presence of an organic carbon source, usually given in the form of acetate, it can grow more quickly heterotrophically, or by providing both inorganic and organic carbon, *C. reinhardtii* can also grow mixotrophically (Harris, 2009).

Different media compositions are suitable for each growth type. *Chlamydomonas* can proliferate autotrophically on the Sueoka's High-Salt medium (HSM), while the Tris-Acetate-Phosphate (TAP) Medium is widely used for mixotrophic growth. Both recipes used Hutner's trace element mixture developed by Hutner *et al.* in 1950, but TAP's high cost is a disadvantage. Alternatively, the HSM medium can be supplemented with acetate and used for mixotrophic growth (Harris, 2009).

As mentioned earlier, media composition, light, and temperature are vital parameters in regulating algae growth (Borowitzka & Vonshak, 2017). The optimal growth temperature for this species is 20-25°C, with a tolerated range as low as 15°C and as high as 32.5°C (Harris,

2009). For phototrophic growth in the absence of sunlight, illumination can be provided by cool, white fluorescent bulbs, and with a light intensity range of 200-400μ mol/m2s (Harris, 2009). Illumination can be continual or with day/night intervals for synchronized growth (Harris, 2009).

Proper agitation is also critical. It is necessary to prevent cell sedimentation, clumps, and cell attachment to the walls of the container. It also allows equal exposure of all cells to light, thereby avoiding the self-shading effect characterized by the formation of dead zones with attenuated light intensity, which may interfere with the algae growth rate (Shigesada and Okubo, 1981). A well-mixed medium also allows the equal distribution of nutrients in the medium, but most importantly, agitation is crucial for aeration. The need for gas exchanges between the air and the media is essential for autotrophic growth, as the CO_2 in the air is the sole source of carbon for photosynthesis (Huang et al., 2017; Shigesada and Okubo, 1981).

Microbial growth is characterized graphically by a growth curve divided into 5 phases, as schematically represented in **Figure 2.2** (Lavens and Sorgeloos, 2000; Basu, 2015). The "lag phase" begins after inoculation and represents slow growth and adaptation of the algae to the new environment. This stage is then followed by the "exponential phase" or "logarithmic (log) phase," where microorganisms grow at maximum growth rate (Basu, 2015). This phase is the most attractive for studying biomass and by-product production (Basu, 2015), and it is usually characterized by a cell density in the range of 10^5 to 10^7 cells/mL (Harris, 2009). The maximum cell density is important for harvesting and is dependent on light intensity, temperature, and media composition (Harris, 2009). The combination of continuous illumination and the addition of organic carbon (e.g., acetate) give the best results in liquid culture, yielding doubling times of 5-8 hours (Harris, 2009). During the "log phase," the nutrients are being rapidly consumed, leading to the scarcity of nutrients, and, consequently, to the "stationary phase," in which the cell density remains the same. The "death phase" starts when the number of cells begins dropping rapidly (Lavens & Sorgeloos, 1996; Basu, 2015).

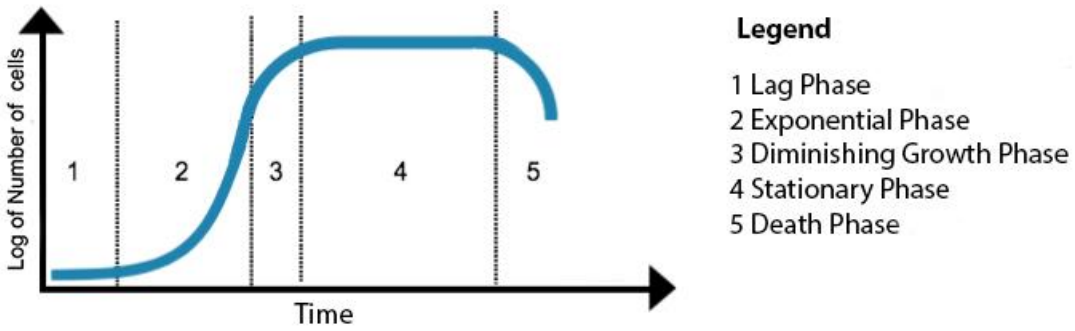

Figure 2.2 Graphic representation of the changes and evolution in the number of algal cells through time. The distinct growth phases are enumerated from 1 to 5 in the curve above. The cells grow slow in the beginning while adapting to the new growth conditions. Once adjusted to the new media, the cells multiply exponentially until they hit the stationary phase, where the number of viable cells remains the same. When the nutrients in the culture get exhausted, the cells start dying, and the culture enters the death phase. The image is in accordance with similar figures found in the literature.

For starting growth in liquid media, inoculation of experimental flasks or large-scale culture systems directly from Petri dishes is discouraged due to low cell concentration and cell adaptations required in order for the microorganisms to adapt from a solid to a liquid culture. Instead, a group of colonies is first added into a small volume, a "starter culture." An aliquot of the "starter culture" at mid-log phase (1-5 x 10^6 cells/mL) is then used to inoculate increasingly larger volumes during the scale-up process (Harris, 2009).

2.1.3 Mass culture

Large scale systems allow the production of algae in industrial volumes, which can have an economic impact by significantly enhancing the quantities of algae biomass and by-products produced (da Silva and Reis, 2015). Several cultivation systems have been developed for the mass culture of algae, all sharing standard features, such as illumination (natural or artificial), the supply of CO_2, and aeration (Huang *et al*., 2017).

Large culture systems in algaculture can be divided into two categories: open reservoirs and closed systems. The two essential factors that need to be considered when choosing between these two types of systems is the strain to be used and the cost of the overall production (Masojídek & Torzillo, 2008). Open reservoirs refer to relatively large, open ponds (**Figure 2.3**) that use natural lighting. These artificial lakes often have depths that range between 10cm

and 30cm, as well as rotating arms or paddlewheels that provide agitation (Masojídek and Torzillo, 2008).

Open ponds are economically more advantageous when compared to closed systems. Still, they are limited by several drawbacks, including the limited number of species that can grow in the pond due to the difficulty in controlling the growth conditions in an outdoor environment and problems of contamination (Masojídek & Torzillo, 2008).

On the other hand, closed systems, also known as photobioreactors (PBRs), offer the benefit of control over the culture's conditions. Reduced risk of contamination, increased reproducibility, and the flexibility to adjust and optimize for a specific algae species are additional gains in closed systems (Masojídek & Torzillo, 2008). One significant drawback associated with PBRs is their high capital costs, which include, but are not limited to, manufacturing and operational power. The most promising closed systems with low power consumption are column airlift, flat-panel airlift, and hanging bags (**Figure 2.3**). Column airlift and flat-panel airlift systems are still capital intensive (Huang *et al*., 2017). The simplest form of PBRs involves vertically suspended bags (**Figure 2.3A**), supported by study frames and aeration system, containing a liquid culture of algae with air or CO_2 being pumped by an aerator into a sterile plastic bag (Masojídek & Torzillo, 2008; Huang *et al*., 2017). Thanks to their low cost, hanging bagsare becoming increasingly attractive for commercial purposes (Huang *et al*., 2017). However, like other systems, they come with disadvantages, including inadequate mixing, inhibition of cell growth in dead zones, and leakages (Huang *et al*., 2017).

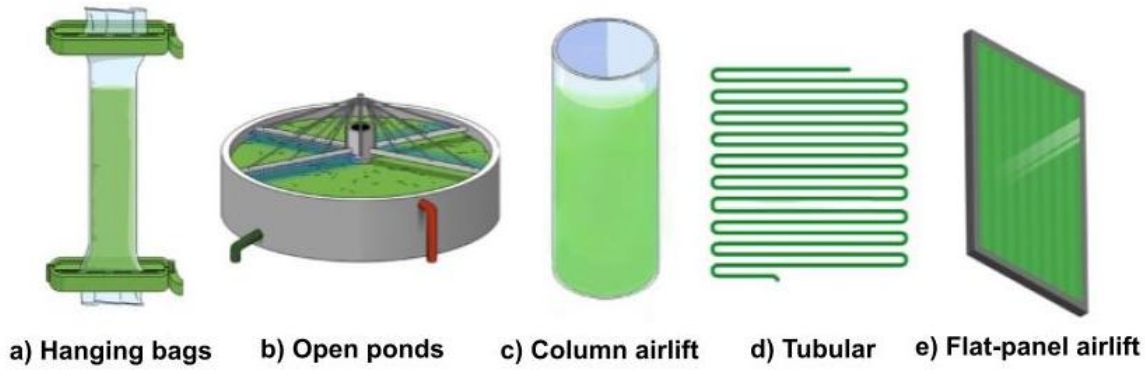

Figure 2.3 The variety of photobioreactors for algal cultivation in large-scale. (a) Plastic hanging bags; (b) an open raceway pond; (c) column airlift; (d); tubular bioreactor; and (e) flat-panel airlift.

Despite growing interest, there is no perfect large-scale system available yet for algae cultivation (Huang *et al*., 2017). Even though mass production of algal biomass has become increasingly attractive, there are still technical and operational practicalities that need to be overcome in order to transfer laboratory volumes to an industrial scale and achieve feasible commercialization (López Expósito et al., 2017). A key requirement for a successful large-scale culture is the reliable and effective monitoring of biomass productivity as well as early detection of contaminants, or other issues that might arise (Borowitzka and Vonshak, 2017). The hanging bags were chosen for this work because a closed system minimizes the risk of contamination and offers more control over growth parameters, as mentioned previously. Moreover, they have a simpler design than other closed PBRs, are less expensive to manufacture, and could, therefore, be more straightforward to install on Mars.

2.1.4 Estimation of Biomass

Estimation of algal biomass is critical in algaculture (Butterwick and Talling, 1982). It helps monitor growth and consequently help achieve the maximum yield of biomass and the product of interest (Basu, 2015). Sadly, accurate estimation has long been a problem (Chioccioli et al., 2014). The ideal method would need to be reliable, rapid, have a low limit of detection, and only require a small amount of sample (Butterwick and Talling, 1982).

The concentration of algae cells can be estimated through a variety of direct or indirect methods. As the name suggests, direct cell counting uses a counting chamber and light microscopy to calculate the number of cells present in liquid culture directly. Despite *Chlamydomonas*' motility, they can easily be counted with a compound microscope (10X ocular, 10X objective) by simply mixing a small sample of liquid culture with fixatives, such as tincture of iodine or Lugol's solution (Harris, 2009). One particularly challenging aspect of cell counting is the fact that in liquid cultures, *Chlamydomonas* tend to form cell aggregates (palmelloids), which are the result of incomplete separation of mother and daughter cells during cell division. Palmelloids, shown in **Figure 2.14**, are counted as four individual cells or multiples of four, which can lead to inaccurate cell counts (Harris, 2009).

Gravimetric analysis through Cell Dry Weight (CDW) offers an accurate measurement of the biomass through direct weighing of the dry mass after removal of the moisture content by freeze-drying or oven-drying. Dry freezing uses low temperatures and vacuums, rather than heat, which is preferable due to its speed and the fact that it preserves the integrity of entire cell structures when compared to heat treatments (Fellows, 2017). However, gravimetric analysis involves centrifugation or filtration. These additional steps make DCW time-consuming and, therefore, not ideal for monitoring purposes (López Expósito et al., 2017).

In contrast, indirect monitoring techniques measure parameters that correlate to the number of cells present in the culture, such as light scattering and chlorophyll, which are later calibrated to dry biomass (López Expósito et al., 2017). Among the indirect methods, also known as off-line, optical density (OD) is the most used, and it can be described as a logarithmic measurement of absorbed light versus transmitted of light (Chioccioli *et al*., 2014; López Expósito et al., 2017). The OD can be read at 750 nm in a bench-top spectrophotometer. At this wavelength, the cell concentration will not suffer interference from the light absorbed by chlorophyll and other pigments (Chioccioli *et al.*, 2014). Though this is a simple, inexpensive, and rapid method, results are often unreliable (Chioccioli *et a*l., 2014). The presence of contaminants and changes in the media might lead to fluctuations in opacity. Besides, cell size, concentration, and cell shape can all vary with culture conditions and can, therefore, also lead to incorrect extrapolation from OD to dry biomass weight (Chioccioli *et al*., 2014; López Expósito et al., 2017).

The search for improved methods for continuous monitoring is ongoing. New protocols have been developed with promising rates of success (López Expósito et al., 2017). To name a few, flow cytometry, two-dimensional fluorometry, in situ microscopy, and infrared (IF) spectroscopy, all presenting potential in replacing conventional techniques (Höpfner et al., 2010; Reardon et al., 2013; Chiocciolo et al., 2014; Lopez-Exposito et al., 2016).

Vibrational Spectroscopy has proven to be a powerful tool for chemical analysis in an array of fields (Hashimoto et al., 2019). Molecular chemical bonds have different vibrational properties (Driver et al., 2015) and this branch of spectroscopy studies the vibrational energy

of these molecular bonds (Hashimoto *et al*., 2019). Vibrational Spectroscopy includes infrared and Raman scattering spectroscopy, which, when used together, can provide complementary information about molecular bonds (Hashimoto *et al*., 2019). Algal cells contain five main types of biomolecules: proteins, carbohydrates, pigments, nucleic acids, and lipids, each of which produces characteristic features in vibrational spectroscopy (Parab & Tomar, 2012). Vibrational spectroscopy is rapid, non-destructive, uses small amounts of samples with no previous preparation, and can be performed in situs providing real-time information regarding different cultivation conditions and cell metabolism (Dupuy & Laureyns, 2002; Parab & Tomar, 2012; Bartosova *et al*., 2013; Ji *et al.*, 2014).

Raman spectroscopy has already been exploited for lipid and starch detection in different algae, including the *Chlamydomonas* genus. Raman is complementary to Fourier transform infrared spectroscopy (FTIR) (Hashimoto et al., 2019). Both techniques measure vibrational energy in molecules and collect data that is then compared to reference libraries. FTIR is an absorption spectroscopy technique that measures the energy absorbed by the sample after infrared light excites the molecules within it (Barth, 2007). The light absorbed corresponds to peaks in the spectrum, as shown in **Figure 2.4**. In comparison, Raman measures the energy that is scattered after the sample is excited by a laser with a single wavelength (Wahadoszamen et al., 2015). Since water has a weak Raman signal, Raman spectroscopy is often used to monitor liquid samples (Li et al., 2016).

In FTIR, the spectral regions that are most important in biological samples include the fingerprint region (600–1,450cm^{-1}), the amide I/II area (1,500–1,700cm^{-1}), the region associated with stretching vibrations in the higher-wavenumber region (2,550–3,500cm^{-1}), and the lower wavenumbers typically related to the carbon fingerprint (Baker et al., 2014). **Figure 2.4** shows a classic biological spectrum with the most important biomolecules, such as carbohydrates and proteins shown in different colours.

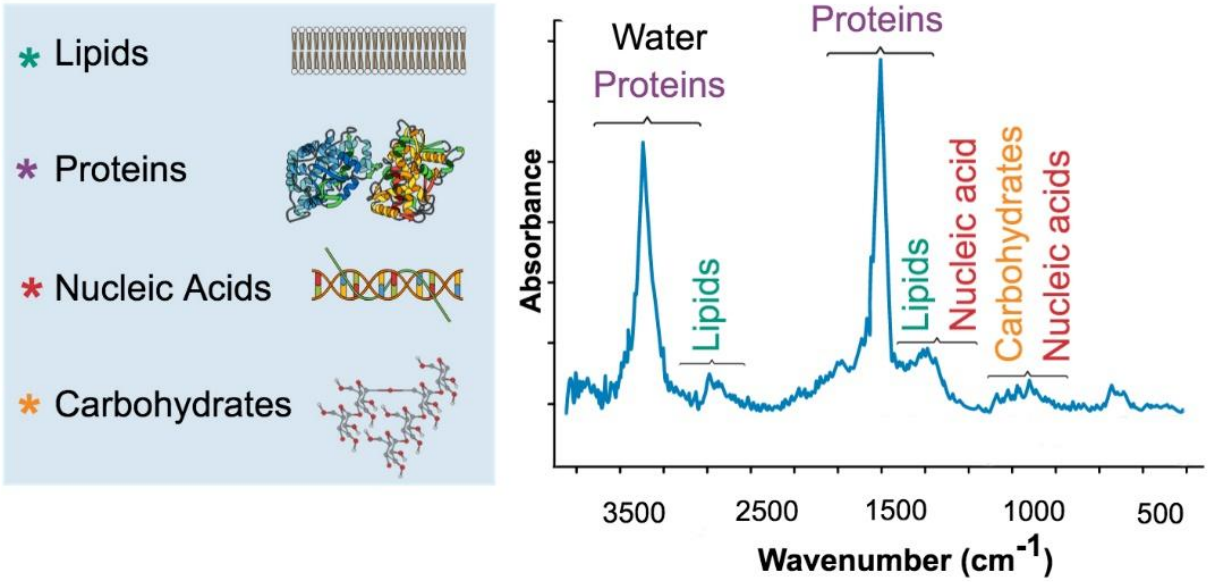

Figure 2.4 Representative biological FTIR spectrum showing the peaks associated with biomolecules, shown in different colours: lipids in green, proteins in purple, nucleic acids in red and carbohydrates in yellow. The image is adapted from the literature (Baker et al., 2014; Rohman and Man, 2010).

It has already been suggested that FTIR can be a powerful and extremely useful tool in the expanding field of algae research (Driver *et al*., 2015). This technique can provide information about the abundance of carbohydrates and other biomolecules present in a sample; it can help identify different algae species found in a specimen collected directly from the environment; and can discriminate algae responses to environmental stress, such as nitrogen or phosphorous limitation (Grace et al., 2020; Driver et al., 2015). FTIR spectroscopy has already been employed to identify biomolecules in algae and detect lipid accumulation in response to nutrient stress (Grace *et al*., 2020). In 2010, Dean and others made use of FTIR to successfully identify the content of lipids and carbohydrates in batch cultures of *Chlamydomonas reinhardtii* and *Scenedesmus subspicatus* over time.

Even though FTIR and Raman are known for providing complementary information when used together, only a handful of studies reported their simultaneous use when studying algae (Grace *et al*., 2020). Recently, Grace and team employed both techniques to analyse lipid accumulation and biomolecular transition during various growth phases in three algae: *Monoraphidium contortum*, *Pseudomuriella* sp., and *Chlamydomonas* sp. (Grace *et al*.

2020). More information regarding Raman spectroscopy and FTIR is presented in the "Estimation of Starch" section.

2.1.5 Harvesting Biomass

In algae biotechnology, the process of harvesting refers to the separation of the algal biomass from the liquid medium (Singh & Patidar, 2018). This step is a challenging one due to its high capital cost (Lopez-Exposito et al., 2017). It is estimated that biomass recovery represents 20-30% of the total cost of production (Dassey & Theegala, 2013; Jasper et al., 2017; Branyikova et al., 2018). The high value is related to both the energy and time required, as well as the equipment expenditures (Branyikova et al., 2018).

There are several methods available for dewatering and concentrating biomass, each with their own limitations and disadvantages, and different rates of success (Singh & Patidar, 2018; Branyikova et al., 2018). Biomass can be separated mechanically from the growth media via filtration or centrifugation, biologically with natural or forced sedimentation, chemically with flocculating agents (Singh & Patidar, 2018; Jasper et al., 2017; Branyikova et al., 2018).

Mechanical centrifugation is among the most attractive procedures, as a result of its reliability, and its high rates of biomass recovery, which consistently exceeds 90% (Branyikova *et al.*, 2018; (Singh & Patidar, 2018). Centrifugation works similarly to sedimentation. Sedimentation occurs naturally through Earth's gravity, while in a centrifuge spinning produces a more rapid particle sedimentation (Singh & Patidar, 2018). Centrifugation is energy intensive, however, and when working with higher volumes can become time-intensive (Branyikova *et al*., 2018). Its efficiency also varies in different algae species due to differences in cell sizes and densities (Jasper *et al.*, 2017; Singh & Patidar, 2018).

There has been an increasing demand to improve liquid-solid separation for commercial purposes. Currently, optimization is centered on combining different technologies in a two-step or multi-stage process (Singh & Patidar, 2018), with the goal of pre-concentrating the biomass before harvesting, thereby increasing harvesting efficiency and decreasing operational costs (Lam, 2017; Singh & Patidar, 2018).

Centrifugation can be paired with flocculation. Flocculation is a cost-effective, pre-concentrating technique that works by aggregating cell particles to form a precipitate or floc after changes to the media or addition of a flocculant or coagulant (Scholz *et al.*, 2011; Agunbiade *et al*., 2016). A coagulant/flocculant is a natural or synthetic compound that promotes the aggregation of cells and increases the settling velocity of the cell particles (Scholz *et al.*, 2011). By pre-concentrating the cells 20-100 times with flocculation, centrifugation can be enhanced, and harvesting times considerably reduced (Scholz *et al*., 2011; Branyikova *et al.*, 2018). Several coagulants and flocculants have been successfully used in algal cultures, including multivalent metal salts, polyelectrolytes, and chitosan. (Scholz *et al*., 2011) and can be effective even at low concentrations (Branyikova *et al*., 2018). The main difference between coagulation and flocculation is that coagulation neutralizes the electrical charges of suspended particles, changing their physical state, while flocculation makes these colloidal particles collide and form larger and heavier flocs (Dotto et al., 2019; Scholz *et al*., 2011).

Chemical flocculation aided by positively charged coagulants, such as polyvalent metals, has been reported in *Chlamydomonas* (Scholz *et al*., 2011; Fen *et al*., 2017). Since the surface of algae cells is generally negatively charged, a positively charged coagulant (e.g., calcium chloride) is added, thereby minimizing electrostatic repulsion among cells resulting in their aggregation (Branyikova *et al*., 2018; Pugazhendhi *et al*., 2018), as schematically represented in **Figure 2.5.**

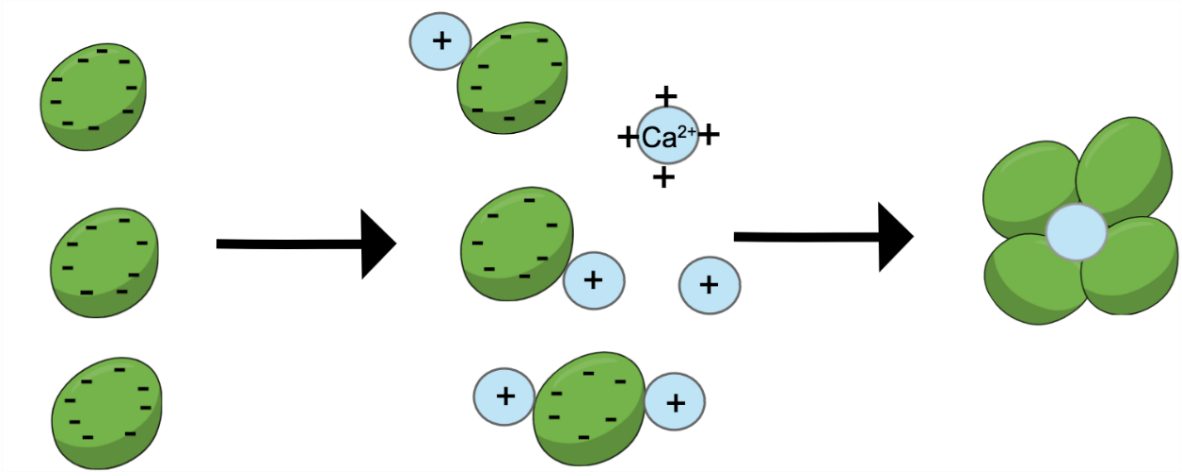

Figure 2.5 Schematic representation of the neutralization mechanisms of coagulation, in which microalgae's negative surface charge, represented in green, is cancelled, by a positive charged coagulant. The image is based on various illustrations from the literature.

Calcium chloride has proven to be an efficient coagulant for promoting flocculation in *Chlamydomonas reinhardtii* cell-wall deficient strains. Scholz et al. (2011) reported flocculation rates higher than 80% in the mutant cw15 after combining the divalent cation with methanol. Later, Fan et al. (2017) showed that both WT and cell-wall deficient strains efficiently flocculate (over 90%) at elevated pH upon the addition of bivalent metal ions such as calcium and magnesium.

2.1.6 Techniques Employed in the Treatment of Microbial Biomass

The harvesting process followed by biomass pre-treatment. The production of starch from biomass often requires two additional steps: I) pre-treatment of biomass to break down the cell wall and II) gelatinization of starch to make the starch available for subsequent microorganism culturing.

Chlamydomonas reinhardtii has a rigid multilayered cell wall made of two layers,formed of carbohydrates and polypeptides (Imam, 1985). This complex wall constitutes a physical barrier for intercellular compounds, such as carbohydrates, and, in order to liberate sugars or other compounds, it is necessary to disintegrate it (Choi *et al*., 2010; Lam, 2017; Velazquez-Lucio *et al.*, 2018). The efficiency of this step plays a key role in the final amount of sugars available and is, therefore, an essential step of the overall process (Velazquez-Lucio *et al.*, 2018).

Methods for rupturing the cell wall include chemical, thermal, and mechanical treatments (Lam, 2017; Kaapore *et al*., 2018; Velazquez-Lucio *et al.*, 2018), as depicted in **Figure 2.6**. These methods include One of the most promising techniques is enzymatic hydrolysis. Certain enzymes, such as amyloses, cellulases, and amyloglucosidases, break down the polysaccharides present in the matrix. The attractiveness of this process comes from the fact that it is a simple technique to carry out on a large scale. However, these enzymes can be costly (Velazquez-Lucio *et al*., 2018).

Hydrothermal treatment is another suitable process for the disintegration of the cell wall. High temperatures denature proteins and break down bonds within the cell wall. This type

of pre-treatment can be achieved with temperatures usually ranging from 60 to 180°C for a short time, typically less than 60 minutes (Velazquez-Lucio *et al*., 2018). Hydrothermal hydrolysis can be enhanced using acids or alkaline solutions as a reaction medium instead of water, resulting in decreased hydrolysis times. Using acidic solutions however can also lead to toxic waste and undesirable compounds, which could potentially interfere with subsequent microorganisms to be used further down the process (Velazquez-Lucio *et al*., 2018).

Electromagnetic treatment by microwaves also offers an expeditious outcome by rapidly superheating the cells (Kaapore *et al*., 2018). Disruption can also be achieved with low temperatures (below –10°C) through ice crystals formed during freeze and thaw cycles (Velazquez-Lucio *et al*., 2018). Sonification or ultrasonification, a disruption process that uses a probe and acoustic sound waves to agitate and break cell membranes, is a popular type of mechanical treatment (Liu et al., 2022). Moreover, electricity can be employed to disintegrate the cell wall. In the Pulsed Electric Field (PEF) method, cells are treated with short, high voltage pulses leading to the formation of pores – electroporation - and increased permeability of cell membranes, allowing for the release of intracellular content (Lam, 2017; Velazquez-Lucio *et al.*, 2018).

One major drawback of the mechanical methods is the high energy consumption (Lam, 2017). Nonetheless, these processes are preferable at the industrial level (Lam, 2017; Velazquez-Lucio *et a*l., 2018), where solid (bead milling/bead beating) and liquid (high-pressure homogenizer) shearing have become the most popular methods (Lam, 2017; Velazquez-Lucio *et al*., 2018).

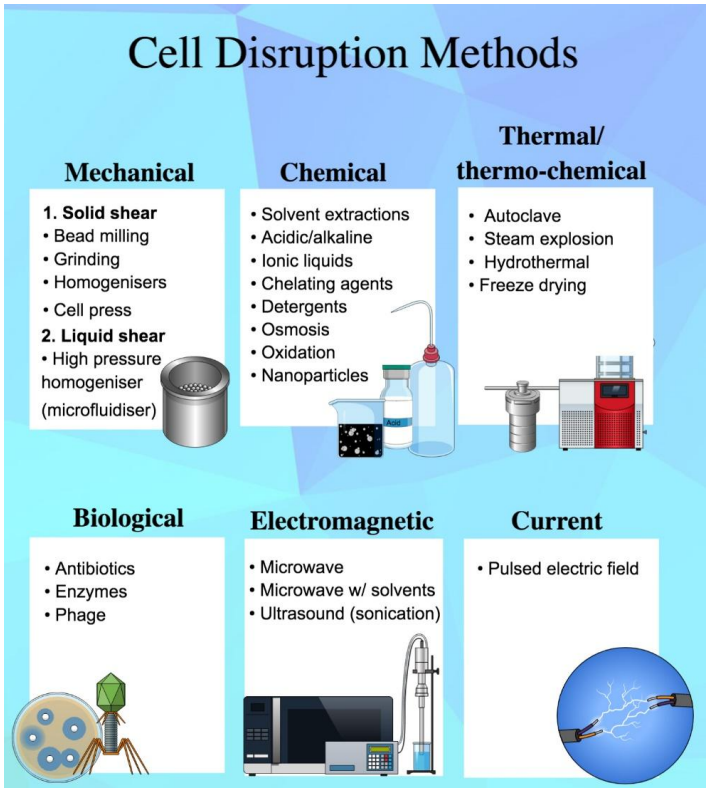

Figure 2.6 Summary of different cell disruption methods used in algae research. Based on their mechanisms of action, the methods are divided into the following types: mechanical, chemical, thermal, electromagnetic, biological, and current. The figure includes information from Kaapore *et al.* (2018).

Despite the rates of success of the techniques discussed above, a pre-treatment step still adds time and cost to the overall process, regardless of efficiency. To overcome the need for pre-treatment, in addition to WT, a cell wall deficient *Chlamydomonas* strain was also investigated. The absence of this structure would likely make intracellular compounds, such as starch, substantially more accessible and easier to extract, in comparison with strains with intact cell walls.

2.1.7 The Hydrolysis of Starch: Gelatinization, Liquefaction, and Saccharification

A stated earlier, the pre-treatment of biomass is required for two primary purposes: the breakdown of the cell wall (discussed above) and the modification of the starch structure. The second is imperative to increase starch accessibility to amylolytic enzymes that convert the starch into simple sugars, such as glucose (Velazquez-Lucio *et al*., 2018).

Starch exists inside semi-crystalline granules that are highly stable, which presents a challenge to the amylolytic enzymes (Velazquez-Lucio *et al*., 2018). Starch can be degraded into simpler carbohydrates in three consecutive steps: gelatinization, liquefaction, and saccharification (Hernandez *et al*., 2007). Gelatinization is the loss of the semi-crystalline granules encapsulating the starch; liquefaction refers to partial hydrolysis of the starch, resulting in reduced viscosity; and saccharification is the complete hydrolysis of starch into monosaccharides (Hernandez *et al.*, 2007).

Starch is insoluble in water at room temperature but becomes soluble when heated. Thus, the most common method employed in gelatinization is hydrothermal hydrolysis. At high temperatures, the hydrogen bonds of the granules are cleaved which results in the gradual loss of the granular structure (Hernandez *et al.*, 2007). The granules dissolve by first swelling irreversibly, and consequently bursting (Hernandez *et al.*, 2007; Schmiele *et al.*, 2019). During this process, the crystalline is melted, amylose is released, and viscosity increases (Schmiele *et al.*, 2019). Gelatinization is commonly used to facilitate the next procedures (Hernandez *et al.*, 2007).

Liquefaction follows gelatinization. After the dissolution of the granules during gelatinization, soluble polysaccharides released can now undergo enzymatic hydrolysis (Alde, 2008). Starch can be partially hydrolysed through conventional acidic treatments. However, acids are being replaced by thermostable enzymes, such as α-amylases. These enzymes catalyse the hydrolysis of internal α-d-(1–4)-glycosidic bonds converting polysaccharides (e.g., starch) into oligosaccharides (Alde, 2008; Choi *et al*., 2010). Dextrins, a mixture of glucose molecules, are the outcome of liquefaction and the intermediate by-product of the process (Alde, 2008). In liquefaction, enzymatic treatments are substituting conventional acidic treatments as they need less heating energy, use milder conditions, and are less costly while obtaining higher yields (Choi *et al.,* 2010; Velazquez-Lucio *et al.*, 2018). Liquefaction results in loss of viscosity, making the solution suitable for further processing in the saccharification step, where dextrins will be treated by further hydrolysis (Alde, 2008; Choi *et al.*, 2010).

In this final step of saccharification, the terminal α-(1-4)-glycosidic bonds in dextrins are cleaved, ultimately releasing individual glucose molecules (Alde, 2008). Aminoglycoside (AMG) is routinely selected in saccharification to break down dextrins into simpler, fermentable sugars (Velazquez-Lucio *et al.*, 2018). In addition to AMG, cellulases and hemicellulases have also proven to be successful in this stage of the process (Velazquez-Lucio *et al.*, 2018). Saccharification can be performed individually or simultaneously with fermentation (Alde, 2008). The advantage of doing it separately is the opportunity to adjust experimental conditions, such as pH and temperature, for optimal performance (Alde, 2008). On the other hand, simultaneous saccharification and fermentation (SSF) can help reduce investment costs and avoid product loss (Olofsson et al*.,* 2008).

In starch hydrolysis, the high cost of industrial enzymes is an obstacle, and it is therefore preferable to skip some of the steps involved in the pre-treatment of biomass and starch saccharification. In order to reduce production costs, the term consolidated bioprocessing (CBP) has been proposed and is gaining popularity in biorefinery (Zhang e*t al*., 2010). CBP is the single-event conversion of lignocellulosic biomass into valuable compounds where enzyme production, carbohydrates hydrolysis, and fermentation with solubilized sugars, are all combined in one step (Levin *et al.,* 2015; Minty & Lin., 2015). CBP uses the same microorganism to perform all tasks (Ali *et al.*, 2016). The number of microorganisms fit for CBP can be significantly increased with the help of synthetic biology. Molecular genetic tools can help introduce hydrolytic genes into an organism whose product-producing ability is well-established, and vice-versa (Zhang *et al*., 2010).

As starch is common in nature, a variety of microorganisms have developed amylolytic enzyme systems to hydrolyse and utilize it as a food source (Zhang *et al.*, 2010). Alpha-amylases, for example, are used in different industries and derived from organisms such as *Bacillus* sp. (Ubalua, 2012). Members of this genus produce thermostable enzymes that can hydrolyse saccharides at high temperatures, thereby dominating the alpha-amylase as well as the "liquefying" enzyme market (Ubalua, 2012).

Moreover, in addition to producing alpha-amylases and other relevant enzymes, *Bacillus* sp. synthesizes PHAs with several commercial applications (Shamala *et al*., 2012). Due to its enzymatic activity and biopolymer yields, *Bacillus subtilis* is the organism of choice in this body of work. *Bacillus* sp.and PHAs will be discussed further in the following chapter.

2.1.8 Estimation of the Starch Content

The estimation of starch content is of great interest to many industries, particularly the food sector (Velazquez-Lucio *et al*., 2018). Throughout time, a range of methods has been employed to quantify this carbohydrate. (Velazquez-Lucio *et al*., 2018., McCleary *et al.,* 2019). Nowadays, starch is measured by colorimetric methods after acidic or enzymatic treatments (Ji *et al.*, 2014).

Due to corrosion issues and other, enzymatic hydrolysis - gelatinization of starch in the presence of enzymes - has become standard practice (Velazquez-Lucio *et al.*, 2018). This method is reliable, accurate, and has been endorsed by the Association of Analytical Communities and the American Association of Cereal Chemists. The procedure is usually referred to as AOAC Method 996.11 or AACC Method 76.13 (Velazquez-Lucio *et al.*, 2018; McCleary *et al*., 2019) and can be detailed in three main steps. Biomass is first incubated in a water bath at elevated temperatures where, in the presence of thermostable α-amylase, starch is hydrolysed to dextrins. Dextrins are ultimately broken down to glucose with the aid of amyloglucosidase (AMG). In the third step, the release of glucose is measured with a spectrophotometer at 510 nm after incubation with a glucose oxidase/peroxidase (GOPOD) reagent (Velazquez-Lucio *et al.*, 2018; McCleary *et al.,* 2019). In 2008 Megazyme Total Starch assay kit, which is widely used, introduced a thermostable alpha-amylase that allows simultaneously incubation of this enzyme together with AMG. Recently, McCleary made slight improvements to this method resulting in a facilitated protocol with quicker outcomes (Mccleary e*t al.*, 2018).

Although the AOAC method is seen as the standard methodology, it is still an invasive and demanding approach in terms of reagents and quantity of sample required. Additionally, its accuracy and reliability depend on the efficiency of starch extraction and solubilization (Ji

et al., 2014). Spectroscopic techniques, such as FTIR and Raman Spectroscopy, both previously mentioned in the "estimation of biomass" section, can be used as a rapid solution for the characterization and quantification of biomass as well as starch content (Kizil *et al*., 2002; Ji *et al*., 2014). Both offer rapid, non-invasive solution that only requires a small volume of samples without previous preparation. Furthermore, the two provide consistent results with little expertise (Dupuy, 2002; Bartosova *et al*., 2013; Ji *et al.,* 2014).

The main goal of this chapter is the development of a start-to-finish process that includes large-scale cultivation of microalgae, *C. reinhardtii* in particular; monitoring of starch accumulation; efficient and time-saving biomass harvesting; and finally, biomass pretreatment for the release of carbohydrates that can be used as feedstock in bioplastic production. Different techniques were evaluated for each step to determine the most appropriate for the system developed.

2.2 Material and Methods

Two culture systems were developed to grow *Chlamydomonas reinhardtii* in the laboratory: Erlenmeyer flasks for small-scale experiments and hanging bags for production of larger volumes.

2.2.1 Implementation of a small-scale culture systems

A wild type (CC-1690) and TN72 cell-wall deficient mutant (CC-5168) strain of *Chlamydomonas reinhardtii* were obtained from Prof Saul Purton Purton's collection at University College London, UK. The TN72 mutant also referred to as CC-5168, is a cell wall deficient strain which lacks photosynthetic capabilities due to a mutation in the psbH gene. Cell-deficient *Chlamydomonas* strains are also commonly referred to as cw15 (Zhang et al., 2022). CC-5168 was created in 2016 at Dr Purton Laboratory by inserting an aadA cassette in the middle of the psbH gene, which led to the deletion of a large part of the psbH genomic region, resulting in a photosystem (PSII) deficient transformant, which lacks photosynthetic activity and is resistant to spectinomycin (Wannathong et al., 2016). The WT and the

chloroplast transformant can be purchased from the Chlamydomonas Resource Center (Wannathong et al., 2016).

Both strains were photoheterotrophically grown in Tris-Acetate-Phosphate (TAP) medium or Sueoka's High Salt Medium (HSM). Media composition can be found in **Table 2.1** and **Table 2.2**, respectively. Sodium acetate can be added to HSM media for mixotrophic growth, as shown in **Table 2.1**. In this body of work, only half of the acetate required for HSM media was added in hanging bags filled with this media to minimize organic carbon source use.

Table 2.1 Composition of Sueoka's High Salt Medium (HSM) for a total media volume of 1 L. [1]Sodium acetate, hydrate or anhydrous, can be added for mixotrophic growth. [2]The quantity of agar required for producing agar plates is also included. The media was created by Sueoka (1960) and its recipe is available in the Chlamydomonas Resource Center (www.chlamycollection.org).

Stock solution	Composition of Stock Solution	Amount required (per litre)
Beijerinck's salt solution		5 mL
	Ammonium Chloride	16 g
	Calcium Chloride Dihydrate	2 g
	Magnesium Sulphate Heptahydrate	4g
Sodium acetate(anhydrous)[1]		1.2 g
Sodium acetate (hydrate)[1]		2.0 g
Phosphate Solution		5 mL
	Dibasic Potassium Phosphate	288 g
	Monobasic Potassium Phosphate	144 g
Hutner's trace elements		7 mL
Agar[2]		15 g

The recipe for Hutner's trace elements, published by Hutner et al. (1950), which is made with eight stock solutions can also be found in the Chlamydomonas Resource Center in the following webpage: *https://www.chlamycollection.org/trace.html*.

Table 2.2 Composition of Tris-Acetate-Phosphate (TAP) for a total media volume of 1 L. The media was created by Gorman & Levine (1965) and its recipe is also available in the Chlamydomonas Resource Center. [1]The mass required for agar plates can also be seen in the table.

Stock solution	Composition of stock solution	Amount required (per litre)
Beijerinck's salt solution		25 mL
	Ammonium Chloride	16 g
	Calcium Chloride Dihydrate	2 g
	Magnesium Sulphate Heptahydrate	4g
Hutner's trace elements		7 mL
X40 TAP stock solution		25 mL
	Trizma Base	96.8 g
	1M Potassium Phosphate	40 mL
	Glacial Acetic Acid	~ 30/40 mL[1]
1M Potassium Phosphate	1M Monobasic Potassium Phosphate	250 mL
	1M Dibasic Potassium Phosphate	~160/170 mL[1]
Agar[1]		15 g

Both wild type and cell-wall deficient cultures were grown under continuous illumination provided by a 120 cm long light panel holding eight T5 white fluorescent lamps (Lumii, UK). The cultures were submitted to constant shaking at 120 rpm by orbital shakers (Benchmark Scientific Orbi-Shaker, USA) to guarantee gas exchange with the environment. The light panel was placed horizontally above the flasks. Light irradiance was measured around 35.37 $\mu mol_{photons}\ m^{-2}$ s.

Cultivation was performed in Erlenmeyer flasks at room temperature (~ 20°C). Starter cultures were prepared by inoculating 25 mL of sterile TAP in 50 mL Erlenmeyer flasks from agar plates and grown into late log phase. Sub-cultures containing at least 1 x 10^5 cells/mL were then added to 1 L flasks with 400 mL of fresh TAP to an initial OD_{750} of 0.05, as described by Cui et al., 2020. The 400 mL cultures were used for experimental purposes or as an intermediate-scale culture for mass production of *Chlamydomonas,* as shown in **Figure 2.7**. All experiments were carried out in triplicate. Old agar plates were kept under low light in a cold room or fridge (18°C) as stock cultures for up to six months.

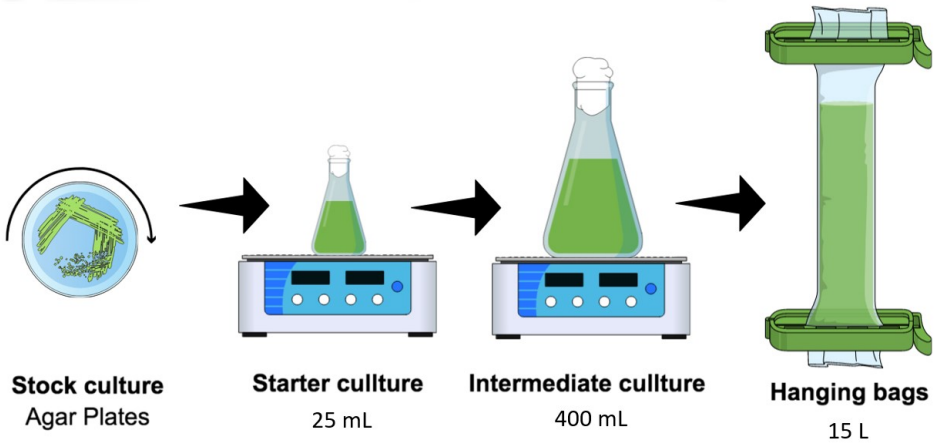

Figure 2.7 The sequence of steps involved in the growth of *Chlamydomonas* in the developed system. Stock cultures are grown in Petri dishes at room temperature and re-streaked often to keep the cultures fresh. Fresh agar plates are used to inoculate starter cultures when necessary. Starter cultures (25 mL in 50 mL flasks) are grown to log phase within two to three days at room temperature and are aerated by constant shaking at 120 rpm and continuous illumination. When ready, starter culture is used to inoculate the intermediate scale (400 mL in a 1 L flask). Intermediate-scale cultures may be used for experiments or to initiate a large-scale culture in hanging bags with a maximum volume of 15 litters.

2.2.2 Large-scale production of algae by hanging bags

Hanging bags were the photobioreactor of choice. A metal stand was designed and customized to meet operational criteria with an online platform known as Vectary Studio. The stand was built at the Building BloQs workshop (London, England), after several online discussions and in-person meetings and visits to the facility.

The metal frame with 160 cm in height and 60 cm in width was designed to fit a total of six hanging bags, each capable of holding 20 L of total volume. The stand possesses a perforated middle panel 5.5 cm thick, to which the light systems are attached, and electricity cables can pass through. A wide square surface was added on the bottom to help support 120 kilograns of lliquid culture (six hanging bags filled with 20 L each). On the top of the bioreactor, two rails with a 5 cm distance between them were added to each side for different light exposure. The closer rail was placed 11 cm while the other 16 cm from the middle panel. Light intensity slightly changed with distance, 43.95 $\mu mol_{photons}\ m^{-2}\ s^{-1}$ and 48.12 $\mu mol_{photons}\ m^{-2}\ s^{-1}$, respectively. A wide square surface was added on the bottom to help support a maximum of 120 kilograms of liquid culture (six hanging bags filled with 20 L each). Each side of the frame supports three hanging bags and two light panels (Lumii, Uk). A 3D model of the stand was first created and then manufactured at the Building BloQs facility, both shown in **Figure 2.8**. Two horizontal poles were also added to the top of the stand to give flexibility in positioning the bags further away or closer to the light panels.

Continuous illumination was provided by two light panels containing eight fluorescent lights (Lumii, UK), on each side. EnviroGro by LUMii T5 lighting panels were selected due to the flexibility of use they offered. They can be hung horizontally in the small-scale system or vertically in the bioreactor. Each light panel carries eight fluorescent T5 lamps and separate power switches, which allows control over light intensity.

Aeration was supplied with aquarium pumps (Hidom 2.0w Aquarium Air Pump Single Valve HD-601, China). The addition of a 0.2 μm syringe filter (Fisherbrand) in the air tubing offered a sterile supply of air.

Sterile polyethylene tubing rolls (1000-gauge, UK Packing, UK) were cut to appropriate lengths and heat-sealed (Pacplus IS300C 300mm) at both ends to ensure a sterile environment. Metal strips with tightenable bolts were handmade to size and added to the bottom of the bags to prevent leakages and at the top, to assure that the bags were stably fixed to the support.

The media composition followed the same HSM or TAP recipes tested in the small-scale system. All reagents were mixed before autoclaving and pumped with a peristaltic pump (Watson-Marlow 323, UK) aseptically into the bags. Large-scale culturing was inoculated by with 400 mL of intermediate culture at the log phase per bag. The photoreactor was operated at room temperature (~20°C). Cultures were grown for a week with cell counts measurements taken daily. The biomass was harvested at the beginning of the stationary phase.

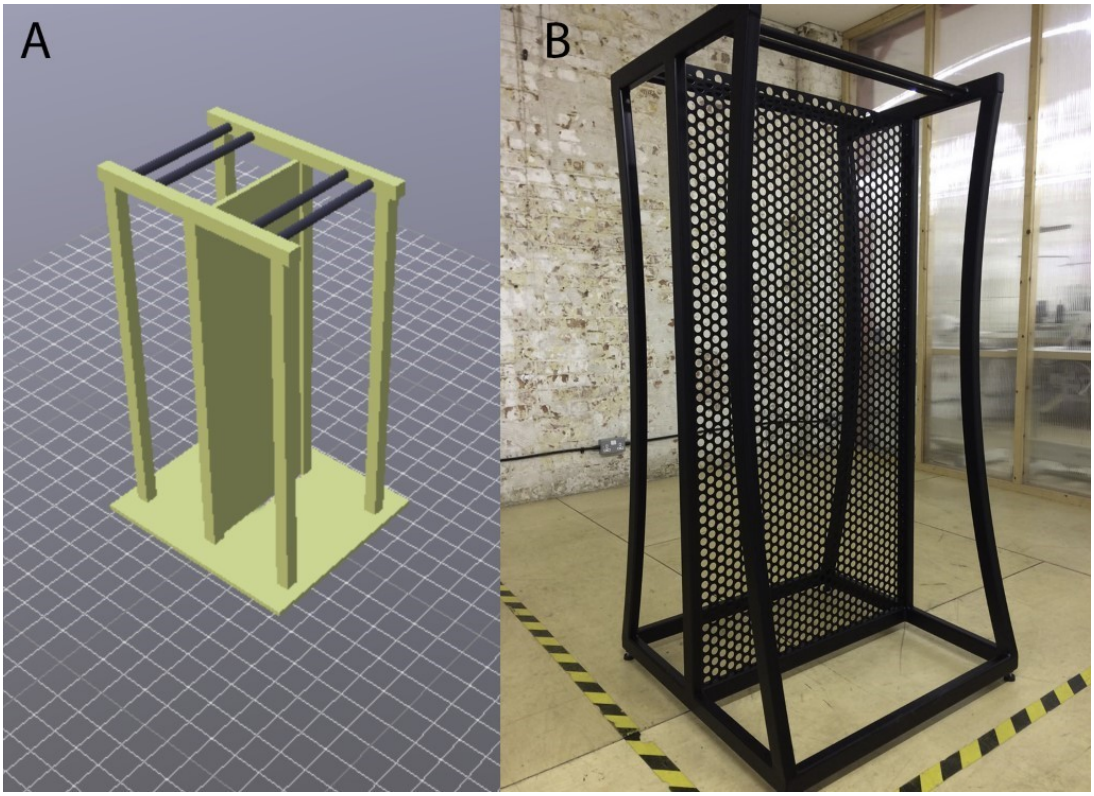

Figure 2.8 The customized stand that was built to support the hanging bags. (A) 3D model of the stand. (B) The metal frame after completion.

Leakage related issues were eased with doubled heat seals and by the introduction of metal clamps that clip together different layers of plastic. The clamps were handmade to size in one of the workshops at the University of Westminster. These metal strips were also used to overcome another challenge. Each hanging bag weights approximately 20 kilograms. Properly fixing the bags to the top poles of the stand was found to be difficult, but the clamps provided a strong and stable solution.

2.2.3 Operation of the hanging bags bioreactor

The protocol designed for operating the hanging bags was adapted from Cui, 2022, with the most significant modifications being to the techniques employed for aeration and harvesting. Aquarium pumps substituted a gas airline and CO_2 supply to reduce complexity. The total volume per bag is 15 L of HSM media supplemented when stated with acetate for mixotrophically growth. Even though many steps involve sterilization, the overall process is not 100% sterile. However, all stages in both protocols were designed to minimize contact of the culture with the environment.

Ten litre plastic carboys were used for preparing and storing culture media. These carboys were fitted with a filling/venting cap and a short length of silicone tubing attached to an autoclavable and reusable 0.2 µm filter (Sartorius, Midisart), in order to keep media sterile after autoclaving for storage and bag-filling. A second, longer, length of silicone tubing was fitted with a 1 mL pipette tip, with the other end to be later connected to the carboy filter to introduce culture media into the bags by peristaltic pump. Aeration tubes were assembled from silicone tubing with a 200 µL pipette tip at one end and a luer fitting at the other to later attach to a single-use air filter.

Growth media were prepared in the 10 L carboys and autoclaved at 121°C for 30-45 minutes, then allowed to cool at room temperature before use. Carboy cap filters, silicone tubing, pipette tips and luers were all autoclaved wrapped in foil.

The bioreactor hanging bags were constructed from layflat polyethylene tubing extra heavy duty with 1000-gauge thickness (UK Packing, UK). The circular cross-sectional area of a liquid-filled layflat tube is 134.5 cm^2, and so 15 L of culture gives a liquid height of 111 cm (with approximate cylindrical volume). A gas headspace of one-third the culture medium height was used, namely 37 cm, and a further 15 cm of tubing are required at the top and bottom for clamping, which resulted in a total hanging bag length of 180 cm. The layflat tubing was cut to this length for each hanging bag, and then heat sealed for 3 seconds at 15 cm from the top and bottom, in a line strictly perpendicular to the bag length to minimise potential leaks. The tube bottom was firmly wrapped around a metal strip three times and then secured tightly

with bolts to a matching strip to ensure a water-tight seal. The tube top was similarly sealed, with the metal strips then providing a secure attachment for hanging of the bag on the culturing frame top railing.

To fill the hanging tubes with culture medium, the top of the bag was locally disinfected by spraying 70% EtOH and a small opening created 5 cm below the top clamp using sterile scissors. The autoclaved 1 mL pipette tip attached to the length of silicone tubing was inserted through the hole, the tubing connected to the carboy cap and a peristaltic pump running at 300 rpm used to fill the hanging bag with 15 L of culture medium. After filling, the top hole in the hanging bag was closed with an autoclaved foam bung. The media in the hanging bag was inoculated with starter culture using a sterile serological pipette through the same access hole at the top.

For aeration of the hanging bag culture, the (non-sterile) air supply tubing from an aquarium air pump was connected to the autoclaved air inlet tubing with 200 µL pipette tip via a sterile single-use filter with luer fitting. Thus, air from the aquarium pump was filter-sterilised before entering the culture. A clamp is applied to the air tube to prevent media back-flowing down it during insertion. The bottom of the hanging bag is disinfected with EtOH spray, and the plastic wall then pierced with the 200 µL pipette tip of the aerating tube. Aeration of the culture is begun by powering on the peristaltic pump and removing the tube clamp. Proper aeration is verified by observing a steady stream of bubbles rising through the column of culture medium.

After inoculation of the hanging bag (as above), visual observations helped verify the equal dispersion of the green-coloured inoculum throughout the medium by the stream of aeration bubbles. Sampling of the culture was achieved by sterile serological pipette through the small access hole at the top of the hanging bag, and the sterile foam bung replaced afterwards.

This large-scale bioreactor set-up can be seen in **Figure 2.9**, showing the hanging bags with well-homogenised algal culture and stream of aeration bubbles, suspended from the frame

by the top metal strips, with bunged access port at the top and aeration line inserted at the bottom. The light panels for illumination are visible behind the hanging cultures.

Figure 2.9 The bioreactor in operation.

At the termination of a culturing experiment, the aeration tube was clamped and the aquarium pump and lighting panels turned off. For flocculation of the cultured cells, a measured volume of calcium chloride liquid stock at the desired concentration was introduced into the media by serological pipette through the sampling port. The cells were allowed to settle for the time required by the flocculation protocol, after which a dense green sediment was observed at the bottom of the culture bag, and the remaining media visibly much less cloudy and tinted – the ‘clear area’ in flocculation terms.

To drain the cleared culture medium, a small puncture was made 5 cm above the precipitate and a clamped disposal tube with attached pipette tip was inserted. The clamp was opened and the medium drained into a disposal carboy. The flocculated algal cells were

harvested by removing the clamped aeration tube and inserting another pipette-tipped length of silicone tubing to drain the cell-dense fluid into 750 mL polypropylene bottles for centrifugation and further processing.

2.2.4 Monitoring of algae growth (cell counting and optical density)

The monitoring of algal growth is of crucial importance. *Chlamydomonas*' growth was measured conventionally by direct cell counting, as described below.

Algae concentration in flasks and bags was calculated via direct cell counting using a light microscope (Carl Zeiss Meditec AG, Germany), a Neubauer-Improved counting chamber (Paul Marienfeld GmbH, Germany), and iodine tincture as a fixative. One drop of iodine tincture was added and mixed with 1 mL of liquid culture. Optical density at wavelength 750 nm with a benchtop spectrophotometer (Jenway, UK) was frequently used as well, mainly when individual cells were aggregated or grouped in palmelloids.

The growth curves were plotted with triplicate data obtained from different flasks or bags cultured on different dates to take variation into consideration. Cell count measurements were made in triplicate from samples collected from flasks and bags daily for a period of one week.

2.2.5 Biomass quantification (Dry Cell Weight and FTIR)

The quantification of algae biomass is commonly calculated by dry cell weight. To determine the dry cell weight, entire volumes were centrifuged at maximum speed for 10 minutes. For larger amounts of culture (e.g., 20 or 15 L), consecutive centrifuge rounds were performed where the supernatant was carefully discharged at the end of a round and the remaining culture added to the pellet.

After the whole volume was processed, the pellets were gently washed with deionized water to remove salts from the medium. The biomass was immediately frozen at –20°C during

24 to 48 h and subsequently subjected to freeze-drying under vacuum until a constant weight was weighed.

In comparison to Dry Cell Weight, Fourier-transform Infrared Spectroscopy has the potential to provide an accelerated quantitative analysis of the biomass. Biomass slurry and freeze-dried samples obtained by centrifugation at maximum speed for 10 minutes, were evaluated by Fourier-transform infrared spectroscopy (FTIR). FTIR spectra were recorded by Thermo Scientific Nicolet iS5 FTIR Spectrometer with an iD5 Single-Bounce ATR attachment at Birkbeck, University of London. Each spectrum was scanned 100 times, measuring the region 400-700 cm^{-1}, with a resolution of 4 cm^{-1}. The slurries and dried samples were directly applied to the diamond crystal, and all samples analysed in triplicate.

In order to evaluate accumulation of starch, the *Chlamydomonas* mutant strain (CC-5168) was grown in a 400 mL flask with TAP medium and constant lighting. 30 mL samples were collected once a day over a period of 8 days. The samples were centrifuged, and the pellet was frozen at –20°C overnight, as described earlier. The samples were lyophilized, and the dry powder was used for FTIR analysis, as described above.

2.2.6 Harvesting biomass (centrifugation efficiency and flocculation)

Different factors, such as rotation speed and centrifuge time, can significantly affect the performance of centrifugation. Centrifugation can be time-consuming, which is a constraint when processing large and industrial volumes. The necessity to deliver more immediate outcomes lead to the evaluation of different centrifugation times.

Different harvesting times were tested in a benchtop centrifuge (Thermo Scientific Heraeus Megafuge 40), at maximum speed (4,700 x g) in 750 mL polypropylene bottles (Fisher Scientific, UK). The time intervals evaluated were the following: 5, 10, 20, 30, 45, and 50 minutes. This experiment was performed in quadruplicate to balance the weight in the centrifuge.

To determine the harvesting efficiency (%) of each time tested, optical density at 750 nm was read before and after each centrifugation round. The samples were taken with a pipette from the clarified zone. The numbers were plotted into the following equation (**Equation 2.1**) published by Japer *et al*., 2017:

$$Harvesting\ efficiency\ (\%) = \frac{(D2 - D1)}{D2} \times 100 \qquad \textbf{(Eq. 2.1)}$$

In the previous equation, D1and D2 are the readings of optical density at 750 nm before and after harvesting, respectively.

Flocculation can help improve the efficiency of centrifugation. In previous studies (Fan et al., 2017; Scholz et al., 2011), high pH values and the addition of Ca^{2+} were shown to trigger flocculation on wild type and cell-deficient strains of *Chlamydomonas reinhardtii*. (Fan et al., 2017).

Flocculation protocol was adapted from Fan et al., 2017. Flocculation experiments were first carried out on culture of WT (CC-1690) and mutant (CC-5168) grown in 400 mL TAP flasks, as described before. After the cells enter the stationary phase, 100 mL aliquots were transferred from each one of the 400 mL cultures to new vials and subjected to different pH treatments. The pH in each flask was measured at the beginning and at the end of each pH adjustment.

2M stock solutions of sodium hydroxide (NaOH) and hydrochloric acid (HCl) were used for gradual pH adjustments. After the addition of NaOH or HCl, the flasks were vigorously mixed for 30 seconds and let settle for 15 minutes. After this time period, OD measurements were taken at 750 nm with a table-top spectrophotometer (Jenway, UK). The analysis was performed on small amounts of sample removed from the "clearing zone" with a pipettor. The pH tested were 2 and 12. These small volumes were used to determine OD at 750 nm, and flocculation efficiency was determined as described earlier by Jasper et al., 2017.

After the pH measurements were recorded, 12 mL aliquots from each 100 mL flask were transferred to 15 mL disposable tubes to evaluate the sedimentation rates after addition of different concentrations of calcium chloride.

A 5M stock solution of calcium chloride was prepared, then diluted to the following final concentrations: 0, 1, 2.5, 5, 10, 30 and 62 mM. The concentration range is similar to Scholz et al., 2011. After the addition of calcium chloride, the test tubes were incubated for 15 minutes without agitation. At the end of the 15 minutes period, aliquots from the clarifying zones located in the middle of the test tubes, between the precipitate and supernate, were again removed and analysed. Flocculation efficiency (%) by $CaCl_2$ was later calculated by cell counts according to the following equation (**Equation 2.2**) described by Fan et al., 2017:

$$Flocculation\ efficiency = \left(1 - \frac{A}{B}\right) \times 100 \qquad \textbf{(Eq. 2.2)}$$

A selected $CaCl_2$ concentration was tested in 15 L bags. Cell counts taken before and after sedimentation-flocculation were used to determine flocculation efficiency by the equation above, (**Equation 2.2**) provided by Fan et al., 2017.

2.2.7 Biomass Pre-treatment and Starch hydrolysis

The pretreatment protocol was modified from Webber et al. 2022 and was conducted in triplicate by either acid hydrolysis with sulfuric acid or sonification. Pretreatment was investigated in *Chlamydomonas* wet biomass WT (CC-1690) and mutant (CC-5168) grown on the photobioreactor and Spirulina (SevenHills Wholefoods, Sheffield, United States) and *Chlorella* (MySuperFoods, New Jersey, United States) commercial powder.

For sonification, microalgae biomass with a concentration of 35 g L^{-1} was prepared in a total of 10 mL volume of deionised water in triplicate (ThermoFisher). The tubes were placed inside a glass beaker with ice. The sonification was performed with a probe (Bandelin

electronic, Philip Harris Scientific) with an amplitude of 100% and the following times: 5 seconds, 5 minutes and 15 minutes.

Acid hydrolysis was performed in triplicate inside glass test tubes with caps. The protocol selected was adapted from Augustino et al. (2019) A concentration of 35 g L^{-1} of all three algae biomass was vortexed and suspended in 10 mL of deionised water. A 3% of sulfuric acid dilution was prepared inside a fume hood. Hydrolysis at an elevated temperature (100 °C) was carried out in a heat block for 30 minutes. After the tubes cooled to room temperature, the solution was neutralised with a stock solution (50%) of sodium hydroxide (NaOH) until the pH reached approximately 6. Microscopic observations are a qualitative approach that help visualise physical and structural changes induced by the different pre-treatments and the efficiency of the different treatments in disrupting cells (Weber et al., 2019). The cells treated with acid and sonification were visualised under a light microscope (Carl Zeiss Meditec AG, Germany).

2.2.8 Chlorophyl and photosynthetic pigments extraction and sugar content determination

The protocol was adapted from Zavrel et al., 2018. The main modifications to the original protocol were using Eppendorf and cuvettes instead of a 96-well plate for reading optical density values. The protocol determined free glucose and storage starch content after the pre-treatments described earlier. The protocol was used on all three microalgae biomass: *Chlamydomonas* sp. (WT and CC-5168), *Chlorella* sp., and Spirulina.

Pigment extraction was performed with methanol. Glucose and other free polysaccharides were determined by the Phenol-Sulfuric Acid Method. Stored carbohydrates were evaluated using the Phenol-Sulfuric Method as well after free polysaccharides were removed from the samples with 30% KOH and ethanol and starch/glycogen degraded by HCl hydrolysis. Saccharides content was determined with the help of a glucose calibration curve. All four protocols are detailed next.

To remove photosynthetic pigments, 1 mL of mixed suspension was centrifuged at 15,000 × *g* for 5 min inside an Eppendorf. After discarding the supernatant, the pellet was mixed with 1 mL of pre-cooled methanol. The Eppendorfs were covered with aluminium foil and placed in the dark inside a fridge (4 °C) for 20 minutes. The samples were centrifuged at 15,000 × *g* and 4 °C for 5 min, and the supernatant was discarded. This step, including the addition of methanol, was repeated (2-3 times) until the pellets lost their green colour.

To determine soluble cellular saccharides, 60 µL of the pellets were suspended in deionised water and placed inside a fume hood where 500 µL of 5% phenol was added and incubated for 15 minutes. In a new Eppendorf, 60 µL of this reaction was mixed with 150 µL of sulfuric acid and incubated for 5 minutes. The solution was added to a 1 mL cuvette with 630 mL of water in a 1:3 dilution. A spectrophotometer (Jenway, UK) was placed inside the fume hood to read OD at 490 nm. D-glucose was used for calibration, as shown in **Table 2.3**.

To determine the content of storage carbohydrates, pigment extraction of 1 mL solution was performed as described earlier. 400 µL of 30% KOH was added to each pellet; the solution was pipetted up and down and incubated at 95 °C for 90 minutes on a heat block to remove free glucose. Samples were cooled at laboratory temperature for 10 minutes, and 1.2 mL of ethanol pre-cooled on ice was added to the samples. The samples were mixed and left overnight in a freezer (-20 °C). The next day, the samples were centrifuged at 20,000 × *g,* 4 °C for 60 min, the supernatant was discarded, and the pellets were dried in the fume hood overnight. The following day, 100 µL of 1 N HCl was added to the dry pellets, mixed up and down with a pipette and incubated at 95 °C for 30 min. The samples were cooled down for 10 min and neutralised with 100 µL of 1 N NaOH. 300 µL of distilled water was then added, and the solution was centrifuged at 15,000 × *g* at room temperature for 10 minutes. 500 µL of the supernatant was transferred to a new Eppendorf. In the fume hood, 500 µL of 5% phenol was pipetted into the solution and incubated for 15 minutes. As described before, 60 µL of each sample was added to a different Eppendorf, followed by adding 150 µL of sulfuric acid and a 5-minute incubation. The solution was then added to a cuvette with 630 mL of water in a 1:3 dilution.

The saccharides content was determined by a D-glucose calibration curve obtained with the following dilutions, shown in **Table 2.3,** made with a D-glucose stock of 500 µg mL $^{-1}$:

Table 2.3 Volumes and respective concentrations used for making the dilutions used to obtain the D-glucose calibration curve. Table and values from Zavrel et al., 2018.

Eppendorf Number	Volume of glucose stock (µL)	Volume of water (µL)	Final glucose concentration (µg mL^{-1})
1	25	475	25
2	50	450	50
3	75	425	75
4	100	400	100
5	300	200	300
6	500	0	500

The concentrations for the calibration curve were made inside a fume hood by mixing 60 µL of glucose-phenol concentration and 96% of sulfuric acid and later adding to a cuvette with a 1:3 dilution, as described above.

2.2.9 Determination of sugar content as glucose

The carbohydrate concentration (µg mL^{-1}) of each sample was determined by the following equation (**Equation 2.3**) adapted from Zavrel et al., 2018:

$$Concentration = \frac{A490 - \beta}{\alpha} \times 3 \qquad \textbf{(Eq. 2.3)}$$

In which A490 is the absorbance measured at 490 nm, α is the slope and β the intercept coefficients from the linear regression model (y = αx + β) obtained from the glucose calibration curve. The final concentration was determined by multiplying the dilution factor (1:3) used in the current work.

2.2.10 Statistical analysis

FTIR spectra were plotted with Excel. D-glucose standard calibration curve was also created in Excel. All other graphs were made with software GraphPad Prism 9 (GraphPad Software Inc., USA). Treatment efficiency (%) was determined by **Equation 2.4**:

$$Treatment\ efficiency\ = \left(\frac{B - A}{B}\right) \times 100 \qquad \textbf{(Eq. 2.4)}$$

in which B is the concentration (μg mL^{-1}) of saccharides of released sugars after sulfuric treatment and A the concentration of initial soluble sugars.

All experiments were performed in triplicate unless stated otherwise. All graphs and growth curves include error bars representing standard deviation. When necessary, analysis of variance (ANOVA) was performed with GraphPad Prism 9. A two-way ANOVA with multiple comparisons was used to assess the statistical significance between the results of WT and mutant during flocculation tests. A one-way ANOVA with multiple comparisons was used to study statistical significance among the various microalgae species (Chlamydomonas, Chlorella and Spirulina) during the evaluation of carbohydrate content. The differences were statistically significant at $p < 0.05$ level. After ANOVA, pairwise comparisons between groups were automatically calculated within Prism.

2.3 Results and Discussion

Currently, there are numerous commercially available *Chlamydomonas* strains. The WT CC- 1690 algal strain, also known as Sager 21gr, chosen in this study originates from Dr Ruth Sager and the Sidney Farber Cancer Institute (Sager, 1955; Zhang et al., 2022). This strain has been the subject of numerous studies, including cDNA libraries, the Chlamydomonas Genetic Project, and even stress-related experiences (Zhang et al., 2022); over the years it has become the most prevalent used strain in *Chlamydomonas* research (Zhang et al., 2022).

From all the cell wall mutants available, TN72 was selected due to its application in genetic engineering. This strain can serve as a recipient strain for targeted insertion of foreign genes into the chloroplast resulting in scar-less fusion of a transgenes to the promoter/5′UTR element of the highly expressed endogenous genes (Wannathong, et al., 2016). Moreover, this strain was chosen since it is a recipient strain for chloroplast transformation using different expression vectors commonly utilised in Prof Purton's laboratory. By using TN72 as recipient strain together with vectors developed at Prof Purton's laboratory, CC-5168 is capable of creating new transgenic lines within just a few weeks with a simple and inexpensive system (Wannathong, et al., 2016).

Both strains can be visualised in **Figure 2.10** microscopically and on agar plates. The lack of cell wall and consequently flagella on the mutant results in morphological differences including the loss of defined shape and smaller size. Wall-deficient mutants, form flatter and irregular (**Figure 2.10C**) colonies on agar when compared to its counterpart (Harris et al., 2009). In addition to shape layout, cell wall offers protection against environmental stressors. Consequently, mutants are more sensitive to physical disruption, such as centrifugation (**Figure 2.10D**), and to changes in culture conditions (e.g., pH, lighting) (Harri et al., 2009). Zhang and colleagues shown that photosynthesis deficient mutant cells (CC-5325) had larger cell volume than the WT. In the current work, the contrary was observed; the cw15 mutants are smaller in size when compared to CC-1690 (**Figure 2.10B**). This change could be the result of lack of optimization regarding growth conditions for the mutant strain, which might require more carbon source (e.g., acetate) since it is not capable of getting energy through light. Furthermore, the differences in coloration were another physical difference observed between CC-1690 and CC-5168 (**Figure 2.10A and Figure 2.10C**). The latter is characterized by a lighter green, which is related to reduced amount of chlorophyll and other photosynthetic pigments (Zhang et al., 2022) due to the lack of PSII and photosynthetic activity.

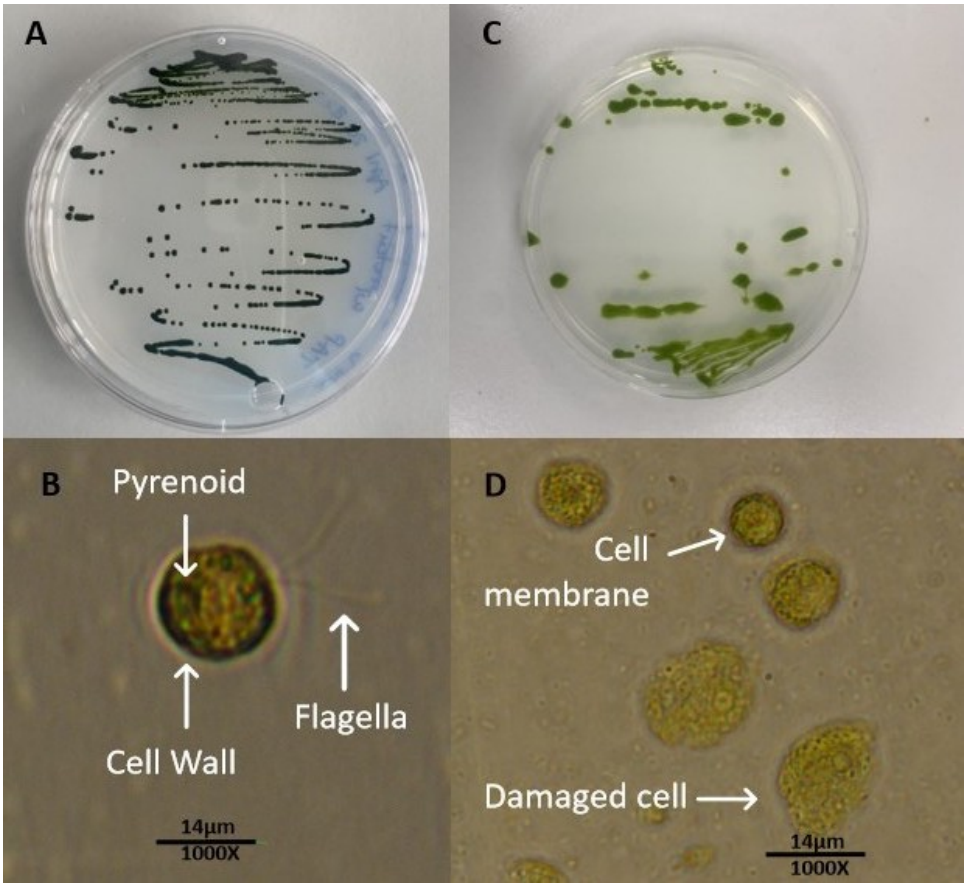

Figure 2.10 Macroscopic view of *Chlamydomonas* colonies on TAP agar (A and C) and light microscopic images (B and D) of liquid cultures (TAP) of WT cells (A-B) and TN72 mutant (C-D).

2.3.1 Implementation of a small-scale culture system

Both *Chlamydomonas* strains were grown under the same controlled conditions in the small-scale system and in photobioreactors (PBRs). Among all the above-described techniques commonly used to monitor algal growth, most research studies on *C. reinhardtii* uses cell counts to measure culture density (Cui et al., 2021). The different growth phases discussed earlier can be easily distinguished in **Figure 2.11**. **Figure 2.11A** displays the growth curves of WT *Chlamydomonas* grown in different media (HSM, HSM supplemented with acetate and TAP) and at various stages of the scale-up process (starter, intermediate and hanging bag). **Figure 2.11B** compares the growth curves of CC-1690 and CC-5168 in the intermediate flask with TAP and PBRs with HSM supplemented with acetate. All experiments were performed at room temperature. Both curves show the number of cells per mL through a period of 1 week.

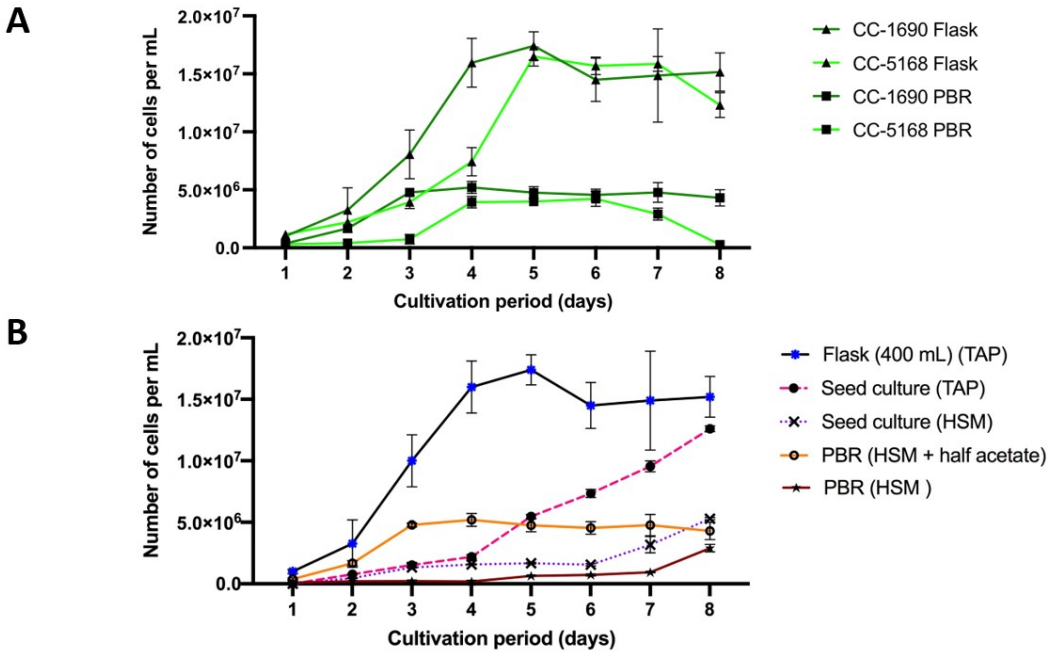

Figure 2.11 Growth curves for *Chlamydomonas* sp. in the developed systems. A) Comparison of WT (CC-1690) and mutant (CC-5168) in the small systems and in the photobioreactor. B) The different growth curves of WT *Chlamydomonas* in distinct stages of the small-scale system and in the photobioreactor cultured with two different media conditions: HSM and HSM supplemented with half of the acetate recommended by the literature. Error bars represent the standard deviation of the data points.

Based on the literature, *Chlamydomonas* doubling time ranges between 6-8 hours (Harris, 2009; Zhang et al., 2022). In the curves above, the number of measurements obtained during the exponential phase are insufficient to determine the doubling time of *Chlamydomonas* under the different conditions tested here. All curves follow the general trend with minor exceptions; they all exhibit a sharp transition between the lag and exponential phase, as expected. These results can indicate that factors such as the amount of light and agitation are sufficient in the implemented system. One of the differences between WT (dark green) and wc15 mutant (light green) in **Figure 2.11A** is the fact that the mutant reaches the death phase sooner ($6^{th}/7^{th}$ day) than the WT, which can be due sudden nutrient depletion resulting in quick starvation and death (Basu, 2015) or higher susceptibility to contaminating organisms due to the lack of cell wall; as mentioned earlier, due to the lack of wall, mutant cells might be more sensible to external factors, such as light intensity. The first reason is more plausible since, unlike WT, which can produce energy through photosynthesis, the mutant depends on organic carbon provided in the media for survival. When media content is exhausted, the mutant can no longer produce energy and quickly dies. Another difference is

that the mutant takes longer to reach the exponential phase. Again, this is because the WT grows faster since it produces energy mixotrophically, while the mutant can only grow heterotrophically. Cell concentration in the mutant is slightly lower than the WT due to their nutritional differences. However, due to the fact that in both systems (flask and PBR) an organic source is provided the algae concentration difference was minor between WT and mutant in the two systems.

The two major differences between the starter curve with TAP and the intermediate curve it is the steepness of the slope of the log phase and the maximum number of cells reached in the two cultures. In the starter culture, the highest number of cells was seen on the third day. This value was $1.7E^{+6}$ cells/mL, which is considerably less than the one observed in the intermediate culture. This discrepancy might be due to solid-to-liquid transition and adaptations of cells in the starter culture reinforcing the need for this step and avoidance of direct inoculation from agar plates. Due to the lack of PBR optimization and the fact that only half of the sodium acetate (0.6 g/L of sodium acetate anhydrous or 1 g/L of sodium acetate hydrate) recommended by the literature for HSM mixotrophic growth was provided in the bioreactor, the curves associated with the hanging bags had much less cell concentration than the flasks with TAP medium. Only half of the acetate was provided to minimize the organic carbon source use in the system, which is one of the main aims of this thesis. Since both the mutant and WT strain followed a normal growth curve all hanging bags-associated experiments were performed with HSM medium and half the amount of sodium acetate recommended to reduce carbon source-related costs. One of the parameters that might be negatively affecting cell growth inside the bags is aeration. Large air bubbles are not capable of mixing a culture as well as small air bubbles, as discussed in Chapter 6, under the future work section.

2.3.2 Implementation of a large-scale system

The bags were initially prone to contamination, which was observed microscopically. To reduce the risk of contamination, the volume per bag was reduced from 20 L to 15 L to include a headspace, as described in the Material and Methods and recommended by the literature. The headspace acts as a barrier between the medium and the external environment

by minimising gas exchange and contamination by airborne contaminants. This solution fixed the contamination problem.

Two other challenges associated with hanging bags are leakages and dead zones characterized by no growth as a result of the shading effect. The aquarium pumps of choice provide sufficient aeration to make air bubbles travel from the bottom of the bag to the top, mixing the medium and avoiding the formation of dead zones at the bottom of the bags. Once the testing of the new system was finished, large-scale cultivation was initiated in the bioreactor. The entirety of 400 mL cultures of the WT grown in TAP media were used to inoculate individual bags (Harris, 2009). The hanging bags' results can be seen in **Figure 2.16**.

Bags containing HSM medium exclusively were compared with bags enriched with half of the acetate recommended. These two were used to compare autotrophic and mixotrophic growth in the WT, respectively, as shown in **Figure 2.16B**. TAP medium is the most used media in *Chlamydomonas* research. Unfortunately, it is also the most expensive, has previously stated, and, therefore, undesirable for scale-up. TAP can continue to be used in small-scale experiments. Still, it would be preferable to substitute it with HSM in the bioreactor. Additionally, TAP does not provide conditions for photoautotrophic growth. Using autotrophically grown algae as a feedstock is one of the goals of this body of work since sunlight and CO_2 are abundant on Mars, while organic carbon sources are scarce. Since the mutant strain requires organic carbon to grow and the WT grew poorly with HSM in hanging bags (**Figure 2.16B**), a compromise was established, in which the bags were cultivated with HSM and half of the sodium acetate hydrate (1g/L) recommended for mixotrophic growth when using the HSM medium, which is (2 g/L).

2.3.3 Analysis of biomass components by FTIR

In FTIR spectroscopy, biomolecules such as proteins and lipids can be identified based on vibrations such as stretching (symmetric and asymmetric) and bending (scissoring, rocking, wagging, and twisting) of their molecular bonds and functional groups when these absorb infrared radiation. In FTIR spectra, these vibrations are translated into peaks at characteristic wavenumbers.

Lipids, for example, have carbon-hydrogen (C-H) bonds in the fatty acids long tails. These bonds can be seen in the FTIR spectrum around 2800-2950 cm^{-1}. Carbohydrates, including starch, contain C-O bonds that typically occur at low frequencies in the 800-1200 cm^{-1} region. The N-H bonds of amides, which are found in DNA and prevalent in proteins, can be seen in the 1500-1700 cm^{-1} region (Shapaval *et al.*, 2019).

The FTIR spectrum from WT *Chlamydomonas reinhardtii* sludge grown in a hanging bag with HSM medium supplemented with acetate is presented in **Figure 2.12,** whereas the assignments for the major peaks are shown in **Table 2.4**. As seen in **Figure 2.12A**, the most prominent bands were obtained in the wavenumber range 3000-3600 cm^{-1}, followed by the 1655-1637 cm^{-1}, and 1200-1000 cm^{-1}. Parts of the spectrum with detailed information of the regions associated with important biomolecules are provided in the following **Figure 2.12B**.

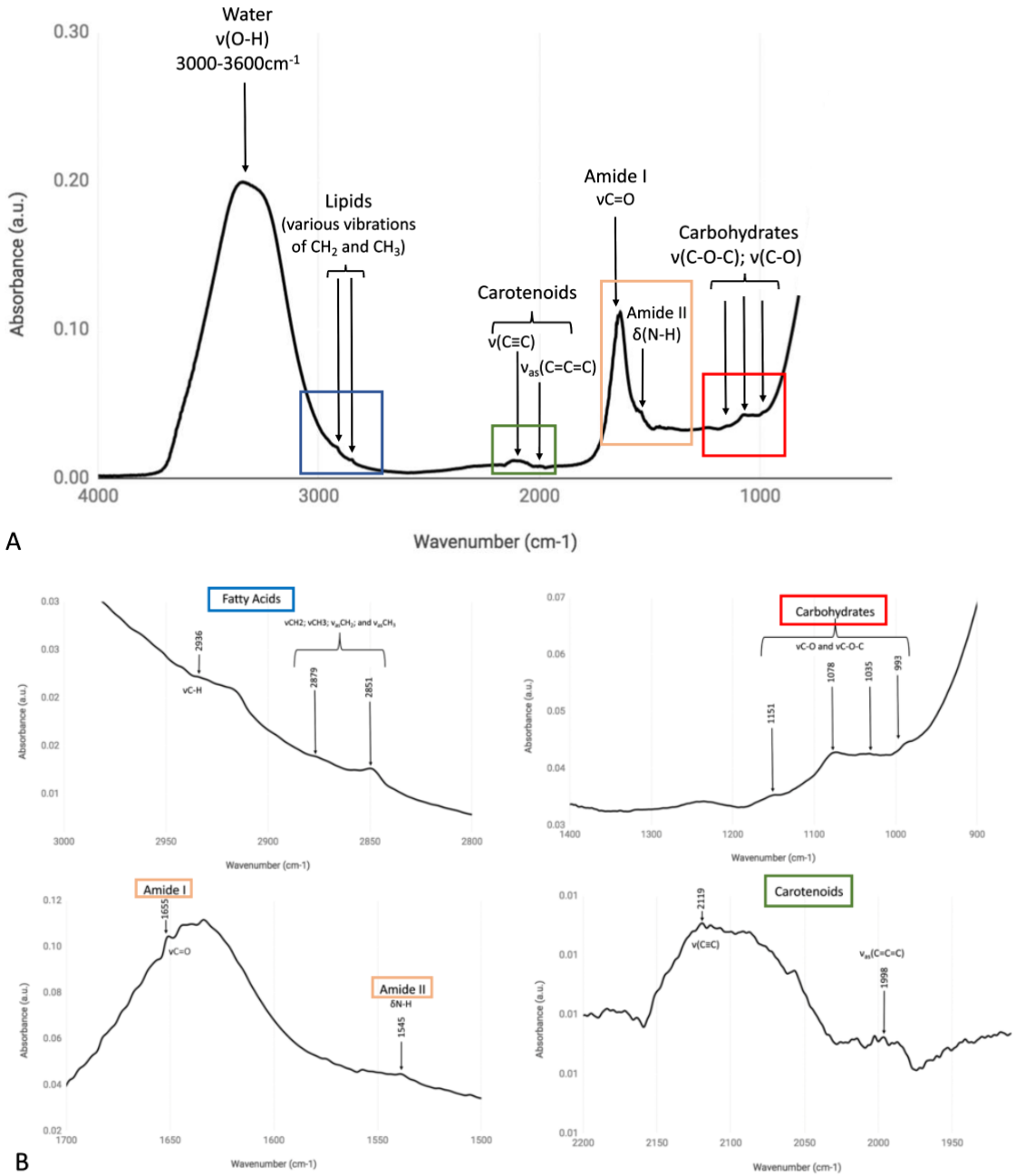

Figure 2.12 (A) FTIR spectra of WT *Chlamydomonas reinhardtii* sludge with the regions assigned to important biomolecules marked in different colours. Lipids are in blue, carotenoids in green, amides in orange, and carbohydrates in red. (B). Close-ups of the most important regions of the FTIR marked with the respective colours. ν = symmetric stretching, νas = asymmetric stretching, and δ = bending.

Based on the literature, a typical FTIR spectrum of starch has the following three distinctive regions: the 2900-3000 cm^{-1}, associated with C-H stretching, the 1100-1150 cm^{-1}, (C-O, C-C, and C-O-H stretching); and 1100-900 cm^{-1}, attributed to C-O-H bending (Warren *et al*., 2016). All three regions were seen in this study, with different levels of intensity.

Table 2.4 Band assignment for the FTIR spectra of the *Chlamydomonas* sludge, where ν = symmetric stretching, νas = asymmetric stretching, and δ = bending.

Wavenumber (cm^{-1})	Wavenumber in the Literature	Band Assignment	Literature Reference
993	800-1200 1100-900	νC-O-C of polysaccharides δC-O-H	Several sources Warren *et al.*, 2016
1035	1036	νC-O of carbohydrate	Driver *et al.*, 2015
1078	1086	νC-O of carbohydrate	Driver *et al.*, 2015
1151	1149	ν_{as}C-O-C of polysaccharides	Abdullah *et al.*, 2018
1249	1245	ν_{as}P=O of nucleic acids and phosphorylated proteins	Driver *et al.*, 2015
1428	1415	CH_2 scissoring	Abdullah *et al.*, 2018
1458	1455	$\delta_{as}CH_2$ and $\delta_{as}CH_3$ of lipids and proteins	Driver *et al.*, 2015
1545	1545	δN-H of amides related to Amide II	Driver *et al.*, 2015 Dean *et al.*, 2010
1637	1637	δC-O associated with OH group	Abdullah *et al.*, 2018
1655	1655	νC=O of amides related to Amide I	Driver *et al.*, 2015 Dean *et al.*, 2010
1998	1927 and 1929	ν_{as}(C=C=C) stretching of the allene functional group in carotenoids and other algal pigments	Lorand *et al.* 2002
2119	2260 – 2100	ν(C≡C)	Coates, 2006
2851	2850 – 2890 including band at 2872	νCH_2, νCH_3, $\nu_{as}CH_2$, and $\nu_{as}CH_3$ of fatty acids	Driver *et al.*, 2015
2936	2931	νC-H	Abdullah *et al.*, 2018
3365	3000-3600	νO-H of water	Several sources

The third most prominent region (1200-1000 cm^{-1}) in the overall spectrum, shown in **Figure 2.12**, is commonly associated with carbohydrates, including polysaccharides (Warren *et al*., 2018; Dean *et al.* 2010). Dean *et al*. 2010 used FTIR to study changes in lipid and carbohydrate content in *C. reinhardtii* in response to limiting nitrogen concentration. Their FTIR spectra showed nine distinct absorption bands over the wavenumber range of this region (1900–800 cm^{-1}). In the present study, the most defined peaks in this region were seen at 1035 and 1078 cm^{-1}, both assigned to C-O stretching, and the band at 1151 cm^{-1}, attributed to C-O-C asymmetric stretching (Driver *et al.*, 2015; Abdullah *et al.*, 2018).

Additionally, the presence of a band around 990 cm^{-1} was also observed. This peak was also mentioned by Pozo *et al*., 2018 who studied the FTIR spectra of 13 starches. Bands located within the 1100-900 cm^{-1} range were assigned to C-O-H bending in previous starch spectra (Warren *et al*., 2016), whereas bands within the region 1200-800 cm^{-1}, are associated with vibrational changes in carbohydrates (Abdullah *et al.*, 2018).

Figure 2.12 also shows a peak at 2936 cm^{-1}, within the spectra; region commonly associated with CH stretching (Abdullah *et al*., 2018). Lipid-related CH_2 and CH_3 symmetric and asymmetric stretching are found in the 3000–2800 cm^{-1} range (Driver e*t al.*, 2015) was attributed to the peak at 2851 cm^{-1}. No band was detected at 1740 cm^{-1}, a wavenumber previously used to determine the relative lipid content through lipid:amide ratio (Driver *et al*., 2015).

The most prominent band was seen at 3365 cm^{-1}. This broad peak commonly found between 3650-300 cm^{-1} is associated with O-H stretching of water molecules (Kizil *et al.*, 2002; Abdullah *et al*., 2018; Pozo *et al*., 2018). The presence of this peak was expected due to the abundant water content present in the sludge. Changes in dried-freeze samples in the spectrum region **(**1047-1000 cm^{-1}**)** are the result of hydration-induced structural modifications (Warren *et al*., 2018); in previous studies, an increase of the 1022 cm^{-1} feature was reported in amorphous samples, whereas in dried starches, the peaks 1000 and 1047 cm^{-1} were more defined, showing water sensitivity in this region of the starch spectrum (Warren *et al.*, 2018).

One of the most defined peaks in the second most prominent region was seen at the wavenumber 1655 cm^{-1} which was attributed to ν(C=0) stretching of amide I (Dean *et al.*, 2010) and reflects the high amount of protein in the sludge (Warren *et al*., 2018). The δ(N–H) bending of amide II (1556 cm^{-1}) was also present.

The presence of peaks around 2100 cm^{-1} and ~2000 cm^{-1} was noted. Both bands were assigned to vibrations in carotenoids bonds. The peak at ~1998 cm^{-1} was attributed to the stretching of allene (C=C=C), a unique functional group present mostly in carotenoids (Takaichi *et al.*, 2011).

The acetylenic functional group (C≡C) is an uncommon structure in biomolecules (Coates, 2006) but has been found in carotenoids (West *et al*., 2016). Acetylenic carotenoids have only been reported in algae (Takaichi *et al*., 2011). The peak at 2119 cm^{-1} was assigned to the stretching vibration of this triple bond. A bump in this region can also be seen in the spectra of *C. reinhardtii* growing in TAP (non-stressed) while absent in the nitrogen and phosphorous-

limiting spectra, in the work of Driver *et al.,* 2015. Carotenoids are photosynthetic pigments that, together with chlorophylls, help algae capture light (*Takaichi et al*., 2011). This change in peak intensity could be due to the loss of photosynthetic activity as a result of abiotic stress. Stress caused by harsh environmental conditions can lead to changes in the photosynthetic apparatus (Devadasu *et al*., 2018).

Similarly, to the present study, the amide peak reported by Driver and colleagues was more intense than the lipids and the carbohydrates when they cultured *Chlamydomonas* under optimal conditions. In contrast, the intensity of amide, which contains nitrogen, is much lower than the lipids and carbohydrates bands under nitrogen starvation (Driver *et al*., 2015).

Overall, a prevalent protein-associated peak was observed in the *Chlamydomonas* sludge. Since FTIR is a semi-quantitative method, the lower band height associated with carbohydrates suggests that these macromolecules were present in smaller amounts. The low levels of polysaccharides maybe be due to the fact that *Chlamydomonas* grew under optimal conditions without nutrient limitations and therefore did not produce energy storage compounds. Thus, the carbohydrates present may be limited to structural functions. FTIR proved to be an efficient method for the quick quantitative evaluation of carbohydrates such as starch and other important biomolecules present in a small, non-treated sample of *C. reinhardtii*.

2.3.4 Analysis of starch accumulation and consumption over time

The FTIR spectra of the *Chlamydomonas* mutant strain collected once a day for a period of 8 days were recorded, as described in the Material and Methods, to evaluate the accumulation and degradation of starch in the mutant strain in the small-scale system, using a volume of 400 mL, TAP medium and constant lighting. The current experiment used freeze-dried samples instead of sludge in an attempt to remove interference from water features (predominantly over 3000- 3600 cm^{-1}) and obtain better-defined peaks. Indeed, it was found that peak discrimination improved and thus all further FTIR experiments were performed with dried samples instead of sludges. In particular, the 1000 and 1047 cm^{-1} bands are more defined in the dried samples, as observed by Warren et al. (2018), and the lipid-associated peaks beyond

3000 cm^{-1} are better differentiated without the broad water feature. The peak associated with the stretching of the C-O bond of carbohydrates, at around 1078 cm^{-1}, became the most prominent peak in this experiment.

Overall, peak intensity related to lipids, carbohydrates, carotenoids and amide I increased in the first few days, with the highest peaks observed on the 3rd day. After day 5, all peaks gradually lost intensity, with all major peaks showing the lowest peak intensity on the last day (day 8), as shown in **Figure 2.13**.

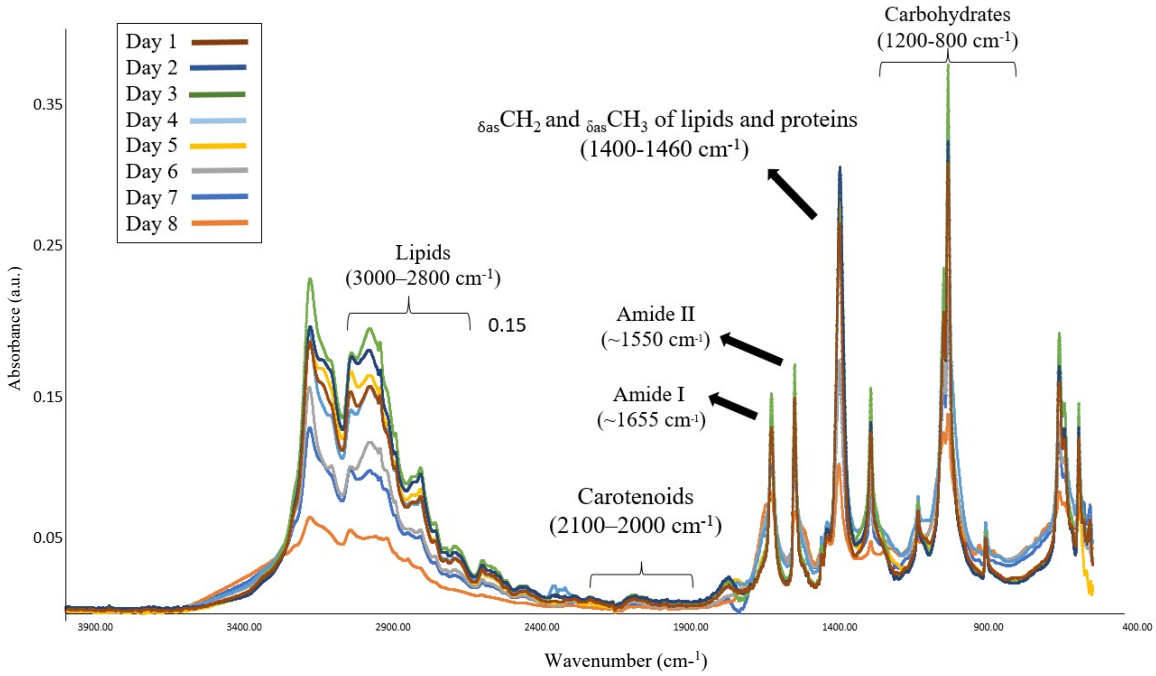

Figure 2.13 FTIR spectral changes of *Chlamyaomonas* mutant over a period of eight days in TAP medium.

Concerning starch, all four major peaks in the carbohydrate regions (1200-800 cm^{-1}) were present. All of them increased in the first few days, with maximum absorbance seen on day three, as can be visualized in **Figure 2.14**, which may indicate maximum starch accumulation. After day 5, all of them lost intensity over time. Comparing the FTIR results to the growth curves shown earlier (**Figure 2.11**), day 5 marks the beginning of the stationary phase for the mutant in the 400 mL flask. This time point therefore likely corresponds to the start of starch and lipids consumption by the mutant in response to the lack of nutrients in the media.

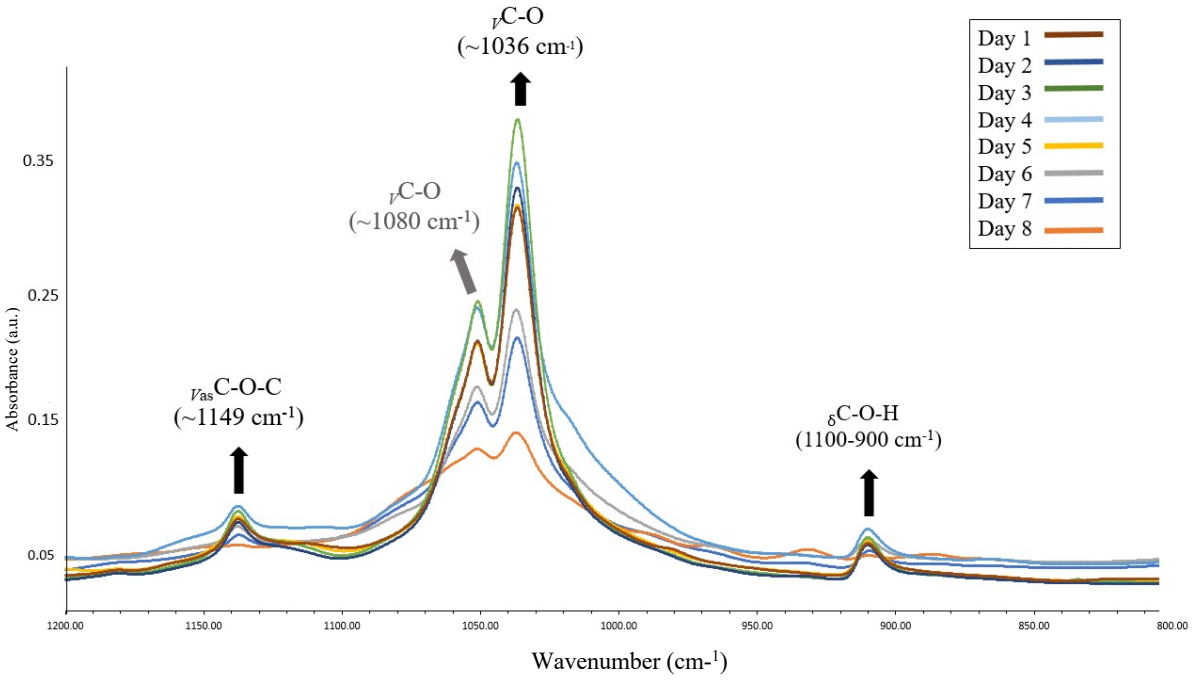

Figure 2.14 FTIR analysis of starch accumulation and degradation in the *Chlamydomonas* mutant strain over a period of eight days.

The maximum starch accumulation occurred on day 3, corresponding to the beginning of the exponential phase on the curves. Stretching of the C-O bond of carbohydrates was the highest peak seen in all spectra. FTIR starch-associated peaks decreased slightly after day three but remained roughly constant until the beginning of the stationary phase on day 5. The daily changes and slight decreases in peak height between days 3 and 5 can result from daily fluctuations in microalgae starch production caused by slight environmental conditions (e.g., light and temperature). Moreover, these fluctuations may not reflect actual changes in starch production, as they may result from subtle variations in sample collection and handling that can influence FTIR peak intensity and mimic daily starch differences. After day 5, peak intensity started decreasing over the remaining days, probably due to the start of consumption of internal storage compounds due to the lack of nutrients in the medium. At day 8, similar to other peaks (e.g., lipids, Amide I), starch-associated peaks reached their lowest intensity. The peaks related to the stretching of C-O-C and C-O-H of carbohydrates were lost entirely. These observations confirmed the growth curve results, in which, at the end of one week, the mutant cells reached the death phase in the 400 mL flask supplemented with TAP medium. Most cells start dying on day eight due to the exhaustion of nutrients in the media and internal storage

compounds such as lipids and starch, as this mutant strain lacks the photosynthetic capabilities of the WT and can not obtain energy through light.

FTIR analysis helped detect the day starch accumulation was the highest in the 400 mL flasks with TAP. It also allowed the observation of the accumulation and degradation of starch during the mutant's distinct growth phases. FTIR can be therefore used to detect and semi-quantify starch quantities in other microalgae systems and media, such as the bioreactor developed in this work.

2.3.5 Harvesting by centrifugation

Centrifugation is a time- and energy-expensive process, and so means were sought to optimise the process and identify the best harvesting time. Volumes of 400 mL of WT culture grown until the stationary phase were tested in the 750 mL centrifuge bottles for different periods of time.

Jasper *et al*., 2017 demonstrated that higher harvesting efficacy was obtained with higher rotational speeds in *Chlamydomonas* and other algae. Following these reports, maximum speed (4700 x g) was chosen and used to test different centrifuge times. Absorbance values taken before and after centrifugation were recorded and plotted in the formula introduced by Jasper *et al.*, 2017 indicated in the Materials and Methods. Absorbance measurements were chosen for the calculations over cell count due the appearance of cell clumps and agglomerates in the sediments which made cell count challenging.

Centrifugation efficiency values ranged from 76.6 % ± 10.5 to 95.6 % ± 2.12, as shown in the **Figure 2.15**. Harvesting efficiency was found to peak at 96% after 45 minutes, after which the graph plateaus and no further gains are made with longer centrifugation times.

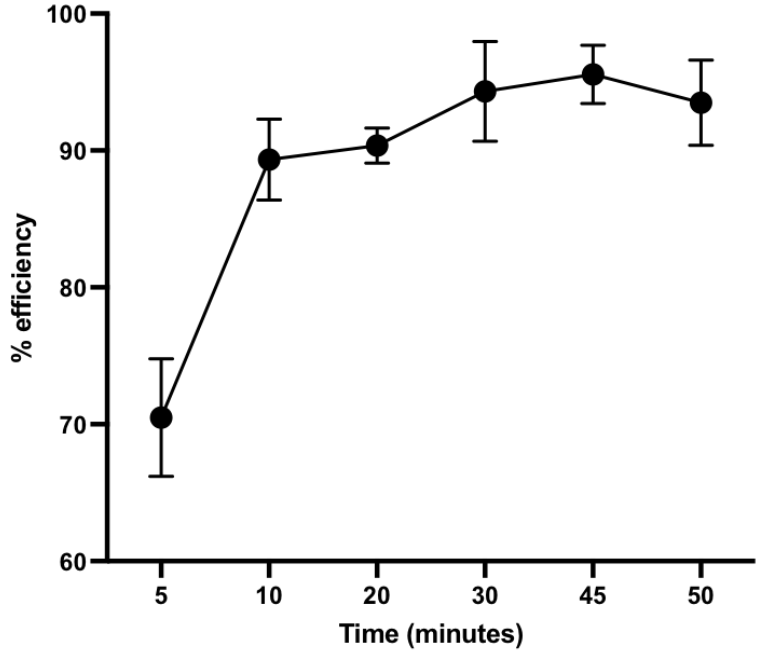

Figure 2.15 Harvesting efficiency for the different times tested at 4700 x g in a benchtop centrifuge. Error bars represent the standard deviation of the data points.

The simultaneous use of all four bottles allows the centrifugation of a maximum of 3 L per centrifuge round. If every centrifuge round lasted 45 minutes, the harvesting time of an individual 15 L bag would take approximately four hours. Centrifugation for 20 minutes still yielded an efficiency of 90.35 ± 1.28%, and so as an expedient compromise in this study, centrifugal rounds at 4700 x g for 20 minutes were adopted as the standard protocol harvesting.

With this protocol, the harvesting of a 15 L bag could be completed in less than two (1.6) hours, which is a notable decrease. Nonetheless, when operating the bioreactor at full capacity (6 bags), 90 – 120 L will need to be harvested, putting the total time required for harvesting between 9 to 12 hours, which is not practical. Further improvements to the harvesting step are necessary for large-scale production. Flocculation has been proven to help increase centrifugation efficiency in *Chlamydomonas.* The ability of this technique to help dewatering hanging bags will be discussed next.

2.3.6 Flocculation-based harvesting

The role of pH and a metal cation in the efficiency of cell coagulation-flocculation on *Chlamydomonas reinhardtii* was investigated. WT and mutant cultures were grown in Erlenmeyer flasks with 400 mL of TAP medium, as described earlier. Coagulation-flocculation tests were performed at the beginning of the stationary phase. At this stage, the pH of the cultures was measured between 7 and 8. Absorbance readings were taken at 750 nm with a benchtop spectrophotometer (Jenway, UK) and plotted in the formula introduced in the Material and Methods by Jasper *et al.*, 2017 (**Equation 2.1**). Similar to the centrifugation tests, absorbance at 750 nm was chosen to evaluate flocculation's efficiency over cell count due to the formation of cell agglomerates and precipitate.

The impact of different pH values on coagulation-flocculation efficiency was first explored. Different pH adjustments in the growth medium have been shown to trigger self-flocculation in algae in the past. In previous studies, a number of pH adjustments increased the flocculation efficiency up to 90% in algae (Liu et al., 2013; Wu et al., 2012) suggesting its harvesting potential in algae biotechnology (Fen *et al*., 2017).

In this experiment, untreated aliquots with pH ~8 were used as control and as a reference for natural-occurring sedimentation. WT and mutant cells were subjected to two pH changes in the extreme ranges of the pH scale. The pH values tested were as low as 2 and as high as 12. Flocculation–sedimentation efficiencies were analysed in the flasks after a 15-minute wait. Both WT and mutant were tested under the same conditions but showed contrasting results, as shown in **Figure 2.16**. Significant differences in coagulation-flocculation between WT and mutant strains as a result of pH changes have been reported previously, such as Fan e*t al*., 2017.

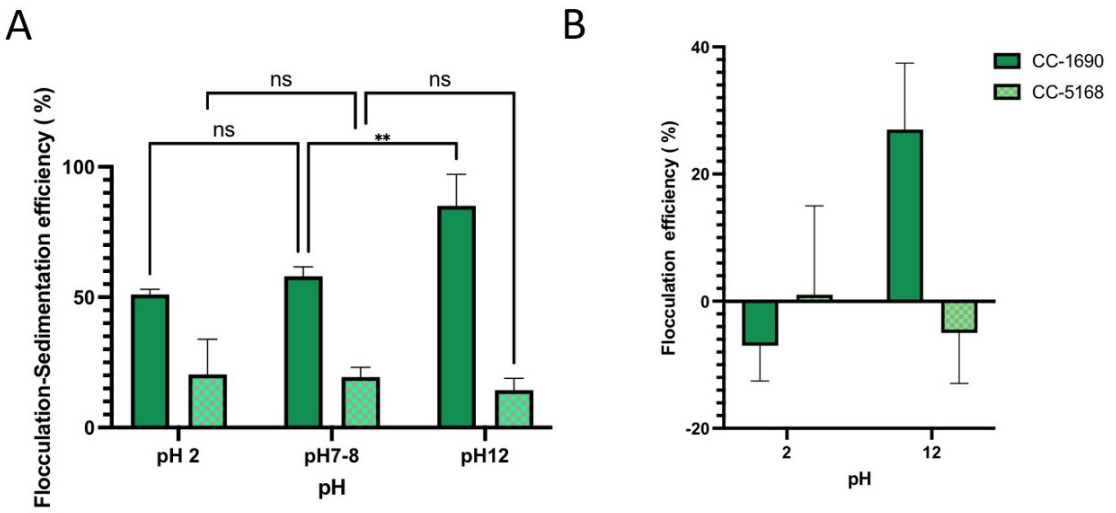

Figure 2.16 Sedimentation-flocculation yields observed in both WT (CC-1690) and mutant (CC-5168) cells grown in TAP medium based on OD measurements. (a) Sedimentation-flocculation results in all three pH ranges. (b) The efficiency of flocculation at pH 2 and 12 when the percentage of sedimentation (pH ~ 8), used as control, was subtracted. ** indicates statistically significant difference. Error bars represent the standard deviation of the data points.

Flocculation by pH was ineffective in the mutant. Maximum flocculation-sedimentation efficiency was around 20% in the pH ~8 (**Figure 2.22A**), with no significant change at either high or low pH. Flocculation of the WT cells was significantly (p-value<0.001) more effective at pH 12 than neutral sedimentation, at 85% This was an increase of almost 30% (27%) when compared to natural sedimentation (**Figure 2.22B**). The discrepancy in the flocculation performance between strains can be attributed to phenotypic differences (Fan *et al*., 2017). Similar results were reported by Fan's research team. They observed low flocculation efficiency in cell-wall deficient mutants when compared to WT (Fan *et al*., 2017). Similarly, they also obtained the best flocculation outcome in WT cells at relatively elevated pH (above 10).

In the literature, coagulation-flocculation triggered by low pH has been associated with the protonation of carboxyl and/or sulphate groups that neutralize the negative surface charges of the cells. Whereas the flocculation elicited by elevating the pH can be due to metal ions still present in low concentrations in the media (Fan *et al*., 2017).

The effect of increasing amounts of calcium chloride was tested in aliquots of culture without previous pH treatment (pH ~ 8) for several reasons. First, since flocculation by pH was inefficient in the mutant, pH was not considered for flocculation in hanging bags, since one of the aims is to obtain standardised harvesting protocols for multiple strains. Moreover, extremes of pH interfere with the coagulation effect of $CaCl_2$: calcium chloride and sodium hydroxide, which was used to increase the pH of the solution, react to form calcium hydroxide. This precipitate impacted the turbidity of the liquid solutions and, consequently, the OD measurements. To avoid this issue, the experiment evaluating the different coagulant concentrations in the two strains was repeated, as shown in **Figure 2.17**, without pH pretreatment and measured by cell counts instead of optical density and plotted in the **Equation 2.2**. provided by Fan *et al*., 2017, which was shown earlier. A 12 mL aliquot was left untreated (0 mM of $CaCl_2$) for each strain and utilized as a control.

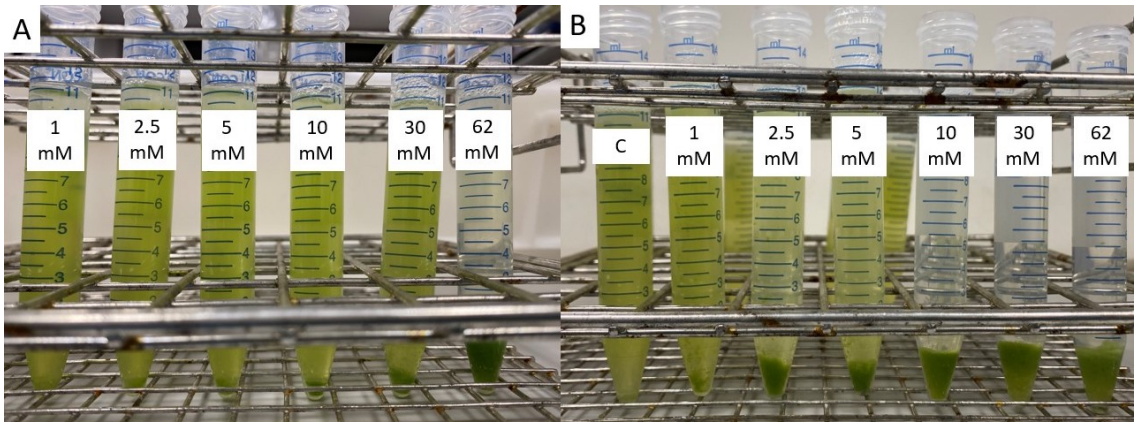

Figure 2.17 Macroscopic observations of the flocculation-sedimentation results by $CaCl_2$, in the WT and mutant at near neutral pH range. Increasing concentrations (1 to 62 mM) of calcium chloride in (a) WT *Chlamydomonas* cells in TAP medium, and (b) the mutant cell in TAP medium.

Flocculation was best achieved by adding calcium chloride – 62 mM, which can be visualized in the **Figure 2.17**, where both strains displayed flocculation efficiency above 80%, as can be seen in **Figure 2.18**. Flocculation was more efficient on the mutant approaching 100% of flocculation efficiency at the highest concentration (62 mM), which is characterized by no remaining cells in the supernatant, whereas the WT, was less responsive to lower levels of flocculant. Comparable results were observed by Scholz et al. (2011), who also reported higher efficiency in this pH range in the mutant probably due to the fact that this strain lacks

flagella and therefore motility. A WT flocculation-sedimentation efficiency higher than 50% was observed at 30 mM concentration of $CaCl_2$. With smaller concentrations, efficiency in the WT remained the same, whereas Scholz et al. (2011) reported a decreased flocculation efficiency in the WT with increased flocculant concentrations.

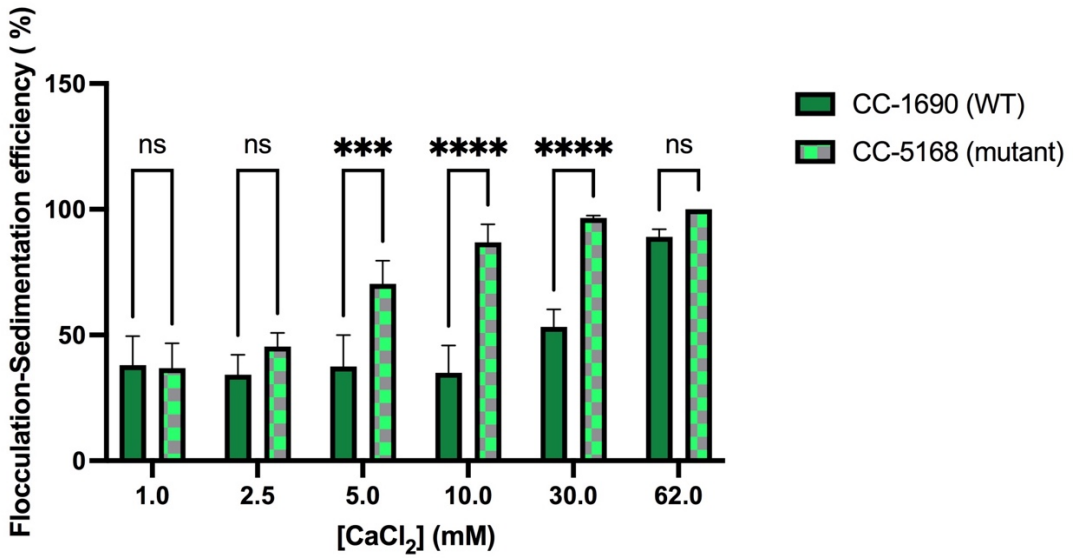

Figure 2.18 Flocculation-sedimentation efficiency in WT and mutant cells with increasing concentrations of $CaCl_2$ (1 to 62 mM) in the near neutral pH range. ** indicates statistically significant difference. Error bars represent the standard deviation of the data points.

As mentioned before, previous studies showed that efficient flocculation of the cell-deficient cw15 mutant can occur with 15mM $CaCl_2$ at pH 8 (Scholz *et al*., 2011). At this pH, calcium and phosphate present in the media form octacalcium phosphate, which can act as a precipitating agent in some algae (Scholz *et al.*, 2011). On the other hand, a recent study showed that the addition of divalent cations, including Ca^{2+}, did not impact flocculation in both WT and mutant cells (Fan *et al*., 2017). The contrasting results seen in the literature could be the result of testing algae cells at different concentration and/or different growth phases. In the current study, flocculation-sedimentation evaluation was performed at the beginning of the stationary phase since this is the time point chosen for starch harvesting. The differences between WT and mutant results are due to cell size, motility differences, and differences in the surface charges of mutant membrane versus WT cell-walls (Scholz *et al.*, 2011; Fan *et al*., 2017). Various parameters can influence the concentration of coagulant and flocculant required, including microalgae strain, media's iconic strength, algae concentration, amount of

impurities, and pH of the culture (Feng et al., 2017; Matter et al., 2019; Maćczak et al., 2020). The WT cell are slightly larger than mutant, as discussed earlier. Small cells have a higher surface area, hence higher flocculant dosage might be needed to achieve greater efficiency (Branyikova *et al.*, 2018) but since in the current experiment the mutant was more responsive, its lack of motility was probably one of the factors contributing the most to flocculation.

Coagulation-flocculation by $CaCl_2$ was also tested in hanging bags supplemented with HSM and (half) of the sodium acetate rather than TAP, as exemplified in **Figure 2.19**. In addition to its efficiency in harvesting large volumes of microalgae culture, another reason for studying flocculation in hanging bags is to evaluate the efficiency of the flocculant in HSM rather than TAP medium, since as mentioned above, different media can influence the dosage of flocculant required.

The flocculation was performed during the stationary phase. Sedimentation-flocculation was achieved with a concentration of 30 mM and 5 mM of $CaCl_2$ for WT and mutant, respectively, since they were the lowest concentration at which more than 50% of cells flocculated in the small-scale experiments. Small coagulant concentrations were selected to avoid adding a large amount of $CaCl_2$, which can increase harvesting-related costs and since the bags had fewer cells than the flasks, as discussed earlier and shown in **Figure 2.11**. As previously mentioned, flocculant dosage depends on numerous factors, including algae concentration (Matter et al., 2019).

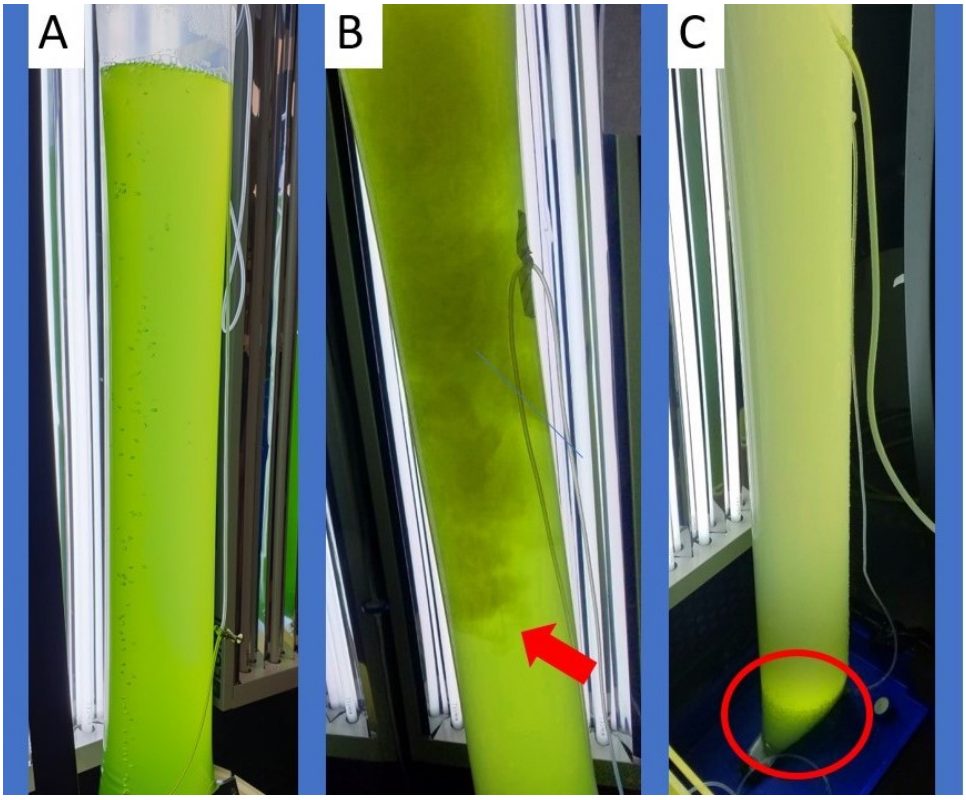

Figure 2.19 Sedimentation-flocculation by calcium chloride in a hanging bag. (a) The figure shows mutant cells growing on HSM medium with (half) acetate in a bag without flocculant. (b) Moments after the addition of calcium chloride, where the flocculant, shown in a darker colour and indicated by the red arrow, can be seen being distributed in the medium. (c) Sedimentation of algae cells on the bottom of the bag, highlighted by the red circle.

The concentration of suspended cells was estimated by cell counting instead of optical density for reasons mentioned earlier. The number of cells before and after the treatment was plotted in the **Equation 2.2** provided by Fan and co-authors and shown in the Material and Methods. The cells sedimented on the bottom of the bag, as can be seen in **Figure 2.19,** and the cleared media/supernatant was removed by a peristaltic pump and discharged. The remaining sediment had considerably less volume and was centrifuged at maximum speed for one-two rounds until fully processed. The flocculation efficiency was around 80% for both strains. The higher efficiency obtained in bags with smaller $CaCl_2$ concentrations is the result of the lower number of cells compared to the flasks. A longer sedimentation time can be explored to help the WT reach a similar flocculation efficiency with a lower flocculant concentration.

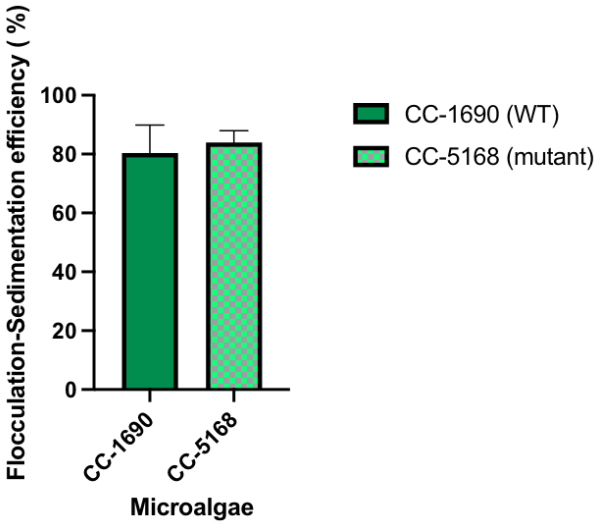

Figure 2.20 Flocculation-sedimentation efficiency obtained for WT and mutant with 5 mM and 30 mM of $CaCl_2$, respectively, in the hanging bags supplemented with HSM. Error bars represent the standard deviation of the data points.

The flocculation-sedimentation-centrifugation technique led to a decrease in the harvesting time, from 96 minutes to approximately 40 minutes or less per one 15 L bag. Total biomass collection time was reduced to less than an hour per bag with a combination of flocculation followed by centrifugation. The time reduction shown here demonstrates the potential of this technique for harvesting purposes in a large-scale system. Approximately 21.43g ± 4.778 and 29 ± 7.5 g of wet biomass was collected per 15 L culture bag with a combination of sedimentation-flocculation-centrifugation for the WT and mutant, respectively.

2.3.7 Cell disruption and starch hydrolysis

The main purpose of pretreatment is to increase the availability of cellular contents, such as starch, for nutrients for subsequent culturing (Feng et al., 2019). Since the bioreactor can be used to cultivate different microalgae, in addition to WT and mutant CC-5168 *C. reinhardtii*, two other microalgae relevant to space exploration - *Chlorella* and Spirulina - were also evaluated to determine the best pretreatment to release stored carbohydrates in all three. *Chlorella* is a relevant species in microalgae pre-treatment research since it has a rigid complex cell wall which makes cell disintegration challenging (Safi et al., 2015). One the other hand, Spirulina has relatively simpler cell wall (Coelho et al., 2020). Nonetheless, Spirulina's cell

wall is a physical barrier and improved accessibility to intracellular content is preferred (Coellho et al., 2020).

When submitted to ultrasound treatments the cells can be disrupted in two major ways, cavitation or accounting steaming (Gerde et al., 2012). The first produces microbubbles that when implode generate shock waves capable of disrupting cells (Gerde et al., 2012). When microbubbles collapse, they can create diversified effects (e.g., fragmentation, perforation, swelling and shrink) which can deform the cell morphology and surface (Liu et al., 2022).

The sonication treatment times chosen were 5 seconds, 5 and 15 minutes. Increasing time were selected to evaluate the response of the three different microalgae with an increase of sonification period since, in general, longer sonification leads to improved release of intercellular content (Liu et al., 2022).

Figure 2.27 shows the microscopic changes of untreated and sonification-treated cells. Similar to the observations of Bigelow et al. (2014), *C. reinhardtii* cells remained intact during the shortest sonification periods (5 seconds). No visual changes were observed in the other two microalgae for the shortest sonification and therefore those microscopic images are not included in **Figure 2.21**. Only a small number of cells lost their oval shape with intermediate sonification (5 minutes), as can be seen by a red arrow in **Figure 2.21B.** After a longer sonification period (15 minutes), almost all cells were disintegrated, as shown in **Figure 2.21C**. In previous studies (Bigelow et al., 2014), sonification of *Chlamydomonas* led to the release of chlorophyll suggesting that sonification is capable of disrupting intracellular structures in this species (Liu et al., 2019). However, careful control is necessary since sonification energy higher than the value needed for cell disruption has been shown in the past to induce oxidation of polyunsaturated fatty acids that can form free radicals and lead to the degradation of lipids and oils, which are also of value for various industries (Gerde et al., 2012). At the end of the 15 minutes, both the mutant and the WT had been disintegrated, as seen in **Figure 2.21L** but there were still oval cells present, as shown in Figure **2.21C**.

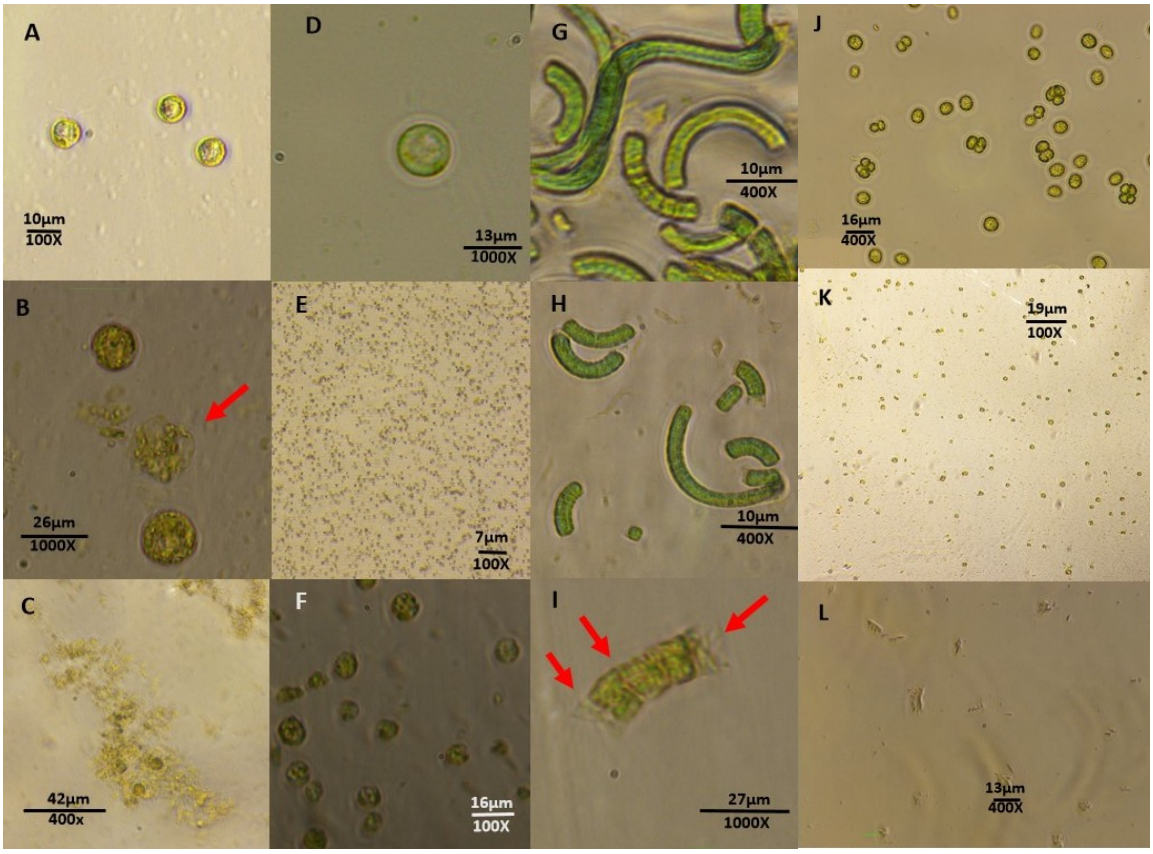

Figure 2.21 Figure 2.21 Microscopic observations of the effect of the sonification on microalgae cells, in particular in *Chlamydomonas* mutant CC-5168 (A-C), *Chlorella* sp. (D-F), Spirulina (G-I) and WT *Chlamydomonas* (CC-1690) (J-L). Untreated cells are shown in the top images (A, D, G and J). Cells treated with 5 minutes of sonification can be seen in the middle row (B, E, H and K). The results from the longest sonication treatment (15 minutes) are presented in the last row (C, F, I and L). Cells treated with the shortest sonification time (5 seconds) are not shown since it had not visual impact on the three microalgae**.**

A 5-minute sonification treatment led to cell disruption in *Chlorella* and increased cell components in the solution, as seen in **Figure 2.21E**. This observation is in accordance with the literature that states that ultrasonic treatment of this microalgae leads to increased UV absorbance values due to the release of chlorophyll and other intracellular content (Liu et al., 2022; Huang et al., 2016). However, at the end of the experiment, similar to the observations of Bigelow et al. (2014), *C. reinhardtii* cells remained intact during the shortest sonification periods (5 seconds). No visual changes were observed in the other two microalgae for the shortest sonification and therefore those microscopic images are not included in **Figure 2.21**. Only a small number of cells lost their oval shape with intermediate sonification (5 minutes), as can be seen by a red arrow in **Figure 2.21B.** After a longer sonification period (15 minutes), almost all cells were disintegrated, as shown in **Figure 2.21C**.

A 5-minute sonification treatment led to cell disruption in *Chlorella* and increased cell components in the solution, as seen in **Figure 2.21E**. This observation is in accordance with the literature that states that ultrasonic treatment of this microalgae leads to increased UV absorbance values due to the release of chlorophyll and other intracellular content (Liu et al., 2022; Huang et al., 2016). However, at the end of 15 minutes, similar to Safi et al. (2015) and Wagger et al. (2022), there were still intact *Chlorella* cells due to its resistant cell wall. *Chlorella* is known for its rigid cell wall composed of cellulose, chitin, proteins, and lipids, among other components (Safi et al., 2015; Wagger et al., 2022; Liu et al., 2022), while *Chlamydomonas* cell walls lack cellulose and chitin in their composition and are made up of mostly carbohydrates and polypeptides.

The microscopic observations of *Chlorella* differ from *Chlamydomonas* and Spirulina since the first increased in size with 15-minute sonification treatment. This could be as a result of sonoporation, which has been previously observed in enlarged *C. vulgaris* during sonification (Liu et al., 2022; Deenu et al., 2013). Changes in *Chlorella'*s round form to irregular shapes, which can be visualized in **Figure 2.21F**, were also observed in this experiment and have also been reported in previous studies, such as Huang et al. (2016).

In **Figure 2.21G**, untreated Spirulina shows well-compartmentalised cells. Several Spirulina were already fragmented due to physical treatments during powder processing (Vernes et al., 2019); whereas others retained a spiral structure, as seen in **Figure 2.21G**. A comparison of untreated and treated Spirulina shows increased fragmentation and smaller fragments with time, as it can be visualized in **Figure 2.21H** and **Figure 2.21I**. Microscopic observations showed, in particular **Figure 22.1I**, that rupture of Spirulina, a multicellular cyanobacteria, was obtained by fragmentation, which is the effect most observed in microalgae sonification (Liu et al., 2022). Due to the multicellular nature of Spirulina, in this study, sonification first led to the separation of individual cells (red arrows in **Figure 2.21I**), and only then were cells disintegrated and intracellular components released. Microscopic visualisation showed that after the longest sonification (15 minutes) there were still small fragments, like the one from **Figure 2.21I,** present in the solution. Previous studies showed complete disintegration of Spirulina cells at 20 minutes (Vernes et al., 2019) and therefore a longer

sonification time was probably needed in this study, however, as explained before, longer sonification can lead to adverse side effects.

Overall, as reported by Safi et al. (2015), sonification helped break the cells of all three microalgae but failed to achieve complete disintegration, in particular, in *Chlorella* sp. which is known for its pretreatment-resistant cell wall.

Conversely, chemical treatments, especially acids, are among the most common and efficient pretreatment methods as they can perforate the cell wall or membranes (Weber et al., 2022). Different acids have been tested in microalgae, including hydrochloric acid (HCl) and nitric acid (HNO_3) (Sign et al., 2000; Martins et al., 2022). Diluted sulfuric acid has been shown to lead to an efficient release of lipids and glucose even in microalgae with resistant cell walls, such as *C. vulgaris* (Weber et al., 2022; Martins et al., 2022). Moreover, sulfuric acid was used since sulphate is less toxic than chloride and the resulting solution will be fed to another microorganism. (Augustino et al., 2019).

The concentration of sulfuric acid (3%) used in this experiment was chosen since it was the most efficient concentration previously found to hydrolyse microalgae (*Scenedesmus* sp.) carbohydrates that were later used, identical to the current work, as a feedstock to produce a bioproduct (bioethanol) by another microbe (*Saccharomyces cerevisiae*) (Augustini et al., 2019). The authors tested different acid concentration combined with elevated temperature of 100 °C. Temperature is essential in acid hydrolysis since it helps break down the cell wall (Weber et al., 2022). As a result, the same temperature was selected for the current experiment.

Visually, thermal acidic treatment led to the alteration of the biomass colour, which was green for *Chlamydomonas* and *Chorella* and blue-green for Spirulina, as seen in **Figure 2.22** before treatment. All three became darker after acid hydrolysis. *Chlorella* and spirulina changed to black since sulfuric acid dehydrates carbohydrates which turn dark when they lose their water content (Augustino et al., 2019). Moreover, acid hydrolysis can lead to structural changes in starches (Wang et al., 2015). Microscopically, all cells in all four microalgae were completely disintegrated as shown in **Figure 2.22**.

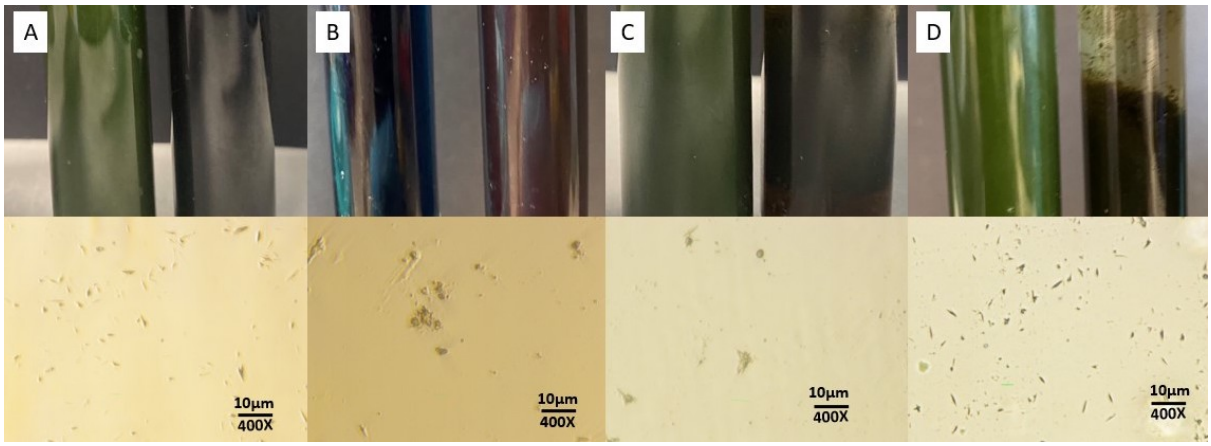

Figure 2.22 Macro (upper row) and microscopic (bottom row) observations from the acid treatment with 3% of sulfuric acid and high temperature. The results for all four microalgae can be vizualized in the following order: A) *Chlorella*, B) Spirulina, C) *Chlamydomonas* WT and D) *Chlamydomonas* mutant.

Since microscopically, acid treatment was more efficient than sonification, quantification of total saccharides and stored carbohydrates after treatment was measured by the protocol described in the Material and Methods, as well as the efficiency of the treatment in releasing stored carbohydrates (starch or glycogen) in all four microalgae.

Several methods can be used to routinely analyse carbohydrates, including physical, chemical, and biochemical techniques (e.g., colourimetric) (Zavrel et al., 2018). As mentioned in the Material and Methods, the protocol chosen to evaluate total saccharides and stored carbohydrates was a slight modification of the protocol developed by Zavrel et al., 2018, which involves the phenol–sulfuric acid protocol and is a combination of previous protocols. In this method, sugars are hydrolysed into simpler forms and measured spectroscopically (Templeton et al., 2012).

The disadvantage of spectroscopic measurements and the D-glucose standard calibration curve is that it is not sensitive to stored carbohydrates, and starch can be confounded with other polysaccharides (Zavrel et al., 2018). Nonetheless, it offers advantages over commercial kits such as the Megazyme, introduced earlier and evaluated in the next chapter. The protocol published by Zavrel et al. (2018) is quick and straightforward, offers sensitive results, has been successfully used in various algae (*Chlorella*, *Galdieria*, *Cyanidium*,

Nannochloris, *Haematococcus*, *Eustigmatos* and *Parachlorella*) and cyanobacteria (*Synechocystis* sp. PCC 6803 and *Cyanothece* sp. ATCC 51142), and only requires standard chemicals and a small volume of sample (1 mL) (Zavrel et al., 2018), which can result in decreased costs compared to enzymatic commercial kits. Additionally, commercial kits do not include the pigment extraction step, which, if not performed, can interfere with spectroscopic analysis (Yong et al., 2019). In this protocol, after the extraction of chlorophyll and carotenoids, soluble glucose was determined using the classical phenol-sulfuric acid method, followed by the removal of free glucose. Starch and glycogen were then decomposed in an acidic environment, liberating glucose from the previously stored carbohydrates. This free glucose was then quantified again using the phenol-sulfuric acid method (Zavrel et al., 2018).

Carbohydrate concentrations were calculated with the linear regression equation obtained with the D-glucose standard curve, which is shown in **Figure 2.23**. The curve was created with the D-glucose concentrations, also detailed in the Material and Methods. The fitted linear equation (Y= 0.0055X - 0.072) had an R-squared value of 0.9967. The various absorbances reads for free sugars, before and after treatment, were therefore entered and calculated with the regression equation.

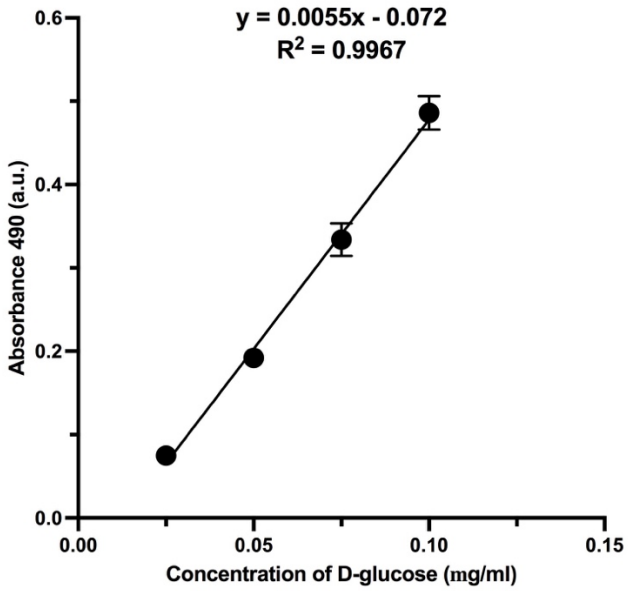

Figure 2.23 D-glucose calibration curve made with different dilutions and measured at 490 nm.

The concentration range of free saccharides, also addressed here as soluble sugars, before sulfuric treatment varied between 90–300 µg/mL in all four microalgae. The total amount of free saccharides was higher (254-568 µg/mL) than stored carbohydrates (245-358 µg/mL) after treatment in all three microalgae, as shown in **Figure 2.24.**

This indicates that pretreatment with 3% of sulfuric acid combined with high temperature was efficient in hydrolysing the majority of complex sugars, including structural and the ones used as carbon storage, such as starch. The wall-less mutant CC-5168 had the highest amount of free sugar and second highest of stored saccharides due to the fact that it has no cell wall, and intracellular components are more easily released to the solvent. Spirulina and *Chlorella* had a similar content of free saccharides. However, Spirulina had more sugar content from stored carbohydrates after treatment showing that the treatment was effective in breaking its softer cell wall and making accessible intracellular components. Spirulina's cell wall is made of several layers composed of lipopolysaccharides and peptidoglycan (Coellho et al., 2020).

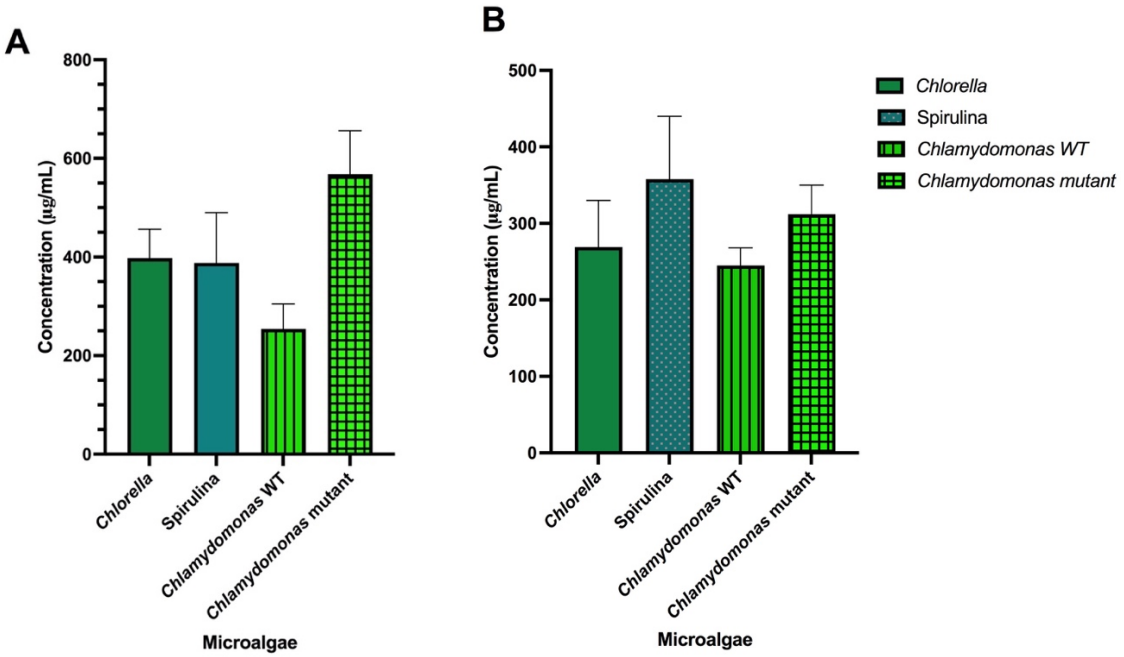

Figure 2.24 Concentration of total sugars (a) and stored carbohydrates (b) in *Chlorella,* Spirulina, *Chlamydomonas WT* and mutant pre-treated with dilute sulfuric acid, H_2SO_4 and elevated temperature (100°C). Error bars represent the standard deviation of the data points.

The pretreatment efficiency with 3% sulfuric acid and high temperature was compared among all three microalgae, as detailed in the Material and Methods. The efficiency of the treatment was determined as a percentage of the released sugars that originated from the breakdown of stored carbohydrates, as shown in **Equation 2.4**. Treatment efficiency for stored carbohydrates was similar among all four strains. Percentage values ranged from 50-70%, as can be seen in **Figure 2.25**. Spirulina had the highest efficiency (66%), probably due to the characteristics of its cell wall, which is less resistant to pretreatment. Moreover, unlike *Chlorella* and *Chlamydomonas*, the main stored carbohydrate in Spirulina is glycogen rather than starch. In microalgae, starch is commonly found inside insoluble granules, which makes it harder to extract and purify (Di Caprio et al., 2022).

Surprisingly, the second highest treatment efficiency was seen in *Chlorella*, which, as mentioned before, has the most resistant cell wall of all three. The fact that *Chlorella* had higher efficiency than *Chlamydomonas* could be due to the initial concentration of carbohydrates already present in *Chlamydomonas*, as discussed above. Since Spirulina and *Chlorella* were both grown under optimal conditions, harvested, and treated to be served as food sources, their nutritional quality, including carbohydrate content, should be near maximum and ideal. While *Chlamydomonas* collected from the bioreactor at the beginning of the stationary phase had a smaller number of cells (**Figure 2.11**) and, therefore, less starch and sugar both before and after treatment compared to the optimized small-scale system and the commercial powders. Moreover, unexpectedly, the treatment was slightly more efficient on the mutant strain than the WT due to the lack of cell wall.

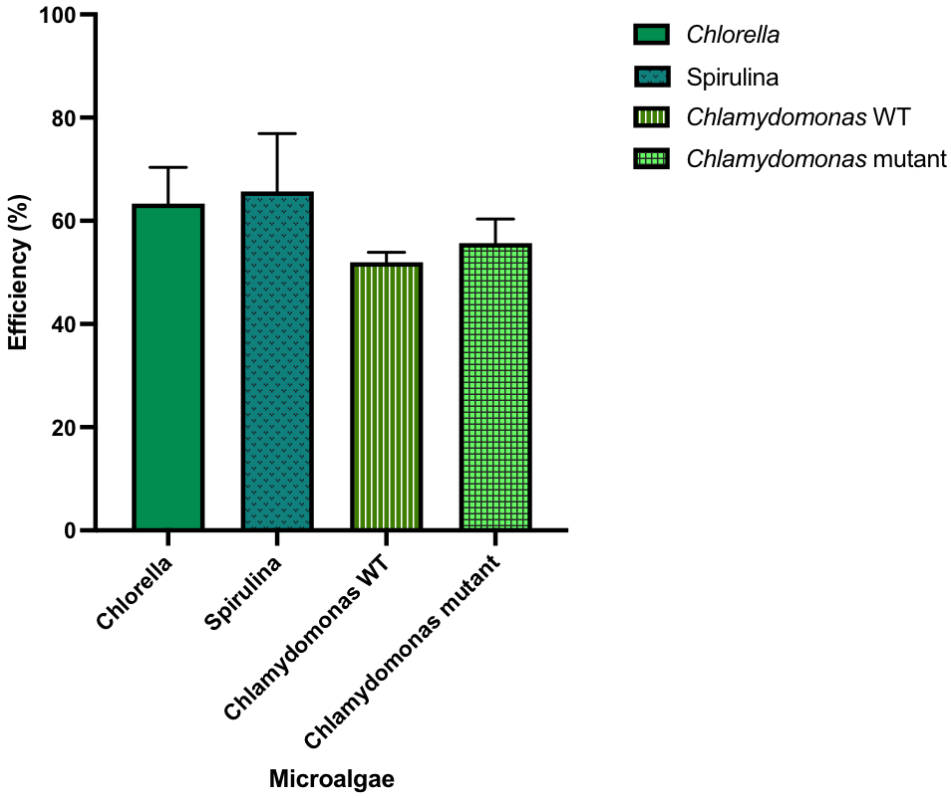

Figure 2.25 Efficiency of the pre-treatment with 3% of H_2SO_4 and 100°C on the amount of stored carbohydrates in the four microalgae tested: *Chlorella*, Spirulina, *Chlamydomonas* WT and *Chlamydomonas* mutant. Error bars represent the standard deviation of the data points.

In summary, more than 50% of stored carbohydrates were released from biomass after releasing soluble sugars in all four showing, showing that this is a promising pre-treatment for microalgae species with significance to deep space exploration. Chang et al. (2017) and Phwan (2019) argue that lower acid concentration combined with high temperature is more desirable than the other way around due to the degradation of fermentable sugars, the lower amount of neutralizing agents required in the subsequent step, and less corrosion of various laboratory equipment (Phwan et al., 2019). Dilute acid hydrolysis has been shown to be a cost-effective solution to produce bioethanol from carbohydrate-rich microalgae biomass (Phwan et al., 2019) and can be explored in bioplastic production as well.

2.4 Conclusions

In this chapter, both a small-scale system and a bioreactor for large-scale cultivation of *Chlamydomonas* sp. were successfully designed and implemented. The cells of both systems followed a normal growth curve trend for WT and the mutant *C. reinhardtii* strain confirming adequate aeration and lighting in both systems. The physical support designed for the hanging bag system successfully endured the weight of six bags and allowed the easy setup and operation of each hanging bag.

The introduction of flocculation reduced the harvesting process time of each hanging bag from 96 minutes to roughly 40 minutes, saving nearly 60% of the time. FT-IR of freeze-dried samples delivered well-differentiated spectra, notably better than sludges and allowed determination of the maximum starch accumulation in the mutant strain at day three and rapid consumption after day 5, which could indicate the beginning of starch utilization by the microalgae as a response to a decline in available nutrients in the media.

The protocol chosen to quantify soluble saccharides and stored carbohydrates was indeed rapid and simple. The minor modifications made to the protocol to adjust to available instrumentation were effectively implemented.

Chemical treatment was found to be more efficient in breaking down starch and releasing glucose than mechanical pretreatment, even in microalgae with resistant cell walls such as *Chlorella*. Acid thermal hydrolysis is, therefore, the method of choice to continue this dissertation's work.

Chapter 3 Production of scl-PHA 3D structures using algae feedstock

I want to acknowledge the valuable contributions of Dr Pooja Basnett and Vittoria Vecchiato, whose feedback and expertise in PHB production were instrumental in experimental design.

3.1 Introduction

3.1.1 Production of PHAs' by *Bacillus* sp.

Industrial-scale production and commercial application of PHAs usually employ Gram-negative bacteria, such as *Cupriavidus necator*, *Methylobacterium organophilum*, *Pseudomonas oleovorans* and *Escherichia coli* in the fermentation process (Valappil et al. 2008; Vu et al., 2021) due to high production rates and capability of these microbes to grow on simple carbon subtracts (Vu et al., 2021). However, PHA synthesis is not exclusive to Gram-negative bacteria. Gram-positive bacteria are also explored in PHA research, mainly in the biomedical field, due to the lack of a lipopolysaccharide-rich outer membrane that can act as an endotoxin, inducing a strong immunogenic reaction and hamper the commercialization of Gram-negative PHAs in this sector (Vu et al., 2021; Chen & Wu, 2005; Marcello, 2020).

PHB was, in fact, first identified and isolated by Maurice Lemoigne in the Gram-positive *Bacillus megaterium* in 1926 (Lemoigne, 1926). As a result, during the initial stages of PHA research, the Bacillus sp. genus was extensively investigated (Valappil et al., 2007). Sign and colleagues (2009) and Valappil and team (2007), reviewed a substantial amount of information regarding PHA production by members of this genus, including the most significant findings discovered throughout the decades.

In 1958, Macrae and Wilkinson identified the conditions under which *B. megaterium* and *B. cereus* produce and degrade PHB. Shortly after, in 1961, Lepecky and Law reported that PHB's most prominent roles are as carbon reserve and sporulation "fuel" (Valappil et al., 2007; Lepecky and Law, 1961; Macrae & Wilkinson, 1958). A few years later, in 1965, Kominek and Halvorson elucidated the start of PHB synthesis during *Bacillus* growth. The synthesis of PHB begins after the cells reach the log phase, with maximum biopolymer accumulation occurring just prior to spore formation, a stage that is then followed by breakdown of PHB during sporulation so that the polymer has disappeared when cells reach the late stationary phase (Kominek & Halvorson, 1965; Valappil et a., 2009).

Bacillus sp. remains one of the most explored bacteria in P(3HB) research (Mohapatra et al., 2017; Marcello, 2020). Reported PHA yields across the genus vary from 11 to 69% with up to 70 g/L of DCW (Singh et al., 2009). Most *Bacillus* species have been given the GRAS (Generally Recognized As Safe) status by the FDA (Food and Drug Administration) (Sign et al., 2009), including *B. subtilis*, the bacterium explored in the current study.

Similar to Gram-negative bacteria, *Bacillus* sp. can accumulate scl-PHAs using both simple (e.g.,glucose) and complex polysaccharides (Mohapatra et al., 2017). Members of this genus, including *B. subtilis*, have the ability to produce and secrete hydrolyzing enzymes such as amylase to break-down complex polysaccharides such as starch. Moreover, they are already used as bio-factories for the industrial production of recombinant proteins (Sign et al., 2009). Furthermore, various *Bacillus* spp. species, in addition to several types of PHAs, produce copolymers with medical importance from different inexpensive substrates (Valappil et al., 2007; Valappil et al., 2008; Marcello, 2020; Sign et al., 2009). For instance, P(3HB-co-3HV), the most investigated PHA copolymer due to equivalent mechanical properties to those of polypropylene (Sankhla et al., 2010), has been produced by *B. megaterium* OU303A to a higher yield (62.43% DCW) when supplemented with glycerol instead of the more expensive glucose (Sultanpuram et al., 2008).

Numerous factors should be considered when selecting the proper PHA-producing system, such as the cost of the carbon substrate, the growth efficiency and PHB accumulation level of the bacteria of interest, mechanical properties of the resulting PHA, and downstream

processing-related costs (Dalton et al., 2022). A species of the *Bacillus* genus was chosen for the current work due to the listed advantages the members of this genus offer to PHA research, one of the most important being safety for medical applications due to the lack of endotoxins (Sign et at., 2009). In summary, *Bacillus* sp. species are also one of the most versatile biopolymers producers capable of producing an array of PHAs and copolymers by using a variety of carbohydrates, including complex polysaccharides thanks to the presence of alpha amylases (Sign et al., 2009 and are already an established producer for industrial scale synthesis of other compounds (Sign et at., 2009).

Specifically to Mars, *B. subtilis* is a robust bacterium capable of forming spores resistant to numerous space-related stressors (Cortesão et al., 2019). Furthermore, when *B. subtilis* was submitted to microgravity and simulated Mars gravity aboard the ISS, no changes in its final cell concentration were observed compared to the ground control experiment, suggesting that this bacterium is suitable for the bioproduction of valuable compounds in space (Santomartino et al., 2020).

3.1.2 Synthesis of PHB using starch and algae biomass as feedstock

Glucose is the most extensively used substrate for the production of PHAs in both research and industry as this monosaccharide is readily metabolised (Jiang et al., 2016; Zhang et al., 2022). Due to the wide availability of starch - a major constituent of many crops (corn, rice, potato, cassava) - and the fact that it can be hydrolysed into glucose interest has grown in the potential of using it as an inexpensive carbon feedstock for PHA synthesis (Jiang et al., 2016; Zhang et al., 2022).

Of greatest importance for supporting a Mars habitat is the production of biopolymers from starch produced by algae. For instance, a strain of *Bacillus pumilus*, isolated from the wastewater of the University of Santa Cruz do Sul (Rio Grande do Sul, Brazil), was able to utilise the hydrolysate of spirulina biomass in conjunction with glucose and glycerol to produce PHB (Werlang et al., 2021).

3.1.3 Medical applications of PHAs and manufacturing 3D structures

One of the main applications of PHAs, as introduced in Chapter 1, is the medical industry. PHAs and other biodegradable materials have been used in the medical field since the 1970s (Bonartsev et al., 2019). 3D PHAs-based scaffolds, for instance, are the subject of extensive research in tissue engineering since they can replace missing or damaged tissues (Capuana et l., 2021). Moreover, nowadays, PHAs are used to manufacture various medical products (e.g., screws, pins, staples, patches), summarised in great detail by Bonartsev et al., 2019.

There are various fabrication methods - from conventional approaches to additive manufacturing techniques - capable of rapidly producing 3D scaffolds with porous structures (Bhushan e al., 2022). The solvent-casting-particle leaching method, where the polymer is dissolved in an organic solvent (e.g., NaCl) known as porogen and poured into a moulded cast followed by solvent evaporation, is one of the simplest processes (Marcello, 2020; Bhushan e al., 2022) and offers a controlled pore shape (Bhushan e al., 2022). Other traditional manufacturing 3D scaffolding methods include freeze drying, phase separation, hydrogels, cryogels and, more recently, electrohydrodynamic techniques, which have all been individually discussed by Bhushan and colleagues (2022), as well as their respective advantages and drawbacks. In additive manufacturing the most frequently employed 3D methods in bone scaffolds and PHB research (Marcello, 2020; Bhushan et al., 2022). FMD, in particular, is the most widely known and common 3D printing technique in various industries and research thanks to fast printing speed, reasonable cost, and various materials, from synthetic to biological, that FMD printers can process (Plavec et al., 2022). Among the biomaterials, PLA is the most suitable and used due to its low print temperature and exceptional adhesion to the 3D printer bed but it is unfortunately also associated with several limitations, including lower biodegradability when compared to other biopolymers such as PHB (Plavec et al., 2022).

Pure PHB is challenging to 3D print due to its tendency to wrap and shrink during the printing process as a result of its high crystallinity and processing temperature, between 170

- 180 °C (Table 3.1), which is close to its degradation temperature, leading to the formation of defective pieces (Menčík et al., 2022; Zainuddin et al., 2023; Plavel et al., 2022).

As recently reviewed by Zainuddin et al., 2023, to overcome this nuisance, some researchers have created blends of PHAs by mixing them with other polymers (mainly PLA) or through the addition of a second material, such as fillers or compatibilizers (Ausejo et al., 2018; Giubilini et al., 2020; Kontárová et al., 2020; Rydz et al., 2020; Mehrpouya et al., 2021; Plavel et al., 2022). An overview of the different printing techniques utilized to produce 3D PHA structures was published by Mehrpouya et al., 2021. PHB alone has been printed by SLS (Pereira et al., 2013), while PHB/PLA composites are frequently produced for FDM purposes, as exemplified in the following studies. A blend of PHB with 20% of biorefinery lignin was successfully melt-extruded by Vaidya and team (2019). The final extruded composite showed a decrease in warpage of 34-78% compared to PHB alone (Vaidya et al., 2019). PLB/PLA blends are known for having low flexibility values (Plavec et al., 2020), which can be increased by adding plasticizers that will help reduce the glass transition temperature and processability (Plavec et al., 2020). Incorporating plasticizers into PHB/PLA blends in a 60-25-15 (wt.%) ratio improved thermal and mechanical properties but slightly worsened printability compared to the PHB/PLA reference blend (Kontárová et al., 2020). In another study, a combination of PHB, PLA and cellulose nanocrystals employed FDM to produce mesh samples (Frone et al., 2020). The authors used cellulose to enhance adhesion and dispersion between PHB and PLA (Frone et al., 2020).

The applications of plastics are dependent on their thermal and mechanical properties. Melting and glass transition temperatures are two of the most important properties for manufacturing either 3D scaffolds or FDM 3D prints (Marcello, 2020). Both tensile strength, and elongation break evaluates a polymer's capacity to stretch. The literature values for the previous properties for PHB, PHB's copolymer Poly(3-hydroxybutyrate-co-3-hydroxyvalerate) (PHBV), polylactide acid (PLA) and polythylene (PE), which is the most used plastic in the world, are shown in Table 3.1 for reference.

Table 3.1 Thermal and mechanical properties of PHB and PLA - the polymers most frequently discussed in this chapter. The table also includes the properties of PE for reference. The parameters shown are the following: melting temperature (Tm), glass transition temperature (Tg), Young's Modulus (E), elongation at break (ε), and tensile strength (R_m). All the values are an average due to variations from several different reports.

Polymer name	Tm (°C)	Tg (°C)	E (GPa)	ε (%)	R_m (MPa)	Literature references
PHB	177	4	3.5	6	40	Valappil *et al.*, 2006
PHBV	170	5	0.11	30-123	2.4-80	Kouhi *et al.*, 2019 Zhao *et al.*, 2021
PLA	150	59	3.6	2.4	68	Byrne *et al.*, 2014 Balakrishnan et al., 2012
PE	130	-30	0.2	620	10	Strong *et al.*, 2016

The objective of this chapter is the production of PHB by a Bacillus strain feed with algae-derived feedstock as sole carbon source. Moreover, the PHB's properties will be investigated as well as its feasibility to produce 3D scaffolds and to be utilized in 3D printing.

3.2 Material and Methods

3.2.1 PHA production by *Bacillus subtilis* OK2

A stock culture of *Bacillus subtilis* OK2 from the University of Westminster, London, UK, collection was incubated at 30 ºC overnight on Nutrient Agar containing (g/L): 1 of meat extract, 2 of yeast extract, 5 of peptone, 5 of sodium chloride, and 15 of agar, as described by Marcello, 2020.

For maintenance, the agar plates were kept at 4ºC after growth and restreaked regularly; a new plate was streaked every week from a single colony into freshly made agar plates for subsequent experiments. For PHA production and experiments/testing freshly grown *Bacillus subtilis* colonies were always used.

A single colony of Bacillus spp. was used to inoculate Erlenmeyer flasks with 150 mL of Nutrient Broth. The starter culture was grown at 30ºC during 16 hours for 140 rpm. For PHA

production, 10% of seed culture were transferred into three Erlenmeyer flasks with 500 mL working volumes of modified Kannan and Rehacek medium (Kannan and Rehacek, 1970), a semi defined medium routinely used in PHA production. The Kannan and Rehacek's recipe, (referred in this chapter simply as Kannan recipe) consisted of the following ingredients (g/L): 5 of ammonium sulphate, 3 of potassium chloride, 2.5 of yeast extract, 35 of biomass hydrolysate or D-glucose, and 1 mL/L of trace elements. The cultures were grown at 30ºC with agitation (140 rpm) for 48 hours, as previously described by Marcello, 2020.

Autoclaved sponge's bungs were used to cover the top of Erlenmeyer flasks. All media was made fresh or kept at 4ºC until use and buffered before sterilization; pH was adjusted to 6.8 with 1M NaOH. D-Glucose was autoclaved separately from the rest of the media under different conditions (110ºC for 10 minutes and 121ºC for 15 minutes, respectively), and mixed post-sterilization. All chemicals were purchased from Sigma-Aldrich Company Ltd. (Dorset, England).

The biomass was harvested by centrifugation (4600 rpm) for thirty minutes. Pellets were frozen down at -20ºC for 24 hours and then lyophilized with Labconco FreeZone benchtop freeze dry system (Labconco, United States) for 2-3 days. The weight (g) before and after lyophilization was recorded. Polymer yield was calculated in terms of cell dry weight (CDW) by the following equation (**Equation 3.1**):

$$CDW = \frac{polymer\ mass}{mass\ of\ lyophilized\ biomass} \times 100 \qquad \textbf{(Eq 3.1)}$$

The productivity of PHB and starch production was calculated based on **Equation 3.2**, which focuses on the amount of PHB or starch (mg) produced per unit volume (L) of culture over time (h), as shown below:

$$Productivity = \frac{weight\ of\ product}{culture\ volume} \times cultivation\ time \qquad \textbf{(Eq 3.2)}$$

3.2.2 Extraction, purification, and precipitation of PHAs

PHA extraction was performed with two different methods. Due to purity reasons, the extractions involving film fabrication and 2D constructs were performed by the Soxhlet extraction method as summarized by Valappil et al., 2007. During Soxhlet extraction, the lyophilized and milled biomass was purified by re-precipitation with approximately 300 mL of ice-cold methanol (Hahn et al., 1995) for 48h at 37 °C followed by chloroform ($CHCl_3$) for 24 h. Concentration of the collected $CHCl_3$ was performed by vacuum rotary evaporation where chloroform is retovaped and PHA is precipitated under continuous stirring conditions. The precipitate is then air-dried and weighted.

A swifter extraction protocol was used to evaluate PHAs' yield at different time points over five days. In the sodium hypochlorite (NaClO) extraction method the lyophilized and milled biomass is incubated with 80 % NaClO and $CHCl_3$ at 30ºC for 2 h at 180 rpm in a 1:4 ration, in which 5 mL of NaClO and 20 mL of chloroform are added to each 0.3 g of dried biomass (Rai et al., 2011b; Lukasiewicz et al., 2018). After incubation, the biomass is centrifuged for 20 minutes at 3900 rpm. The top layer and biomass are discharged whereas the chloroform in the bottom containing the biopolymer is collected and subjected to concentration. The concentration and precipitation step are performed by vacuum rotary evaporation (R-215, Buchi Labortechnick AG, Switzerland), as described above.

The complete process involved in PHB production, from fermentation to polymer characterization, is schematically shown below in **Figure 3.1.**

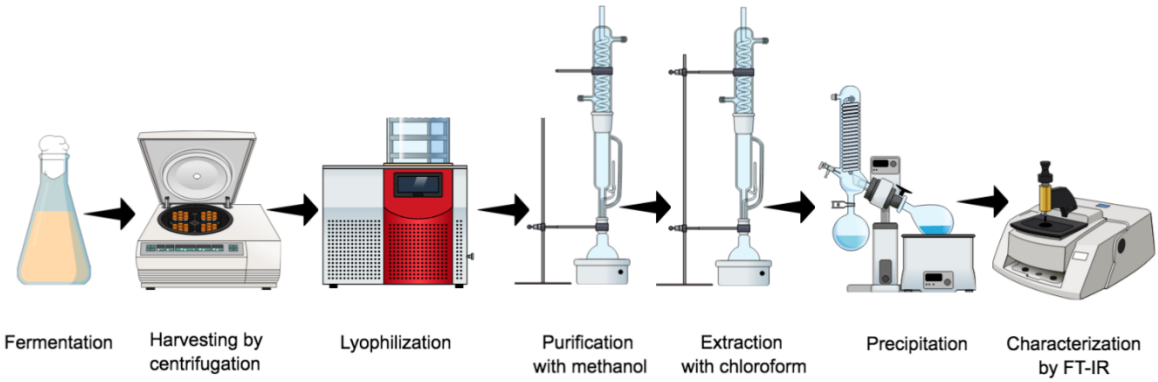

Figure 3.1 Sequence of steps involved in producing PHB from *B. subtilis* OK2. After the cultivation of *Bacillus* on NB broth, the bacterium is grown under limited nutrient conditions that will lead to PHB production in the fermentation step, which will be followed by cell harvesting. *Bacillus* biomass is then freeze-dried and submitted to purification in a soxhlet extractor. Purification precedes polymer extraction which also occurs inside a soxhlet extractor. PHB is then precipitated with chloroform in a rotavapor and characterized by FTIR.

3.2.3 PHA characterization

Characterization of precipitated PHA was performed by attenuated total reflectance Fourier transform infrared (ATR-FTIR) by a PerkinElmer FTIR spectrometer Spectrum Two (PerkinElmer Inc, USA) at the University of Westminster using a spectral range between 4000 to 400 cm-1 and a resolution of 4 cm-1.

Characterization of freeze-dried *Bacillus* biomass cultivated under different conditions was carried out by using again ATR-FTIR spectroscopy with a Thermo Scientific Nicolet iS5 FTIR Spectrometer and an iD5 Single-Bounce ATR attachment at Birkbeck, University of London with the same spectral range and resolution described as above and 100 scans per spectrum.

All spectra were corrected against a background measurement performed before analysis to automatically subtract atmospheric carbon dioxide and water.

3.2.4 Large-scale production of PHA

In order to improve PHA yield, a large-scale protocol was designed and evaluated. The new protocol, detailed below, involves an additional starvation step which can be seen in **Figure 3.2** with a concentration of ammonium sulphate of 5 g/L.

20 mL nutrient broth were inoculated with a single colony of *Bacillus* spp. and incubated for 16 h. All 20 mL were poured into modified Kannan and Rehacek media (second stage) described earlier and incubated for 16 h. The entirety of the volume was poured into a larger volume of further modified Kannan and Rehacek media (third stage) with fewer amount of ammonium sulphate (**Table 3.2**) and grown for 48 h. pH was adjusted with 1 M NaOH.

Table 3.2 Media composition, total volume, pH, and speed of agitation used during the two stages of the large-scale process.

Media (g/L)	**2nd stage**	**3rd stage**
Ammonium sulphate	5.5	5
Potassium chloride	3	3
Yeast extract	2.5	2.5
Biomass hydrolysate/Glucose	35	35
Trace elements	1 mL/L	1 mL/L
Total volume	200 mL	2 L
pH	6.8	6.8
Agitation (rpm)	140	200

All incubation steps were performed at 30ºC. Biomass was harvest by centrifugation as described previously. The soxhlet extraction method detailed earlier was used for PHA purification and extraction. The experiment was performed in triplicate.

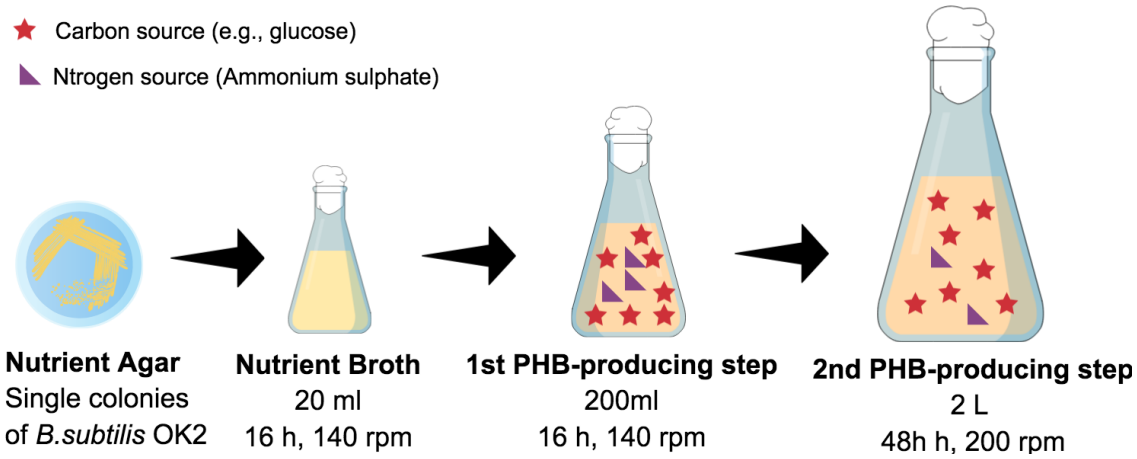

Figure 3.2 Scheme displaying the succession of steps involved in the scale-up process of PHA production by *Bacillus subtilis* OK2. The figure shows how the working volume has the same amount of carbon source (g/L) but lower nitrogen (g/L) compared to the second stage. The growth temperature in very steps was 30ºC. The image is not to scale. The schematic representation is adapted from Marcello, 2020.

3.2.5 Proof of concept: starch as organic carbon feedstock

In order to investigate the ability of *Bacillus subtilis* OK2 to use and grow on starch rather than glucose, commercial soluble starch purchased from Sigma-Aldrich (Dorset, England) was tested as carbon source.

Experiments were performed for 84 h in 0.5 L of modified Kannan and Rehacek media at 30 °C with agitation (140 rpm) inoculated with 10% of inoculum grown on nutrient broth for 16 h. In order to maintain reproducibility all working volume flasks were inoculated with the same optical density of approximately 0.6. The Kannan and Rehacek recipe was used with modifications; these adjustments are associated with the sources of carbon in the medium. The different carbon sources combinations were the following: glucose + yeast extract (YE), soluble starch + YE, and YE only (without a carbon source). The quantity of commercial starch added was the same as glucose (35 g/L). Commercial starch was sterilized separately from the rest of the media using the same conditions used in glucose sterilization (110 °C for 20 minutes).

Optical density was used to monitor the growth of *Bacillus* spp. through time in the different combinations of carbon source. OD was measured at 600 nm every 12 hours for a period of 84 h using the respective media as a blank. Dilutions, using also the respective media, with 10x dilution factor were made when OD reached 1. Temporal measurements were performed with a visible spectrophotometer (Jenway, UK). The experiment was performed in three times. A sampling schedule was designed, where different replicates were measured at different time points to allow data collection during the night while maintaining synchronization across replicates.

3.2.6 Hydrolysed *Chlamydomonas* spp. biomass as glucose replacement

Hydrolysed biomass of WT *Chlamydomonas* spp. was tested as glucose replacement for *Bacillus* spp. Similar to glucose and commercial starch the concentration of biomass added was the same as glucose (35 g/L). Biomass went through acid hydrolysis with 3% of sulfuric acid on a water bath at high temperature, as described in the previous chapter. The solution was subsequently neutralised with sodium hydroxide as described in Chapter 2.

Experiments were performed in a total volume of 0.5 L in triplicate on Kannan and Rehacek media, at 30ºC and 140 rpm, as described earlier. Furthermore, hydrolysed algal biomass was treated separately during the sterilization process as described before, with the sterilization conditions used for glucose and starch. OD was measured at 600mm every 12 hours using the respective media without inoculum as a blank. As before, one of the cultures was inoculated at a different time to determine the overnight OD measurement.

A temporal profile analysis that included OD, pH and polymer yield, was performed. Temporal measurements of pH were obtained by a benchtop pH meter (Jenway, UK), while OD was obtained by using 1 mL plastic cuvettes (Greiner Bio-one, Frickenhausen, Germany) on a visible spectrophotometer (Jenway, UK). PHB yields were obtained by the sodium hypochlorite method described earlier after the biomass was submitted to lyophilization.

3.2.7 Determination of Starch content

The different carbon sources investigated in this chapter were analysed for starch content with the Total Starch Assay Kit (AA/AMG) by Megazyme (Wicklow, Ireland) by following the manufacture's instructions. The carbon sources evaluated were D-Glucose (Dorset, England), soluble starch (Dorset, England), dried biomass of WT and mutant Chlamydomonas obtained from the hanging bangs. Biomass of both strains submitted to the acidic treatment described above were also tested. Each carbon source was weighted in duplicate. OD measurements for each sample were also performed duplicate, as recommended by the manufacturer. Therefore, four OD values were obtained per carbon source.

3.2.8 Determination of PHA content over time by FTIR

Harvesting time is one of the most crucial factors in fermentation. FTIR can be used to analyse PHA content changes over time, including PHA maximum accumulation and start of polymer degradation. PHB accumulation was investigated using modified Kannan and Rehacek media with glucose as carbon source in a 0.5 L working volume and with 10% of inoculum grown on nutrient broth for 16 h at 30ºC for five days at 140 rpm. Volumes of 30 mL were pipetted from liquid cultures into 50 mL falcon tubes daily. A small volume (1 mL) was used for OD measurements, while the remaining was centrifuged at maximum speed for 10 minutes. Pellets were gently washed with deionized water to remove salts from the medium; the sludge was immediately frozen at -20ºC. The frozen sludges were subsequently subjected to lyophilization. A 30 mL volume from the 200 mL seed culture with nutrient broth was also removed and freeze-dried to. be used as control and to determine *B. subtilis'* spectrum without PHB inducing conditions. A small portion of all freeze-dried samples was analysed by a Thermo Scientific Nicolet iS5 FTIR Spectrometer with an iD5 Single-Bounce ATR attachment at Birkbeck, University of London, as described earlier. The remaining mass was weighed and submitted to PHB extraction by the sodium hypochlorite protocol in 15 mL falcon tubes to determine the PHB yield content in each day.

3.2.9 Production of PHB Films by the Solvent Casting Technique

Two PHB films were produced. The first film was created using the PHB produced with glucose, and the scale-up methodology as a control, while the other was fabricated with the PHB produced using algae biomass. The two films were fabricated by the solvent casting technique described by Marcello et al., 2021 with a slightly modified protocol. In brief, 0.3 g of polymer was dissolved in 10 mL of chloroform with ≥ 99.8% purity (Fischer Chemical, Zurich, Switzerland) (5% w/v), stirred for 24 h in glass vials and placed inside glass Petri dishes 6 cm in diameter at room temperature (covered with a lid) inside a fume hood until the chloroform slowly evaporated completely and the films were fully dried (approximately three days).

3.2.10 Evaluation of Wettability by the Water Contact Angle Method

The surface wettability of PHB films was performed by Water Contact Angle using the sessile drop method and a Attension Theta tensiometer (Biolin Scientific, Gothenburg, Sweden). A small, flat circle of each film was cut with a steel scalpel and placed on microscope slide. One drop of distilled water was dropped on the flat film circle. Contact angle measurements and digital images were taken immediately as the drop touched the surface of the film with a lens and automated video camera (Navitar optics) and software (OneAttension software) coupled with the instrument. Two replicates of static contact angle measurements automatically performed by the instrument were used to determine the average contact angle value for each film.

3.2.11 Preparation of salt-leached porous structure and a 3D wrench

The 3D porous scaffolds of PHB produced with glucose and PHB produced with algae biomass were fabricated using solvent-leaching. Two different structures were produced. Sodium chloride (Sigma Aldrich) was used as porogen and chloroform (>99%) as solvent. The ratio of porogen: polymer was 3:1. A total of 0.3 g of PHB was dissolved in 10 mL of chloroform inside a glass vial, followed by the addition of 2.7. g of NaCl, which was subsequently added to the mixture. The lid was covered with parafilm to avoid solvent evaporation, and the solution was stirred for four days. The suspensions were then cast in an

appropriate silicon mould (**Figure 3.3)** to fabricate rectangular scaffolds. A glass slide was placed on the mould to avoid rapid solvent evaporation. The mould was left drying for 24 h inside a fume hood at room temperature.

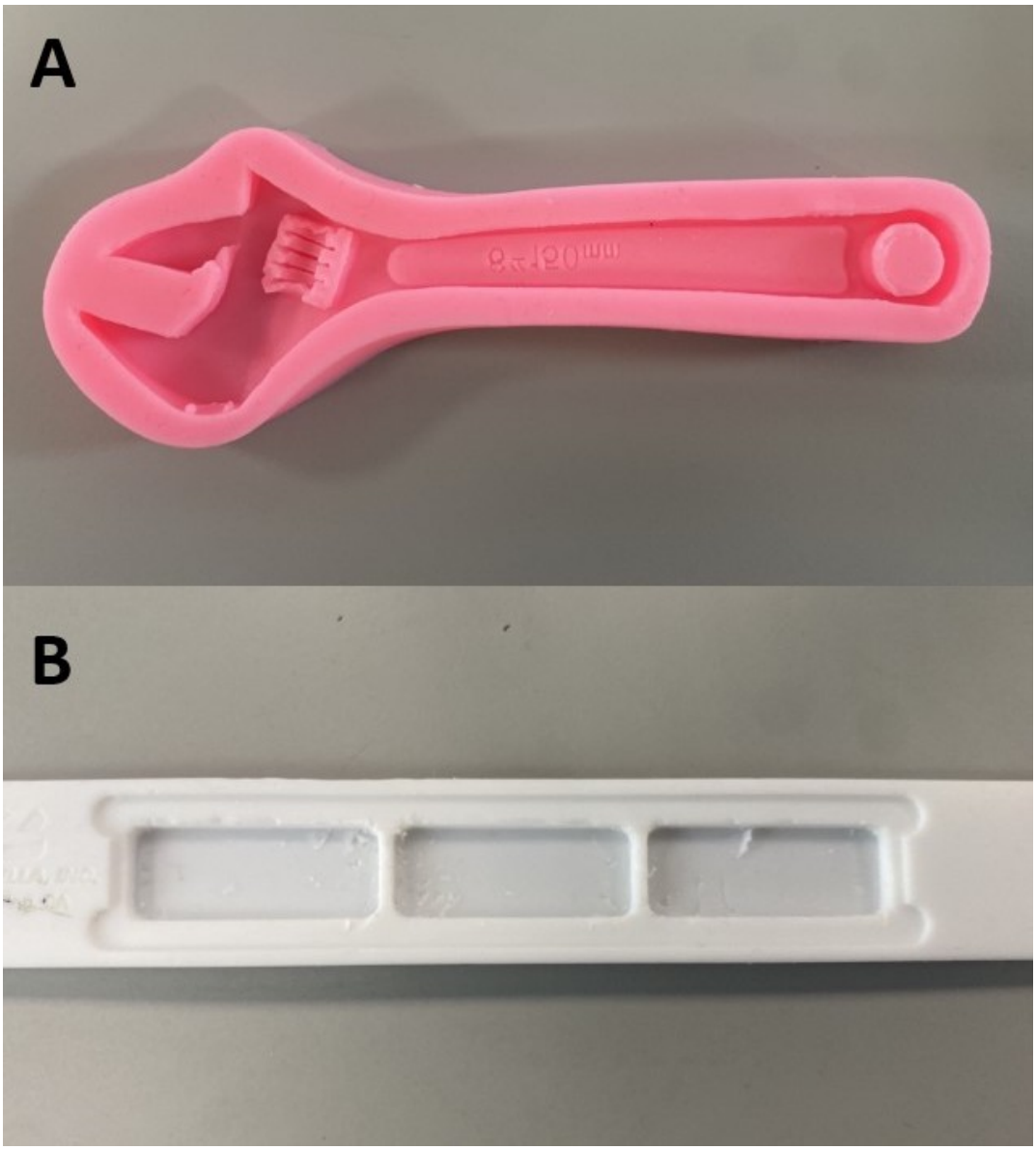

Figure 3.3 Moulds used to make 3D structures via the salt-leaching technique, (a) including a wrench and (b) a mould capable of producing three porous structures with medical significance.

A suspension made of algae produced PHB was also poured into a silicon mould with the form of a wrench (Posionks; EXCEART), shown in the figure above and with the following dimensions: 15 cm X 5 cm X 1.5 cm. A glass cover was also placed on the mould during the drying stage.

3.2.12 Statistical Analysis

All measurements were obtained in triplicate except the FTIR data and when stated by the author. Triplicate or duplicate data was averaged and presented here with the respective standard deviations. Growth curves, statistical analysis and column graphs were made using GraphPad Prism 9 (GraphPad Software Inc., USA). To assess the relationship between peak height and PHB yield (% cdw), a Pearson correlation coefficient (r) and a simple linear regression was determined with GraphPad Prism 9. The associated p-value was also calculated to evaluate the correlation's statistical significance.

FTIR spectra of Bacillus biomass were plotted in Excel while the FTIR spectra of purified PHB were obtained and analysed with the help of Spectrum Quant software (PerkinElmer, Massachusetts, United States). Starch content evaluated by the Megazyme kit (Wicklow, Ireland) was determined by the kit-specific automatic calculator Mega-Calc (Equation 3.3), which was obtained from the following webpage: https://www.megazyme.com/total-starch-assay-kit provided by the manufacturer:

$$Starch\,\% = \Delta A \times F \times \frac{EV}{0.1} \times D \times \frac{1}{1000} \times \frac{100}{W} \times \frac{162}{180} \qquad \textbf{(Eq 3.3)}$$

In which ΔA is the subtraction of sample absorbance minus sample blank read, F represents the factor that converts absorbance reads into glucose value (µ), EV the sample extraction volume and 0.1 is the volume of sample analysed. D represent further sample dilution (if necessary), 1/1000 is the conversion of units (µg to mg), W sample weight (mg) and 162/180 is the factor responsible for converting free glucose into anhydroglucose characteristic of starch.

3.2.13 Three-Dimensional-Printing

3D printing was performed in collaboration with Champion 3D (London, United Kingdom) at the company's facility. Two commercially available filaments optimized for

FDM additive manufacturing were used to print two identical ratchet wrenches with the following dimensions: 15 cm x 5 cm x 1.5 cm. The two chosen filaments – allPHA and NonOilen – both have PHA in their composition and were purchased from ColorFabb and Fillamentum, respectively. Detailed information regarding their chemical constitution can be found in Table 3.7. Both filaments were 1.75 mm ± 0.02 mm in diameter.

The stl file used to 3D print the two objects is shown next in Figure 3.4. The file was designed by Made in Space, Inc., used to 3D print the first wrench aboard the ISS and obtained from the following NASA webpage: https://nasa3d.arc.nasa.gov/detail/wrench-mis.

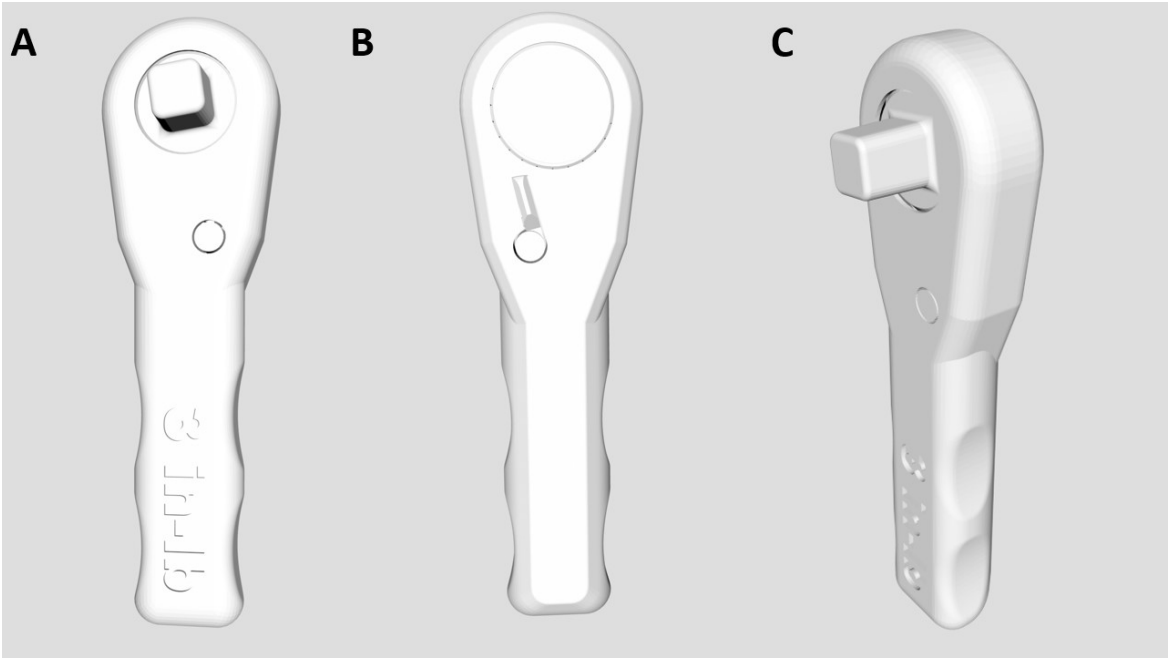

Figure 3.4 CAD model from NASA/Made in Space, Inc. used to 3D print both wrenches in this study. The figure shows different angles of the model including (a) the front, (b) the back, (c) and the side view of the wrench.

The CAD wrench model is composed of three individual pieces, as shown in the figure above. These are the main structure, the ratchet gear, which is the rotating top circle with teeth, and a bottom pawl which prevents the ratchet gear from rotating in the wrong direction. All 3D pieces were sliced using the Simplify3D (Cincinnati, Ohio, United States) software which cut the model into multiple layers as shown in Figure 3.5. The three pieces were printed simultaneously.

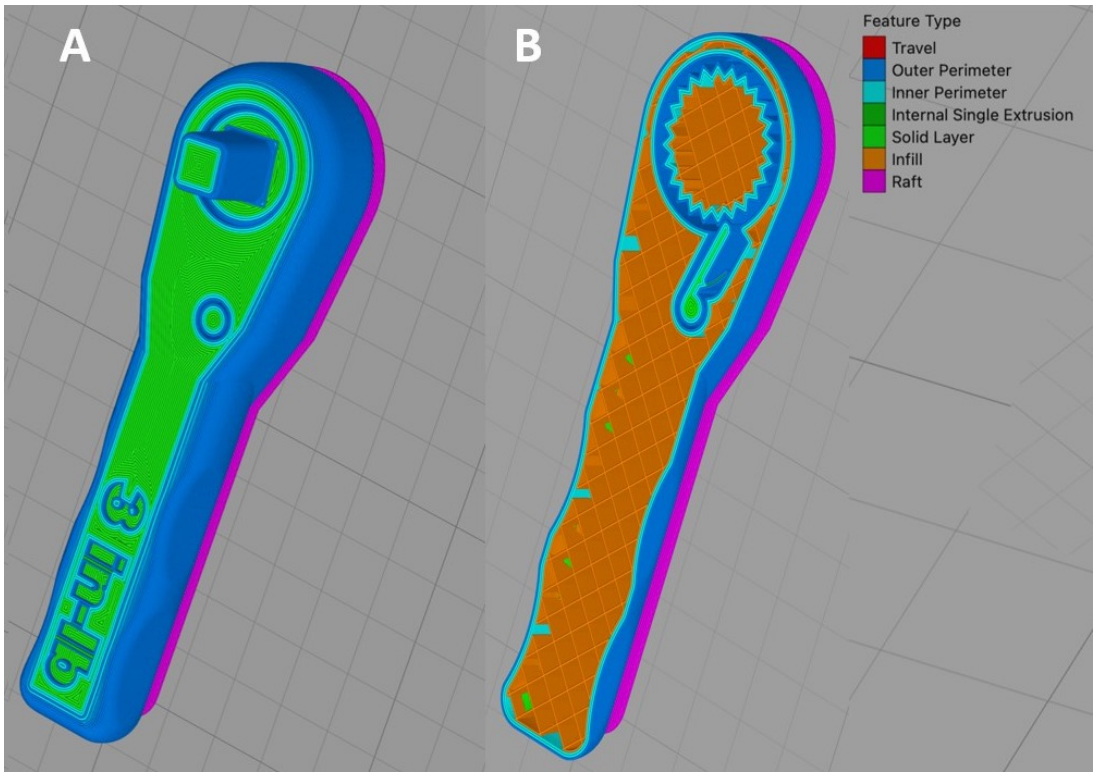

Figure 3.5 The preview of the external (a) and internal (b) layers resulting from the slicing stage performed with Simplify3D software. The legend for the colours shown in the designs is presented on the right side of the figure.

After testing printing parameters, the final products were printed with a Creality 3D CR-10 Max printer and modified extruder that allows a wider range of filament dimeter. A raft, which is a flat horizontal latticework made of filament placed on the printing bed to increase adhesion, was used to aid the printing process which was accomplished with the printing parameters shown in **Table 3.3** which were used for both filaments.

Table 3.3 Final printing parameters used to 3D print two wrenches with two different filaments having PHA in their composition.

Printing parameter	Value
Nozzle temperature	195°C
Bed temperature	0°C
Printing speed	50 mm per second
Layer height	0.2 mm
Filling	20%
Raft separation	0.18 mm

3.3 Results and Discussion

Bacillus spp. was the genus of choice for reasons presented earlier in this chapter (**section 3.1.1**). The *B. subtilis* natto strain OK2 from the University of Westminster collection was first isolated from commercial fermented soybean (Okame natto) produced by the Japanese food company Takano Foods Co. (Ashikaga et al., 2000). The strain was a gift from Professor Fujio Kawamura from the Department of Life Sciences at Rikkyo University (Lukasiewicz et al., 2018).

In terms of bacterial cultivation, *B. subtilis* can grow in an impressive wide range of temperatures (5.5 °C and 55.7 °C) exhibiting optimal growth between 30 – 35 °C (Gauvry et al., 2021; Errington & Art, 2020). Based on the literature, *B. subtilis* is a fast-growing organism with a quick doubling time of 20 minutes under optimal conditions (Errington & Art, 2020) that can grow in non-complex media like nutrient broth. Both nutrient agar and nutrient broth have beef extract (or yeast extract), peptone and sodium chloride (NaCl) in their composition. Peptone provides amino acids as a source of organic nitrogen, NaCl maintains salt concentration, while beef and yeast extract provide a variety of fundamental ingredients for microbial growth, which include vitamins, carbohydrates, salts and other organic nitrogen compounds (Tao, 2023). Yeast extract (YE) composition depends on the manufacturer. Roughly, YE is made of 5% of potassium, small amounts (<1%) of chloride, magnesium,

ammonia, phosphor, phosphate, around 10% of organic nitrogen and 40% of organic carbon (Thompson et al., 2017).

Lukasiewicz et al. 2018 and Marcello, 2020 have already characterised the growth rate and investigated PHB production by the *B. subtilis* OK strain. Therefore, the starting point of this work in terms of media composition and protocols followed previous publications, which protocols were optimized for PHB accumulated using glucose as a carbon source. Past studies include a two-stage system for producing PHB by this bacterium. In the first stage, *B. subtilis* grown on nutrient broth followed by fermentation in PHB-producing media characterized by lack of sufficient inorganic nitrogen. The Kannan and Rehacek medium is composed of YE which is responsible for organic nitrogen and reduced quantities of ammonium sulfate - the source of inorganic nitrogen - which will trigger the cells to produce PHB as a response to nutrient stress. The medium also contains potassium chloride, an important nutrient for bacterial growth. Potassium chloride is a readily available source of potassium, which is necessary for various cellular functions and for maintaining osmotic pressure. The name of the recipe is a reference to the first two authors who developed it when studying PHB synthesis in *Actinomycetes (*Kannan & Rehacek, 1970).

In addition to temperature and media composition, other factors, such as pH and agitation, are crucial during fermentation to obtain maximum bacterial growth and product accumulation. Agitation is responsible for mixing the medium's ingredients and for exposing the culture to oxygen transfer. Acidic conditions have been shown to suppress sporulation in the past (Valappil et al., 2007) which can interfere with PHB accumulation and degradation as discussed earlier. Like other members of the *Bacillus* sp. genus, *B. subtilis* can grow on a wide variety of pH values, from 4.8 to 9.2 (Gauvry et al., 2021). Again, the optimum pH and cultivation speed for PHB accumulation used in the present studied was based in past recommendations and studies.

3.3.1 Evaluation of a modified protocol for the large production of PHB by *B. subtilis* OK2

In order to increase the quantity of PHB extracted, a new protocol with increased working volume and an additional step to further stress the cells, was evaluated. Glucose was used as carbon source in both protocols. In both systems, *Bacillus* sp. was grown following a batch cultivation sequence where one colony of *Bacillus* sp. grows on a seed culture on nutrient broth for bacterial adaptation to liquid media (Lukasiewicz et al., 2018; Marcello, 2020) followed by inoculation of a larger volume with 10 % v/v of inoculum from the previous stage. With the new protocol, 10 % v/v of the previous culture is used to inoculate a larger volume during the third stage of the process. During fermentation, *B. subtilis* produced PHB under nitrogen-limiting conditions and excess of glucose. PHB was purified and extracted using the soxhlet extraction method. The PHB yield at 48 h for both protocols is shown in **Table 3.4**. All stages in both protocols were carried out in shaken flasks.

Table 3.4 Comparison of PHB mass and polymer yield values obtained by culturing *B. subtilis* with two different protocols and their respective ammonium sulphate concentrations. The results shown are average of triplicates; standard deviation values are also included.

$[(NH_4)_2SO_4]$ g/L	**PHB mass (g)**	**CDW (%)**
5.5	0.13 ± 0.03	29.56 ± 3.33
5	0.89 ± 0.01	64.49 ± 15.00

The PHB yield obtained with the previous protocol was 30% of CDW. This value is identical to the ones found in the literature (Lukasiewicz et al., 2018; Marcello, 2020) when batch fermentations of the same strain were performed using the same medium and under similar fermentation conditions in 5 (Lukasiewicz et al., 2018) and 10 L bioreactors (Marcello, 2020). Even though a similar polymer yield was obtained in this chapter, due to the smaller working volume (500 mL), only 0.16 g of PHB were collected per shaken flask in this experiment.

One of the most efficient ways to increase the amount of PHAs produced is by scaling-up the process by producing PHB in a fermenter during the nutrient stress stage. In addition to

higher yields, fermenters used in large-scale production have many other advantages over shaken flasks including a more efficient aeration and increased control of parameters (e.g., oxygen, temperature, and agitation) (Raza et al., 2019; Marcello, 2018). On the downside, these apparatuses can be costly, energy-intensive, complex to operate, and large, adding to the total cargo volume of space missions. On the contrary, shaken flasks are low-tech, simpler to transport, operate and wash. Similar to the ISS, future spacecrafts would have incubators aboard to allow controlled growth of plants and microorganisms. Taking advantage of the fact that incubators and shaken flasks will be taken to Mars, a simple protocol was designed for large-scale production of PHB using shaken flasks and incubators to minimize material and operation related costs and complexity associated with fermenters. The working volume, characterized here as the volume used during PHB production in the last phase of the fermentation during nitrogen starvation, was increased from 500 mL to 2 L. Increased working volumes is one of the approaches researchers use to obtain higher biomass quantities. However, higher biomass quantity does not necessarily correlate with increased biopolymer yields, therefore, polymer yield was also investigated by cell dry weight.

To attempt to improve the amount of PHA produced, an additional fermentation step was added. As mentioned, previously PHB is produced in medium when carbon is in excess (e.g., 35 g/L of glucose) and nitrogen is limiting. Ammonium sulphate, a common source of inorganic nitrogen in microbial cultivation protocols, is the main provider of inorganic nitrogen in this study. In the last step of the scaling-up process a second nitrogen starvation step was added. By further decreasing the concentration of ammonium sulphate in the medium from 5.5 to 5 g/L, the cells were further stressed in hopes of accumulating even more PHA. Media composition in both stages can be seen in **Table 3.2**. These protocol modifications resulted in a substantial increase in PHA yield when the two protocols were compared. The amount of PHB, which can be visualized in **Figure 3.6**, doubled from 30% to 64% of CDW from the initial system to the scale-up method, respectively, as shown in **Table 3.4**.

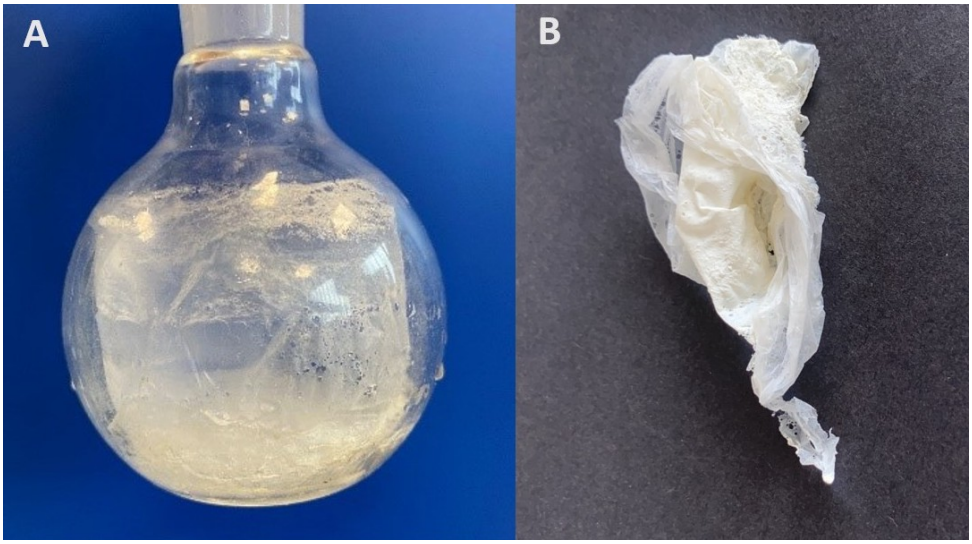

Figure 3.6 The amount of PHB obtained with the three-stage protocol as (a) visualized inside the round bottom flask after the precipitation step and (b) after overnight air drying.

In addition to nitrogen content, the agitation speed was also changed in the last stage. The speed was increased from 140 to 200 rpm to adjust for the use of a larger volume. Increasing agitation during scale-up processes might be necessary and it is a common practice to ensure uniform culture mixing and proper gas exchange. In addition to excess carbon and the limitation of nitrogen, the agitation rate is also known to affect PHB yields (Musa et al., 2016). Culture aeration, which is influenced by agitation, plays a significant role in biopolymer accumulation and cell growth (Musa et al., 2016). Therefore, optimizing agitation within a specific range is a valuable strategy for enhancing PHB yield; increased agitation promotes nutrient and oxygen transfer, manages beneficial levels of shear stress, and maintains favourable growth conditions (Wei et al., 2011). To evaluate how the different agitation speeds contributed to the increased yields, an experiment to evaluate PHB yields with different agitation speeds, ranging from the original speed to the scaled-up version, should be considered in the future.

3.3.2 Characterization of PHB

PHAs can be preliminary characterized by FTIR and more fully analysed by Gas Chromatography Mass spectrometry (GC-MS). Since a previous author (Marcello, 2020) identified P(3HB) by this *Bacillus* spp. strain, preliminary analysis by FTIR is sufficient for

the current work. The range of wavelengths scanned in this study, which was 400 – 4000 cm^{-1}, was the same reported in the literature (Trakunjae et al., 2021). In FTIR, PHAs are indicated by the presence of a characteristic peak found at around 1720-1740 cm^{-1} (Marcello, 2020).

The purified biopolymer produced by *B. subtilis* was analysed by FTIR, as described in the Material and Methods (**section 3.2.3**) The spectrum obtained was comparable to the spectrum previously described for this strain in the literature by Marcello (2020), which was characterized by a prominent peak at 1720 cm^{-1}. In the current work, the presence of a distinguishable peak at 1721 cm^{-1}, which can be seen in **Figure 3.7**, confirmed the presence of P(3HB). As mentioned earlier, the peak in this spectral region is the most frequently associated with PHAs.

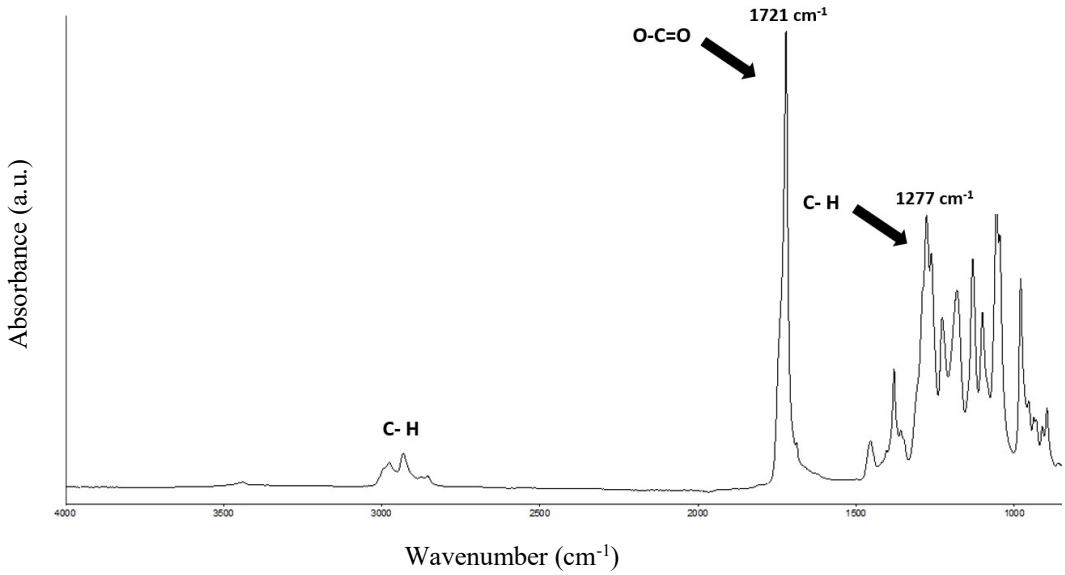

Figure 3.7 FTIR spectrum of the biopolymer produced and extracted from Bacillus subtilis OK 2 with 35g/L of glucose and with the three-stage scale up protocol.

The characteristic peak between 1720-1740 cm^{-1} relates to the stretching of the carbonyl group in the ester linkage of the molecular chain of polyesters' crystalline structure (Marcello, 2020; Trakunjae et al., 2021). A higher wavenumber for this peak indicates material with higher amorphous composition and is associated with mcl-PHAs (e.g., 1727 cm^{-1}), while lower wavenumber values, such as 1721 cm^{-1}, indicate higher crystallinity and are associated with scl-PHAs, such as PHB (Marcello, 2020; Kann et al., 2014). A second PHB marker, frequently

associated with the identification of this biopolymer is the peak at 1277 cm^{-1} which corresponds to the -CH group (Trakunjae et al., 2021).

Moreover, PHAs also present absorption bands at around 2900 cm^{-1} (Marcello, 2020; Trakunjae et al., 2021). This spectral region, more specifically peaks at 2975 cm^{-1} and 2933 cm^{-1}, relates to the stretching of carbon-hydrogen bond of methyl (CH_3) and methylene (CH_2) groups, respectively (Trakunjae et al., 2021). Similar to Marcello (2020), in this experiment, the peaks around 2900 cm^{-1} are not prominent suggesting once again the presence of a scl-PHA since prominent peaks in this are produced by mcl-PHAs instead of scl-PHAs, (Marcello, 2020; Kann et al., 2014). These FTIR spectral feature assignments are summarised in **Table 3.5**.

Table 3.5 Band assignments for the most prominent peaks found in this study and their correspondent band assignments based on information found in the literature.

Wavenumber (cm^{-1})	**Wavenumber in the literature (cm^{-1})**	**Band Assignment**	**Literature reference**
1000 - 1453	1000 - 1300 (Series of peaks)	νC-O bond of ester group	Trakunjae et al., 2021 El-Kadhi et al., 2021
1277	1282 - 1267	-CH group	Trakunjae et al., 2021
1721	1740- 1720	νO-C=O of ester bond	Trakunjae et al., 2021 & Marcello, 202; several sources
2977	2975	νC-H of methyl of group	Trakunjae et al., 2021 & Marcello, 2020
2933	2993	νC-H of methylene group	Trakunjae et al., 2021 & Marcello, 2020

Moreover, a series of peaks between 1,000 and 1,300 cm^{-1} can be found in PHB's FTIR spectrum at 1034 and 1097 cm^{-1}; these peaks correspond to the stretching of the C–O bond of the ester group (Trakunjae et al., 2021; El-Khadi et al., 2021). Finally, a band of minor

relevance, which can be found at around 3443.7 cm^{-1} is related to a terminal OH group (Trakunjae et al., 2021).

3.3.3 PHB Accumulation Over Time

In outer space applications, FTIR can quickly detect bacterial pathogens (Filip et al., 2004) inside living facilities, allowing rapid identification and contamination prevention. Additionally, FTIR can also be used to detect desired cellular components (Filip et al., 2004), as discussed in Chapter 2, such as PHAs and the ideal time points to harvest the desired product. PHB accumulation in *Bacillus* spp. supplemented with glucose was analyzed over time by FTIR and compared to PHB yield harvested at distinct phases of bacterial growth, over a five-day culture. *B. subtilis* OK2 grown on nutrient broth rather than PHB-producing media was also investigated by FTIR to be used as a reference.

The Sodium hypochlorite (NaClO) extraction protocol was used to determine PHB yield over time. While the NaClO method exhibits lower accuracy and purity compared to the gold standard Soxhlet extraction, it is particularly advantageous for its compatibility with smaller sample sizes, such as those typically obtained from bacterial cultures during evaluations of PHB content at various time points. In contrast, the Soxhlet extraction is more suitable for larger samples. The use of the NaClO method for yield estimation is common in the literature (Balakrishnan, 2011; Hahn et al., 1995; Jacquel et al., 2008). Moreover, it can be convenient when determining PHB yield through culturing time; its rapid nature allows for monitoring of PHB production, enabling adjustments of parameters for optimization of PHB production.

When Filip and co-authors (2004) cultivated *B. subtilis* at 30 °C in a minimum-strength nutrient broth, the FTIR findings resulted in a spectrum with distinctive absorption bands at 3300 cm^{-1}, 3000-2800 cm^{-1}, 1700-1200 cm^{-1} (1660, 1544 and 1235 cm^{-1}) (Filip et al., 2004). These regions correspond to changes in nucleic acid structures, cell wall components and proteins, respectively (Filip et al., 2004). Detailed information regarding the FTIR peaks associated with *B. subtilis* can be found in **Table 3.6**.

Table 3.6 FTIR absorption bands found here in *B. subtilis* OK2 cultivated in nutrient broth and the respective assignments based on literature information found in Filip et al., 2004 who also investigated *B. subtilis*.

Wavenumber in the current study (cm^{-1})	**Wavenumber in Filip et al., 2004 (cm^{-1})**	**Band Assignment**
618	540	C-O; P-O-C bonding of phospholipids and RNA
1100	1080	ν_{as}C-O-C of aliphatic esters
1228	1235	δN-H of Amide III
1655	1660	Amide I (δNH_2; νC=O; and νC=N)
1544	1544	Amide II
	3000-3600	νO-H of water
2900 - 3000	3000	νNH_2 of nucleobases
	2960- 2927	νC-H in aliphatics of cell walls

The spectrum of *B. subtilis* cultivated in nutrient broth was included in this study (**Figure 3.8**) as a reference to differentiate the PHA (1720 – 1740 cm^{-1}) and the Amide I band (1600 -1700 cm^{-1}), which have remarkably close wavelengths and are some of the bands with the highest intensity in this study. The spectrum of *B. subtilis* cultivated in nutrient broth is shown below (**Figure 3.9)** and shows the Amide I band at 1645 cm^{-1} to be the most prominent peak. The carbonyl stretching of ester bonds at 1721 cm^{-1}, dominant in PHB, was also detectable. Since NB does not trigger the accumulation of PHB due to the absence of nutrient stress, this band was minimal. The peak at around 3300 cm^{-1} was attributed to water.

Moreover, the spectra in nitrogen-limiting conditions had an additional peak. In almost every spectrum, a strong absorbance peak was observed at around 1721 cm^{-1} confirming the presence of PHB in different time points, as shown in **Figure 3.9**. PHB absorbance increased from the first to second day until reaching maximum accumulation at 48 h after inoculation, an observation that agrees with a past study (Marcello, 2020) using the same bacterial strain but a different technique (polymer yield by cell dry weight). The peak on day three was slightly lower, suggesting polymer degradation, probably due to nutrient and carbon deficiency. On day five, the peak was absent indicating complete polymer degradation. The last time point had

the same absorbance value of the *B. subtilis* OK2 grown on nutrient broth, showing the polymer content was minimal on day five.

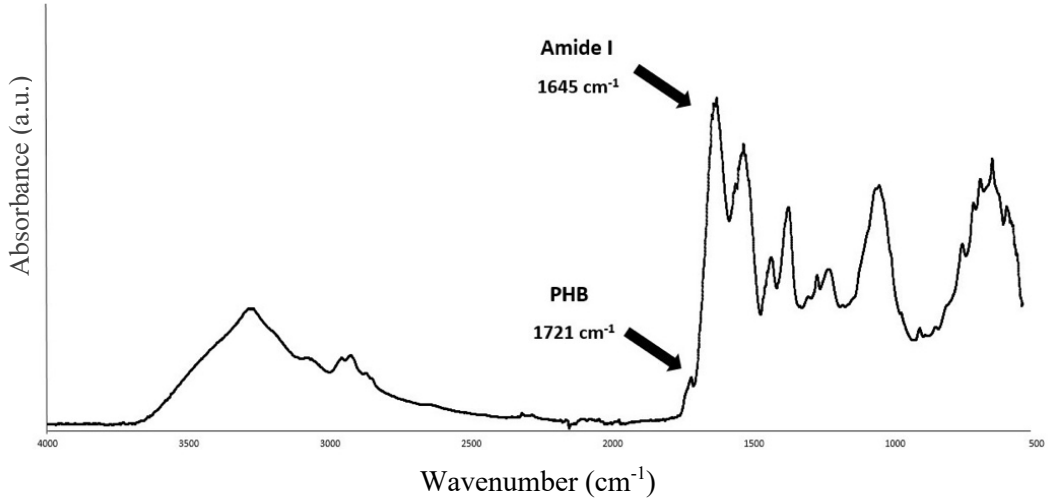

Figure 3.8 FTIR results of *Bacillus subtilis* OK2 cultivated on nutrient broth.

Similarly, the peak at 1277 cm^{-1}, the second PHB marker, exhibited a similar pattern through time, with its highest absorption peak at 48 h and complete disappearance by day 5. Except for PHB, all other major peaks, including the ones from the 3000 cm^{-1} and 1600-500 cm^{-1} regions decreased over time, specifically from 24 to 96 h, reaching their lowest intensity at day four (96 h), believed to reflect the structural changes occurring during this period in the bacterium cells as a result of nutrient stress. Though most peaks lost intensity, they all remained detectable. Interestingly, the same peaks increased again the next day (120 h), likely due to PHB consumption and consequently cell recovery and therefore a delay in sporulation.

Bacillus spp. is one of the best studied bacterial genera in terms of response to various stressors, and in particular nutrient deprivation (Hashuel & Ben-Yehuda, 2019). Upon nutrient exhaustion, the Gram-positive bacterium can enter a quiescent state and form spores (Hashuel & Ben-Yehuda, 2019). Spore formation requires a considerable amount of carbon (Wang et al., 2016), and even though the PHB content/spore formation relationship is controversial (Wang et al., 2016), past research has suggested a link between PHB consumption and sporulation in *B.cereus* (Valappil et al., 2007), *B. thuringiensis* (Navarro et al., 2006) and *B. megaterium* (Slepecky and Law, 1961).

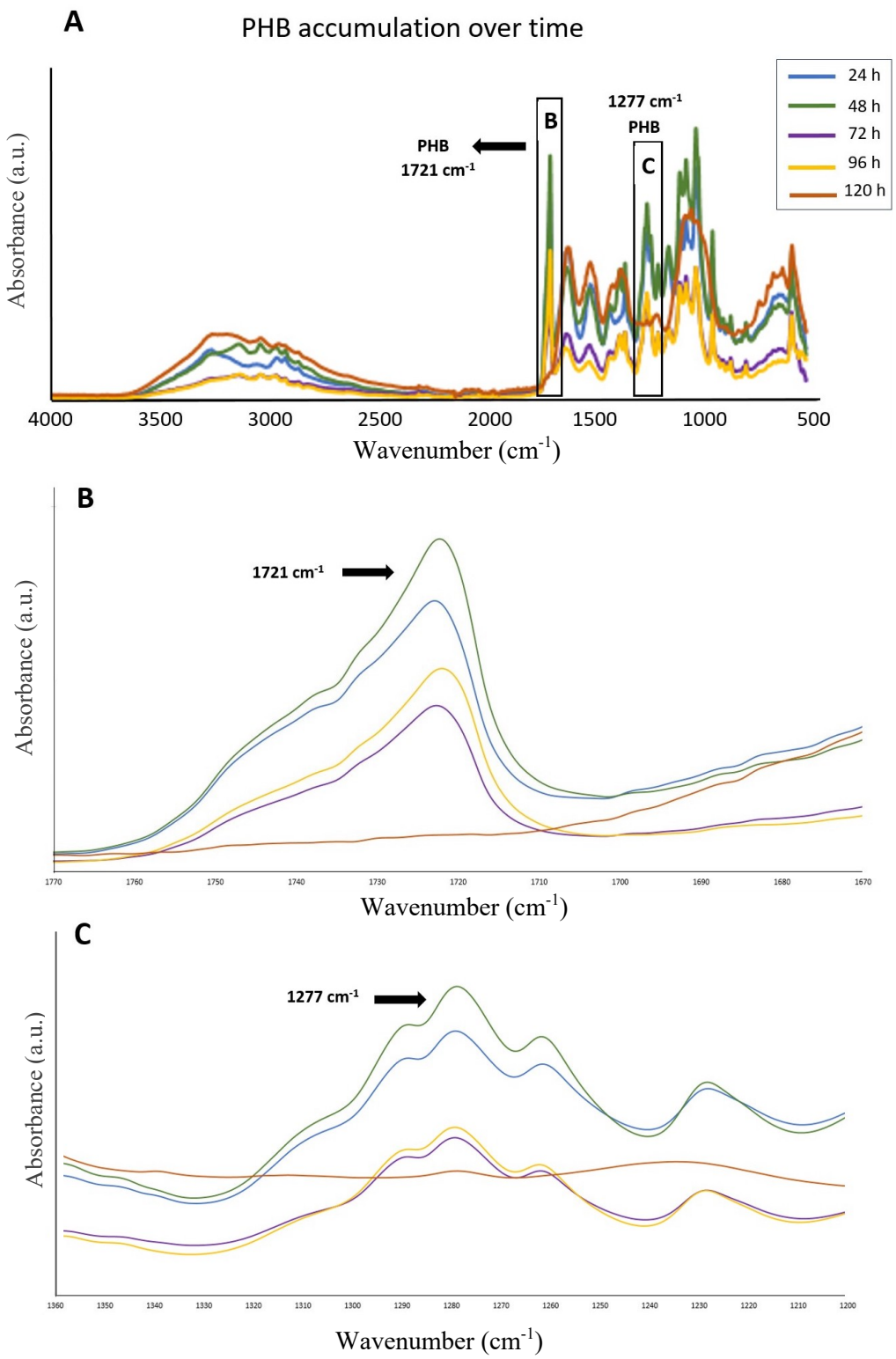

Figure 3.9 FTIR spectra of *B. subtilis* OK2 dried biomass harvested from PHB-producing media (0.5 L) supplemented with 35 g/L of glucose after 24 h (blue); 48 h (green); 72 h (purple); 96 h (yellow); and 120 h (orange). A) Shows all the spectra juxtaposed while b) and c) focus on the most prominent peaks of PHB (1721 and 1277 cm^{-1}) in greater detail.

Filip and co-authors (2004) studied IR-spectral changes of starving *Bacillus subtilis* cells over a period of a few days. The most prominent variations they observed was reduction of absorbance of proteinaceous features, namely Amide I and II (1550 and 1660 cm^{-1}) and hydroxyl groups OH (550 - 630 cm^{-1}) vibration, which was also seen in the present study. The bands responsible for cell wall components such as lipids and carbohydrates (2900 and 3300 cm^{-1}) (Filip et al., 2004) diminish on the third and four days as well. Revealingly, both the latter and the amide-associated bands increase in intensity in the last day when the PHB peaks are barely detectable.

The changing spectral feature at 1721 cm^{-1} due to PHB was quantified by calculating the peak height over time (maximum peak absorbance - baseline absorbance) and its correlation to PHB yield is shown in **Figure 3.10**.

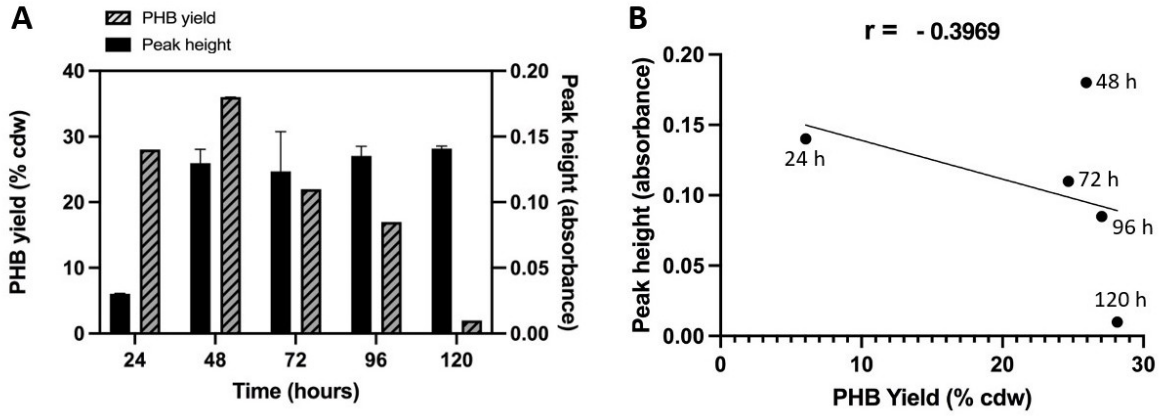

Figure 3.10 Comparison between peak height at the 1721 cm^{-1} FTIR feature associated with PHB and the actual extracted PHB yield for *B. subtilis* OK2 supplemented with glucose over 5 days. (a) The group bar chart allows the visualization of the changes in peak height and PHB yield (% cdw) during the 120 hours. Error bars represent the standard deviation of the data points (b) The scatter plot with simple linear regression and the Pearson correlation coefficient shows the weak negative correlation between the two variables with a p-value of 0.2541.

Following FTIR analysis, the remaining cell mass was used to evaluate the actual extracted polymer yield in each time point, as detailed in section 3.2.1, and compare it with the results obtained with the spectrophotometer.

As shown in **Figure 3.10A**, both the 1721 cm^{-1} FTIR spectral feature and the actual extracted yield indicate an increase in PHB within the *Bacillus* cells over the first 48 hours of culturing. However, while the extractable PHB yield then plateaued and remained at around 28%, the FTIR peak height decreased after 48 hours. At 120 hours, the 1721 cm-^{1} peak is almost absent in the FTIR spectrum but extractable PHB remains high. A scatter plot (**Figure 3.10 B**) was created to determine the correlation between peak height and PHB yield over the days. The correlation coefficient of -0.3969 indicates a slight negative correlation between the two variables, which is not statistically significant (p-value 0.2541). The weak negative relationship is unexpected and implies that the yield and peak height exhibit an inverse correlation, particularly after the cell approaches the stationary phase after 48 hours. In this phase, the extractable PHB remains high, but the peaks decrease readily. A possible reason for the reduction in the 1721 cm^{-1} peak — due to stretching of the carbonyl group within the ester linkages of the polymer — is structural changes within the PHB stored as the culture enters the late stationary phase and the cells prepare to mobilise this carbon-store with starvation and begin sporulation. FTIR spectroscopy and extracted PHB data are only in agreement until 48 hours, which is the optimum time to harvest the produced biopolymer from the culture: after this time point there are no further gains in extractable PHB.

3.3.4 Proof of concepts: starch as organic carbon feedstock

The experiment aimed to analyse the effect of modifications of the medium composition in terms of carbon source on the growth of *B. subtilis*. Since the Kannan medium allows for the elimination and replacing individual medium components it was selected for this experiment over nutrient broth. The latter is commonly purchased as a powder and provides all the ingredients necessary for growing a wide range of bacteria, not allowing the selection and substitution of single media constituents.

The preferred carbon substrates of *Bacillus subtilis* are glucose and malates (Meyer et al., 2013). However, the gram-positive bacterium can also utilise starch as carbon feedstock since it is capable of hydrolysing this polysaccharide into maltose and maltodextrins, which will be subsequently converted into glucose-6-P and enter glycolysis (Schönert et al., 2006).

Schönert and co-authors (2006) elucidated the mechanism by which *B. subtilis* uses glycogen and starch for its metabolism (**Figure 3.11**). The process starts with extracellular starch/glycogen hydrolysation and the formation of maltose and maltodextrins by an α-amylase named AmyE (Schönert et al., 2006). PTS transport maltose into the cell's interior, which is phosphorylated and later hydrolysed into glucose and glucose-6-P in the cytoplasm by MalA. (Schönert et al., 2006). Conversely, maltodextrin-specific ABC transporter takes up and transports maltodextrin without suffering phosphorylation (Schönert et al., 2006). In the cytoplasm, maltodextrins are degraded into glucose-1-P by maltogenic amylase or neopullulanase YvdF and later converted by PgcM into glucose-6-P (Schönert et al., 2006).

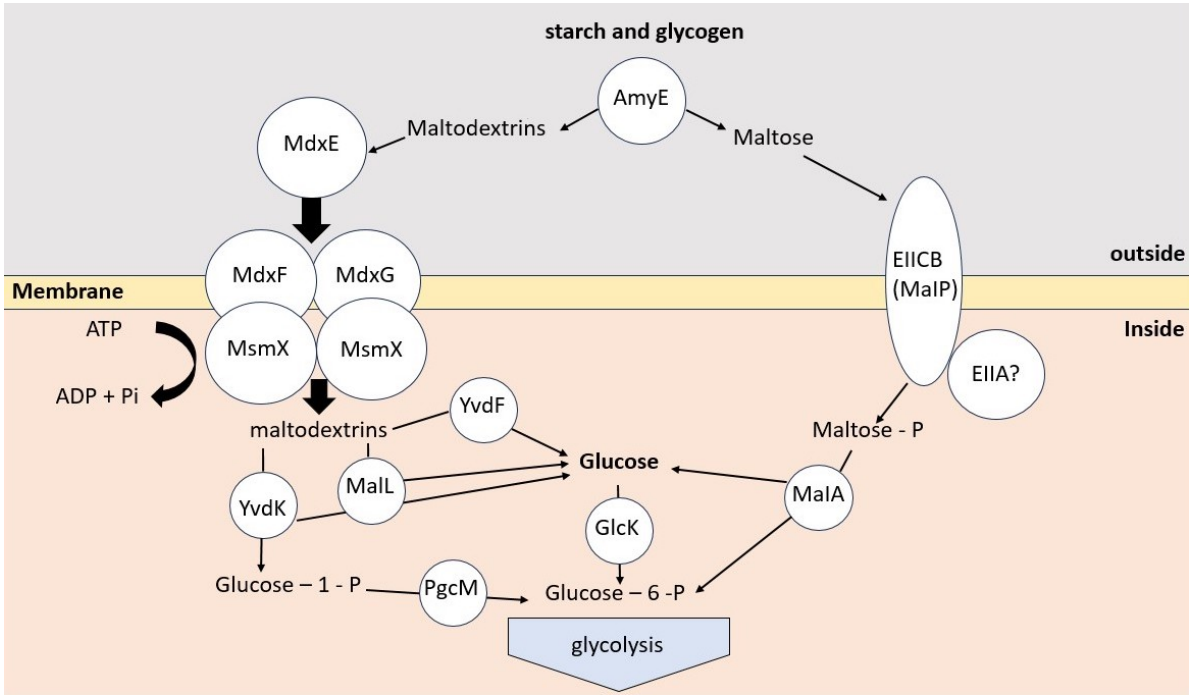

Figure 3.11 Schematic model showing the utilization model of starch and glycogen by *B. subtilis,* including the enzymes involved (shown in circles) in the extracellular and intracellular stages. In which, yvdK is maltose phosphorylase; yvdF a neopullulanase; mdx g and mdxF are components of the ABC transporter; mdxE a maltodextrin binding protein; malL an α-phospho-glucomutase; pgcM a beta- phospho-glucomutase; MsmX an ATPase; and AmyE an α-amylase. Image adapted from Schönert et al., 2006.

The choice of soluble commercial starch for the proof-of-concept experiment was based on simplicity and control. Commercial starch provides a readily available substrate for bacteria. Its consistent and well-defined composition also provides a precise platform for controlling experimental variables. Moreover, it also minimizes potential interference from

biomass and other cell components. Lastly, using commercial starch as a starting point establishes a clear reference point for future comparisons with microalga-derived starch.

In *Bacillus* sp. research, starch is commonly used as feedstock to study and induce alpha-amylase production (Bakri et al., 2012; de Souza & de Oliveira Magalhães, 2010; Ubalua, 2014). More recently, the medium components' high cost has led researchers to investigate starch and other products as substrate substitutes for this Gram-positive bacterium. For instance, a recent study investigating different carbon sources for *B. subtilis natto* BS1m and surfactin biosynthesis in this bacterium showed that starch was the best carbon source, providing the most efficient surfactin production, followed by glucose (Koim-Puchowska et al., 2021).

In the current study, for the proof of concept, glucose was replaced by commercial starch to investigate if *B. subtilis* OK2 could uptake and grow on starch. This experiment used commercial starch as an analogue for *Chlamydomonas*' spp. starch. Soluble starch was chosen rather than insoluble since insoluble starch requires heat pre-treatment to become soluble and more easily available to be uptake by different microbes.

As seen in the following growth curves, when glucose was replaced by commercial soluble starch, *B. subtilis* OK2 did not grow as well as on glucose since the log phase is slower and the maximum OD was lower for starch. However, *B. subtilis* OK2 grown on starch exhibited a growth curve closer to the glucose one, referred to here as the "standard" curve, in comparison to the yeast extract curve. The latter finding is unsurprising since *B. subtilis* is a well-known alpha-amylase producer (Raul et al., 2014). However, the maximum cell concentration obtained with starch (OD ~8) was less than the one observed when the bacterium was cultivated with glucose (**Figure 3.12**), which was OD ~10 and was slightly lower than Marcello, 2020, who studied the same bacterial strain with the same media, pH and temperature in 10 L fermenters. In both studies, maximum OD was observed at around the same time, 60 h in this study and 50 h, which was the last time point, and it was still exhibiting a growth increase, in the past study. The Lag phase in the current results lasted until 24 h for both starch and glucose. At 72 h the cells supplemented with glucose entered the stationary phase after a drop in biomass was observed. The cells fed with starch entered stationary phase slightly

earlier, as soon as they reached maximum OD. In industry, dozens to hundreds of measurements are required when studying marketable products. In academia, a few OD values are sufficient to help determine the proxy growth trend of most organisms in a timely manner (Myers et al., 2013). UV–vis spectrophotometric optical density, which is a semi-quantitative analysis, can only provide an approximately estimation and it is associated with drawbacks already discussed in Chapter 2. Moreover, OD measurements are highly dependent on culture conditions such as media composition, cell's geometry, growth phase and spectrophotometer model (Myers et al., 2013).

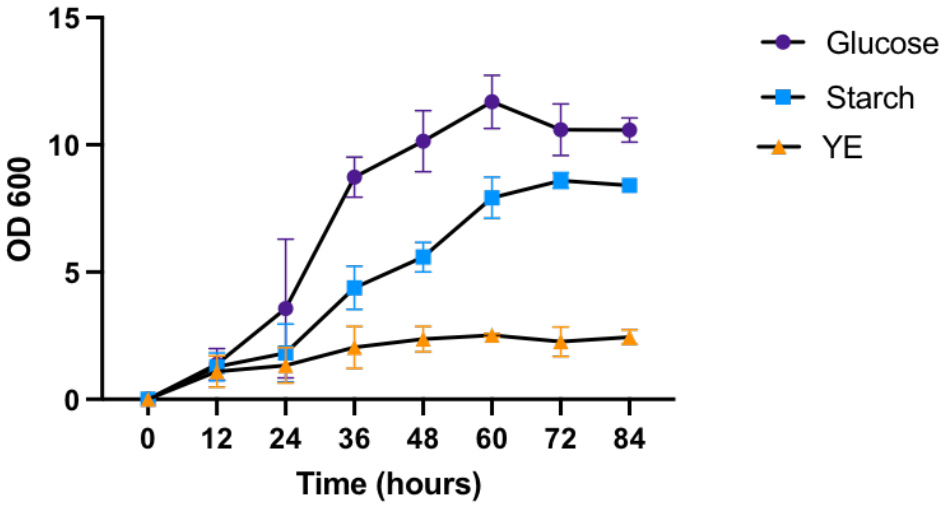

Figure 3.12 *B. subtilis* OK2 growth curves based on OD measurements at 600 nm obtained from three different media conditions with a 0.5L working volume over a period of 84 hours. The media evaluated was (a) Kannan and Rehacek recipe supplemented with glucose as sole carbon source (b) followed Kannan and Rehacek recipe supplemented with starch instead of glucose and (c) lastly, the growth tendency when the bacterium grew exclusively on yeast extract (YE). Error bars represent the standard deviation of the data points.

One possible reason that led to starch being less effective than glucose in terms of growth rate is that starch is not readily available for the cells to uptake since it requires synthesis of amylase and prior extracellular degradation of starch into simpler saccharides as described earlier. Another possible reason for the lower cell concentration associated with starch could be that *Bacillus* sp. growth conditions, mainly temperature and pH, were not ideal for maximum amylase activity and, consequently, maximum starch degradation by this strain. Future work could involve investigating the proper conditions for the most efficient enzymatic activity or

increasing the concentration of starch, which was given at the same concentration of glucose for a straightforward comparison.

Yeast Extract (YE) is one of the best nitrogen sources for different bacteria (Hakobyan et al., 2012). Ammonium sulphate is added to the Kannan recipe as a source of inorganic nitrogen, while YE's amino acids mixture provides organic nitrogen. However, YE also contributes to bacterial growth with vitamins, growth stimulants (Hakobyan et al., 2012) and carbon (Tachibana et al., 2019). YE was therefore studied without the addition of other ingredients, including carbon source, to investigate the extent of its contribution to *Bacillus* spp. growth. Once more, OD measurements were used to track cell growth. The findings can also be found in **Figure 3.12**.

As expected, the organism grew exclusively on YE since this ingredient has critical ingredients that support bacterial growth. However, maximum OD value was ~2, which is five and four times lower than the one obtained with glucose and starch, respectively showing that is the combination of other ingredients including the addition of carbon sources which contributes more to *Bacillus* growth. Even though the growth seemed to follow the standard growth curve introduced in Chapter 2, the different growth stages were not as noticeable. Nonetheless, it can be concluded that YE is a major media component capable of supporting *B. subtilis* OK2 growth.

3.3.5 *Chlamydomonas* spp. hydrolysed biomass as glucose replacement for PHB production

The previous experiment confirmed that *B. subtilis* OK2 is capable of growing on soluble starch as a sole carbon source. The next step of the project was producing PHB by replacing glucose/starch for WT *Chlamydomonas* biomass pre-treated by acidic hydrolysis. WT was chosen over the mutant due to the higher content of starch determined by the Megazyme kit after treatment, as seen below in **Figure 3.13**.

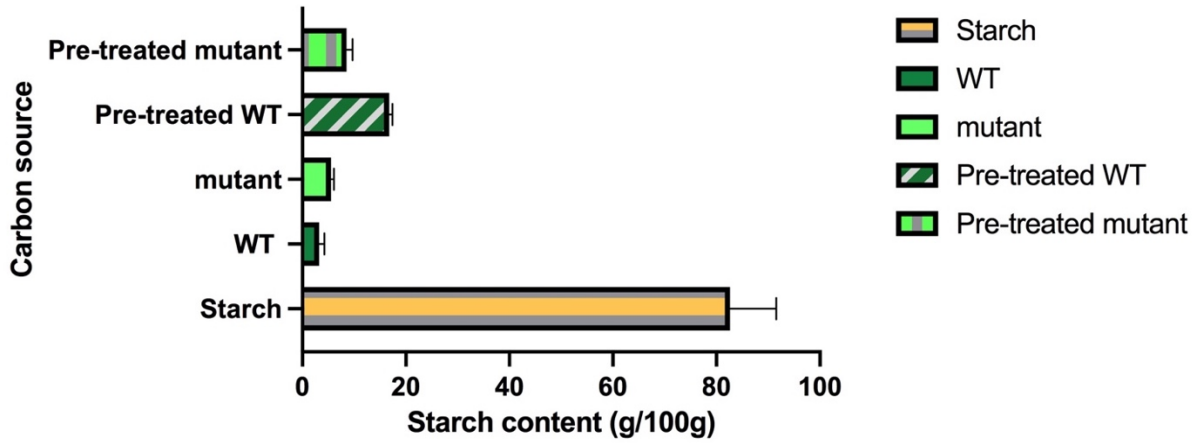

Figure 3.13Starch content for the different carbon sources studied in this chapter. Starch content was determined by the Megazyme Total Starch Assay Kit. The pretreatment involved acid hydrolysis with 3% sulfuric acid at high temperature. Error bars represent the standard deviation of the data points.

The kit selected, which was introduced in Chapter 2, quantifies free glucose in samples by measuring the production of quinoneimine, which turns red in the presence of peroxidase. All samples were subjected to hydrolysis with α-amylases, a step that can be skipped in soluble starches but was kept for close comparison among all tested carbon sources. Free glucose is then converted by mathematical calculations to anhydroglucose, which is the glucose form present in starch.

Since pre-treated WT exhibited the highest amount of starch with (16.75g/100g ± 0.67) it was selected as the feedstock of choice for polymer production. Distinct stages of the polymer production process can be seen in **Figure 3.14**. In the different figures a green tone can be seen. The colour is the result of the presence of photosynthetic pigments which indicates that the purification protocol with methanol was not sufficient, more rounds of purification was needed due to the complexity of the extract. In such case, in addition to pigments, the final unpurified polymer might still also have attached extracellular polymeric substance (EPS). EPS are organic polymers composed of a mixture of carbohydrates, proteins, and other substances, produced by several microbes, and associated with the formation of biofilms (Costa et al., 2018). EPS are known for being capable of interacting with other polysaccharides (Nishanth et al., 2021) and can therefore interfere with PHB properties if present. For instance, a past

research showed that PHAs EPS fibres decreased PHB's crystallinity and improved its mechanical properties (Zhao et al., 2021).

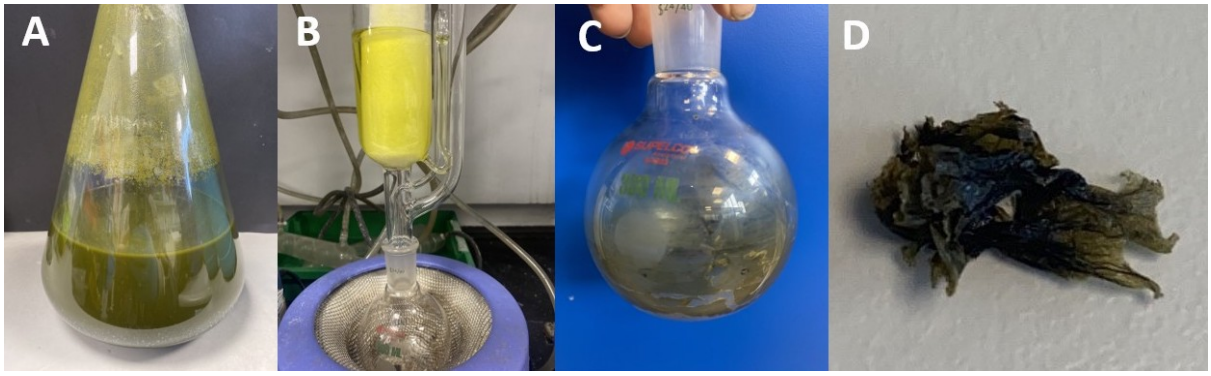

Figure 3.14 Production of PHB using hydrolysed biomass algae (35 g/L) as feedstock which includes a) fermentation in Kanan recipe, b) purification, c) precipitation via rotary evaporation, and d) the final product after being airdried.

The polymer obtained, shown in the above figure (**Figure 3.14**) was more flexible and smother in nature when compared to the glucose produced PHB. Due to the green colour of the extracted product, the polymer was placed in a 10 mL chloroform solution for 2 h to further reduce the colour. Since chloroform is the solvent of choice for the 2D films and 3D porous structures the green colour was gradually lost in the following experiments, as can be seen ahead. This observation means that polymer extraction using pure culture of *Chlamydomonas* spp. as feedstock should include more rounds of polymer purification with ≥ 99% methanol.

A temporal analysis that included the three main paraments ($OD_{600,}$ PHB yield and pH) was performed, as mentioned before. Nitrogen concentration and the amount of reducing sugars are two important parameters in the temporal profile of PHA production. Since the project's goal was to validate fermentation and determine if and what PHB *B. subtilis* OK2 yield can produce using *Chlamydomonas* hydrolysed biomass as the sole carbon source, those two parameters were skipped. Nonetheless, evaluating nitrogen and reducing sugars concentration over time is recommended in Chapter 6, which discusses future work and optimisation of PHB content.

As expected, a pH decrease was observed over time. The pH value lowered from ~7 to ~6 during the first 24 h. pH decreases during fermentation are attributed to the consumption of

amino acids and calcium content, which are responsible for the buffering capacity of the media and production of acids during microbial growth (Zannini et al., 2022). Marcello, 2020 also observed a decrease in pH from 6.8 to 5.2 while studying the temporal growth of this strain under similar conditions and supplemented with glucose as carbon source. The drop in pH was more evident in the past study in which the final pH values at around 48 h were close to five rather than six and exhibited a drop within the first fermentation hours as a result of rapid ingredient consumption. The most considerable pH drop in the present study was also seen in the first few hours (12 h) but the overall swifter pH decrease obtained in the current results might be the result of slower carbon and nutrient consumption probably due to the fact that bacterial cells are not utilizing the algae feedstock as well as commercial D-glucose. In fermentation, after a certain time, pH has a tendency to increase when the cells run out of carbon and start consuming the acids produced in the earlier stages of fermentation. Since pH increased towards the end of the second day (~60 h), one can conclude that at this time point the carbon had been completely exhausted in the medium.

Maximum OD was ~9. Visually, the culture colour changed from clear dark green to an opaque Earth-tone green (**Figure 3.14**), indicating bacterial growth. However, the OD values observed, shown in **Figure 3.15**, were higher than expected an observation in parallel with the previous section where optical density was discussed. Exponential phase was still obtained at 2 h and stationary phase at 60 h (OD ~9).

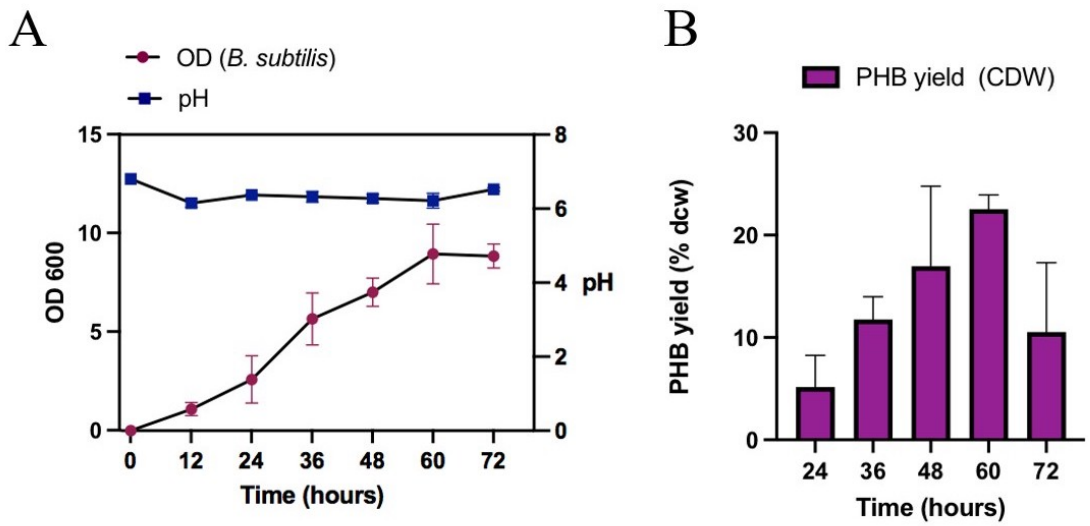

Figure 3.15 Temporal profile of *B. subtilis* OK2 cultivated using 35 g/L of *Chlamydomonas* biomass which was hydrolysed before it was fed to the bacterium as a carbon source. All the measurements were obtained over a period of three days. (a) Optical density and pH shown on the left are an average of triplicates and (b) PHB yield values shown on the right are the results obtained with duplicates.

B. subtills OK2 was able to produce a maximum PHB yield of 23% ± 1.45 of CDW and 0.18 ± 0.1 g/L of PHB when grown on WT *Chlamydomonas* hydrolyzate with a productivity of 7.6 mg/L/h. Maximum accumulation was seen at 60 h, which was slightly later than the one observed with glucose. A gradual increase of PHB yield (% CDW) was observed through time with a decrease on the third day. PHB yield was slightly lower than the glucose counterpart. The lack of a difference between the results between glucose and algae pre-treated biomass can indicate that in fact, the concentration of starch in the *Chlamydomonas* solution might not be 7-8 times lower than glucose as discussed earlier or/and that B. subtilis could be also using other types of *Chlamydomonas* related sugars and cell constituents for its metabolism. Moreover, the PHB yield obtained with the hydrolysate (23% ± 1.45 of CDW) was similar to the PHB yield obtained with glucose (29.56% ± 3.33), as mentioned above. This observation suggests that the *Bacillus* cells produce a similar amount of PHB with both substrates. However, despite the similar yield of dry cell weight, the concentration of PHB with the hydrolysate (0.18 g/L) was approximately half compared to that with glucose (0.32 g/L). This could be because *Bacillus* exhibited fewer and slower growth when supplemented with the hydrolysate, reaching a maximum optical density (OD) of ~9 at around 60h (Figure 3.15A), while the *Bacillus* supplemented with glucose reached an OD of ~10 at 48h under similar

conditions (Marcello, 2020). These findings underscore the importance of substrate selection in PHB production, as it directly impacts the growth rate and, consequently, the yield of PHB.

The outcome of this experiment links the main two goals of this thesis, which is the production of PHB by *B. subtilis* OK2 using pre-treated *Chlamydomonas* biomass grown in a low-tech bioreactor, as schematically shown in the **Figure 3.16**. The quantities of feedstock required and amount of product obtained for each stage are also shown in the scheme. Overall, per 0.5 L of *Bacillus* culture, 0.1g of PHB can be obtained. To put this into context, 1.5 L of the *Bacillus* is sufficient to produce enough biopolymer to create three porous structures with medical significance or one 2D film similar to those shown in **Figure 3.18.** Overall, 0.5 L of *Chlamydomonas* culture at the start of the two-phase system produces ~0.1g of PHB. This is a relatively low efficiency, but represents the production of functional bioplastic from photosynthetic growth suitable for a Martian habitat, and as both the photosynthetic bioreactor and *Bacillus* fermentation stages can be further optimized, the overall efficiency has potential to be improved in the future.

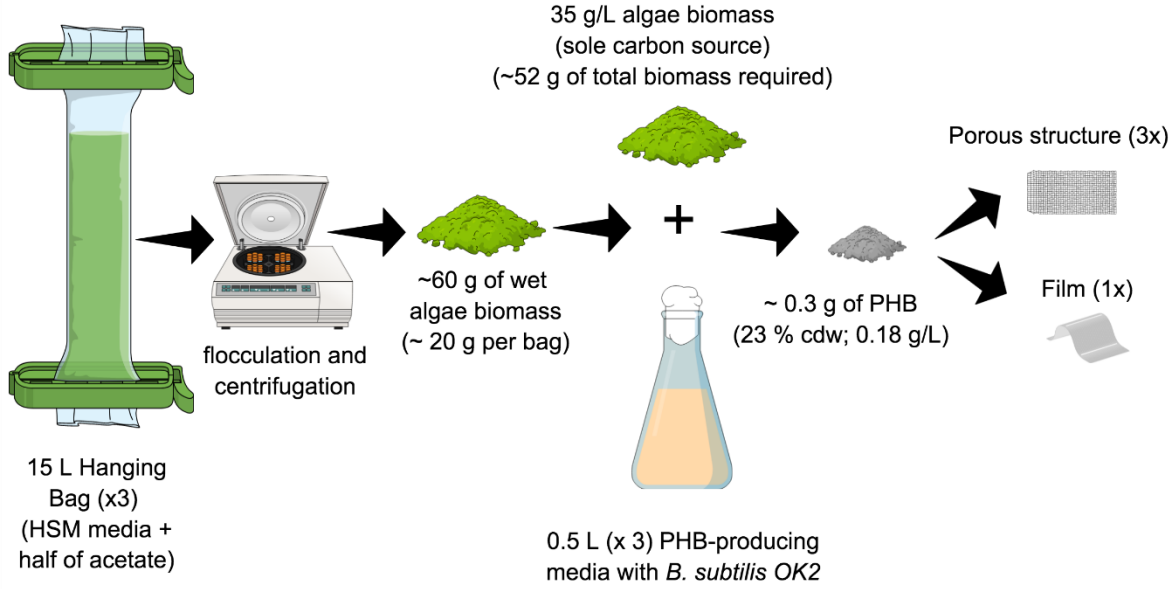

Figure 3.16 Schematically representation of the process, from algae growth in the bioreactor to PHB production and its applications. All the quantities required to operate the systems and amount of products obtained in each stage are shown in the figure.

To increase the amount of polymer, one can also test increased amounts of biomass. Other parameters should be investigated and optimized as detailed in Chapter 6. The scale-up process described earlier for glucose can also be used to increase the amount of polymer than can be obtained when using WT *Chlamydomonas* as feedstock. Alternately, synthetic biology can help introduce amylases into *Chlamydomonas* to help hydrolize starch and simultaneously increase available sugars and remove the pre-treatment step making the process quicker. Since the last approach offers two advantages over one it was the selected one to continue optimizing the process which will be addressed in the following chapter (Chapter 5).

3.3.6 Spectral differences between PHB obtained from glucose and algae

PHB extracted from *B. subtilis* OK2 grown on algal-derived feedstock was analysed by FTIR and compared to the PHB spectrum (**Figure 3.7**) produced on glucose medium, as shown in **Figure 3.17**. Both spectra are similar, including the presence of PHB's characteristic peaks 1721 and 1277 cm-[1] confirming the presence of pure PHB and this strain's capacity to produce PHB with algae as a sole source of carbon feedstock.

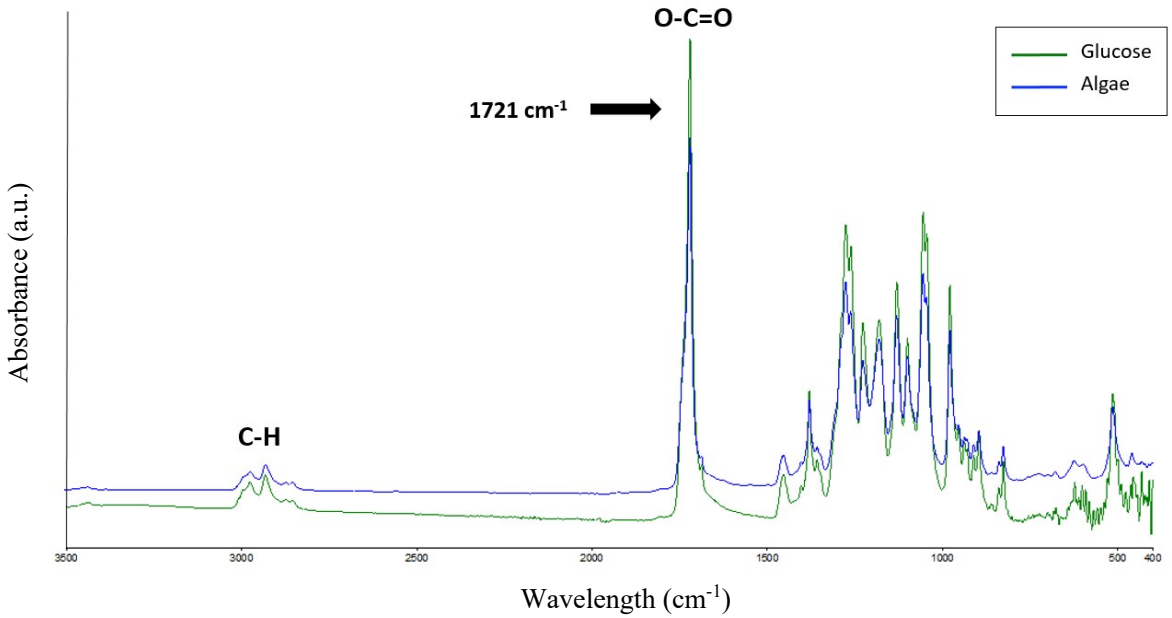

Figure 3.17 FTIR spectra of PHB obtained with glucose (green) and hydrolysed *Chlamydomonas* biomass (blue) as sole carbon source.

3.3.7 The hydrophilicity of solvent-cast PHB films

The PHBs obtained with glucose and algae biomass were used to fabricate solvent-cast films, as seen in **Figure 3.18**, which can be used in the packaging industry and to analyse polymer' properties. Despite its limitations, such as cost and safety handling (Anbukarasu et al., 2015), chloroform is one of this technique's most frequently used solvents thanks to its high solvation capacity (Byun et al., 2012). The resulting films are also smoother and less cloudy

than those produced by other solvents (e.g., acetic acid) since evaporation of this solvent at room temperature occurs at a slower rate (Anbukarasu et al., 2015).

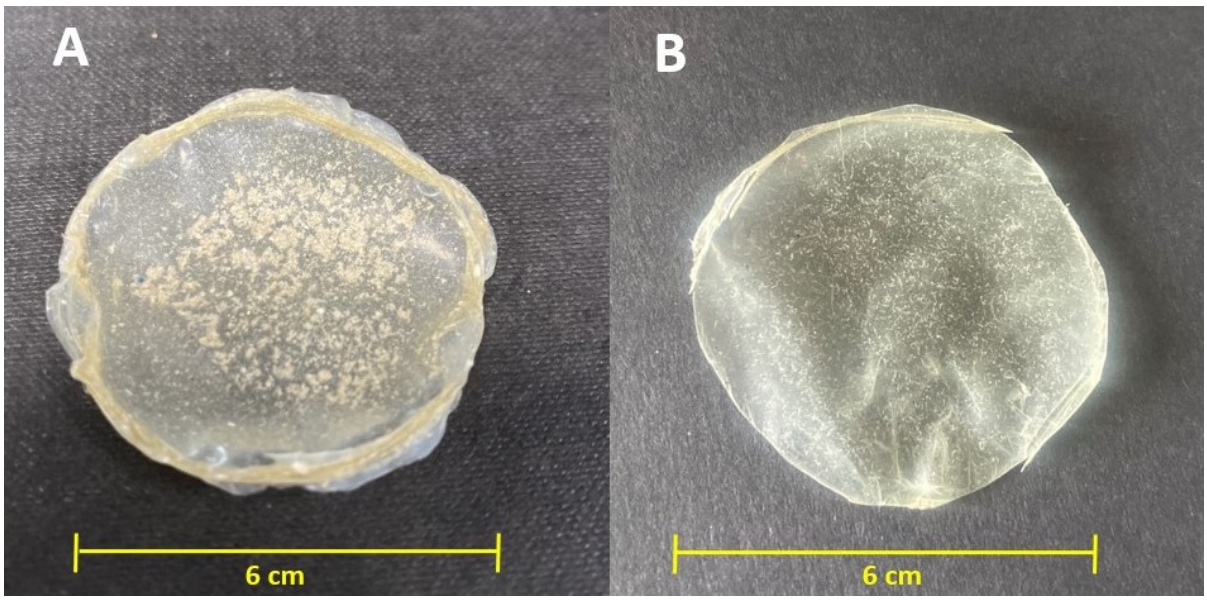

Figure 3.18 Solvent cast 2D films were produced with PHB by *B.suttilis* OK when suplemented with 35g/L of glucose (left) and 35g/L of hydrolized algae biomass (right). Both were trimed with scissors.

Differences between the two films were observed during macroscopic observations. In the one on the left, produced with glucose, impurifications could still be seen in the middle of the circle. Furthermore, Glucose-produced PHB, referred to as standard PHB, resulted in a thick, brittle white opaque film. The second film was more flexible, thinner, less opaque and less "sandy." The higher malleability could be a result of lower crystallinity as discussed earlier in this chapter. One can therefore conclude that algae-based feedstock is therefore capable of producing malleable plastic that can be used to create pastic films with various applications.

Neither film was perfectly smooth. This observation is in agreement with the findings from the literature, which state that PHB films exhibit a rough surface due to the presence of pores and protrusions (Rai et al., 2011; Anbukarasu et al., 2015; Marcello et al., 2021) which have been attributed to its high degree of crystallization (Kai et al., 2003; Li et al., 2016c; Marcello et al., 2021).

In addition to macroscopic observation, the materials' wettability was also characterized. Adeshion is an important property of polymers and solid materials (Orf et al., 2017). A polymer's adhesion is influenced by its wetting behaviour (Rios et al., 2012; Su et al., 2021), or in other words, the ability of a solid surface to remaintain in contact with a liquid (Zhao & Jiang, 2018).

Wetting is commonly evaluated using the water contact angle technique, also called WCA, a rapid and straightforward method (Chang et al., 2018). WCA measures the hydrophobicity or hydrophilicity of a polymer's surface by measuring the angle at which a liquid droplet (e.g., water) extends along the solid's surface (Zhao & Jiang, 2018). When the liquid being tested is water, and the WCA measurement is below 90°, the surface is defined as hydrophilic and hydrophobic when WCA is above 90°. If the contact angle equals 90°, the surface is considered intermediate-wet.

The recorded values for water contact angle for both PHB films were below 90.0°, as seen in **Figure 3.19**, meaning that they were both hydrophilic. Standard PHB, shown on the right, was 75.0°, closer to 90.0°, much less hydrophilic than algae-produced PHB, which was approximately 40.0°. The value for standard PHB was almost identical to the one found in the literature. Chang and colleagues (2018) reported a water contact angle value of 76.0° for untreated PHB films cast with chloroform.

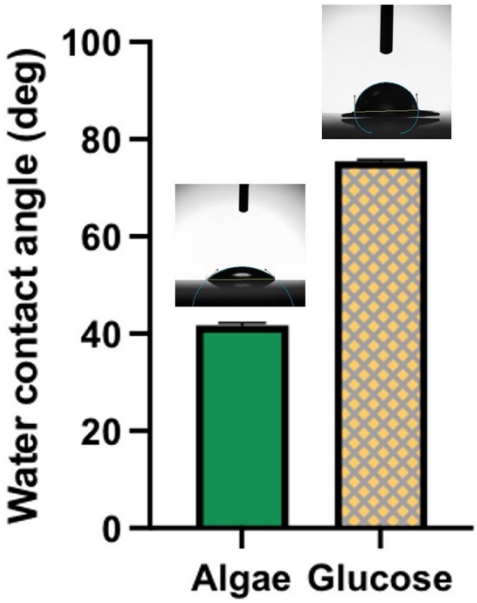

Figure 3.19 Water Contact Angle values measured for PHB 2D films poduced with 35g/L of hydrolized algae biomass (left) and glucose (right) by *B. subtilis* OK2. The measuremtns are averages of duplicates.

The algae PHB surface had a contact angle twice as low as the standard PHB and, therefore, lower adhesion. The improved hydrophilicity of the film's surface was probably a result of the cleavage of hydrophobic residues and the formation of new hydrophilic groups (Wang et al., 2006; Chang et al., 2018). The difference between the two contact angles was probably due to impurities, such as algae cells on the PHB produced with biomass rather than glucose, which conferred a green colour to the film. It has been shown that algae can decrease the hydrophobicity of silicon rubber in the past (Yang et al., 2019) since, by nature, algae is hydrophilic, leading to water accumulation (Kumagai, 2007).

Therefore, algae biomass and cells can be used to increase PHB's hydrophilicity. Different ratios of PHB and algae concentration can be mixed and investigated to increase the wettability of PHB films. Both superhydrophobic (WCA>150°) and superhydrophilic (WCA<10°) surfaces are of interest in the biomedical field; for instance, superhydrophobic surfaces can resist bacterial adhesion, while superwettable offer the advantage of facilitating cell attachment (Su et al., 2021).

One of the challenges preventing PHB's widespread application is the difficulty in producing flexible PHB films that can be thermally processed, which is limited by its high crystallization and melting temperature (Anbukarasu et al., 2015). Heat treatment, co-polymerization and blending are some of the approaches being explored to overcome this roadblock (Anbukarasu et al., 2015). This result shows that algae should be explored in PHB blends to increase its wettability and processing (Stoudt, 2017).

3.3.8 The efficiency of salt leaching in producing 3D structures

Medical instruments will be necessary during deep space missions for medical emergencies such as surgeries, where tissue replacement might be necessary. Biopolymers can be processed into porous scaffolds, which can be used for tissue engineering (Ambekar and Kandasubramanian, 2019; Socci et al., 2023; Tessmar and Göpferich, 2007). Solvent casting leaching is one of the main techniques for fabricating 3D porous constructs (Marcello, 2020). One of the main advantages of this technique is the small quantity of polymer required to produce the final product and the fact that it can also be employed to fabricate larger structures if necessary (Tessmar and Göpferich, 2007). Salt leaching is achieved by mixing the polymer in a suspension with a porogen, usually salt or sugar, and an organic solvent (e.g., chloroform) (Marcello, 2020). Inorganic salts (e.g., ammonium carbonate) and sugars are the pyrogens of choice since they are insoluble in organic solvents and removable by water, leaving only behind the polymer structure, which is insoluble in water, during the washing phase (Tessmar and Göpferich, 2007). Another advantage of salt-leaching is that it can be coupled with other methods, such as 3D printing, to obtain 3D structures with dual and increased porosity (Marcello, 2020; Tessmar and Göpferich, 2007). Moreover, the final structures can be redissolved and poured into different moulds.

Salt leaching was first described in 1993 and 1994 (Mikos et al., 1993; Mikos et al., 1994). Sodium chloride (NaCl) was the first and is currently the most frequently explored porogen (Tessmar and Göpferich, 2007; Tran et al., 2011) as it has proven efficient for producing crystallized solid porous.

One of the main goals of salt-leaching is to produce scaffolds with uniform porosity that can otherwise result in thin films with decreased porous accessibility (Tessmar and Göpferich, 2007). One of the most critical steps in the methodology is a slow drying rate commonly achieved by using a glass cover. Moreover, the porogen/polymer ratio is a critical parameter for controlling pore size and quantity (%) of porosity (Prasad et al., 2013; Marcello, 2020). The literature reports that the optimal crystal dimensions to develop interconnected pores similar in size in PHA scaffolds range from 100-300 μm (Marcello, 2020).

In attention to all the details mentioned above, the possibility of developing 3D scaffolds with algae produced PHB via salt leaching was investigated. The resulting products, shown in **Figure 3.20**, were shaped by the mould structure, and distributed uniformly with an interconnected porous structure, as seen macroscopically. The thickness size of the medical structure was around 3mm. The structure fractured when force was applied, the resulting trimmed square can be seen in the figure below.

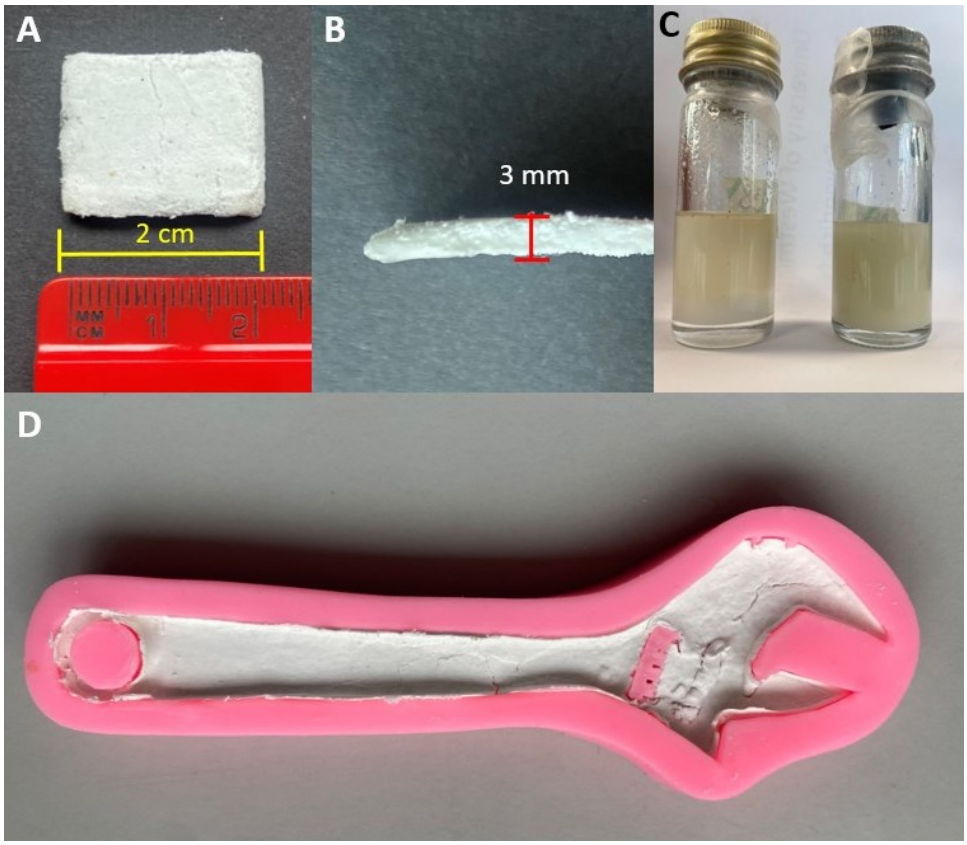

Figure 3.20 3D scaffolds fabricated using the salt-leaching technique. Front (a) and side (b) view of porous structure with medical relevance and (d) wrench. The image also includes (c) sample preparation.

In addition to the medical field, the possibility of producing 3D structures useful for the astronaut's routine life via salt leaching was also investigated. For this study, a wrench mould was selected since a wrench was the first object with practicality printed in space, as discussed in Chapter 1. A silicon mould was chosen considering that silicon is one of the most common materials used to make scaffolds due to its resistance towards chloroform. Nonetheless, concerns regarding the effect of chloroform on the silicone rubber wrench mould, which was softer than the medical structure, was first investigated by producing a 2D film. Since chloroform did not dissolve the mould, the solution with sodium chloride was poured next. Salt-leaching was capable of producing a solid structure with a rubber-like structure (**Figure 3.20**). However, the structure was not strong enough to be functional and was also prone to break easily. The later was probably due to the content of salt. Future attempts should include testing of reduced salt concentrations and different poragen:polymer ratios.

The scaffold square with medical relevance, which can be used to repair damaged organs or tissues (Kwon et al., 2020) was less prone to break probably due to its smaller dimensions (2cm x 2cm). One can therefore conclude that salt-leaching is an optimal choice for manufacturing 3D compact structure. Other techniques should be explored for larger objects.

3.3.9 Additive manufacture with PHA-based filaments

Finally, the possibility of using PHA-based filaments in fused deposition modelling FDM 3D printing to produce tools useful for space exploration was investigated. Due to temperature-related limitations, 3D printing with the PHB obtained by *Bacillus* sp. was not possible with the University of Westminster's CELLINK INKREDIBLE+ printer (Sweden). PHB has a melting temperature of 170 °C, while the bioprinter has a maximum printing temperature of 130 °C.

As discussed in Chapter 1, the printers being developed for space exploration and the ISS are based on FFF and FMD-based technology, which use filament as printing material (Denine and Siegfried, 2022). Due to the PHB's brittle nature, the biopolymer is blended with plasticizers or other polymers to facilitate its use in 3D printing applications (Pereira et al.,

2012). Blending tests and experimentation with different plasticizers and blend compositions would be necessary to attempt printing with the PHB obtained from the laboratory. Subsequently, the selected blend must be transformed into a filament first to be used by most FDM printers available. Both these steps are time-consuming and would constitute a separate chapter due to the amount of work involved. Due to time constraints, two commercial PHB blends were evaluated instead. Moreover, since exotic blends can damage printers and nozzles, the two blends were also printed commercially with the help of experts who have previously printed with similar material. Nonetheless, Chapter 6 includes the steps necessary for manufacturing filaments with PHB blends created in the laboratory for future reference.

The work presented here was conducted in collaboration with Champion 3D (London, United Kingdom), experts in 3D printing with biodegradable material. The additive manufacturing technique selected was FMA since NASA used an FDM printer to manufacture the first 3D object to meet astronauts' needs in space, a wrench, as shown in Chapter 1. Most filaments can be purchased in two different dimeters, 1.75 and 2.85 mm. In this study, the size of 1.75 mm was chosen over the latter since it heats and melts faster resulting in a faster printing and less filament oozing.

PLA/PHA blends, introduced earlier in this chapter, have started to be widely researched thanks to their favourable printing properties (Plavec et al., 2022). As a result, a few PLA-PHA filaments, optimized for FDM, have been made commercially available in recent years. Three PHA-based filaments suitable for FDM printing are currently on the market, listed in **Table 3.7**.

ColorFabb (Belfeld, The Netherlands) distributed the first PLA/PHA filament, sold under the name allPHA®, which was characterised by a blend of PLA with the PHB's copolymer Poly(3-hydroxybutyrate-co-3-hydroxyvalerate (P(3HB-co-3HV)) in an 88:22 ratio (Ausejo et al., 2018). The copolymer was added to improve PLA's ductility resulting in a 40% increase in elongation break and a 25% decrease in mechanical strength (Kaygusuz & Özerinç, 2019; Ausejo et al., 2018; Marcello, 2002).

The NONOILEN® filament from Fillamentum Manufacturing Czech (Hulin, Czech Republic) combines PLA with PHB to increase biodegradability by three times that of the PLA counterpart (Plavec et al., 2022). The blend is made of > 10% of PLA, > 30 % of PHB and < 15 % of oligomer plasticiser concentration (Plavec et al., 2022). The exact composition of blends is frequently not disclosed due to commercial purposes. The recyclability of this filament was investigated in multiple printing rounds; reprocessing did not result in significant changes in the thermophysical properties (Plavec et al., 2022).

PLAyPHAb® from 3D Print Life (Southborough, Massachusetts, United States) is another filament that offers more flexibility, according to the manufacturers' website, than the PLA filament from the same company. PLAyPHAb® also meets the ASTM D6400 standards for biodegradable materials.

Table 3.7 List of commercially available filaments with PHAs in their composition and respective manufacturer, market name, nozzle temperate range, and composition where * indicates unknown material.

Manufacturer	Name	Blend composition	Nozzle temperature
ColorFabb	allPHA	PLA/PHBV	190 – 200 ºC
Fillamentum	NonOilen	PLA/PHB/oligomer plasticizer	175 – 195 ºC
3D Print Life	PLAyPHAb	PLA/PHA*	210 – 250 ºC
3D Print Life/Algix	ALGA	PLA/remediated algae	185 – 210 ºC

3D Print Life (Southborough, Massachusetts, United States) has also commercialised another product relevant to this thesis. The Alga® filament is an algae-based filament from a partnership between 3D Print Life and Algix (Meridian, Mississippi, United States). As per information from the manufacturers, the filament is made of PLA resin and nuisance invasive algae collected from lakes, ponds and other water reservoirs by the dissolved air flotation technique.

The first step in additive manufacturing is designing or selecting an already available design and exporting it in a file format supported by CAD (Computer Aided Design) software. STL (Standard Triangle Language or Standard Tessellation Language) files encode and "describe" to the printer the 3D surface geometry of the object of interest.

The 3D ratchet wrenches obtained here, which can be seen in **Figure 3.21**, were made using the commercial PLA/PHA filaments (NonOilen and allPHA) described earlier and the same STL that NASA and Made In Space used to print the wrench aboard the Internation Space Station. The file (**Figure 3.5**) was made available to the public in 2015 by NASA and can be obtained as described in the material and methods section.

The aim was to print 3D wrenches similar in size to the 3D mould studied in salt-leaching for comparison. Therefore, the dimensions selected in terms of length (15 cm), height (5 cm) and width (1.5 cm) were the same as the wrench obtained by salt leaching. The two filaments selected - NonOilen and allPHA - were chosen since they are PHB-specific. The first has PHB in its composition while the other blend is made off PHB's copolymer PHBV, as discussed earlier.

The wrenches, shown in **Figure 3.21**, were a result of the deposition of 130 layers of material. The printing settings used the nozzle temperature range recommended by the manufacturer and listed in **Table 3.7**, but no heated bed. Each construct took approximately two hours and a half to print and were printed with the same printing settings. Initially, problems arose when trying to stick the initial layers to the heat bed. To overcome this issue a glass bed was tested but without success. The solution was a sticker bed (BuilldTak, Gent, Belgium) and a raft (**Figure 3.22**) placed between the bed and the first layer of printed wrench, which when attached temporarily provided greater adhesion.

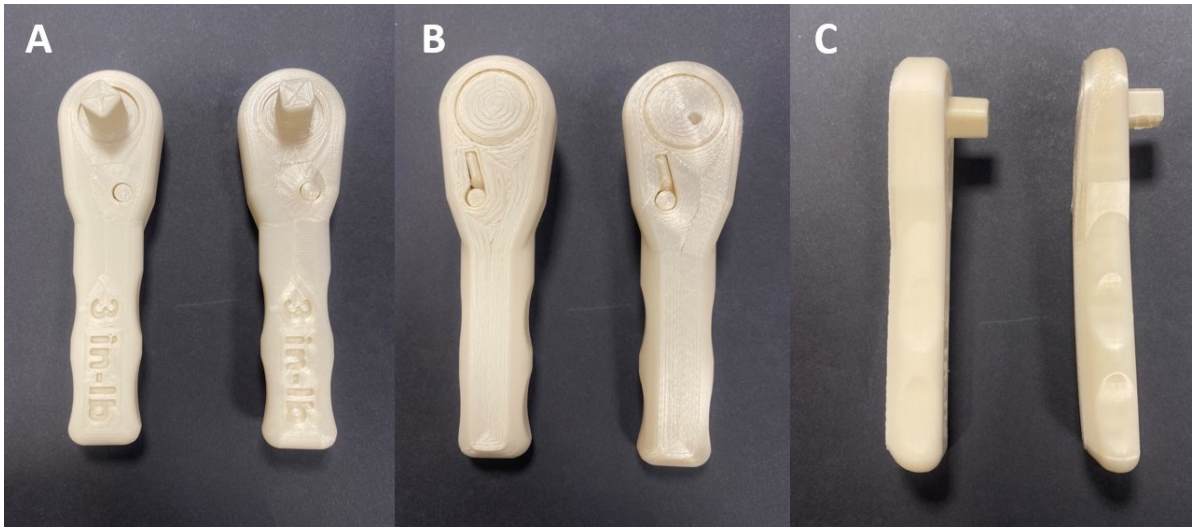

Figure 3.20 3D printed wrenches obtained by FDM with the NASA/Made in Space, Inc. stf file. As before, the figure shows different angles of the wrenches including a) the front, b) the back, c) and the side view. In every image, the wrench produced with allPHA (ColorFabb) is on the left while the NonOilen (Fillamentum) product in shown on the right. Visually, both wrenches can be distinguished by the presence/absence of a gloss finishing characteristic of the latter one.

Despite initial difficulties, **Figure 3.21** shows that the wrenches fabricated via 3D printing resulted in layered, solid and rigid structures. Additive manufacturing was more efficient than the salt-leaching method regarding repeatability and the structure's shape and stability. Kwon and colleagues (2020) reported similar results when comparing poly(ε-caprolactone-ran-lactic acid) scaffolds created by salt leaching and FDM (Kwon et al., 2020). In the current study, the structure from the mould was flattened, probably due to structural disintegration and rapid collapse due to irregular pore structure (Kwon et al., 2020).3D printing is, therefore, a preferable technique for PHA-based 3D structures that needs further exploration. Chapter 6 presents a few guidelines regarding future work with additive manufacturing.

Although both blends were successfully utilized to print wrenches, the differences in material composition were clear and resulted in slightly different products. Overall, the blend with copolymer (allPHA) was easier to print, exhibiting less oozing/stringing and a more opaque colour. A common issue observed in both was material warping deformation when the pieces cooled down, which is a common issue in FDM 3D printing (Alsoufi & Elsayed, 2017). In this study, the edges tended to bend inwards showing that despite the addition of an adhesive to prevent the material from peeling off, the process still suffered from poor adhesion to the bed. Other factors involved in material shrinking during 3D printings are printing parameters,

including printing temperature (Alsoufi & Elsayed, 2017). The shrinking effect was more accentuated with PHB blend (NonOilen), as shown in **Figure 3.22**. Surprisingly the filament (allPHA) with copolymer P(3HB-co-3HV) was able to work properly. The wrench gear efficiently rotated left and its movement was successfully locked by pressing the pawl. Unfortunately, the PHB/plasticizer blend did not move, believed to be due to the hard nature and stiffness of PHB. Poly(3-hydroxybutyrate-co-3-hydroxyvalerate) on the other hand is known for having increased elasticity due to lower elastic modulus and higher impact resistance than PHB (Biron, 2012). Alternatively, the printing parameters of NonOilen could be further optimized in an attempt to print a functional wrench with minimal wrapping deformation.

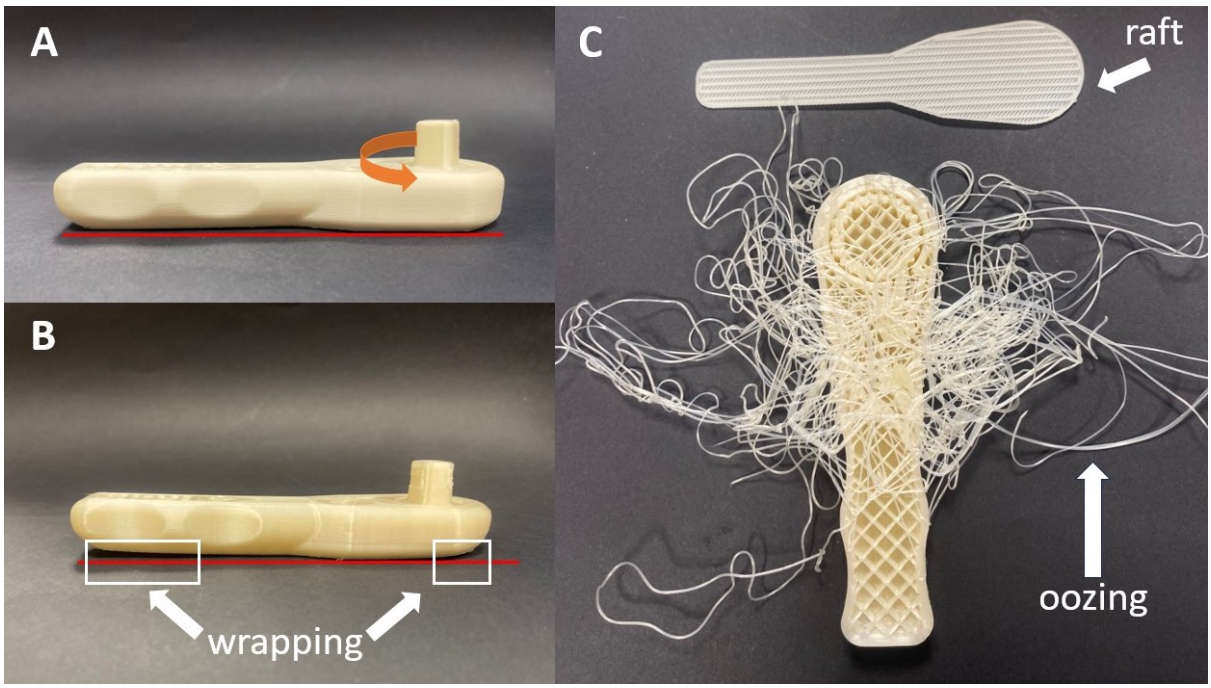

Figure 3.21 Details regarding the final 3D printed constructs and the printing process. Differences in wrapping intensity can be seen between a) the structure produced with allPHA and b) the NonOilen wrench. The horizontal red lines help visualize the wrapping intensity of the second. The first was fully functional as exhibited by the rotating orange arrow. The prints were possible due to the aid of a raft showed in (c) which also shows the oozing printing difficulties associated with printing both filaments. The internal sliced structure can also be visualized in the latter image.

3.4 Conclusions

The freeze-dried biomass of *B. subtilis* and extracted PHB resulted in a well-differentiated FTIR spectra. Under the new scale-up protocol, which is characterized by an additional nitrogen-limiting stage, PHB accumulation is maximum at 48 h, which is in agreement with Marcello (2020) who cultivated the same strain with the same media but with a more hightech scale-up process involving the use of a bioreactor instead of flasks during the fermentation step. The new protocol used here resulted in twice the amount of polymer produced, and so offers a more effective solution to produce large quantities of PHB inside spacecrafts and Mars habitats with limited instruments.

FTIR as a technique for evaluating the ideal harvesting polymer time was investigated. Despite a weak negative correlation between actual extracted polymer yield and FTIR results, the latter was able to determine that maximum accumulation of PHB occurred on the second day of fermentation.

The *Bacillus* strain also showed less but satisfactory growth when cultivated with commercial soluble starch and hydrolysed algae biomass rather than glucose, confirming the variety of substrates *B. subtili*s can grow with. *B. subtilis* produced 23% ± 1.45 of CDW and 0.18 ± 0.1 g/L of PHB when supplemented with WT *Chlamydomonas* biomass as solo carbon source pre-treated at 100°C with 3% of sulfuric acid.

The polymer obtained with *Chlamydomonas* spp. biomass was less brittle, stiff and less hydrophobic than the one obtained from glucose culture. The differences might be due to the lack of sufficient polymer purification and therefore presence of extracellular polymeric substances. The less crystalline nature and increased flexibility of the biopolymer obtained with *Chlamydomonas*-derived biomass is a drawback when constructing solid structures. However, it can be advantageous when producing 2D films for the packaging industry and other areas where PHB's brittleness is a limitation.

Two commercial PLA/PHA blends were able to produce rigid printed wrenches. However, 3D printing results showed that the blend with copolymer PHBV was easier to print, less prone to wrap and the only one to properly work. The observation shows that more research is needed in order to use PHB to manufacture through FDM routine objects useful for astronauts in space.

Chapter 4 Self-liquefaction of starch in Chlamydomonas sp.

I want to acknowledge the valuable contributions of Dr Henry Taunt, who assisted in the overall experimental design, and Dr Jing Cui, who provided support and technical expertise in the Golden Gate technique.

4.1 Introduction

As discussed previously, microalgae starch can be used as a carbon source for heterotrophic bacteria capable of producing essential bioproducts such as biopolymers. Despite the fact that different microalgae strains are capable of accumulating biopolymers such as PHB (Chapter 1), bacteria are known for producing higher yields (Koch et al., 2020), as discussed in **Chapter 1** and **3**.

In spite of that on Earth it is more cost-effective to produce starch from various crops (e.g., corn, potatoes and wheat), on Mars, the presence of food crops will be limited by the large space and high energy requirements needed to maintain and harvest these crops. Microalgae cultivation in hanging bags offers a lowtech solution with simpler requisites including the lack of organic carbon source, as discussed in Chapter 1. However, similar to crop-derived starch, microalgal starch must be first converted into simpler saccharides to serve as feedstock (Wang et al., 2014). Different treatments are available to hydrolyse starch into simpler sugars, as explored in **Chapter 2.** All the discussed treatments involve laboratory reagents and/or instrumentation which is a non-ideal scenario for non-terrestrial applications.

This chapter's main aim is to simplify the liquefaction of starch into smaller saccharides by focusing on eliminating the pretreatment step. Due to the advantages mentioned elsewhere, enzymatic treatment with enzymes such as amylases has become a preferred method. Amylases

are enzymes, introduced in previous Chapters, capable of facilitating starch degradation into smaller saccardies such as the disaccharide maltose which is then converted into glucose (Schonert et al., 2006). Therefore, molecular biology has been used to insert these enzymes into microbial strains with industry value, such as the unicellular fungus *Saccharomyces cerevisiae*, for instance, to directly convert starch into a desired product (e.g., ethanol) (Purkan et al., 2017).

The present study investigates the genetic manipulation of *Chlamydomonas reinhardtii* with a thermophilic amylase to facilitate degradation of starch through simple heat activation, aiming to eliminate the steps involved in biomass pre-treatment and starch hydrolysis, as discussed in Chapter 2. The new mutant will be able to self-liquify its own starch under high temperature (Wang et al., 2014). Even though the cells will be lysed by a simple and suitable method for Mars, elevated temperature will also help denature and rupture membranes, increasing their permeability which will lead to the release of reducing sugars from the cells' interior (Wang et al., 2014).

The thermophilic amylase of choice, which will be introduced later on in this chapter, will be genetically attached to the Granule Bound Starch Synthase I (GBSS1), which is localised on the starch granules. Starch biosynthesis and synthases are introduced in Chapter 1. This strategy will simplify starch purification and collection, which will require no more than sedimentation in some algae systems (Dauvillée et al., 2010). Starch granules are dense and can therefore be easily separated from the rest of the cellular components by centrifugal force in wall-deficient strains. Centrifugation can be used as a simple harvesting technique after cell disruption, which will lead to precipitation of starch and the starch bound-amylase in the pellet leading to its separation from the rest of the cell content which is less dense and therefore will be present in the supernatant. Subsequent to starch and starch bound-amylase harvesting, the precipitate will undergo thermal treatment which will activate the amylase and induce starch liquefaction of the polysaccharide into maltose which, as mentioned earlier, will be later converted into glucose.

Identically, to CC-1690 and CC-5861, the new mutant will follow the same scale-up process described in Chapter 2 to be cultured inside hanging bags. Moreover, large-scale cultivation will be followed by flocculation combined with centrifugation to reduce the biomass harvesting time significantly compared to sole centrifugation. After a simple treatment, such as cell lysis, suitable for Mars habitation, centrifugation will separate the starch granules and the amylase from the rest of the cell content, as explained earlier. **Figure 4.1** schematically represents the overall process. Details regarding the choice of molecular technique, details regarding plasmid construction will be introduced next.

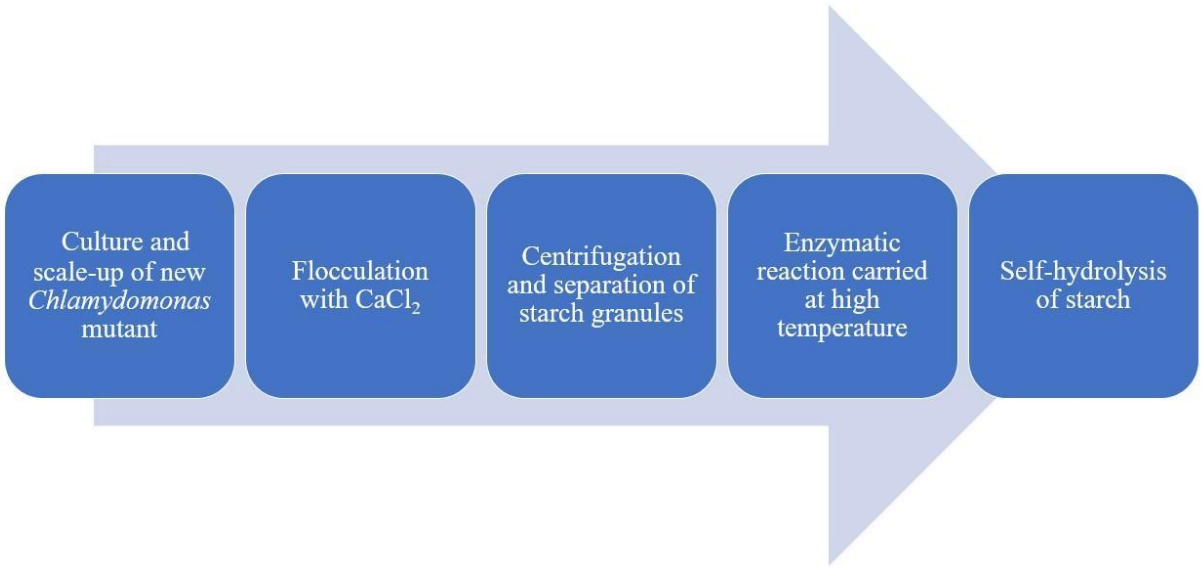

Figure 4.1 Schematic representation of the proposed pipeline involved in the large-scale cultivation of a genetically engineered *C. reinhardtii* mutant capable of self-liquefying starch into simpler sugars, which will serve as feedstock for non-terrestrial polymer production by the heterotrophic bacteria *Bacillus subtilis* OK2.

4.1.1 *Chlamydomonas reinhardtii* chloroplast as a biofactory for recombinant proteins

C. reinhardtii has become a model organism in various areas, as introduced in the second Chapter, including as a platform in algal molecular biology, thanks to a sequenced and annotated genome (Manuell and Mayfield, 2006). More than 5000 mutants of this green algae

have been developed over 70 years and deposited on *Chlamydomonas* "centres" such as the Chlamydomonas Resource Center (CRC) from the University of Minnesota, USA (https://www.chlamycollection.org), which is the most extensive collection of *Chlamydomonas* mutants to date (Tran and Kaldenhoff, 2020).

Transgenes can be expressed through nuclear, chloroplast and mitochondrial transformation (Tran & Kaldengoff, 2020). The plastome has several advantages as a location for the production of recombinant proteins, one being high protein yields (Tran & Kaldengoff, 2020). The *Chlamydomonas'* circular plastome was sequenced for the first time in 2002 by (Maul et al., 2002). More than 100 foreign genes have been introduced and expressed in the *Chlamydomonas* plastome (Adem et al., 2017; Jackson et al., 2021; Larrea-Álvarez and Purton, 2021). A comprehensive summary with the list of proteins with therapeutic relevance (e.g., antibodies, bacterial and viral antigens, and immunotoxins) produced in its chloroplast have been published by Almaraz-Delgado et al., (2014). In the current work, the main reason for choosing plastome transformation is the fact that starch and GBSS are both found in the chloroplast, where starch biosynthesis takes place, as discussed in Chapter 1.

Its ~204 kb genome is presented in **Figure 4.2**, and it is characterised by the presence of several short-dispersed repeats (SDRs), which contribute to its highly repetitive DNA sequence content (~20%) (Jackson et al., 2021). In **Figure 4.2**, distinct colours indicate different gene functions; for instance, dark green represents genes associated with photosystem II (Taunt et al., 2018). Arrows indicate neutral sites for insertion of transgenes (Taunt et al., 2018). *Chlamydomonas*' chloroplast genome is a typical polypod circular plastome with two single-copy regions interlaced by two inverted repeats encoding 108 genes, including duplicates (Taunt et al., 2018; Jackson et al., 2021). Of the 108 genes, 8 are rRNA genes, 29 are tRNAs, and 71 are protein-encoding genes, with the majority encoding critical components of the photosynthetic machinery (Taunt et al., 2018; Jackson et al., 2021).

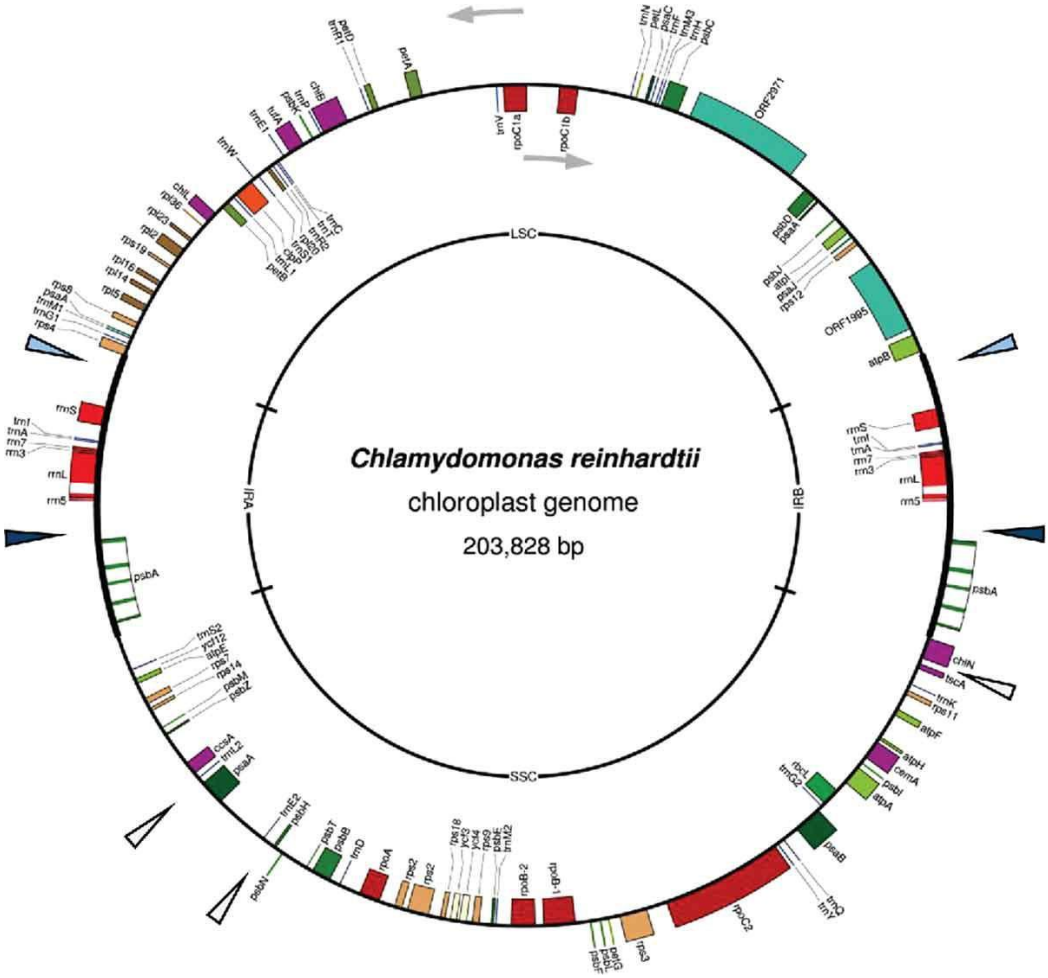

Figure 4.2 *Chlamydomonas reinhardtii* chloroplast genome. The image was published by Taunt et al., 2018 which was generated using sequence information from GenBank (BK000554) and OGDRAW (ogdraw.mpimp-golm.mpg.de) for map design, as detailed by the authors. The image is republished in this thesis under a Creative Commons License.

Increased expression of transgenic proteins in the chloroplast is aided by codon optimization of the gene of interest (Maifuelf et al., 2017). The most commonly used are glass bead transformation, in which cell-wall-less strains are mixed with small glass beads and are agitated in a bench-top vortex; electroporation, which uses an electric field to temporarily make algal lipid membranes permeable, allowing DNA to be uptaken by the cells; and lastly particle bombardment, also known as biolistics. This technique involves metal particles (e.g., gold or tungsten) and similar to electroporation does not require the removal of the cell wall; the particles are coated with DNA being accelerated by a biolistic device into targeted algal cells (Tran & Kaldengoff, 2020). Particle bombardment which directly delivers DNA being

accelerated to the host location is often the most efficient and chosen method for chloroplast transformation (Ozyigit and Yucebilgili Kurtoglu, 2020; Tran and Kaldenhoff, 2020).

4.1.2 The Choice of Amylase

After reviewing the literature, three amylase candidates were considered for heat-activated self-hydrolysis of starch. Choi and colleagues (2010) used a combination of two commercial hydrolytic enzymes: a 57.6 kDa α-amylase from *Bacillus licheniformis (*Termamyl – 120L) and a glucoamylase from a genetically modified strain of *Aspergillus (*AMG 300L) for starch liquefaction in *Chlamydomonas.* After evaluating pH, temperature, enzyme concentration and residence time, the authors determined that the optimal conditions required for the starch hydrolysis were 0.005% α-amylase at 90°C for 30 minutes for liquefaction followed by 0.2% glucoamylase at 55°C and pH 4.5 for 30 min for saccharification. This combination was considered for this study since it successfully converted *Chlamydomonas reinhardtii* UTEX 90 into a suitable fermentable feedstock for *Saccharomyces cerevisiae* for ethanol production, resulting in almost all starch being released and converted into glucose, however, a pH value closer to neutrality is preferable.

The second option was a glucoamylase gene (GLO1) from *Saccharomycopsis fibuligera* inserted in *Saccharomyces cerevisiae* by Purkan et al. (2017) for the direct conversion of starch to ethanol by this recombinant *Saccharomyces* strain. However, the activation temperature of 30°C was considered too low for this project since it is not in the thermophilic temperature range (45 – 85 °C). A thermophilic temperature is desirable to avoid enzyme activity during the *Chlamydomonas* cultivation step, which has a mesophilic optimum growth temperature range.

The thermophilic amylase (arAmyBH) from the hyperthermophilic bacterium *Thermotoga neapolitana*and was the final option considered since it had already been successfully inserted and expressed in C. *reinhardtii* by Wang and team (2014). After evaluating the optimal conditions, the authors selected a pH value of 5.5 and a temperature of 60°C. Even though the amylase was activated and capable of hydrolysation, the results indicated that recombinant arAmyBH alone was insufficient to degrade all algal starch in the

transformant cells and was supplemented with another commercial endo-amylase for complete hydrolysis. Similar to the present study, they developed an expression system for integrating heterologous genes into *Chlamydomonas*' chloroplast between the psaB and trnG genes without interfering with any functional gene and added a 6xHis-tag coding sequence to the C-terminus, which was kept in this study for protein purification purposes. The main difference between their method (Wang et al., 2014) and the current one is the fact that amylase will be fused to the GBSS1, which will allow a simplified harvesting step, as described earlier in this chapter.

4.1.3 The choice of recipient *Chlamydomonas* strain

The chosen recipient strain was the same used by Dauvillée et al. (2010). It was the Bafr1 made available by Steven Ball laboratory (Lille, France) in 2009. This is a GBSSI-defective mutant obtained by deletion of *sta2* through insertional mutagenesis of the cw15 arg7 strain CC-4324 (also known as Ball strain 330), as described in the *Chlamydomonas* collection (https://www.chlamycollection.org). BafR1 is a cell-wall less mutant strain deficient in the granule bound starch synthase I (GBSS) enzyme the GBSS gene as a result of a complete deletion at the STAT2 knockout of the gene (Dauvillée et al., 2010). The use of a knockout STA2 strain line has to do with the fact that GBSS was selected as the region of interest to fused and localise the amylase and will therefore be reintroduced into the strain during chloroplast transformation. The potential of foreign proteins to be fused to *Chlamydomonas*' GBSS and to be expressed has been already explored in malaria research (Dauvillée et al., 2010). *Plasmodium falciparum* Major Surface Protein MSP1 was linked to GBSS and the polysaccharide matrix, resulting in the successful expression of antigens in *C. reinhardtii*, demonstrating the potential of this species to be used as an edible vaccine against malaria (Dauvillée et al., 2010).

The synthetic arAmyBH gene, the gene encoding the amylase of interest, was fused to the STA2 gene, which encodes GBSSI, a protein involved in starch biosynthesis pathway, in particular the synthesis of amylose and elongation of amylopectin chains (Han et al., 2019; Watterbled et al., 2002). GBSS proteins are present in all organisms that accumulate starch, from *C. reinhardtii* to vascular plants, as a result of the commonality of starch metabolism (Dauvillée et al., 2010).

4.1.4 Modular Cloning and Golden Gate

Cloning methods have improved with the arrival of standardised cloning systems; Golden Gate method, which was developed by Engleret al. (2008), is a modular cloning technique that allows the insertion of multiple genes in a single, quick, easy one-pot reaction (Engler et al., 2008). The Golden Gate method is therefore well-suited for the easy and rapid assembling of constructs with multiple DNA fragments, linear or circular (Mukherjee et al., 2021; Jackson et al., 2021; Bird et al., 2022). This technique uses Type IIS restriction enzymes that cut DNA outside recognition sites and join DNA parts through ssDNA sticky ends (Engler et al., 2008; Jackson et al., 2021; Taylor et al., 2019). The literature emphasises the importance of the proper design of the endonuclease's restriction sites (Bird et al., 2022; Engler et al., 2008) and summarises the list of the various toolkits developed based on this methodology (Bird et al., 2022).

The Golden Gate method involves the hierarchical assembly of DNA fragments into higher and higher levels, as shown in **Figure 4.3**, which allows assembled DNA parts to be used for subsequent assembly stages (Bird et al., 2022). In "Level 0", essential DNA parts such as promoters, terminators, and genes of interest can be stored inside plasmids (Weber et al., 2011; Bird et al., 2022). In "Level 1", various individual transcriptional units can be assembled simultaneously from Level 0 parts in a single digestion/ligation reaction (Jackson et al., 2021) since it is more practical to assemble transcriptional units separately (Bird et al., 2022). Next, L1 individual transcriptional units are combined together in conjunction with selective markers, and flaking regions required for plastome transformation into higher-level constructs (Level 2 or more) (Jackson et al., 2021).

The Start-Stop assembly developed by Taylor and colleagues (2019) for cyanobacteria is an adaptation of the Golden Gate method in which the overhangs where DNA fragments join correspond to start (ATG) and stop (TAA) codons, avoiding the presence of scars at sensitive coding areas and resulting in a scarless DNA assembly (Taylor et al., 2018). More recently, this method was adapted to microalgae chloroplast in a new system called Synthetic Toolkit for Engineering Plastids (STEP). The present study uses STEP, the novel modified version of the Golden Gate platform developed for rapid algal plastome transformation. A dual system

based on the STEP system (Taunt et al., 2024) was created to allow the assembly of two constructs in parallel using restriction-ligation reactions and the hierarchical assembly with start and stop codons as fusion sites. The construct with GBSS and amylase (GBSS-arAmyBH), occasionally referred to as rrnS-psaA-GBSS-amylase-HA-rbcL (which specifies its promoter and terminator) will be responsible for the hydrolysis of starch. The construct with both STA2 and mVenus referred to here as GBSS-mVenus or rrnS-psaA-GBSS-mVenus-rbcL will provide the ability to visualise the GBSS bound-amylase inside *Chlamydomonas*' chloroplast. The schematic representation of the steps used in assembling both constructs is shown in **Figure 4.3** and detailed in the following paragraphs.

Two constructs were designed in parallel via Golden Gate as explained earlier to fuse the chosen amylase and the gene encoding for mVenus to the GBSS's STA2 gene. The mVenus is a yellow fluorescent protein derived from *Aequorea victoria* and published by Kremers et al. (2006), frequently used in molecular biology to track protein production and localisation, including in *Chlamydmonas* spp. (Molino et al., 2022) through confocal microscopy.

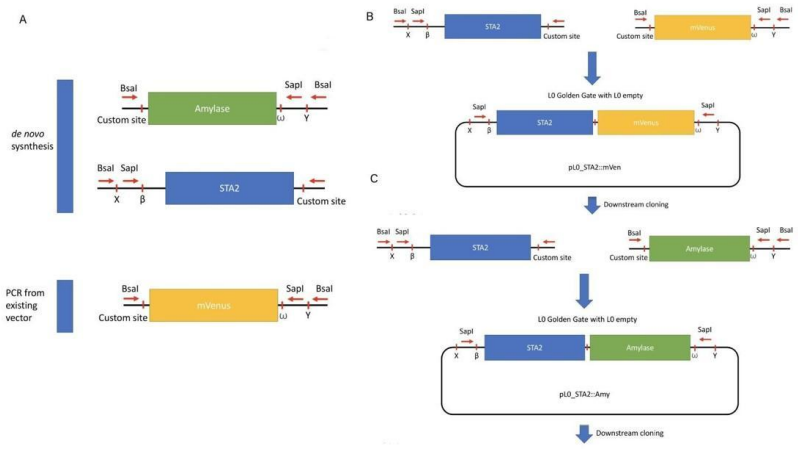

Figure 4.3 The dual system proposed for this project based on the STEP system will allow a) the creation of two different constructs in parallel including b) the GBSS:amylase and c) the GBSS:mVenus. All three fragments were be commercially synthesised. Alternatively, mVenus which was also obtained by direct mutagenesis can be constructed through PCR amplification as shown in this figure.

4.2 Materials and Methods

4.2.1 Plasmid construction

Vectors (pSS117 and pSS102) with genetic elements (16S_psA promoter and a rbcL transcriptional terminator) were obtained from the Purton Lab Collection (University College London). Before bench work, L0, L1, and L2 assembled constructs were designed in Benchling (https://www.benchling.com/) with start and stop codons in the restriction sites. Level 0 and L2 vectors (pSS117) contain an ampicillin-resistant gene (ampR) which confers the ability to grow on media supplemented with ampicillin, while the L1 vector (pSS102) confers tetracycline resistance for selection purposes.

The arAmyBH gene (GenBank KF703932), developed by Wang et al., 2014 was the amylase of choice, as will be discussed in the following section. Insertions containing digestion sites of Type IIS restriction enzyme SapI and BsaI (NEB) were introduced into the sites upstream and downstream of the two genes of interest, *Chlamydomonas'* GBSS and arAmyBH in Benchling.

A (GS)4 flexi-linker was added to the end of the STA2 gene to prevent steric hindrance. PredoAlgo (http://www.grenoble.prabi.fr/protehome/), a sequence analysis software for intracellular targeting prediction used to discriminate chloroplast from mitochondrial proteins in *C. reinhardtii* (Tardif et al., 2012), was used to search and remove transit peptides.

4.2.2 Codon optimization

Codon optimization of *Chlamydomonas*' STA2 was achieved with Codon Usage Optimizer (CUO), a multiplatform software (github.com/khai-/CUO) developed for the Algae Department at University College London (UCL) to optimise the genes to be transformed into the *C. reinhardtii* chloroplast genome.

4.2.3 Synthetic DNA fragment synthesis

Restriction sites for type IIS enzymes (SapI and BsaI) for all three genes, GBSS, arAmyBH and mVenus, were introduced in Benchling. The protein translation of each gene was also verified *in silico* with Benchling. Finally, the three individual gBlocks gene fragments were synthesised by Integrated DNA Technologies (IDT). After arrival, the three gBlocks fragments were resuspended in an elution buffer and incubated for 20 minutes at 50 °C, as recommended by the manufacturer.

4.2.4 Golden Gate Assembly

DNA cloning was performed by a Golden Gate-based assembly system using start and stop codons, as described by Jackson et al. 2022. As mentioned earlier, two constructs, GBSS-arAmyBH and GBSS-mVenus, were produced. GBSS DNA fragment was separately fused to amylase and mVenus into the Level 1 vector (pSS102), also referred to as P1 AB empty, using one-pot restriction-ligation assembly reactions with SpaI, as described below. The GBSS-arAmyBH and GBSS-mVenus, from both L1 constructs, were then cloned individually into L2 vectors (pSS117) together with the *aadA* gene for streptomycin and spectinomycin resistance as a selectable marker (Cui et al., 2021) and sequences for homologous recombination in *Chlamydomonas* by using BsaI.

All enzymes, buffers and reagents were obtained from New England Biolabs (NEB). One-pot restriction-ligation Golden Gate Assembly reactions following a previous protocol (Jackson et al., 2022) were performed in a total volume of 20 µL with ten units of the appropriate restriction endonuclease (SapI or BsaI), T4 DNA ligase (400 U), 60 fmol of each PCR assembly fragment in 10X T4 DNA ligase buffer, and 20 fmol of the backbone plasmid. Reactions were cycled in a thermocycler (T100 thermo cycler, Bio-Rad) at 37°C for 15 minutes, followed by 30 cycles of 5 minutes at two different temperatures (37°C and 16°C), and subsequent heat shock at 65°C for 20 minutes, incubation at 37°C for 15 minutes, and a final hold at 4°C. All reactions were performed in PCR tubes adding water first and the enzymes last. All Golden Gate reactions were performed in a laminar flow hood.

4.2.5 *Escherichia coli* transformation

The DNA product from Level 0 and Level 1 restriction-ligation assembly reactions was transformed into *E. coli* competent cells DH5α (DH5α for subcloning by Thermo Fischer Scientific). These cells contain the genetic marker φ80dlacZΔM15 for blue/white colour screening, recA1 to reduce the occurrence of unwanted recombination and to increase insert stability, and endA1 to increase the quantity and quality of the plasmid, as described by the manufacturer. Each transformation was followed by selection in Lysogeny Broth (LB) plates (containing 15 g l^{-1} bacteriological agar). As appropriate, LB plates were supplemented with ampicillin (100 μg ml^{-1}) or tetracycline (10 μg ml^{-1}). The media with tetracycline was also supplemented with 0.1 mM of IPTG (isopropyl β- d-1-thiogalactopyranoside) and 40 μg ml^{-1} of X-gal (5-Bromo-4-Chloro-3-Indoyl β-D-Galactopyranoside) for the blue-white screen.

DH5α chemically competent cells were transformed following Thermo Fischer Scientific's high-efficiency protocol, with slight changes to the protocol: 1~1 ng of each plasmid was incubated with 50 μl of the competent cells on ice for 30 minutes, followed by a heat shock at 42°C for 30 seconds and re-cooled on ice for 2 minutes. A volume of 250 μl of thawed and room-temperature Super Optimal broth with Catabolite repression (S.O.C.) medium was added for cell recovery, followed by a 1-hour incubation at 37 °C, 225 rpm. 50 μl of the cell suspension was then plated and spread with glass beads on LB agar plates with the relevant antibiotic for selection. The plates were incubated overnight at 37°C. Two colonies per plate were selected and used to inoculate 5 ml LB broth, which was supplemented with the relevant antibiotic if necessary. Cultures grew overnight in 14 ml round bottom polypropylene falcon tubes, which were not firmly closed to allow gas exchange, at 37 °C with continuous shaking at 225 rpm and the respective antibiotic. A small volume of the overnight culture (1 mL) was combined with glycerol and stocked at – 80 °C while the remaining 4 ml was used for DNA extraction as described next.

4.2.6 DNA Extraction and Sequencing

Plasmid DNA was isolated using the GeneJET Plasmid Miniprep Kit (Thermo Scientific), which uses silica-based membrane technology, according to the manufacturer's

instructions. In brief, the protocol starts with alkaline (SDS) lysis to liberate the plasmid DNA from inside *E. coli* cells, followed by neutralisation and binding of the lysate to the silica membrane present in a spin column. The DNA of interest adsorbed in the membrane is then washed for contaminant removal and finally eluted with Elution Buffer (10 mM Tris-HCl, pH 8.5). A smaller volume of elution buffer (30 µL) was used than that recommended by the protocol in order to concentrate the DNA. DNA concentration and purity evaluated by the A260/280 ratio were measured with a NanoDrop100 (Thermo Fischer Scientific) using elution buffer as a blank and following the standard protocol.

The purified Plasmid DNA from L1 constructs were sequenced by Source Bioscience (Cambridge, United Kingdom) using Sanger sequencing. Sequencing primers and plasmid DNA were supplied at the concentration required by the sequencing service, which are 3.2 pmol/µl and 100 ng/µl, respectively. Plasmid DNA was diluted with water to obtain the final concentration of 100 ng/µl. A total of 11 µl were sent for each construct, 5 µl for each primer (forward and reverse) and 10% of total volume as extra volume to account for pipetting mistakes. L0 and L1 sequencing primers, referred to as HT 181 and HT 201, were developed and provided by Prof Saul Purton laboratory (University College London, United Kingdom) as shown in **Table 4.1**. A total of 20 µl were sent of each primer for sequencing two L0 and two L1 constructs.

Table 4.1 The primers used for sequencing the L1 constructs.

Primer Name	Primer Sequence	Direction
HT 181	GGACGACCGAGCGCCTTGG	Forward
HT 201	CCAACTTTTGGCGTATCACGAGGCCCTTTC	Reverse

4.3 Results and Discussion

4.3.1 Vectors construction for Golden Gate Assembly

A total of seven different constructs were designed in Benchling, as shown in **Figure 4.4**: three for L0 level, two for L1 level and another two for L2, with each level containing a

construct for GBSS-amylase and GBSS-mVenus. As can be seen in the constructs, the expression of GBSS-amylase and GBSS-mVenus fusion protein is under the control of a strong 16S rRNA promoter to the 5′ UTR of the psbA gene (Rasala et al., 2011).

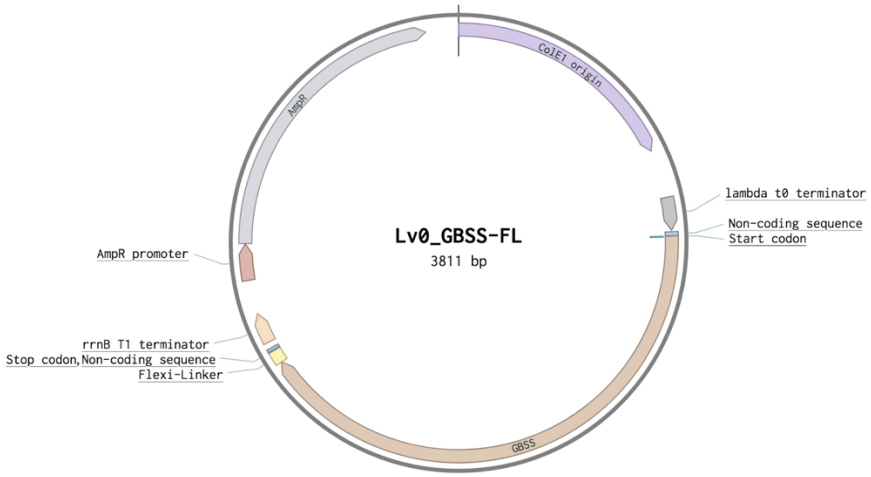

Figure 4.4.A. L0 level construct for the synthesised GBSS gene.

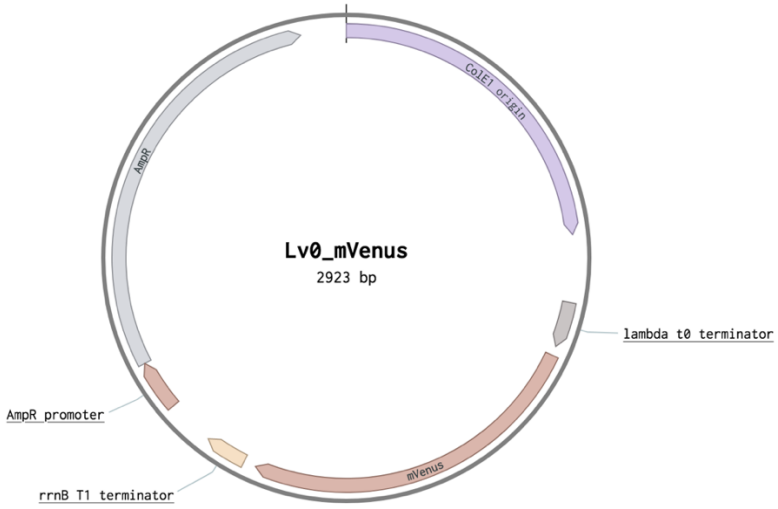

Figure 4.4B L0 level plasmid for the synthesised mVenus gene.

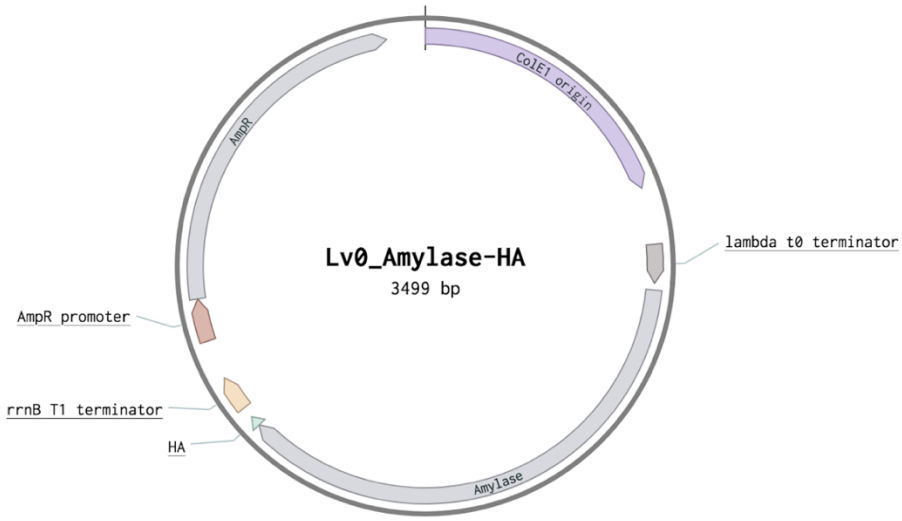

Figure 4.4C L0 level plasmid for the synthesised amylase gene.

Figure 4.4D L1 level plasmid for the GBSS-Amylase construct.

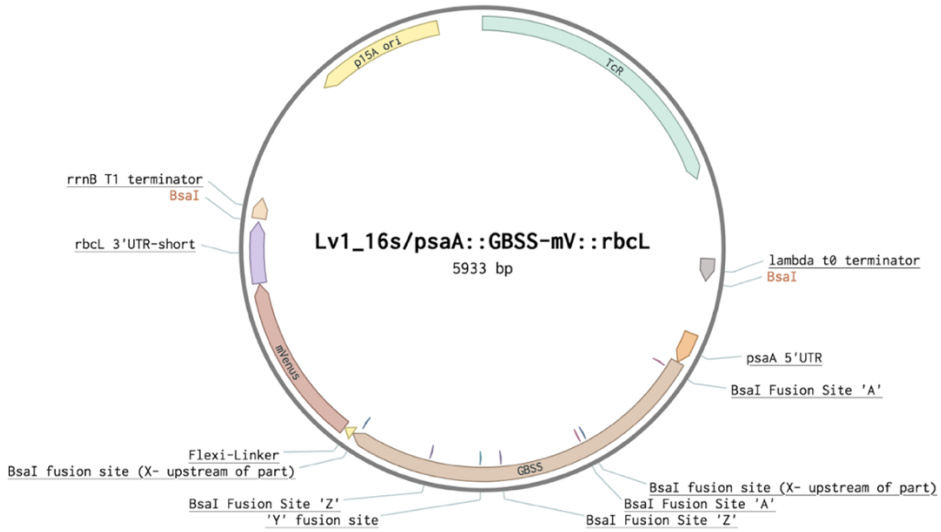

Figure 4.4E L1 level plasmid for the GBSS-mVenus construct.

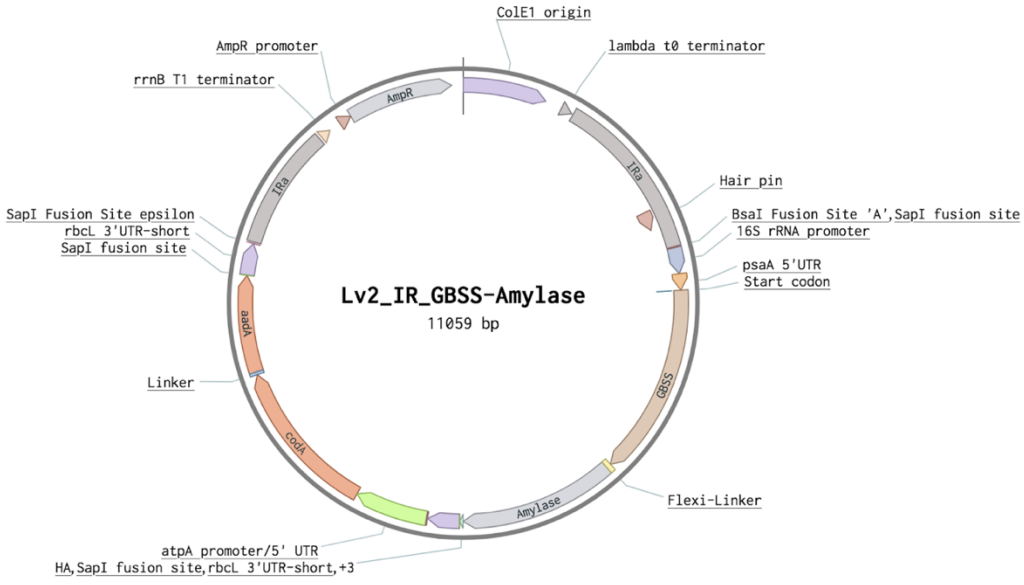

Figure 4.4F L2 level plasmid for the GBSS-Amylase construct.

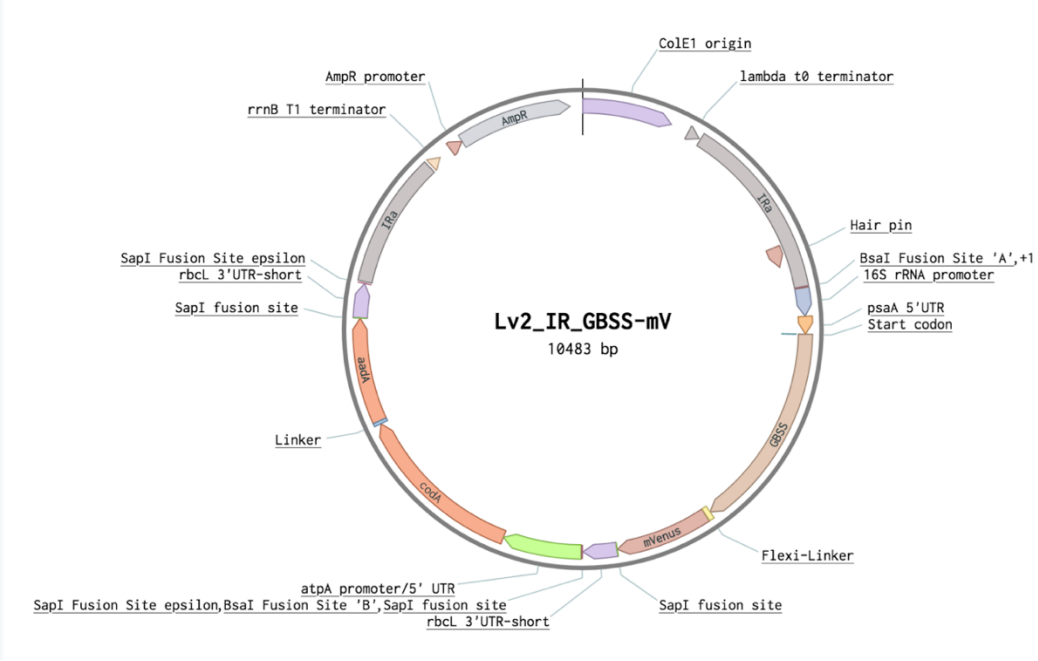

Figure 4.4G L2 level plasmid for the GBSS-GBSS construct.

Figure 4.4 Level 0, 1 and 2 vectors assembled *in silico* with Benchling. The main features of each plasmid is shown in each figure. Each figure is individually labelled to avoid confusion

4.3.2 Assembly of L1 constructs

L0 constructs, shown in **Figure 4.5a** are only necessary for DNA storage and propagation of the plasmid with the gene(s) of interest which is more stable inside a (circular) plasmid than as linear DNA. After a second attempt, L1 constructs were successfully developed. The products from both L1 *E. coli* transformations were plated on LB agar with tetracycline as described earlier. *E. coli* transformant colonies can be seen in **Figure 4.5b**. The L1 blue-white screen on agar plates resulted in only white colonies presumably containing the foreign genes. The fact that no blue (non-recombinant) colonies were obtained confirms efficient digestion with SapI and the insertion of the DNA of interest into the *lacZ* gene in the L1 backbone plasmid (pSS102), and thus disruption of ß-galactosidase activity (Ullman et al., 1957). L1 constructs were verified by DNA Sanger sequencing.

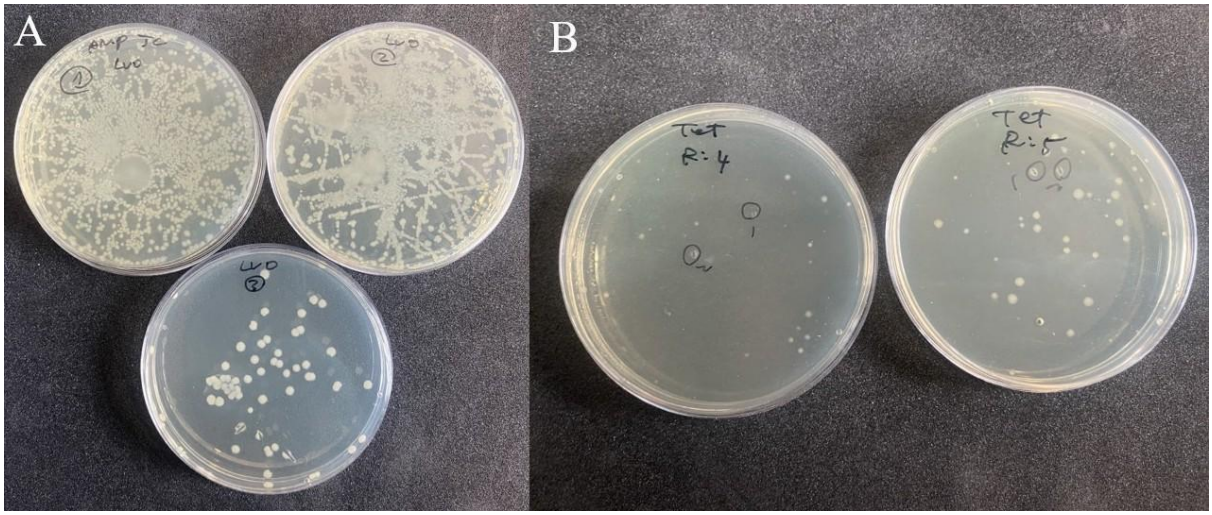

Figure 4.5 E. coli transformants on agar plates for a) L0 and b) L1 levels. a) L0 plates are numbered from 1 to 3, each corresponding to individual genes of interest. Number one shows the result of transformants with the amylase gene, number two with GBSS and number three with mVenus. b) Left plate corresponds to GBSS:Amylase, while GBSS:mVenus transformants can be found on the right plate. The L1 colonies removed for DNA extraction and further used for L2 assembly are marked with a circle.

Two L1 colonies were selected and removed from each plate indicated in **Figure 4.5B** and grown in 5 ml LB liquid with tetracycline. After DNA extraction, DNA concentration and purity (A260/A280) were measured as described in the Material and Methods.

4.3.3 Troubleshooting L2 stage of the Golden Gate Assembly

Two attempts were made to assemble the two L2 constructs with freshly made medium and agar plates the day prior to transformation as discussed above. Both attempts were unsuccessful. During the first try, pink colonies – indicating backbone plasmid without transgenes – were present at much higher numbers than the white colonies, as seen marked in **Figure 4.6**.

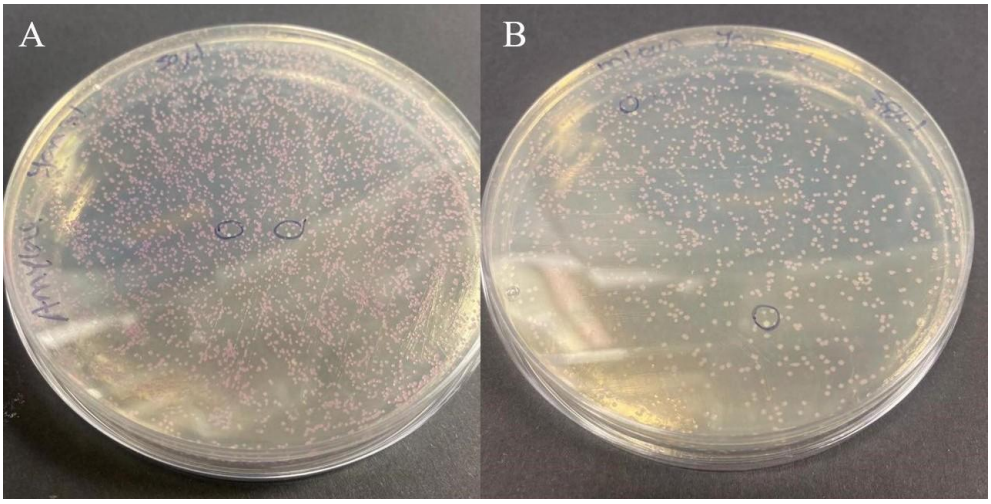

Figure 4.6 Transformation results from the first attempt during L2 assembly. A) The 50 µL transformation product result for GBSS:amylase can be seen on the left, while the b) right plate shows the same result for GBSS:mVenus. As before, the colonies removed for DNA extraction are marked with a circle. Lack of transformant after 100 µL plating during the second attempt is not shown.

pSS117, the backbone of L0 and L2 constructs, is also known as the tinsel purple (tsPurple) due to the presence of a gene encoding a purple chromoprotein. This produces a magenta or pink-purple colour when expressed (Lazarus et al., 2019); the initial light pink tone of a colony changes into darker pink and purple with longer incubation times. When a transgene is inserted into tsPurple, it disrupts the expression of the chromoprotein, and the pink/purple tone is no longer produced, resulting in white-beige colonies. tsPurple was chosen because it is an improved version of the blue-white screening. To ensure differentiation between white and light pink colonies, agar plates were always observed against a black card.

Despite the low number of colonies, DNA was extracted from two selected colonies per construct after growing the colonies in 5 ml LB medium with ampicillin. DNA extraction was performed as described in the Materials and Methods section. DNA concentration values for all four colonies were low, less than 50 ng/µL. Since DNA purity for all four was reasonable (>1.6), 20 µL of each sample was submitted to DNA sequencing. Sanger sequencing confirmed the absence of the transgenes in the backbone plasmid (data not shown).

Troubleshooting approaches between the first and second attempts focused on verifying the *in silico* constructs and adjusting the concentration of DNA fragments in the Golden Gate

one-pot reaction. In this second attempt, no colonies were obtained after transformation, even when the volume plate was increased from 50 to 100 µl, which is the volume recommended by the manufacturer. As a result, a further series of troubleshooting investigations was devised to check the most essential steps involved in the process, in the following order: transformation, activity of BsaI restriction enzyme and the ligation step.

Transformation and *E. coli* DH5α competent cells were tested using pSS117 as a positive control followed by evaluation of the activity of the BsaI enzyme in a digestion reaction using 500 ng of tsPurple as a positive control. Digestion was carried out at 37 °C for one hour using 0.5 µl of BsaI and 1 µl of cutsmart buffer in 10 µl total volume. The digestion product was loaded onto a 1% electrophoresis gel.

In summary, evaluation of transformation efficiency and digestion were conducted in this order. Transformation was the first step addressed due to the lack of transformants on agar plates during the previous troubleshooting attempt. The transformation efficiency calculated was $3.6\ 10^{5}$ CFU/µg, which was lower than that reported as achievable by the manufacturer (10^{6} - 10^{7} CFU/µg), but still fairly efficient. Since transformation with both dilutions tested was successful, and the transformation efficiency was reasonable, the competent cells (which had been kept at –80 °C throughout this project) were ruled-out as the problem causing difficulties in the L2 assembly.

Subsequently, the cutting efficiency of BsaI was evaluated in a digestion reaction using tsPurple as a positive control. Visualisation of the electrophoresis gel (not shown here) revealed that BsaI had lost its enzymatic activity and was not capable of cutting pSS117 into two fragments of 2183 bp and 848 bp in size. Only a single band corresponding to the overall size of the plasmid (3031 bp) could be seen in the gel. Thus, one of the problems with the transformation process had been identified and a new BsaI was ordered. It is at this point, however, that time ran out for this project and the trouble-shooting steps for the Golden Gate assembly were suspended. Further work to complete the trouble-shooting steps would start with confirming the digestion with fresh BsaI, and then verifying the ligation step and the T4 ligase which should also be evaluated in a one-pot digestion reaction as described in the

Materials and Methods using BsaI as restriction enzyme as previously described and tsPurple positive control. The ligation product will be loaded on a 1% electrophoresis gel.

Once the issue is resolved, another attempt at constructing the L2 vectors can be made. Nevertheless, the future steps involved in the construction of the new *Chlamydomonas* mutant are described in the following section.

4.4 Overview of the steps required to conclude the project

After completion of the Golden Gate L2 constructs, they would have been used to transform algal chloroplasts. The selected host, the *Chlamydomonas* BafR1 strain, was obtained from the Chlamydomonas Resource Center (https://www.chlamycollection.org) as CC-4329. The genetic information of the Golden Gate's final construct would have been integrated into the *Chlamydomonas'* chloroplast genome through homologous recombination by biolistic transformation. The new *Chlamydomonas* mutants would have been screened for successful transformation by antibiotic selection on TAP agar plates with spectinomycin followed by growth in liquid culture for further analysis. DNA extracted from selected colonies would undergo homoplasmy evaluation by PCR. DNA sequencing would have followed in order to confirm the correct insertion of the desired constructs.

Protein analysis and accumulation of arAmyBH protein in the *C. reinhardtii* transformants would have been analysed by a combination of western blotting and confocal microscopy. Western blotting would have been performed using monoclonal anti-polyhistidine antibodies to confirm the fusion of the amylase and *Chlamydomonas* starch bound GBSS (Deuvovill et al., 2010; Wang et al., 2014). Confocal laser scanning microscopy (CLSM) would have been used to confirm the localisation of the amylase fused with fluorescent mVenus, inside the chloroplast, more specifically in the pyrenoid where starch is deposited, as discussed in Chapter 1.

Finally, evaluation of the self-liquefaction of starch would have been conducted. Enzymatic analysis of starch content would have been performed similarly to the methodology

described by Wang et al. (2014), which includes lysing the cells and incubating the starch at high temperature (60 °C). After centrifugation of the hydrolysate the supernatants would have been submitted for sugar analysis by the 3,5-dinitrosalicylic acid (DNS) method (Miller, 1959) as described by Wang et al. (2014). After confirmation of the successful self-hydrolysis of their starch grains by the transformed *Chlamydomonas* cells, this transformant can be cultured at scale. The new capability provided by the starch-grain localised amylase means that these photosynthetic cultures can be processed using only simple techniques to provide sugar-rich feedstock for growing bioplastic-producing heterotrophic *Bacillus*.

Once constructed, the mutant containing the thermophilic amylase would have been grown autotrophically with HSM medium under similar growth conditions (e.g., cultivation temperature, agitation speed and illumination) to the WT and the cw15 mutant and would followed the same scale-up system used for the two strains, from agar plates to hanging bags.

4.5 Summary of the transformation attempt

The aim of the work detailed in this chapter was to create a *Chlamydomonas reinhardtii* mutant with a thermophilic amylase bound to the starch granules which will allow both the starch and the enzyme to be harvested together through centrifugation after the cells are lysed by a simple and cost-effective method (e.g., ultrasonication) that will take into account the limitations associated with Martian habitat and spacecrafts. The thermophilic amylase will then digest the starch through heat activation into simpler sugars, which would be used as feedstock for the selected PHB-producing bacteria eliminating the need for acidic treatment discussed in the previous chapter.

Golden Gate was the technique of choice to create this mutant due to its many advantages which includes the quick and easy insertion of various genes by a one-pot digestion/ligation reaction.

However, this work could not be completed due to difficulties in developing the L2 constructs, the final step of the Golden Gate assembly before transformation of the

Chlamydomonas. A series of troubleshooting approaches were attempted as described above but ultimately were not able to identify and resolve the underlying problem before time ran-out on the project.

Chapter 5 Analysis of Microbial Dispersal at a Mars Analogue Habitat

I want to acknowledge the valuable contributions of Dr Michael Macey, who assisted with bioinformatics, inductively coupled plasma spectroscopy (ICP-MS), and soil property analysis. I also want to acknowledge Mamatha Maheshwarappa for collecting the samples studied in this chapter and Dr Dragana Dobrijevic and Dr John Ward for assisting with DNA extraction and sequencing.

5.1 Introduction

Microorganisms are often the source of environmental contamination in pristine and remote locations on our planet (Baker et al., 2003; Schuerger and Lee, 2015; Sjöling and Cowan, 2000; Upton et al., 1997). Carried by future astronauts, microorganisms might escape habitational and research facilities and contaminate the Martian soil interfering with the search for indigenous Martian life (Schuerger and Lee, 2015).

5.1.1 Preventing forward contamination of Mars

Astrobiology focuses on understanding life's origin, evolution, and distribution in the universe (de la Higuera and Lázaro, 2022; Preston and Dartnell, 2014). In this thesis, the unintentional or deliberate transfer of life (viable or dormant) or other biological material (e.g., viruses, bioactive molecules, organics, dead organic matter, dust, etc.) between celestial bodies will be referred to as interplanetary contamination.

Interplanetary contamination considers two types of contamination; forward contamination focuses on the introduction of terrestrial material into the environment of another planetary body, such as the moon and Mars. On the other hand, backward contamination is the biological contamination of Earth’s biosphere with material originating

from another celestial body (Coelho et al., 2022; Goh & Kazeminejad, 2004; Showstack, 2023). For instance, a human mission to Mars will not be considered contamination until a terrestrial biological contaminant is introduced into the Martian atmosphere, terrain, ice caps, sediments, or subsurface. Both types of biological contamination are represented in **Figure 5.1**.

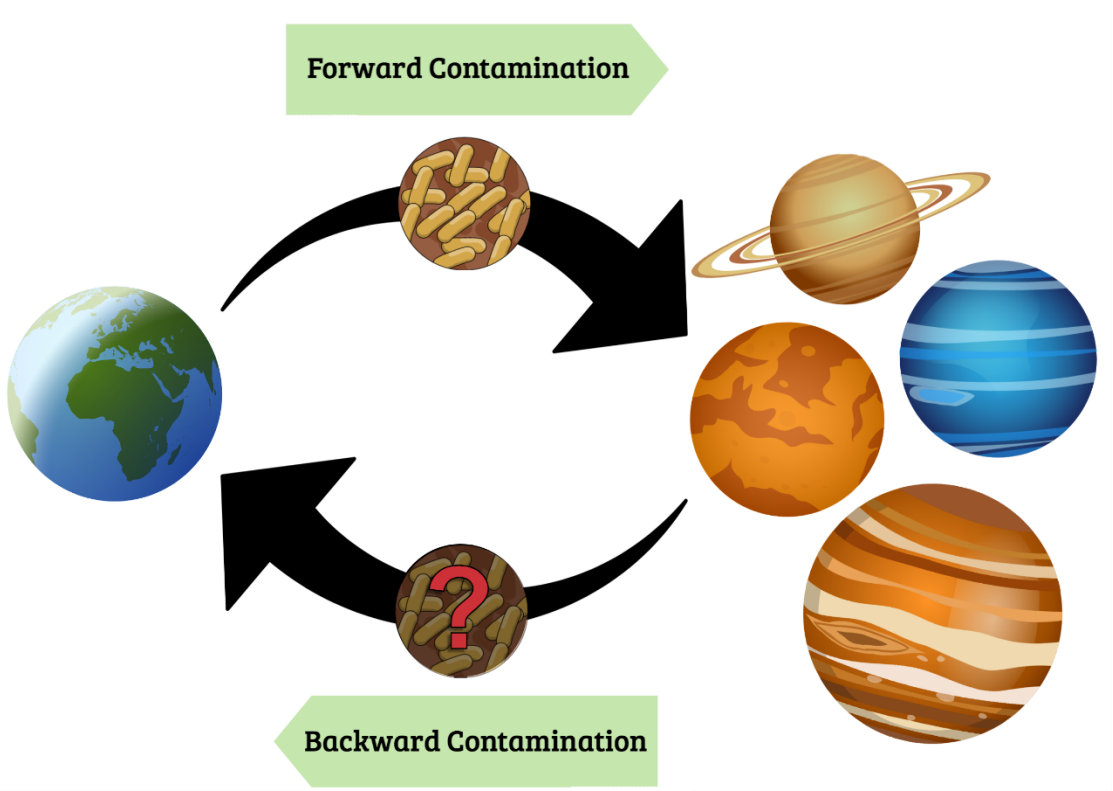

Figure 5.1 Schematic representation of forward and backward contamination between Earth and different celestial bodies. The image was produced in accordance with similar depictions found in the literature regarding interplanetary contamination. The question mark indicates the uncertainty concerning the existence of life beyond Earth. Planet sizes are not to scale.

Life has not been detected outside our planet. If detected, it would be a significant scientific breakthrough. The age-old "Are we alone in the universe?" question has driven the field of astrobiology for decades (Marino, 2023). The indispensable ingredients for all terrestrial life forms are water, carbon, energy sources capable of sustaining metabolism, and essential elements such as hydrogen and nitrogen (McKay, 2014; Preston and Dartnell, 2014). Water is an excellent solvent and transport medium (Preston & Dartnell, 2014). All cells, from bacteria to humans, are predominantly made of water (70%) (Cooper, 2000), which is essential to various chemical reactions. Carbon is also intrinsically linked to life (Westall et al., 2003).

Every terrestrial form of life known to date is carbon-based and made up of a variety of molecules containing one or more atoms of carbon, known as organics (Sephton and Botta, 2005). Organics, which can be made geologically or biologically by living organisms, are preferred targets when searching for habitable planets and moons (Chan et al., 2020; Preston & Dartnell, 2014). Amino acids and nucleobases are among the most important organics and are commonly referred to as building blocks of life as they make up proteins and genetic information, respectively (Sephton & Botta, 2005).

Even though alien life itself, past or present, has not been identified, the ingredients for life have been found in meteorites that have fallen onto Earth and on other celestial bodies. For instance, all five nucleobases have been detected in carbon-rich meteorites (Oba et al., 2022); phosphate minerals have been found in both meteorites and lunar samples (Fuchs, 1969; Li et al., 2022); various amino acids (glutamic acid, glycine, aspartic acid, serine, alanine, β-alanine, and γ-amino-n-butyric acid) were present in a Martian meteorite (Glavin et al., 1999). Robotic missions have detected methane, a potential biosignature gas, in Mars' atmosphere; and complex organics, such as aromatic and aliphatic compounds, have been found on Mars Gale Crater (Geminale et al., 2011; Giuranna et al., 2019; Webster et al., 2014, 2018).

The consequences of both forward and backward contamination can be severe and are potentially of pathogenicity. In backward contamination, unicellular extra-terrestrial life can pose medical risks to humans or environmental threats to our ecosystems. The first possibility is less likely as extraterrestrial microbes are likely extremophilic and adapted to environmental conditions greatly differing from those within the human body. Moreover, alien microbial life will suffer competition from highly adapted human-associated bacteria. Nevertheless, extra-terrestrial pathogens should not be ruled out and should be included in the design of preventive and mitigation protocols.

Backward contamination is a bigger potential threat to agriculture and natural ecosystems as extraterrestrial microbes could act invasive species and potential disrupt the biomes of different environments around the Earth. Astronauts and lunar samples from the Apollo program were subjected to quarantine upon return to Earth (Goh & Kazeminejadb,

2004; Rummel, 2001).. Additionally, astronauts' suits were also decontaminated, but in retrospect, these measurements needed to be more stringent to prevent backward contamination if any lunar microbes were present (Showstack, 2023). While the Apollo quarantine system a rationally cautious approach, it is no longer believed that the lunar surface holds any possibility at harbouring native microbial life. Through its history, the moon has been too dry, unprotected by a lack of atmosphere and benefit of organic chemistry from the development of life (Liu, 2022).

Inversely, Mars has a thin atmosphere and studies have shown that it might have been volcanically active until recent geological time (Broquet and Andrews-Hanna, 2023). Mars is believed to have had a warmer climate and surface liquid water that could have harbour life (Preston & Dartnell, 2014). Polar water ice deposits still exist on Mars (Liu et al., 2022; Titus et al., 2003). Furthermore, Mars might still have liquid water underneath the ice cap of its southern pole (Arnold et al., 2022). Its similarity and proximity to Earth also contribute to the fact that Mars is one of the top targets for searching for extra-terrestrial life together with the icy moons of our Solar system (Goh & Kazeminejadb, 2004; Preston & Dartnell, 2014).

It is unlikely that life can thrive on the Martian surface under the current environmentally hazardous conditions (Preston & Dartnell, 2014). Nonetheless, it may persist underneath Mars' surface, where microbial communities might be shielded from deadly solar and UV radiation (Preston & Dartnell, 2014). The Martian subsurface or surface material containing openings and fissures might offer the necessary protection for biosignature preservation (Preston and Dartnell, 2014). Extant life forms can also be present on some regions of Mars, known as special regions, that can support microbes' growth and proliferation (Rummel et al., 2014). Planetary policies could potentially restrict robotic missions in these areas due to the increased risk of contamination and terrestrial lifeform propagation (Fairén et al., 2017; Schuerger and Lee, 2015).

Some of the Mars robotic missions, such as the Viking landers and Perseverance rover, were designed with *in-situ* instrumentation capable of searching for biosignatures. Unfortunately, those instruments are not as powerful as the equivalent equipment from ground-

based laboratories. Ultimately, researchers want to analyze pristine Mars samples on Earth with the most capable instruments without size, mass and power restrictions associated with space missions. NASA and ESA are designing the first Mars Sample Return mission. The mission will likely include a customized Biosafety Level 4 facility for containment, safe storage and processing of samples returned to Earth in order to avoid backward contamination (Carrier et al., 2021).

In addition to backward contamination, another risk of planetary exploration is forward contamination of extraterrestrial locales. If terrestrial biological material is present in the instruments and on rovers, it can get dispersed into the environment and contaminate, if present, the Martian biota. It can also irreversibly contaminate the collected samples and lead to false positive results and misleading conclusions of the presence of indigenous microbial life (Goh & Kazeminejadb, 2004; Rummel, 2004).

Vehicles and spacecraft are subjected to strict sterilization practices to ensure the responsible exploration of Mars and other planetary bodies (Rummel, 2004; Showstack, 2023). Surface cleaning with chemical sterilants such as isopropyl alcohol; dry-heat or wet-heat sterilization at high pressure of individual components; and equipment assembly in cleanrooms under aseptic conditions and by personnel dressed in full sterile gear are some of the measures in place (Showstack, 2023). Additionally, the rooms and the vehicles are subjected to characterization and quantification of microbial load during assembly and before launch. Sterilization protocols might differ based on the type of mission (e.g., lander, flyby or rover), scientific objectives (e.g., life detection, geological characterisation), and the type of targeted body (Showstack, 2023). For instance, Mars Missions with life-detection experiments, such as the Perseverance rover, are further sterilized compared to vehicles that do not search for past signs of Martian life. Space missions are categorized into five distinct groups based on the parameters mentioned earlier. Since Mars is a location with significant interest in the evolution and origin of life, Mars robotic missions are classified as category IV while Mars sample return as category V (Goh & Kazeminejadb, 2004).

Extremophilic bacteria, capable of adapting to extreme conditions, or dormant life forms, such as spores, capable of undergoing extremely lengthy periods of dormancy, might survive interplanetary transit and contaminate the Martian surface. However, even with the stringiest sterilisation and cleaning protocols the complete removal of all contaminating terrestrial microbes (as their residues of organic molecules) is not possible, and a limited bioburden is accepted. The degree of bioload permitted is dependent on the category or subcategory a particular mission has been classified into.

Microbial species often recovered from the surfaces of uncrewed spacecrafts include bacteria, fungi, and yeasts, and are similar to those identified in dust samples of cleanrooms (Favero, 1971; Favero et al., 1966; La Duc et al., 2012; Puleo et al., 1977). The following genera are the most frequently identified: *Acinetobacter, Alternaria, Aspergillus, Bacillus, Candida, Cladosporium, Corynebacterium, and Flavobacterium Micrococcus Staphylococcus,* and *Streptococcus* (Favero et al., 1966, Favero, 1971, Puleo et al., 1973, Puleo et al., 1977, Taylor, 1974, Venkateswaran et al., 2001; Schuerger, 2004; Schuerger, 2007). Bacteria from the *Bacillus* sp. genus are known to form, under stressful conditions, spores that are highly resistant to various stressors (e.g., heat, desiccation, disinfection protocols, and radiation). For simplicity purposes, *Bacillus* spores are used as a reference in the quantitative analysis of the microbial spacecraft load in Mars Category IV missions. For non-life-searching missions, a maximum of 300,000 spores are allowed per vehicle. For instance, Mars Pathfinder, Spirit, and Opportunity rovers' biological burden did not exceed 3 $x10^5$ viable aerobic spores (Rummel, 1989; Crawford 2005; Puleo et al., 1977; Schuerger et al., 2007). For missions involving Martian "special regions," only 30 *Bacillus* sp. spores per spacecraft can be present after sterilization is concluded to avoid forward contamination of Mars (Changela et al., 2021).

Mission classification into a particular category is determined by the Committee on Space Research (COSPAR), which also delineates guidelines and preventive policies related to planetary protection (Race et al., 2012; Showstack, 2023). COSPAR was formed in 1959 and is currently comprised of several international space scientists who meet every two years to discuss, rectify and update policies (Fairien et al., 2017). Interplanetary contamination has been a concern of the scientific community for decades to such an extent that in 1967 the United

Nations created the Outer Space Treaty defining the foundations for planetary protection (United Nations, 1967). The treaty received worldwide support and has been signed by over 100 nations gaining the status of customary international law.

In addition to extremophilic life carried on robotic missions, the human body contains approximately 8×10^{13} microorganisms that reside commensally with each of us (Sender et al., 2016). Those microbes can reach the surface of Mars through space suits or leak from habitats. Hence any crewed mission will carry a risk of introducing human-associated microbes into the Martian landscape (Schwendner et al., 2017; Meadows et al., 2015). Although the Martian environment does not favour the growth of human-associated bacteria, preventive protocols and contamination risk assessment are still necessary (Schwendner et al., 2017).

5.1.2 Analogue missions as testing and risk assessment opportunities

Terrestrial analogue sites are locations on Earth characterized by topographies and environmental conditions resembling those on Mars or other planetary bodies. These locations are used for activities related to space exploration (Preston & Dartnell, 2014), such as the testing of robotic equipment and field trips involving sample collection. For instance, the Apolo 11 astronauts were trained in aspects of the Moon landing and rock sampling in Húsavík, Iceland and at various locations in the United States (e.g., Cinder Lake) due to terrain characteristics these locations share with the lunar surface.

Some of these analogue locations have stations that have been designed and constructed to emulate space missions. Here, a selected number of academics and/or members of the public co-habit as a team during simulated missions that can vary between weeks and months. During this period, crewmembers live and work inside habitational facilities where they perform routine tasks and scientific research as if they were in space. Occasionally, they also performed extravehicular activities (EVA), dressed in a garment similar to real spacesuits. In addition to spacewalks, instrument testing and evaluation of scientific protocols, these locations also allow the investigation of psychological and physiological effects that isolation and confinement

might have on crewmembers. A number of analogue stations have been used to simulate Mars missions including:

- Australia Mars Analog Research Station (Australia);
- Astroland Agency (Spain);
- Concordia Station (Antarctica);
- D-MARS (Israel);
- European Mars Analog Research Station;
- Flashline Mars Arctic Research Station;
- The Hawaii Space Exploration Analog and Simulation (HI-SEAS) (Hawaii, USA);
- Mars Desert Research Station (MDRS) (Utah, United States);
- Mars500 (Moscow, Russia);
- NASA Extreme Environment Mission Operations (NEEMO) (underwater);
- LunAres Research Station (Poland);
- Solar54 (Argentina).

The MDRS is the longest-running Mars analogue station. The MDRS, built near Hanksville, Utah, United States, similar to the Martian surface, is located in a desert characterized by high soil salinity and cold temperatures. Moreover, the MDRS terrain also shares similar mineralogy content to Mars. Both are rich in phyllosilicates, gypsum and other evaporites (Stoker et al., 2011). Due to these geological similarities, the MDRS focuses less on psychosocial studies and more on field research in analogue Martian terrain, which can be visualized in the satellite images of **Figure 5.2**.

Figure 5.2 Location of Hanksville, Utah, USA (left); MDRS Research Site in Hanksville, UT (right).

Due to the extreme nature of analogue locations, analogue stations are frequently isolated from populated areas and only visited by allowed personnel that strictly follow protocols designed to avoid the disturbance of indigenous life forms. Like the Martian soil, these places have been barely "touched" by humans and can be used to study the impact and extent of contamination that human missions will pose to the Martian landscape. Pristine environments can be contaminated by human-associated microbes, including commensal enteric bacteria, which are some of the best-known human contaminants (Baker et al., 2003).

Enteric bacteria and other human-associated microbes from crewmembers can become disperse throughout the internal environment of living and working facilities, as well as onto spacesuits and vehicles through shed skin and exhalation (e.g., coughing and sneezing) (Baker et al., 2003). Subsequently, even with stringent protocols, human-associated bacteria can be transported outdoors through several microbial hotspots (e.g., spacesuit gloves, spacesuit boots, and vehicles wheels), depicted in **Figure 5.3**. Pressurised spacecrafts or habitat modules are also not perfectly air-tight and microbial leakage into equipment can occur through tiny leaks. Moreover, waste facilities responsible for the process of urine, water, faeces, and other organic waste can be an additional source of environmental contamination (Yair et al., 2021). If contamination of the Martian environment occurs, terrestrial microbes can cofound the detection of indigenous Martian life and so jeopardize our efforts in searching for existing or extant extra-terrestrial microbial life.

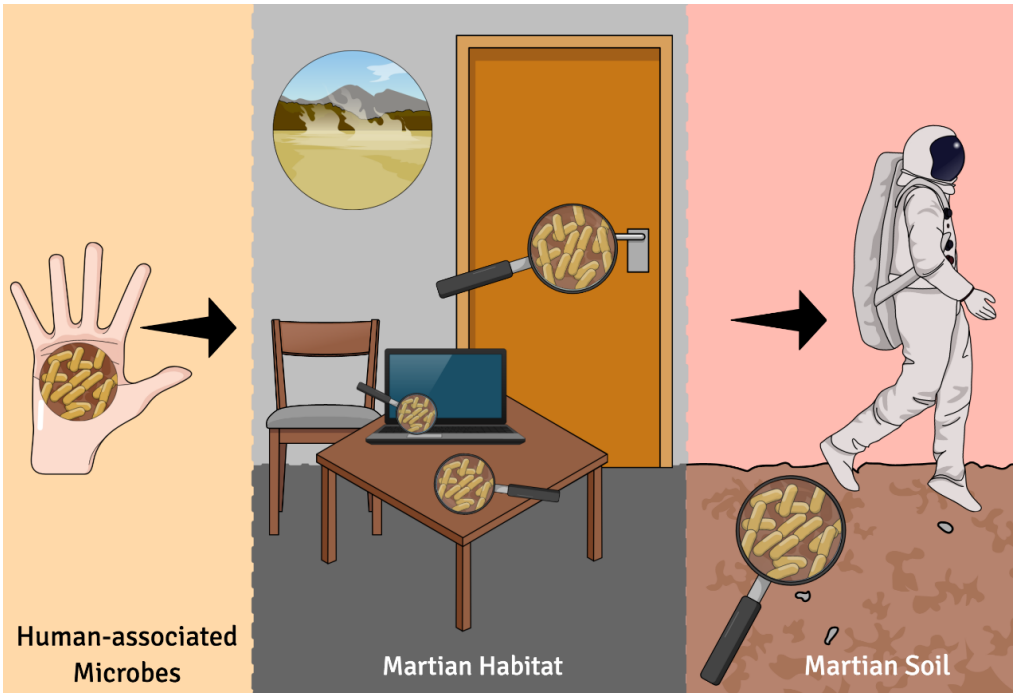

Figure 5.3 Schematic representation of forward contamination of Mars by human-associated bacteria. Commensal microbes can be transmitted into multiple surfaces inside Mars habitats and subsequently leak into the Martian environment.

In addition to the risk of contamination of pristine environments by human-associated bacteria, there is a growing attention being given to the microbial communities found inside analogue habitats. Human-made structures (e.g., residential buildings, hospitals, ISS, etc.) are known to harbour complex microbial communities (Adams et al., 2015; Mayer et al., 2016) which are determined by the interplay of different elements such as the external and environmental conditions, cleaning practices, building characteristics, and their occupants (Adams et al., 2015; National Academies of Sciences, Engineering and Medicine, 2017). Indoor microbiomes can present hazards to built habitats and their residents (Blachowicz et al., 2017; Mayer et al., 2016; Mora et al., 2016); therefore, a growing number of studies aim to decipher the main sources and routes of microbial dispersal and to provide insight into spatial and temporal dynamics of indoor microbiota (Adams et al., 2015). Of interest are the microbial monitoring findings obtained from the International Space Station (Novikova et al., 2006; Sielaff et al., 2019; Vesper et al., 2008) and Mars/Moon analogue habitats such as the Hawaii Space Exploration Analog (HI-SEAS), the Antartica base Concordia, the Inflatable Lunar-Mars Analog Habitat (ILMAH), the MARS500, and the Lunar Palace1 (LP1).

The number of studies focusing on the microbiome of closed habitats and contamination of Mars-like terrains by human commensals in the literature is exceedingly low. Much more information is needed to properly understand the risks microbes pose to crew members, Martian habitats, and its pristine soil.

5.1.3 Microbial monitoring and profiling by culture-independent methods

Microbial monitoring is essential for identifying and tracking potential pathogens and specific contaminants. Space Agencies have designed and implemented protocols for routine characterization and quantification of microbial communities aboard the ISS that are continuously updated as technology advances (Lang et al., 2017; Stahl-Rommel et al., 2021). The current ISS bioload allowances, microbiological specifications, and monitoring requirements are outlined in the ISS Medical Operations Requirement Documents (MORD NASA-2003) (Urbaniak et al., 2020). For instance, the microbiological contamination for potable water aboard the station is surveyed monthly; it should not exceed 5×10^4 colony-forming units (CFUs) of bacteria per litre of water (Urbaniak et al., 2020). Ideally, monitoring protocols should be quick, simple, autonomous, and offer on-site and real-time results.

Microbial monitoring can be performed by various techniques grouped into three primary scientific fields: microbiology, biochemistry, and molecular biology. Microbiological methods are the most traditional; unfortunately, these techniques (e.g., plate-counting and microscopic observations) are culture-dependent, meaning that they rely on microbial cultivation with specific growth requirements, which is fastidious, can be costly, and most importantly, offers an incomplete representation of the microbial composition of a sample (Spiegelman et al., 2005) With current protocols, only an expectational small portion (0.1-1%) of environmental microbes is recovered since the great majority are unculturable (Spiegelman et al., 2005). The latter can be due to the lack of knowledge in terms of specific nutrients required for the growth of certain species; the production of inhibitory substances by other bacteria that prevent the growth of the targeted microbe; and symbiotic relationships that make some bacteria dependent on other microbes and so unsuitable for individual culturing (Wade, 2002).

Biochemical methods, such as mass spectrometry and lipid analyses, are culture-independent. Unfortunately, this type of methodology produces information characteristic of the whole microbial community and is not suitable for characterising individual members of the community (Spiegelman et al., 2005). Both microbiological and biochemical techniques have been used to monitor the ISS water, air, and surfaces (Stahl-rommel et al., 2021). For instance, a portable system capable of identifying lipopolysaccharides on-site was used to detect Gram-negative bacterial and fungal endotoxins on cabin surfaces (Maule et al., 2009).

Lastly, molecular characterization, which provides information regarding the genetic information of organisms, circumvents the disadvantages mentioned above. It is currently the best option to identify the most representative microbes in samples with complex microbial compositions (Spiegelman et al., 2005). Molecular profiling has already been used to characterize the built environment of the ISS through analysis of samples from various surfaces (e.g., swabs and wipes) (Castro et al., 2023; Ichijo et al., 2016; Lang et al., 2017; Venkateswaran et al., 2014). As described by Lang et al. (2017), ISS surface samples are kept at –80°C in freezers aboard the station and inside the cargo spacecraft before being returned to the Earth and analysed in a laboratory. The overall process, from sampling to processing, can take weeks to months (Stahl-Rommel et al., 2021). On Mars and *en-route* to Mars, sample processing needs to be performed in-situ, independent from Earth-based facilities. Recent years have seen the validation aboard the ISS of easy-to-use portable molecular-based tools such as the miniPCR thermal cycler (miniPCR bio TM, Cambridge, MA, USA) and MinION sequencer (Oxford Nanopore Technologies, Oxford, UK) used for DNA amplification and identification, respectively (Boguraev et al., 2017; Burton et al., 2020; Castro-Wallace et al., 2017; Stahl-rommel et al., 2021).

In molecular analyses, nucleic acid (mainly DNA) is directly recovered from cells, eliminating the culturing step. Several commercial protocols are currently available for quick, consistent, and efficient extraction of DNA (Zielińska et al., 2017). Their effectiveness depends on the type of microbe, considering that different membranes and cell wall structures will lyse differently, and on the type of sample (e.g., marine, soil, and habitational structures). Soil is one of the most challenging samples to obtain high quantify of DNA with good purity levels

(Zielińska et al., 2017) due to co-extracted contaminants (Spiegelman et al., 2005; Yeates et al., 1998).

Different manufacturers use different protocols and buffers that might result in quantity and purity differences (Zielińska et al., 2017). Hence, the selection of the appropriate extraction kit should be carefully considered. During nucleic acid extraction from soil, once the DNA is released from the cells, co-excreted compounds, such as humic acids, can introduce bias and interfere with DNA analysis by inhibiting enzymes, such as the Taq polymerase, an enzyme commonly used in DNA amplification (Spiegelman et al., 2005). Thankfully, various extraction kits have been designed to minimize this problem, including the DNeasy ® PowerSoil (Qiagen), which uses a washing solution to remove humic acids, salts and other contaminants and an affinity-binding column with silica membrane that binds DNA (Spiegelman et al., 2005). This kit has been successfully used to analyse a wide variety of soil samples around the globe , including previously collected samples from the MDRS (Direito et al., 2011).

Three steps are involved in DNA extraction: cell lysis, DNA precipitation and purification. The kit's protocol starts with homogenizing the sample with bead-beating tubes provided by the manufacturer, followed by mechanical and chemical lysis of the cells and contaminant removal. The exact composition of commercial buffers is not fully revealed for commercial reasons. However, the precipitation step should be similar to other kits that use salts (e.g., sodium) and alcohol (e.g., ethanol) to neutralize DNA's negative charge and make it less soluble for precipitation and separation from the aqueous solution. In the last step, DNA is eluted with high pH and low-ionic-strength solutions (e.g., Tris-EDTA buffer or nuclease-free water).

Commercial kits commonly used in DNA extraction from soil require 250 mg of the initial sample (Yeates et al., 1998). One of the advantages of this kit is the existence of another version known as DNeasy PowerMax Soil Kit (Qiagen), which uses an increased quantity of the initial sample (10 g) for soils with low microbial load, such as desert samples. Moreover, in addition to topsoils, this kit has also been successfully used to extract DNA from various

swab samples, expanding its application to different types of microbiomes. In a study aimed to compare the efficiency of different extraction kits on vaginal swabs, this was the kit that resulted in the highest DNA yields (Mattei et al., 2019).

After extraction, the nucleic acids can be cloned, amplified or sequenced (Stahl-Rommel et al., 2021). The latter can help distinguish microbial species from one another, even if they share a high degree of similarity (Spiegelman et al., 2005). Molecular characterization methods comprise a broad range of techniques; selecting the best one from microbiome profiling can be challenging. The two most popular ones are Targeted and Shotgun sequencing. They both utilize Illumina Next-generation sequencing (NGS), which, thanks to its sequencing volume capacity, allows the simultaneous sequencing of millions of fragments at a time, which is a great improvement over classic Sanger sequencing, which only sequences a single DNA fragment per run. Shotgun is the most powerful molecular technique since it can sequence all given genomes from complex samples. As a result, in addition to taxonomy classification, shotgun sequencing is used for metagenomic assembly, metabolic functionally, and antibiotic resistance profiling. However, this type of analysis is costly. Gene-based sequencing has become a popular, affordable alternative for microbial characterization. In targeted sequencing, only a selected ("targeted") portion of DNA – usually the 16S ribosomal RNA (rRNA gene) – is amplified. Despite being less expensive, it requires PCR amplification of nucleic acids before analysis.

The choice between targeted or whole genome sequencing should be based on cost and research goals that consider sample type; sequence coverage; cross-contamination; and taxonomic resolution. Since the primary goal of this study is microbial identification (and comparison) instead of metabolic function analysis, the target sequencing technique was selected. Moreover, targeted sequencing is best suited for environmental samples and the identification of rare taxa since gene-targeted databases have higher coverage of bacteria and fungi from environmental sources.

Shotgun sequencing, capable of strain level profiling, has a greater taxonomic resolution. However, the technique can present false positives containing various "closely-

related" genomes from different species or genera if the reference database lacks a perfect representative of the sequenced genome. In targeted sequencing, error-correction bioinformatic tools, such as DADA2, allow the elimination of false positives resulting in improved taxonomic resolution and accuracy.

In targeted sequencing, the 16S rRNA gene, which encodes the 16S subunit of the ribosomal RNA, is the most widely accepted genetic target for microbial identification. Previously, lipid DNA and other genes were used for genotyping. However, ribosomal RNA became the standard marker since protein synthesis is a highly conserved and fundamental function for the survival of all organisms. As a result of its significance, its coding genes are some of the most conserved, presented in high copy numbers and have slower mutation rates (Spiegelman et al., 2005). This 1500 bp long gene also has nine variable regions that intercept the conserved sequences (Spiegelman et al., 2005). The highly conserved regions make the *in silico* design of universal primers possible, while the presence of hypervariable regions, such as V3 and V4, allows the differentiation of distinct bacterial and archeal species (Fadeev et al., 2021). Among all nine variable regions, V3 and V4 were selected because they are the most heterogeneous, thus offering maximum differentiation between organisms (Fadeev et al., 2021).

Fungi are devoid of 16S rRNA genes. However, eukaryotic cells possess '16S-like' ribosomal genes (18s rRNA) frequently used for profiling due to the presence of both conserved and variable regions similar to prokaryotes' 16S rRNA genes. Furthermore, the differentiation of yeast and fungi can be performed by additional ribosomal regions. The Internal Transcribed Spacer (ITS), mainly the ITS1 and ITS 2 genes, are regions of non-transcribed DNA, commonly referred to as "spacer DNA", found between small and large subunits of rRNA.

There has been controversy regarding whether 18S or ITS, is taxonomically more informative (Anderson and Parkin, 2007; Liu et al., 2015). Both have proven helpful in assessing fungal diversity in environmental samples (Anderson and Parkin, 2007). However, due to its non-coding nature and less conserved regions, ITS has shown greater potential for

differentiation of closely related fungal species (Liu et al., 2015) and offers more precise differentiation of fungal species in specimens from environmental sources such as in marine and soil samples (Liu et al., 2015).

In terms of data processing, the analysis of data from both targeted or whole genome sequencing can be complex due to the large-size and complexity of raw data; the necessity for powerful computational resources; programming skills and bioinformatic tools that need expert knowledge and proper training which most biologists lack (Marizonno et al., 2020).

Analysis of gene-targeted sequencing data includes preparation of data, quality control of reads and, at last, microbial characterization. It involves three main overall steps: trimming, error correction and comparison to available databases. Data post-processing starts with demultiplexing. In this step, sequence reads are separated and assigned to their original samples as fastaq data files. Demultiplexing is followed by quality control which involves the removal of contaminant sequences, artefacts, and low-quality reads that might result from sample impurities. Finally, microbial profiling occurs and includes chimera removal and taxonomic assignments to a phylogenetic rank based on comparisons between data and reference databases that are frequently updated, such as the Silva and UNITE for prokaryote and eukaryote (ITS), respectively (Marizonno et al., 2020).

Several bioinformatic platforms have been developed in recent years to simplify the analytical process of raw sequencing data and allow untrained biologists to get familiarised with advanced programming. The Quantitative Insights Into Microbial Ecology (QIIME2) (Bolyen et al., 2019) is a platform that has become one of the most widely used to analyse 16S rRNA gene sequencing data. QIIME2 is free, open source and has several plugins, including DADA2 denoise which provides exact sequence variants or amplicon sequence variants (ASVs) that offer higher accuracy in comparison to clusters of Operational Taxonomic Units (OTUs) (Chiarello et al., 2022).

As government agencies and private-sector enterprises prepare for crewed Mars missions, developing a strategic plan for Mars's environmental protection is becoming an

increasingly important topic in the scientific community. Forward contamination of Mars by human-associated microbes is a delicate issue because there is currently no definitive plan to accurately assess the potential environmental risks associated with future human endeavours.

This chapter aims to study and further understand the impact that human-commensal bacteria will have on the Martian environment. More specifically, this study aims to characterize the built environment of a Mars analogue habitat through culture-independent methods and determine the extent of microbial dispersal from inside the habitat into the surrounding soil.

5.2 Material and Methods

The MDRS is a living and working station where seven crew members remain in confinement for the entire duration of the "mission." The MDRS includes the habitational module (Hab), a greenhouse (GreenHab), a repair and assembly module (RAM), a laboratory (The Science Dome), and an observatory (**Figure 5.4A**). To assess the impact of human presence on a Martian analogue terrain, swabs from high frequency touched surfaces around the Hab's interior (**Figure 5.4C)** and an exterior soil sample from the immediate vicinity to the Hab (**Figure 5.4B)** were collected at the end of a two-week mission (MDRS mission number 174) by one of the crewmembers. Sample collection was performed by one of the team members. Sample processing and data analysis were performed at the University of Westminster. After DNA extraction, 16SrRNA gene amplicon and ITS sequencing was performed to identify the bacteria and archaea, and fungi, respectively, and microbial community composition and diversity associated with the humans living in the MDRS was analysed.

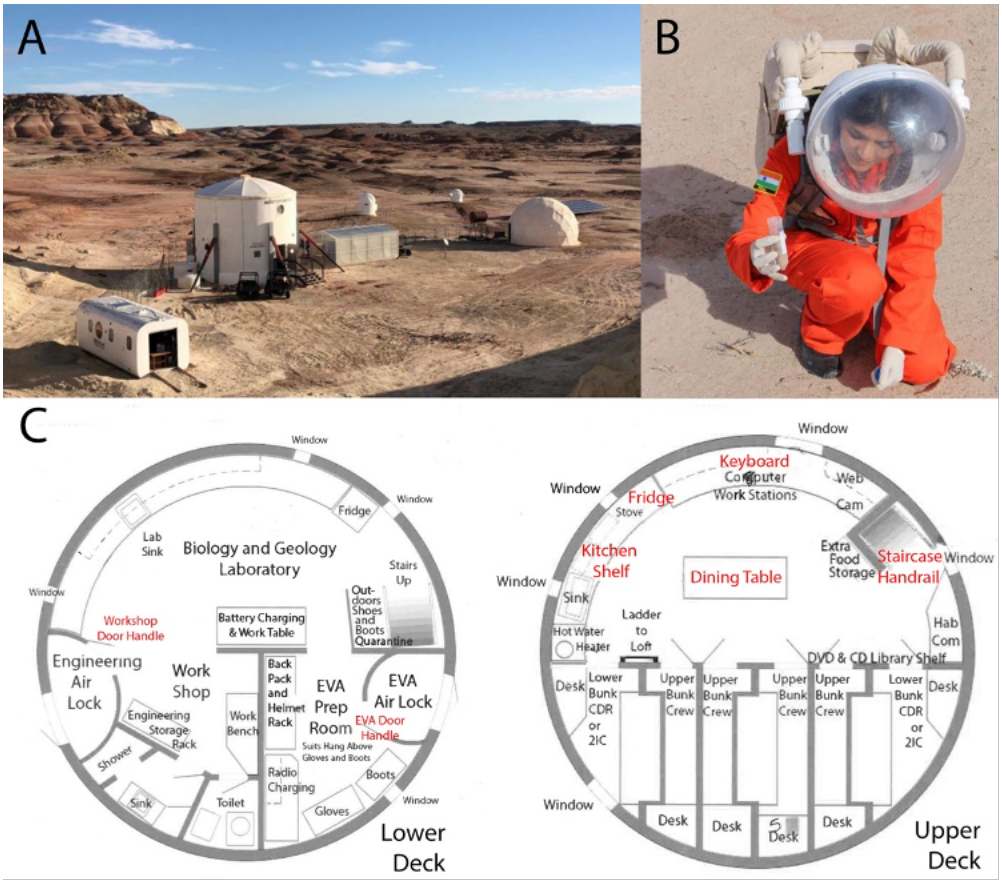

Figure 5.4 MDRS Research Site, Hanksville, Utah, USA. (A) The MDRS layout from left to right: the RAM, the Hab (the tallest building), The GreenHab, the observatory, and the Science Dome (credit: The Mars Society). (B) Soil sampling by a collaborator. (C) The interior layout of the Hab module, indoor sampling, with the swab sampling locations indicated in red text.

5.2.1 Sample Collection

All samples were collected in and around the Hab at the end of the crew's two-week mission in February 2017. Seven swab samples from interior surfaces were collected in duplicate before end-of-mission cleaning, from locations shown in **Figure 5.4**. Four swab samples were collected from the upper (habitational) deck: kitchen shelf (1); fridge door (2); dining table (3); and computer keyboard (4). Three swab samples were collected from the lower deck: workshop door handle (6); the interior handle of the EVA 'air lock' that gives access to the exterior (7); and the staircase handrail (5) that connects both decks. We therefore targeted sampling to dry, high-touch surfaces (HTS) such as handles, handrails and keyboards, as well as kitchen areas associated with food preparation, as recommended in the literature (National

Academies of Sciences, Engineering, and Medicine, 2017). While wearing ethanol-sterilised latex gloves, sterile swab kits (FloqSwabs, Copan, Italy), were moistened in sterile Phosphate-Buffered Saline (PBS) and run across the surfaces. For large, flat, surfaces, such as the dining table, a 10 x 10 cm surface area was swabbed in horizontal, vertical, and diagonal directions. For non-planar surfaces, such as door handles, it was attempted to sample an approximate 10 x 10 cm area, using as much of the surface of the object as possible.

5.2.2 DNA extraction and sequencing

2 mL of sterile PBS was added to each swab container and then agitated for 10 minutes at maximum speed (250 rpm) inside an incubator. The PBS was transferred into a sterile Eppendorf and centrifuged 10 minutes at 15,000 x g speed. The supernatant was removed without disturbing the pellet and transferred back to the swab container to be agitated for another 10 minutes. After a second centrifuge step, the pellet was resuspended in the C1 lysis buffer from the DNeasy PowerSoil Kit (Qiagen) and transferred to the bead beating tubes. The manufacturer's instructions were followed for all subsequent steps. The PBS used to moisten the sample-collection swabs in the field was also processed to investigate potential contamination during sampling. 20 g of soil was used for the total DNA extraction with DNeasy PowerMax Soil Kit (Qiagen) following the manufacturer's instructions. DNA quality check, library generation and sequencing on Illumina MiSeq platform was performed by Eurofins Genomics as part of their INVIEW Microbiome Profiling 3.0 service. Three targets were amplified: bacterial V3-V4 hypervariable region of the 16S rRNA gene, the entire 16S rRNA gene for archaea, and the fungal internal transcribed spacer gene, ITS1. A "blank" was also analysed to characterize the kitome present in this study. The phosphate-buffered saline (PBS) buffer used during surface sample collection was added to an unexposed swab kit. Following the same protocol as that used for the samples, the PBS was subjected to DNA extraction and 16S rRNA and ITS sequencing to enable the identification of contaminants in the swabs, PBS, and reagents in the Qiagen/MoBio PowerSoil DNA extraction kits.

5.2.3 Bioinformatics analysis

QIIME2 pipeline (Bolyen et al., 2019) was used to process raw sequencing data. The amplicons were demultiplexed and primers and barcodes removed from all reads. All chimeric sequences and the first 15 bp of all sequences were removed by DADA2 noise removal algorithm. ITS and 16S rRNA gene amplicons were trimmed based on the Phred values (fungal ITS amplicons F=260 bp and R = 230 bp; prokaryotic 16S rRNA gene F = 270 bp R = 235 bp) which measures the quality of nucleobase identification. Sequences were subsequently clustered into amplicon sequences variants (ASVs) using the DADA2 algorithm. Phylogeny was assigned to the amplicon sequence variants using Scikit–learn classifier (Pedregosa et al., 2011), which compared the ASVs against the Silva (for bacterial and archaeal 16S rRNA gene amplicons) and UNITE (for ITS amplicons) databases (Kõljalg et al., 2020; Nilsson et al., 2019; Quast et al., 2013; Yilmaz et al., 2014) with a confidence threshold of $p = 0.7$. The ASVs alignment was performed using MAFFT (Katoh and Standley, 2013) and a rooted tree produced. All the amplicons were normalised by rarefaction to 60,000 reads and alpha and beta diversity metrics calculated from the normalised data using QIIME2 (Bolyen et al., 2019) to assess the community diversity and the variation between samples. The alpha diversity metrics were Shannon, Simpson, Chao and the number of ASVs identified. Dice, Bray-Curtis, Euclidean and Jaccard were the beta diversity metrics. The presence of plausible contamination was determined by Principal coordinate analysis (PCoA) by comparing amplicon sequence variants (ASVs) of overlapping ASVs present in the soil sample and at least one indoor sample. Heatmap generation was performed using ClustVis (Metsalu and Vilo, 2015).

5.2.4 Soil analysis

Six samples of soil were collected from different locations in the MDRS area and at various distances from the habitat, as shown in **Table 5.1**. The samples were scooped from the uppermost soil layer and near-surface region.

Table 5.1 Soil samples identification, location, and respective physical descriptions.

Sample	UTC Coordinates		Altitude (m)	Location	Description
	Easting	Northing			
S1	518227	4250724	1372	1 meter from the Habitat	Brown clumps of clay soil that break apart
S2	518229	4250721	1368	2 meters from the Habitat	Pale-brown fine sandy soil with occasional rocks
S3	518229	4250718	1368	5 meters from the Habitat	Rusty-brown clay soil with clumps that break apart
S4	520331	4247314	1331	random	Rusty-brown clay soil
S5	518705	4248545	1349	350 meters from Little Mountains	Beige sandy soil with clumps that break apart
S6	518259	4255749	1369	Dinosaur Quarry	Dark-brown coarse sandy soil

5 g of each sample was weighed in triplicate and placed in individual porcelain crucibles. The crucibles were dried (3 h at 105°C) in an oven for moisture quantification. The weight of the dried samples was recorded and used in the following equation (**Equation 5.1**) to help calculate weight losses associated with water, where DW and DW105 represent the dry weight of the sample before and after heating at 105°C, respectively (both in g):

$$Water\ reduction\ = \frac{DW\ -\ DW105}{DW}\ \times\ 100 \qquad \textbf{(Eq 5.1)}$$

Organic matter content was determined by the loss on ignition (LOI) method, whereby high temperatures drive oxidation and escape of carbon as carbon dioxide. Sample weights were recorded before and after furnace heating (3 h at 550°C). LOI (%) was determined by the equation shown next (**Equation 5.2**), where DW105 represents the dry weight of the sample after oven heating and DW550 is the dry weight of the sample after combustion at 550°C (both in g):

$$LOI\ =\ \frac{DW105\ -\ DW550}{DW105} \times 100 \qquad \textbf{(Eq 5.2)}$$

For pH measurements, 5 g of Milli-Q water was mixed with 5 g of each soil. The pH of each sample was measured using a Mettler Delta 320 pH meter. The probe was washed between samples. The samples were centrifuged (3488 centrifugal force) for 3 minutes (Thermo Scientific Megafuge 40R) and left to rest for elemental analysis. After being soaked in water for four days, the concentration of several elements was determined by inductively coupled plasma optical emission spectroscopy (ICP-OES) with an ICP-OES instrument (Agilent 5110), with an instrument detection limit of 3.6 ppb (parts per billion). One run was performed per sample; each sample's final result is based on five internal runs and accounted for baseline noise and background interferences. The dilution factors used can be found in **Appendix A**. MaDLs for all analyzed elements are presented next in alphabetic order: aluminium 0.08 mg/kg, arsenic 1.5 µg/kg; barium 0.3 µg/kg; calcium 0.01 mg/kg; cerium1.9 µg/kg; cobalt 0.9 µg/kg; chromium 0.3 µg/kg; copper µg/kg; iron 0.08 mg/kg; gallium 5.4 µg/kg; potassium 0.02 mg/kg; magnesium 0.01 mg/kg; manganese 0.002 mg/kg; molybdenum 0.6 µg/kg; sodium 0.17 mg/kg; neodymium 1.8 µg/kg; nickel 2.0 µg/kg; potassium 0.01 mg/kg; lead 3 µg/kg; sulfur 0.01 mg/kg; antimony 5.2 µg/kg; scandium 1.2 µg/kg; selenium 4 µg/kg; silicon 0.01 mg/kg; tin 4.8 µg/kg; strontium 0.001 mg/kg; titanium 3.5 µg/kg; vanadium 0.7 µg/kg; tungsten 3.6 µg/kg; zinc 38.1 µg/kg; and zirconium 15.5 µg/kg.

5.3 Results and Discussion

In order to characterise the interior microbiome of an analogue Martian facility, seven swab samples were collected from frequently touched surfaces within the MDRS Hab (**Figure 5.3C**): (1) kitchen shelf, (2) fridge door, (3) dining table, (4) computer keyboard, (5) staircase handrail, (6) workshop door handle, (7) interior handle of the EVA air lock. A soil sample was also collected immediately outside the habitat airlock, expected to have the greatest abundance of human-associated bacteria, to assess the potential detectability of human-associated microbes from the Hab contaminating the environment.

Sequence analysis identified bacteria and fungi in all swab samples taken from surfaces inside the habitat, with the exception of the staircase handrail where only fungal sequences were amplified. The number of sequence reads was generally higher for fungi (**Appendix B**).

Archaeal sequences were not amplified from any of the samples (**Appendix B**). Similar studies have attributed the difficulty in detecting archaea from surface sampling to differences in environmental distribution: archaea tend to inhabit microhabitats, while bacteria are more broadly distributed in the environment (Aller and Kemp, 2008; Direito et al., 2011). The role of archaea in the microbiome of human-built environments is still unclear due to the lack of sufficient archaeal surveys (Moissl-Eichinger, 2011). Nonetheless, screening for archaea on spacecraft and analogue habitat-associated surfaces remains essential as they are considered by some, due in part to their metabolic diversity, to be the organisms most capable of surviving and proliferating in Martian conditions (Moissl-Eichinger, 2011).

Moreover, the lack of archaea in the data set could be the result of PCR primer mismatches. Common prokaryotes 16S PCR primer sets fail to amplify many archaeal species (Bahram et al., 2019). Different primer sets have been designed and tested recently to overcome this issue (Bahram et al., 2019; Fadeev et al., 2022). For instance, during the investigation of marine microbiomes, Fadeev and colleagues tested alternative primers for community profiling of archaeal species. The primer set (515F-Y/926R) targeted the hypervariable regions V4 – V5 and provided higher sequence coverage than the V3/V4 primer set. 16S rRNA V1/V2 primer sets have also outperformed conventional 16S primers offering a greater resolution of Archaea taxa (Bahram et al., 2019; Bharti and Grimm, 2019).

Despite the current difficulties associated with archaea profiling, screening of archaea remains essential due to their ubiquitous nature and metabolic diversity; some consider Archaea to be the most capable organisms of surviving and proliferating in Martian conditions (Moissl et al., 2008).

5.3.1 Investigating the “Kitome”

One of the challenges that troubles microbiota researchers is the presence of contaminating DNA in extraction kits (Salter et al., 20014). It is now known that kits and reagents contain their own singular microbiome (“kitomes") which may be confounded and mask the actual microbiome of samples (de Goffau et al., 2018; kim et al., 2017, Hornung et

al., 2019, Stinson et al., 2018; Salter et al., 2014, Velasquez-Mejia et al. 2018). The presence of kitomes, which varies between kits, is particularly challenging in samples containing low microbial biomass, (de Goffau et al., 2018; Salter et al., 2014; Stinson et al., 2018), such as desert soil. In these types of samples, the amount of DNA of interest might not be enough to compete with predominant contaminating DNA (Salter et al., 2014).

Concerns regarding the lack of negative controls have also emerged in the last few years in microbiome and kitome research (Hornung et al., 2019). A strength of our study is the use of a "blank." Sterile phosphate-buffered saline (PBS) buffer used during sample collection was added to a sterile swab kit. Similar to the samples, PBS was subjected to DNA extraction and 16S rRNA sequencing to enable the identification of contaminants in reagents and in the swab and Qiagen/MoBio PowerSoil DNA extraction kits.

Kit contaminants identified in previous studies match the sequences of soil and water associated bacteria, including nitrogen fixers (de Goffau et al., 2019; Kulakov et al., 2002). Similarly, the results presented here suggest contamination of the indoor samples with soil and root-associated bacteria such as *Bradyrhizobium*, *Mesorhizobium*, and *Phyllobacterium* (**Appendix C**), many of which fix nitrogen and have been reported previously as contaminating DNA (Salter et al., 2014). *Bradyrhizobium* is known for being one of the most common contaminants in sequencing datasets (Laurence et al., 2014; Salter et al., 2014). A possible explanation for the presence of N_2-fixing bacteria in kitomes was provided by Kulakov et al. (2002). The authors associated its presence with the use of nitrogen instead of air during storage of ultrapure water (Kulakov et al., 2002; Salter et al., 2014).

Fungal contamination was also evident in the current study (**Appendix C**). The majority of contaminating sequences identified in the negative control belong to saprotrophic genera, most specifically *Leptobacillium* and *Exophiala,* which were present in high numbers in the indoor environment.

While it is practically almost impossible to eliminate kitomes all together, the inclusion of controls and attention to sample collection and processing are common procedures used to

minimize contamination risks (de Goffau et al., 2019; Hornung et al., 2019; Salter et al., 2014). Beyond these preventive measures, bioinformatics tools can also be used to help detect ASV's present in the negative controls and subtract them from the actual samples (Edmonds & Williams, 2017; Hornung et al., 2019). Currently, no fully agreed standard protocol exists for interpretation of 16S rRNA sequencing controls and raw data (Hornung et al., 2019). The elimination of the kitome from all samples is a possibility but should be carefully considered and should take into account the number of reads obtained; to exclude contamination from sample results the negative control should have fewer reads than the samples (Edmonds & Williams, 2017; Hornung et al., 2019). In this study, plausible kit contaminants were studied at the genus level. The number of species identified in the control was compared with the ones from the samples. If a certain genus was recovered in a sample and the number of reads was higher in the negative control, that genus was removed for microbiome analysis. Interestingly, fungal, and bacterial contaminating DNA were present in different numbers in the abiotic surfaces but mostly absent in the soil sample (**Appendix C**). Our finding might suggest that the origin of the kitome is the swab kits and/or the PBS used to sample the locations inside the Hab since they were not used during soil collection and processing (**Appendix C**). Thus, the DNA extraction kit can be eliminated as a source of contaminants in this study.

5.3.2 Comparison between the indoor and outdoor-derived microbiomes

Once the contaminating species were identified and excluded, heatmaps and stacked column charts were constructed to facilitate visualization of the remaining taxa. The heat maps, shown in **Figure 5.5,** show that the abundance patterns of bacterial and fungal diversity of the indoor samples do not resemble the outdoor environment. The most abundant bacterial genera, represented by dark red, found in the soil were absent in all seven indoor samples (**Figure 5.5A)**. The same trend was observed for fungi (**Figure 5.5B**). At the genus level, 28 bacterial genera were exclusively found in the indoor samples.

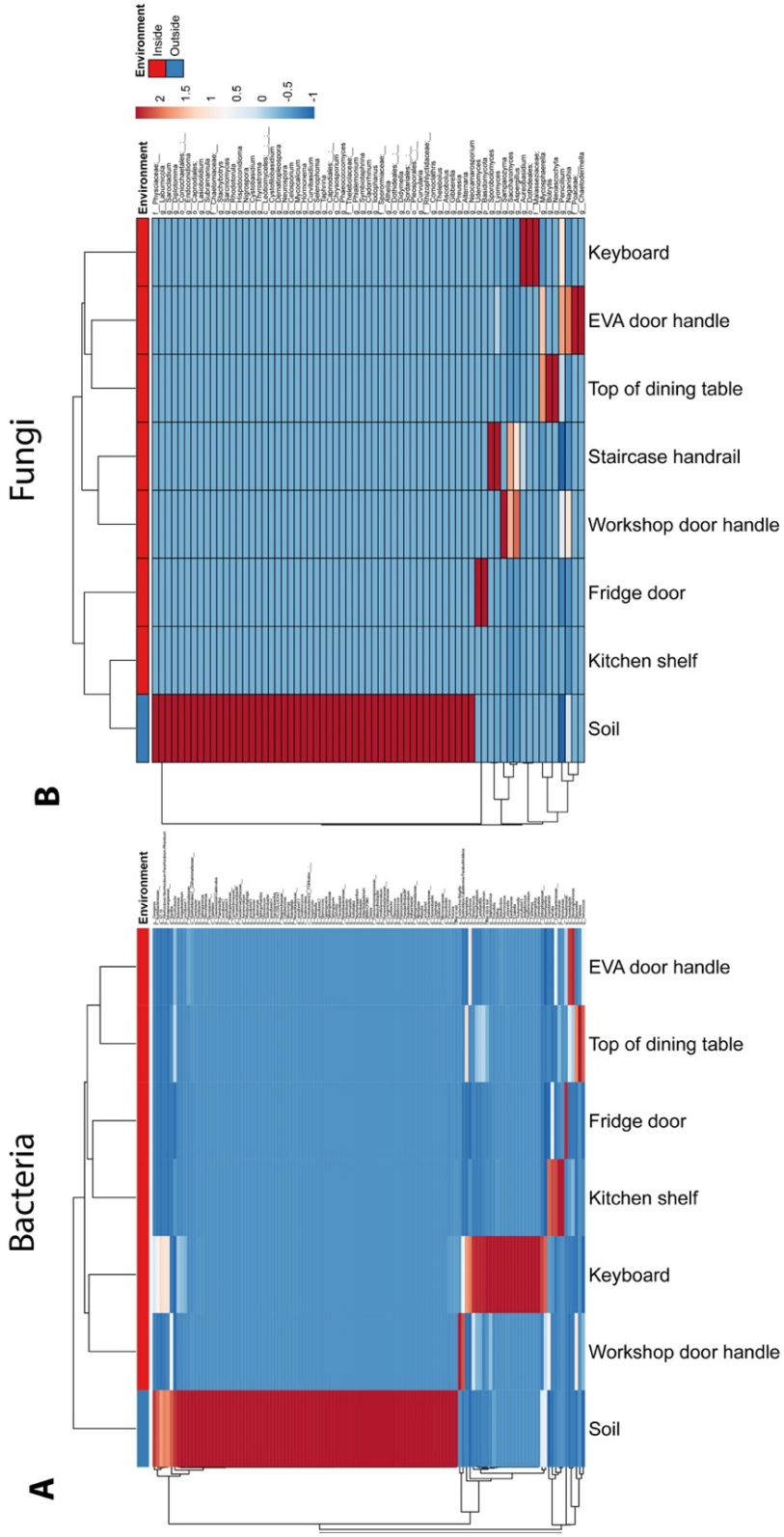

Figure 5.5Heat map of bacterial (A) and fungal (B) diversity and abundance (darker red indicates the most prevalent groups) for all six swabs and the soil sample collected next to the Hab's airlock. Heat maps were constructed using VISCLUST.

The relative abundances (%) of the most abundant microorganisms in the swabs and adjacent soil sample were also calculated. There is no clear consensus on how to present microbial composition in terms of resolution level. The microbial composition of each sample is presented here at the genus level since species belonging to the same genus share various traits. In some instances, when genera were too closely related, ASV's were assigned to a higher hierarchical classification level, such as family.

Analysis of a stacked bar plots (**Figure 5.6A and 5.6B**) confirmed that the predominant genera changed according to the difference in environments (indoor and outdoor). Both figures demonstrate that the swabs have similar microbiome compositions, sharing microbial groups within them while relative abundance differs among the several locations. Which, similarly, to Schwendner et al. (2017), implies that there is a common microbial signature inside the Hab even though each surface had its own microflora. In contrast, the soil yielded a distinct microbial pattern. A range of environmental species were observed in the soil sample. The sample from the terrain also exhibited higher diversity when compared to the locations sampled inside the Hab. These results confirm the complexity and diversity of the soil microbiome which is frequently referred to as the ecosystem with the highest genomic diversity at a global level (Mishra et al., 2022). The bacterial groups identified are discussed in the following section. Overall, the most predominant groups in each sample were frequently associated with similar sample locations discussed in the literature, suggesting a low probability of cross-contamination during sampling and sample processing.

A weakness of this study is the lack of control over potential contamination by the researcher. Unfortunately, the definitive proof of lack of human contamination can be complex. One approach is to limit the number of researchers performing sample processing – advice followed in this study - and further sample and sequence the hands of the researcher itself (Hornung et al., 2019). Alas, it is important to consider that this type of contamination could be unevenly distributed over the samples. Therefore, the presence of a common human-commensal in the samples and its absence in the control could result in false evidence of lack of contamination (Hornung et al., 2019).

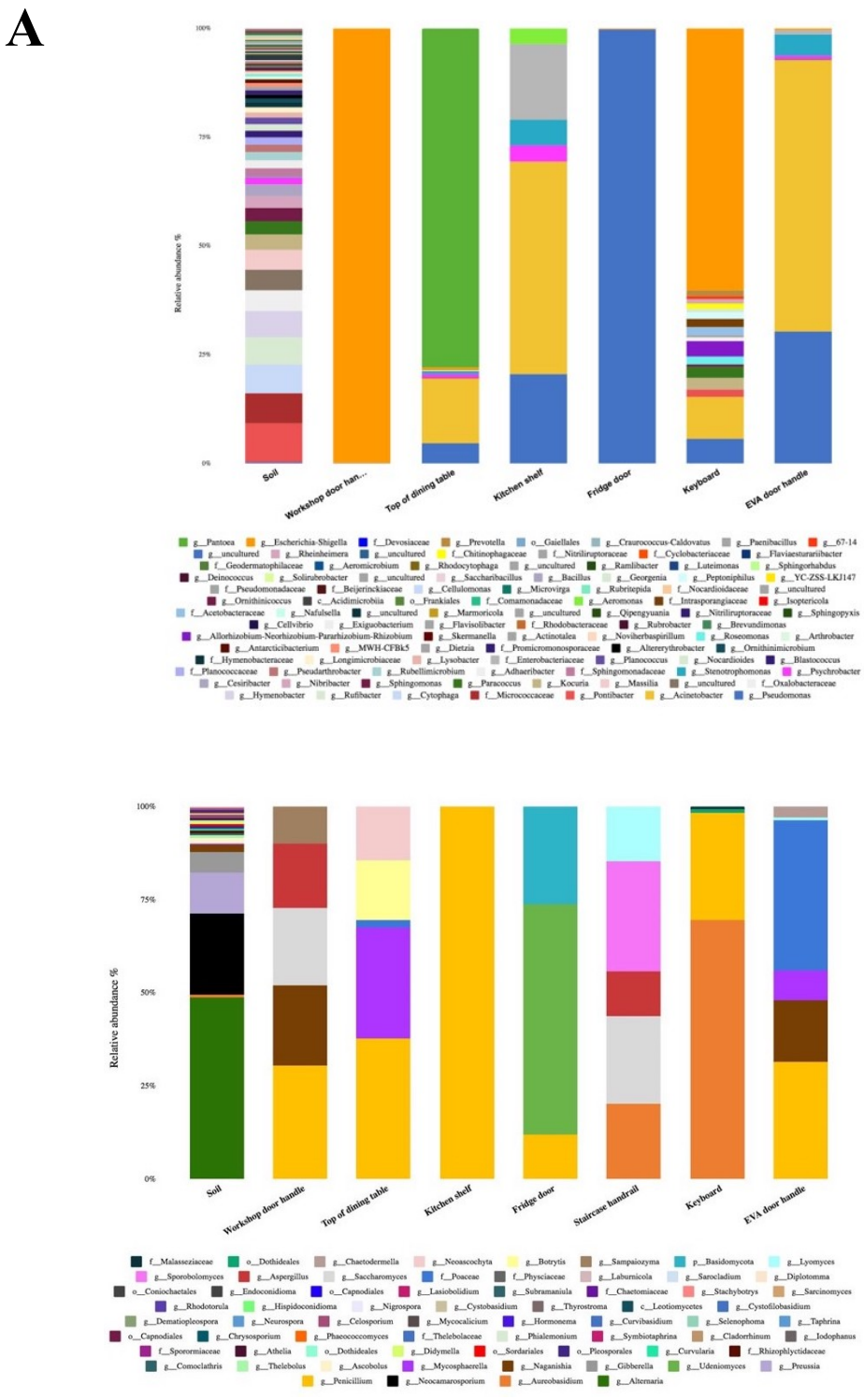

Figure 5.6 Relative abundance percentages of bacterial (A) and fungal (B) genera identification, with some exceptions where genus could not be determined and the microbes were assigned to a higher classification level (e.g., family).

5.3.3 Overview of microbial taxa identified across surfaces inside the Hab

As previously mentioned, microbial monitoring and analysis was performed during previous simulated missions in analogue habitats (e.g., ISS, HI-SEAS, ILMAH, MARS500 and LP1) (Blachowicz et al., 2017; Mahnert et al., 2021; Mayer et al., 2016; Schwendner et al., 2017; Van Houdt et al., 2012; Yang et al., 2022). Overall, the surfaces of Mars500 were characterized by the presence of *Staphylococcus* and *Bacillus* (Schwendner et al., 2017), whereas monitoring of HI-SEAS built environment revealed that *Chryseobacterium*, *Lactobacillus*, *Gardnerella*, *Prevotella*, and *Acinetobacter* were the most frequent bacteria (Mahnert et al., 2021). Li et al. (2021) also investigated built surfaces from the HI-SEAS IV mission and observed significantly higher microbial diversity on plastic rather than wooden surfaces. Mayer et al. (2016) reported an increase of *Actinobacteria* and *Firmicutes* phyla over time during the ILMAH 30-day mission.

In this study, inside the MDRS habitational module, Proteobacteria was identified as the predominant taxa. It had top abundances in all sampled site (**Appendix D**). Even though samples and data were not collected in the beginning of this study, the presence of proteobacterial species all over the surfaces at the end of the mission could be the result of a loss of microbial diversity and a shift in the microbial composition from Gram-positive to Gram-negative bacteria. In the literature, a shift from Gram-positive towards Proteobacteria and other Gram-negative has been associated with increased confinement and cleaning (Mahnert et al., 2021). At the genus level, the Gram-negative *Acinetobacter* (yellow), *Pseudomonas* (blue), *Escherichia-Shigella* (orange) were the most common bacteria found inside the Hab (**Figure 5.6A**).

Identifying the surfaces with the greatest interest for these types of studies can be challenging. As per recommendation in the literature, the focus was on dry high-touch surfaces (HTS) (e.g., door handles, keyboard, etc.) and kitchen areas associated with food preparation such as the top of the dining table (National Academies of Sciences, Engineering, and Medicine, 2017).

Only members of the *Enterobacterireacea* family were identified in the workshop door handle (99.9%). This family includes human-associated pathogens and commensals such as the closely related *Escherichia* and *Shigella* genera (Schierack *et al*., 2007). In a recent study, members from these genera, together with *Escherichia*, were the most common Gram-negative bacteria isolated from frequently touched hospital surfaces, including door handles (Bhatta *et al*., 2018; Frank et al., 2017). Additionally, this was the sample with the highest bacterial reads (**Appendix B**).

Analysis of the EVA door handle, sample closest to the exterior, revealed the presence of *Acinetobacter* (62.3%) and *Pseudomonas* (30.3%). The majority of reads found in the fridge door were assigned to *Pseudomonas* (**Figure 5.6A**) which can be found in plethora of environments. Despite representing an environmental and water-related bacterial taxon (Mahnert et al., 2021), this genus also encompasses psychrotrophic and psychrotolerant bacteria responsible for the spoilage of refrigerated food (Franzetti and Scarpeluni, 2007).

Most likely, the keyboard was the sampling location less often subjected to cleaning. Not surprisingly, this sample displayed the greatest bacterial diversity (**Figure 5.6A**), with representatives from different bacterial phyla (**Appendix D**) and a high incidence of *Escherichia-Shigella*. While studying intensive care units, Bures et al. (2000) concluded that the incidence of novel and unrecognized taxa was greater on keyboards and faucet handles than on other well-studied ICU surfaces.

Representatives of the Erwiniaceae family made up the largest portion of dining table surface (78.0%) and belonged to the genus *Pantoea* (green) which are associated with plants (Cruz et al., 2007; Llop, 2015). Members of this family were not represented in the other samples, which indicates that the members of the Erwiniaceae family present here are a microbial fingerprint of vegetables and fresh fruits when these are placed and prepared on the dining table for consumption (Cruz et al., 2007; Llop, 2015).

Almost half of the bacteria identified in the kitchen shelf belonged to the *Acinetobacter* genus (48.8%), which is commonly described as a skin-associate bacteria (Mahnert et al., 2021)

and will be discussed further ahead. Curiously, the kitchen shelf had the lowest number of bacterial reads (**Appendix D**).

Characterizing and screening the mycobiome is deemed important. In addition to some fungal species being harmful to humans, technophilic fungi can corrode structural materials and lead to habitat deterioration (Blachowicz et al., 2017; Mora et al., 2016; Novikova et al., 2006). Ascomycota, the largest phylum of fungi, was abundant in all our swab samples (**Appendix E**). Identical to the results presented here, Blachowicz et al. (2017) also reported Ascomycota as the most predominate phylum inside the ILMAH (90%). At the genus level, as seen in **figure 5.6B**, the most predominant genera detected through the ITS1 region was *Penicillium* (yellow), seen in all seven swabs, followed by *Aureobasidium* (orange). Novikova and authors (2006) also reported *Penicciilum* (and *Aspergillus*) as the most dominant fungal population aboard the ISS, whereas inside the inflatable module, *Epiccocum*, *Alternaria and Pleosporales* - fungi frequently found in common residential spaces – were the most frequent genera with increased abundance over the occupation time (Blachowicz et al., 2017).

The observations regarding the microbiota of the Hab, which is not the main goal of this study, are limited by the lack of temporal data. Nevertheless, it has been shown that microbiota of space-like habitats as a result of human presence changes over time (Blachowicz et al., 2017; Schwendner et al., 2017). In the past, confinement has been correlated with loss of microbial diversity (Schwendner et al., 2017), but more recently, Mahnert and colleagues (2021) observed a (slight) diversity increase in HI-SEAS built-surfaces.

5.3.4 Human-associated microbes inside the Hab

Astronauts are probably the most important sources of contamination in space habitats (Novikova et al., 2006; Schwendner et al., 2017; Yang et al., 2022). Commensal microbes that inhabit multiple parts of the human body, such as skin or respiratory airways, get dispersed via skin flakes, perspiration, or coughing, consequently shaping the in-house biome (Baker et al., 2003; Blachowicz et al., 2017; Novikova et al., 2006).

Numerous genera can be indicative of human microflorae. Some of the best-known cutaneous residents are Gram-positive bacteria from the *Staphylococcus*, *Streptococcus, Corynebacterium*, *Propionibacterium, and Brevibacterium* (Cogen et al., 2008; Cosseau et al., 2016). *Acinetobacter* is the Gram-negative bacterium most frequently isolated from skin microflora (Cosseau et al., 2016), whereas coliform bacteria are frequent representatives of the human gastrointestinal tract and include genera from the *Enterobacteriaceae* family (e.g., *Escherichia, Shigella, Pantoea,* etc.).

In the present study, enteric bacteria were traced to all indoor locations (**Figure 5.5**). The EVA door handle and the fridge door had the lowest relative abundances, which may reflect a more thorough cleaning schedule and hygiene practices in these areas. Additionally, the EVA door handle might be more likely to be touched only when wearing gloves. In contrast, a large number of *Enterobacteriaceae* were found in the keyboard (60.2%) and kitchen shelf (17.4%). Members of *Escherichia-Shigella* genera were highly abundant on the workshop handle (>90%), while *Pantoea* was the most predominant genus (78%) on the kitchen table, as mentioned earlier. Although *Pantoea* species are well-established plant pathogens, recent studies report the presence of *Pantoea* in various clinical isolates (Soutar and Stavrinides, 2019; Walterson and Stavrinides, 2015).

Sequences of skin-associated *Staphylococcus* and *Streptococcus* were seen in the keyboard which could be the result of frequent and direct touch from crewmembers. ASV's assigned to *Acinetobacter* were present in all indoor samples to varying proportions. Even though this genus is recognized as a skin taxon, these bacteria are also frequently isolated from human-made surfaces, including indoor spaces with strictly controlled conditions such as cleanrooms (Mahnert et al., 2021, 2019). Mahnert et al., 2021, observed higher abundance of *Acinetobacter* in the HI-SEAS built surfaces (e.g., main room and bedroom) than on the crew's skin. This finding made the authors consider the potential role of this bacterium as a microbial indicator for confined human-built environments. In the present analysis, members of the phyla Firmicutes and Bacteroides, which represent more than 90% of the human gut bacteria (Kosiewicz et al., 2011), were also present (**Appendix E**).

In addition to bacteria, many fungi have also been identified as human commensals (Auchtung et al., 2018; Limon et al., 2017). *Penicillium* was the most common fungi inside the Hab. The presence of *Penicillium* in healthy human stools is documented (Limon et al., 2017). This genus showed a consistent presence in all sampled surfaces, in the following order of abundance: kitchen shelf (100%), top of dining table (37.8%), EVA door handle (31.3%), workshop door handle (30%), keyboard (28.9%), fridge door (11.9%), and staircase handrail (<1%).

Human skin and oral cavity harbor *Aspergillus* (Limon et al., 2017), which was present in the workshop door handle and staircase handrail. *Aureobasidium* is a genus frequently encountered in healthy oral mycobiota (Underhill and Iliev, 2014). Sequences assigned to this genus were recovered from the staircase and keyboard.

Moreover, a handful of bacterial and fungal genera found inside the Hab include potential human pathogens and opportunists. *Pseudomonas*, *Escherichia*, *Aspergillus*, and *Aureobasidium*, to name a few, encompass species that are known for causing infectious diseases in humans (Limon et al., 2017; Mora et al., 2016). These findings emphasize the necessity to monitor the microflora of confined environments in analogue and future Mars missions to avoid the spreading of harmful microorganisms. Confined conditions can aggravate bioaccumulation and microbial transmission due to increased physical proximity among occupants; furthermore, spaceflight can compromise immune responses while enhancing antibiotic resistance and bacterial virulence of some microbial species (Blachowicz et al., 2017; Mahnert et al., 2021; Mayer et al., 2016; Mora et al., 2016; Schwendner et al., 2017; Yang et al., 2022).

5.3.5 Microbial taxa identified in the soil

In terms of DNA concentration, the overall amount of DNA recovered from the soil sample closest to the Hab was very low (<15 μg/μl), as seen in **Table 2.** Unfortunately, the vast majority of microbes in the soil are hard to recover through traditional extraction and culturing laboratory methods, which prevents the accurate interpretation of microbial diversity (Andrew et al., 2012; Fierer and Jackson, 2006).

Microbiological analysis was also performed on the sample collected closest to the airlock due to its proximity to the Hab, its inhabitants and the likelihood of recovering commensal DNA. Most of the bacteria identified in the soil belonged to the following phyla: Bacteroides, Actinobacteria, and Proteobacteria (**Appendix F**). Members of these phyla have been found in deserts worldwide, including MDRS soil samples from past studies (Direito et al., 2011; Sun et al., 2018). In this study, *Pontibacter* (8.9%), *Cytophaga* (6.5%), *Rubibacter* (6.3%), and *Hymenobacter* (6.1%) were identified as the most abundant genera. Members of these genera contribute and occupy a vast array of natural sources from soils to various aqueous environments (Kirchman et al., 2003; Roiko et al., 2017; Sun et al., 2018).

The results also showed the presence of extremophilic species as predicted. Deserts are extreme environments characterized by environmental stressors that limit the types of resident microbes (Sun et al., 2018; Vikram et al., 2016). The MDRS is located in a cold desert with intense daily temperature variations that can reach as low as –36°C (Sun et al., 2018; Vikram et al., 2016). Direito and team (2011) studied extremophiles in the MDRS soil and observed a higher abundance and diversity of bacteria when compared to fungi. Similar to the current study, no archaea were detected in the soil sample collected closest to the station.

Extremophiles are of great scientific interest in astrobiology. They have implications for the origin of life and the search for life on other planetary bodies (Merino et al., 2019; Sun et al., 2018). Among the extremophiles recovered, the psychrophile *Hymenobacter glacialis* (Roldán et al., 2020) and other cold-loving bacteria such as *Planomicrobium glaciei* and *Psychrobacter cryohalolentis* were identified. Halotolerants such as *Anditalea andensis* and UV radiation-tolerants (e.g., *Rufibacter tibetensis*) were present. Moreover, as expected, nitrogen-fixing bacteria (e.g., *Azotobacter vinelandii*) were also recovered.

Additionally, the fungal distribution patterns in the soil were also studied. At the phylum level, like the indoor samples, Ascomycota was also the predominant soil phylum in proximity of the Hab (**Appendix G**). Taxa from this phylum can originate and occupy a wide variety of sources, from soils to waterbodies. At the genus level, the taxa detected by ITS1, in order of abundance, were the following: *Alternaria* (48.7%), *Neocamarosporium* (21.8%) and *Preussia*

(11%). Alternaria is widely detected in cryptogamic soils worldwide (Bhatnagar & Bhatnagar, 2005), which are desert soils with a fragile surface crust characterized by the presence of cyanobacteria and lichen. Both *Alternaria* and *Preussia* are frequently isolated from the soil and decaying vegetation (Gonzalez-Menendez et al., 2017; Thomma, 2003). *Neocamarosporium* species, which are typically halotolerant and distributed in saline regions (Gonçalves et al., 2019), were also recovered. This finding is in accordance previous publications, such as Bhatnagar and Bhatnagar (2005), who discussed the presence of halophiles and haloalkaliphiles in desert crusts.

5.3.6 Human-associated microbes in the soil

Monitoring pristine environments for microbial contamination as a result of human activity is essential for mitigating environmental contamination and for improving practices that can help reduce the risk of contamination (Baker et al., 2003). On Mars, human presence can lead to the introduction and propagation of human-associated bacteria or other non-indigenous microbes into the Martian landscape, affecting the native diversity, the differentiation between endemic and nonindigenous population and consequently the search for life on Mars (Schuerger and Lee, 2015; Yair et al., 2021). The future impact of astronauts on Mars' pristine landscape has become an international concern as explained earlier in this chapter.

Although extreme environmental factors may limit the viability of human-associated microbes in pristine environments (Baker et al., 2003), plausible contamination in analogue locations have been reported in places such as the vicinity of camp sites in Antarctica (Baker et al., 2003), during a rover traverse in the Arctic (Sjöling & Cowan, 2000), and more recently, in Israel's Ramon crater (Schuerger & Lee, 2015).

In this body of work, as described in the Materials and Methods **(section 5.2.3**), the presence of plausible contamination was determined by PCoA. The plots were constructed by comparing ASVs shared with the soil sample and with at least one indoor swab. The microbiome distribution of the overlapping samples was separated into two different clusters. **Figure 5.7** shows the visible differentiation between swabs and soil in both fungi and bacteria

plots. Indoor samples clustered together on the right side of the bar (red). The outdoor environment, represented in blue, was isolated from the rest on the left side of the graphs. The results are consistent with the unlikely soil contamination from taxa inside the Hab.

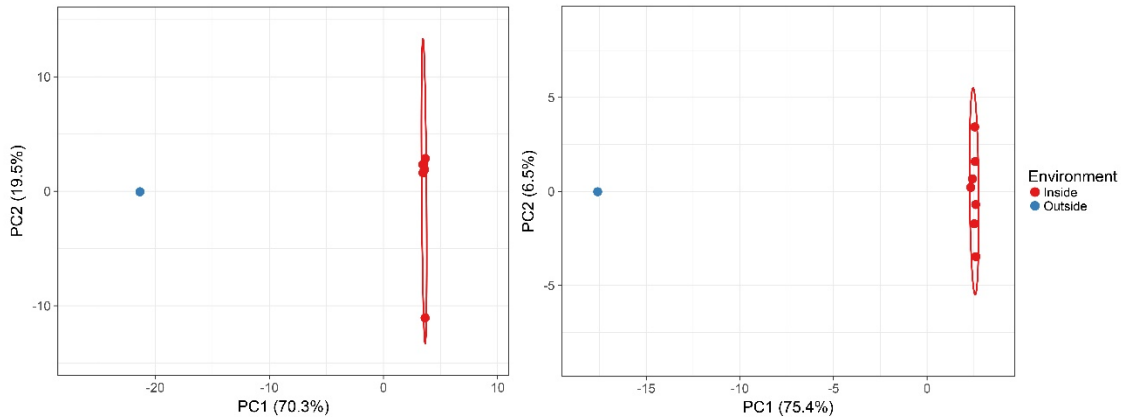

Figure 5.7 Principal coordinate analysis (PCoA) of dissimilarities among samples collected from the Hab (red) and soil (blue) for bacteria (left) and fungi (right).

Three overlapping bacterial groups were identified as the following: *Paracoccus*, *Cesiribacter,* and *Psychrobacter* including the species *Psychrobacter cryohalolentis,* previously isolated from the saline permafrost (Yair et al., 2021). None of the bacteria genera shared between both sample types are commonly associated with humans. The *Cesiribacter* genus includes species isolated from desert and volcano soils (Xu et al., 2015).

Seven fungal DNA sequences were also shared between our outdoor and indoor sample locations, but as seen in the plot, they were also grouped separately. Two fungal sequences were identified as *Leptobacillium leptobactrum*, one was unassigned, and the remaining were as follows: *Mycosphaerella tassiana, Aureobasidium pullulans, Exophiala oligosperma*, and *Rhinocladiella similis*.

The difficulty in detecting bacteria (Andrew et al., 2012) of human origin with molecular methods in the immediate surroundings of a Mars analogue station has been reported before (Upton et al., 1997). Lack of plausible contamination could be the result of low shedding

from the habitat (Schuerger & Lee, 2015), low survival rate, or to the fact that astronauts operated in simulated spacesuits outside the Hab, avoiding direct interaction with the environment. The detection limit of the selected genotyping method could also be a factor, even though 16S rRNA sequencing is an extremely sensitive assay. Estimation of the lower detection limit by bacteria-free water spiked with *E. coli* resulted in bacteria detection in all tested concentrations ($10^1 – 10^6$ cells/mL) (Brandt and Albertsen and 2018).

An additional reason could be the soil morphology and properties. While processing the soil samples, morphologic differences were observed throughout the different locations close and away from The Hab. Previous research demonstrated that soil properties affect soil microbiome with most studies focusing on parameters such as pH, water content, and organic matter (Andrew et al., 2012).

5.3.7 Analysis of soil properties and DNA recovery

Even though aridisol represents one of the largest terrestrial ecosystems by surface area on Earth, little is known about its microbial compositions (Merilä et al., 2010; Mishra et al., 2022). In addition to biotic variables such as the presence of plants and abiotic factors (e.g., extreme temperature fluctuations and UV radiation), bacterial diversity, composition and distribution can be influenced by edaphic variables such as pH and moisture content (Andrew et al., 2012). A better understanding of the relationship between soil properties and microbial amount is essential. In order to evaluate the influence of carbon content, soil moisture, and mineralogy on DNA recovery, desert samples at increased distances from the airlock (1, 2 and 5 meters) were collected together with three randomized locations, as described in the methodology and detailed in **Table 1**.

The MDRS has a diverse geology (Fierer and Jackson, 2006). **Figure 5.8** and **Table 1** show how samples that were collected within a few meters of distance were different morphologically. Some samples were easier to process and consequently extract DNA than others. The samples were loosely divided into "brown or beige sandy soil " or "brown-red clays" which, similar to Mars, are a result of oxidation (Stoker et al., 2011). Large rocks, if

present, were removed before processing the samples. All sampling coordinates are on the Jurassic-aged Morrison formation (MF), composed mainly of clay-rich material and mudstone deposits and nearly devoid of vegetation (Stoker et al., 2011).

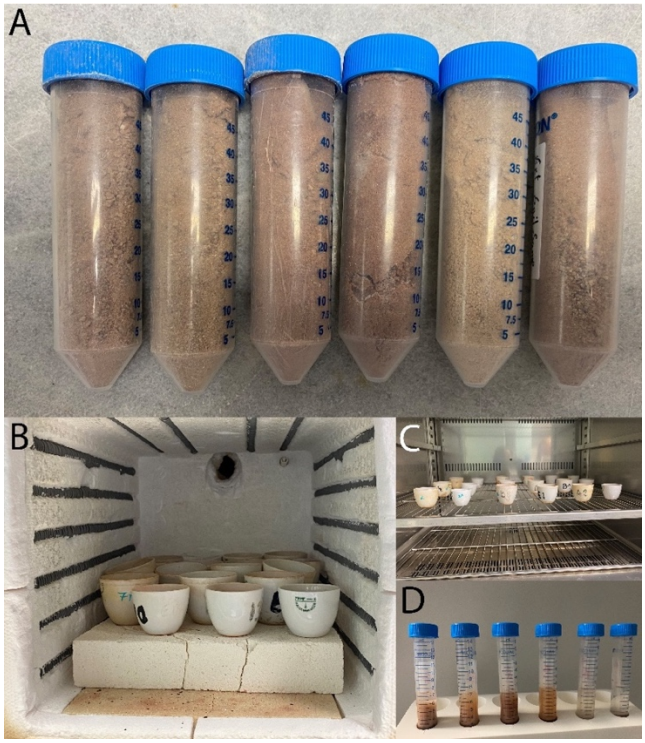

Figure 5.8 Soil Samples (A) and sample processing (B, C and D). (A) shows the different colour tones and textures across all samples. During sample processing, the soil was heated in a furnace and oven (B and C, respectively) for determination of water and carbon content. Milli-Q water was added to samples for pH measurements and ICP-OES analysis (D).

In terms of DNA concentration, the overall amount of DNA recovered was very low (<15 µg/ul), as seen in **Table 2.** Unfortunately, the vast majority of microbes in the soil are hard to recover through traditional extraction and culturing laboratory methods, which prevents the accurate interpretation of microbial diversity (Andrew et al., 2012; Fierer and Jackson, 2006). A correlation between DNA amount and sample morphology was not observed since the two samples with the highest DNA concentration (S4 and S5) were visually contrasting (**Table 5.2** and **Figure 5.8)**; S5 is a sandy-like soil, whereas S4 is composed of brown-red clay.

Analyzing edaphic factors from each location uncovered similar results to past studies from the same area (**Table 5.2**). Low water content was obtained, which is characteristics of deserts and Mar analogue soils. A slightly alkaline pH was also seen. Soil pH has been deemed a significant factor in shaping nutrient availability, microbial activities and therefore composition (Stoker et al., 2011; Zhang et al., 2019). Since the pH values across all samples were similar, they were not considered a factor influencing the differences in recoverable DNA concentration. All pH values were within the neutral to slightly basic range (7.47 - 8.58). Similar values have been reported by Stoker and colleagues in the proximity of the MDRS. Other authors (Fierer and Jackson, 2006; Wang et al., 2019) obtained slightly higher pH reads from the area, including in the Morrison formation. Alkaline pH is common in most arid regions (Fierer and Jackson, 2006; Zhang et al., 2019) but acidification of the MDRS soil has also been reported in the literature (Clarke et al., 2014).

Table 5.2 Results from chemical analysis of the soil samples and amount of DNA extracted per location. Organic matter and moisture percentages are averages of triplicate measurements.

Sample	pH	Organic matter (%)	Moisture (%)	DNA amount (ng/µl)
S1	7.5	1.97	3.42 ± 0.98	2.6
S2	8.25	1.84	2.42 ± 1.04	3.8
S3	8.25	1.10	1.65 ± 0.12	2.8
S4	8.58	5.11	9.27 ± 6.84	7.2
S5	7.47	3.74	4.63 ± 3.03	14.7
S6	7.73	0.97	0.54 ± 0.08	3.7

In accordance with previous soil analysis at the MDRS and identical to Martins et al. (2011), the highest OM content obtained was 5%. The current results show a strong correlation ($r = 0.9312$) between water content and OM (**Figure 5.9A**), which was expected since OM improves water retention in soils due to increased aggregation of soil particles (Arshad and Coen, 1992).

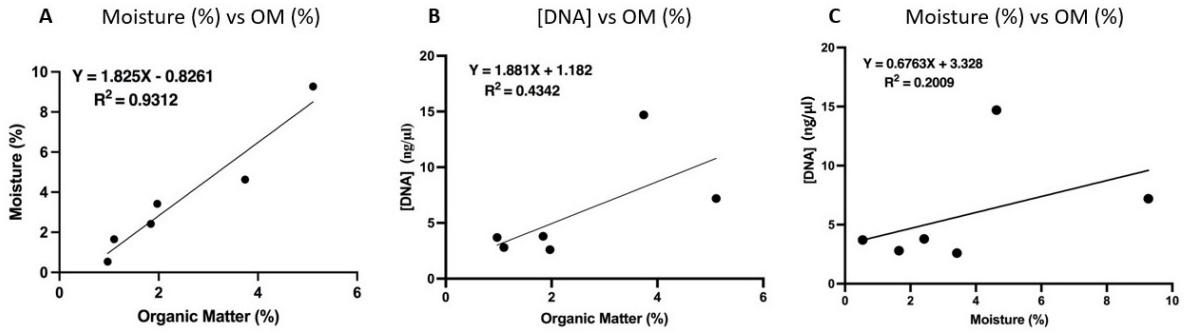

Figure 5.9 The scatter plots with simple linear regression and the square of the Pearson correlation coefficient showing the positive correlations between (a) moisture content and organic matter, (b) DNA concentration and organic matter and (c) moisture content and organic matter.

Moreover, in the present study, a moderate correlation with a correlation coefficient of 0.4342 between organic content and DNA concentration was noticed, as shown in the **Figure 5.9B.** The samples with the highest percentages of organic matter (S4 and S5) also had higher amounts of DNA. Such observation might suggest that the OM in the soil was utilized as a carbon source by the soil microbiota (Stoker et al., 2011). OM is known to increase nutrient availability and soil biota activity (Arshad and Coen, 1992), therefore, in the samples with low OM values, organic content was probably a limiting factor for microbial growth.

Moisture is another crucial factor; high water content promotes microbial proliferation whereas low water availability can limit microbial growth and activity (Stark and Firestone, 1995). Since precipitation is closely linked to water scarcity and soil moisture (Stark and Firestone, 1995), low water content is commonly seen in desert areas, including the present samples (<5%). A positive but weak correlation between water content and DNA concentration (r = 0.2009) is reported. Nevertheless, S4 and S5 were the samples with the highest amount of both (**Table 5.2C**).

While a positive correlation between DNA concentration and both moisture and organic matter was anticipated, the observed weakness of these correlations is likely due to the presence of other interfering factors, such as clay minerals, which may hinder DNA extraction.

S4 and S5 are two of the three samples collected furthest from the MDRS. S5 was taken from the small mountain range close to the MDRS. Both S4 and S5 were sampled in remote

locations, where the frequency of human presence is low. S3 was the sample with the lowest water content (<1%) and some of the lowest organic matter (1%) and DNA concentration (<4 μg/ul) observed in this study.

Additionally, differences in microbial abundance within soil samples could result from distinct mineral compositions among the different locations (Martins et al., 2011). Spectrophotometric techniques, such as Inductively Coupled Plasma Optical Emission Spectroscopy (ICP-OES), have become standard practice in elemental analysis (Sah and Brown, 1997). The concentration of several elements was determined using ICP-OES, which allows the simple, sensitive and simultaneous analysis of a wide range of minerals (Sah and Brown, 1997). The concentrations of thirty-one elements were above the machine's detection limit (3.6 part-per-billion per mass) (**Appendix A**). Minerals with concentrations below or at MaDL (maximum detection limit) were excluded for discussion. The MaDL is the lowest detectable concentration of an element that can be reliably distinguished from background noise in an ICP-OES instrument. The MaDL value gives an idea of the instrument's sensitivity for a particular element, which differs from the machine limit and refers to the instrument's specific technical limitation.

As expected, among the most frequent elements in this study were Ca, K, Mg, and Na (**Figure 5.10**). These are the most common positive ions in soil extracts (Stoker et al., 2011). Sodium was the most frequent cation in all locations, followed by sodium. The highest concentration (506 mg/kg) was observed for sulfur (purple), the dominant anion in all locations.

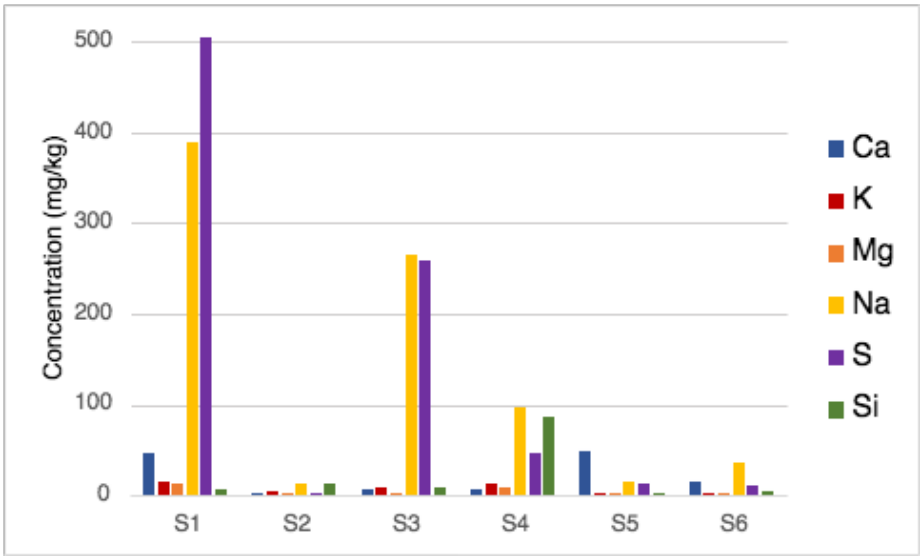

Figure 5.10 Most common elements found in each sampling location.

Some frequent elements in the results were more variable than others, such as Ca and Si. In contrast, a similar distribution pattern within the samples collected closest to the MDRS was obtained (**Figure 5.10**). Here, higher levels of both sulfur and sodium were observed when compared to the remaining locations. This could be explained by the fact that the Morrison Formation, where the research station is located, is characterized by the presence of salt and gypsum (calcium sulfate dihydrate) deposits (Direito et al., 2011). The presence of clay minerals in the area (Direito et al., 2011) likely contributed to the presence of silica, calcium, potassium, and magnesium to various degrees in every sample.

S4 and S5, the samples with the highest DNA concentration, had different elemental compositions. The main minerals in S4 were sodium and silica, whereas S5 was predominantly characterized by calcium. S3, one of the samples with the lowest DNA concentration, was equally made up of sodium and sulfur, the two main elements in almost every sample. In summary, the elemental analysis agrees with previous geology and mineralogy studies from the MDRS but do not correlate with DNA recovery.

As expected in desert samples, water content, and DNA concentration results obtained in this study were low. The data presented here show a moderate positive correlation between

recoverable DNA and carbon content, suggesting that such edaphic factors influence microbial presence to a greater extent than soil morphology or elemental composition.

5.4 Conclusion

While earlier chapters have explored how microbial cultivation can be used to support a human presence on Mars, a significant concern surrounds the possibility of terrestrial microbes leaking out of pressurized habitats or other surface infrastructure to contaminate the Martian environment. Such an outcome would potentially greatly interfere with the interests of astrobiology and the detection of microbial life on Mars that could be demonstrated to be unambiguously indigenous. The work reported here attempted to address the risk of such forward contamination occurring by characterizing the microbiome within an analogue Martian habitat and testing for the presence of human commensal microbes in soil samples collected from the immediate vicinity.

This study was not able to detect evidence of human commensal microbes – or other microbes from the interior of the MDRS – present in the soil immediately outside the habitat 'airlock' door. As described above, however, this attempt was partially frustrated by background DNA sequences present in the analytical equipment used for collection and extraction – the 'kitome' – that needed to be removed from the sequence analysis. The hard nature of some desert samples could also have impacted negatively on sample processing and consequently the recovery of microbial DNA. Microbial cells escaping from the habitat interior would also be expected to be present in low numbers on the surrounding ground, even in comparison to the low numbers of environmental microbes surviving in the desert soil, and so any such contaminant cells may have fallen below the threshold of detection by DNA extraction, PCR amplification, and sequence identification. In this sense, failure of detection does not necessarily mean that human commensal or other habitat-associated microbes were not present in the surrounding soil.

If habitat-associated microbes were to leak into the desert soil, the harsh desert environment would likely result in low survival rates. We found here that DNA concentrations

that could be extracted from the desert soil correlated with moisture and organic matter content. Nonetheless, this contamination risk necessitates the monitoring of microbial environmental contaminants and microbial accumulation inside confined habitats. A better selection of controls and improved and standardized practices to detect microbial contaminants are also necessary. These protocols should include analysis of kitomes and researcher's microbiome, and improved bioinformatic tools for eliminating contaminants. This study is the first investigating dispersal of human-associated microbes from the MDRS into the soil and can provide information for environmental monitoring as a result of human presence in a Mars-like landscape. Furthermore, the presence of potential pathogens and variation in microbial profile inside the Hab implicate the need to screen space-like habitats comprehensively to protect their inhabitants and built-structures from deterioration.

Once we settle, the contamination of Mars with human-associated microbes may be inevitable, even with the best prevention protocols. Avoiding the propagation of such microbes is extremely important. Since the survival and presence of microbes correlates with edaphic factors, detailed knowledge of soil properties can help select locations for future settlements and therefore reduce the risk of forward contamination. In particular, the designation of special regions where microbial propagation is more prone to happen should also extend to avoiding these locations for human missions.

Chapter 6 Conclusions and Future work

6.1 Conclusions

A start-to-finish biphasic system for producing bioplastic with hydrolysed alga biomass was successfully developed. A hanging bag photobioreactor was capable of cultivating large volumes of *Chlamydomonas* cultures. Overall, each 15 L hanging bag of wild-type *Chlamydomonas reinhardtii* grown under mixotrophic conditions with half of the organic carbon recommended by the literature, more specifically 1 g/L of sodium acetate (hydrate), could produce approximately 20 g of wet biomass. The wet biomass, harvested by combining flocculation with calcium chloride and centrifugation, was hydrolysed with 3% sulfuric acid at a high temperature and used as the primary carbon source by *B. subtilis* Ok2. The study's key finding showed that the *Bacillus* strain successfully fermented 25 g/L of algae-derived carbohydrates with 3.2 g/100g of starch and produced 23% ± 1.45 of CDW and 0.18 ± 0.1 g/L of PHB in nitrogen-limited media. The PHB produced was more hydrophilic than the one obtained with commercially purified glucose, commonly used in PHA production. The polymer's hydrophilic nature results from the presence of extracellular polymeric substance cells due to insufficient purification, which resulted in the production of 2D films with increased flexibility, which is preferred in some industries, such as packaging.

Different methodologies were evaluated in Chapter 2 in both WT *Chlamydomonas* (CC-1690) and cell-deficient mutant (CC-5168) to determine the most efficient and time-saving techniques for each step of the process. FTIR helped monitor starch accumulation and degradation over time and was able to determine maximum starch accumulation at day 3. Flocculation with calcium chloride helped reduce harvesting time via centrifugation in both strains with similar efficiency. However, due to a lack of flagella and motility, the mutant required less flocculant concentration. Chemical pre-treatment with diluted sulfuric acid at a high temperature was microscopically more efficient than mechanical treatment with sonification in the *Chlamydomonas* strains and in Spirulina and *Chlorella*,

which were also evaluated due to their significance in space exploration. The treatment was capable of releasing more than 50% of microalgae biosolids (e.g., stored carbohydrates), from the biomass after the removal of soluble sugars in all strains.

In Chapter 3, a WT *Chlamydomonas* hydrolysate obtained by acid pre-treatment was used as the organic carbon source for PHB-producing *Bacillus subtilis* OK2. The Gram-positive bacteria were able to produce PHB, as stated earlier, with maximum accumulation at 60 h. A low-tech large-scale protocol for increased polymer content was designed for non-terrestrial applications and successfully resulted in a double amount of polymer, which was ~64.49 ± 15.00 of CDW. FTIR was also used in this chapter to monitor PHB accumulation in *Bacillus* and determine the time point for maximum PHB accumulation at 48 h, which was the same observed with PHB yield. FDM successfully printed commercial filaments with PHB/PLA and PHBV/PLA blends into the same object with utility for astronauts ever printed in space. However, the wrench manufactured with the PHB blend did not function properly due to PHB's brittleness.

Chapter 4 reports the attempt to genetically insert and link an amylase into *Chlamydomonas's* GBSS to obtain a quicker and more straightforward starch harvesting protocol. The arAmyBH amylase was chosen for this project since it has an enzymatic activity in the thermophilic range, which will allow controlled hydrolysis of starch after cultivation is completed. Moreover, this amylase has been previously expressed in *Chlamydomonas reinhardtii*. Golden Gate was the technique of choice due to the simplicity of the one-pot reaction and the fact that it allows the insertion of multiple genes. In parallel, GBSS was also linked to a mVenus, a gene encoding a fluorescent protein which will facilitate visualisation of the amylase in the *Chlamydomonas*'s pyrenoid. The cloning pipeline involved designing constructs for each hierarchical level - from Level 0 to Level 2 - with start and stop codons at the restriction sites to allow a markless mutagenesis. Before cloning, mVenus, GBSS and amylase were designed and synthesised with the appropriate binding sites to be digested and ligated with Type II restriction endonucleases. The Chapter has yet to be concluded due to challenges in obtaining the Level 2 vectors. Nonetheless, the steps involved in the early stages of cloning were successful. L0 constructs and both L1 constructs with GBSS linked to mVenus

and amylase separately were verified by Sanger sequencing. A detailed plan was designed to address potential issues and how to resolve the problem. Time constraints did not allow the project's conclusion; nonetheless, the issue was identified. Restriction enzyme BsaI lost its enzymatic activity since it could not cut into different fragments with varying sizes in the plasmid tspurple used as control. Nevertheless, L1 and L1 constructs were obtained with incredible simplicity showcasing the power of the Golden Gate technique.

Chapter 5 focused on the potential contamination risk future crewed missions will carry to the Martian surface. Various high-touched surfaces inside a Mars analogue habitat were sampled with swabs at the end of a two-week simulation mission at the Mars Desert Research Station (Utah, United States). The swab samples were used to evaluate the microbial composition in terms of bacteria, fungi and archaea inside the habitat through 16S and ITS sequencing. A soil sample adjacent to the habitat's airlock was also collected to evaluate the presence of human-associated microbes that might have escaped the habit and contaminated the terrain. No human-associated microbes were detected in the soil samples, which were characterised by environmental species, including extremophiles. The indoor samples showed great diversity among the different sampled locations. Human-associated genera, such as *Escherichia* and *Shigella,* were predominantly amplified from the door handle of the workshop. *Acinobacter* and *Pseudomonas* were also frequently seen across the swabs. The fungal genus *Penicillium* was present in all indoor samples. Due to the difficulties associated with DNA extraction from the soil samples, water content, organic matter and mineralogy were analysed. The results showed that soil characteristics might interfere with DNA recovery and should be taken into consideration in future studies.

6.2 Future work

The main focus of this thesis was the development of a biphasic system for the production of malleable and 3D printable biodegradable polymer using algae-derived feedstock. Based on the results and some preliminary findings the overall outcome is promising.

The main limiting step of this biphasic system is the primary cultivation of microalgae in the hanging bags. Aeration was provided by aquarium pumps and a 1 mL microlitre pipette tip which produced a stream of small bubbles. More effective gas exchange into the growth medium may be achieved with more complex bubble diffusers, although potentially with increased risk of contamination. Yang et al., (2018), for example, found greatest biomass productivity with a diffuser producing bubbles of 1.5mm diameter.

For reasons of research operating costs, these experiments were conducted with simple aeration, rather than a CO_2 line. Enhancing the levels of dissolved CO_2 in the culture medium could possibly be expected to increase WT *Chlamydomonas* growth rate and final cell density, which in turn could improve the rate of through-put and mass of harvestable starch feedstock from the microalgae culture. Furthermore, incorporating a CO_2 line into the system would enable the WT Chlamydomonas to grow solely through photosynthesis. This could eliminate the need to add an external organic carbon source to the cultivation bags. In the context of a Martian habitat, CO_2 is facile to provide by simply pressurizing the atmosphere. A more complex photobioreactor system with heat control would also improve both cultivation time and harvestable mass of produced starch: Ivanov et al., (2021) found a culturing temperature of 39°C maximized both of these culture parameters. Substitution of the fluorescent light panels with a Light Emitting Diode (LED) system would also enhance the microalgae culturing. While they represent a high initial capital investment, energy-efficient LEDs offer reduced photobioreactor operational costs (Mapstone et al., 2022; Carneiro et al., 2022)), and their emission can be targeted in the red and blue ends of the spectrum and optimized to the specific preferences of different algal species (Mapstone et al., 2022). Furthermore, LED lamps can be flashed or strobed, which has been shown to prevent photoinhibition and enhance photosynthesis and improve the amount and quality of algae biomass (Abu-Ghosh et al., 2015; Mapstone et al., 2022).

Access to larger centrifuges able to spin-down much greater volumes of microalgae culture at a time would also shorten the time involved in extracting the biomass for processing. Continuous flow centrifugation is particularly time efficient: the Extreme Centrifuge available

from Algae Centrifuge (San Francisco, California, United States), for example, delivers 3600×g and can process 75 litres per hour, as reported in the work of Uysal et al., 2016.

In the protocol used by this study, the substantial volume of left-over culture medium after cell harvesting by flocculation and centrifugation was discarded. Design of a protocol to instead recycle spent culture media, and the water and remnant nutrients and minerals it contains, would increase overall efficiency of the system. In the ultimate goal of efforts such as this – the construction of systems to support human habitation on Mars – such a closed-loop system would be necessary. A few studies have already investigated the feasibility of growing industry-relevant algae, including spirulina and *Chlorella*, with recycled culture medium (Depraetere et al., 2015; Hadj-Romdhane et al., 2013; Kim et al., 2011; Rodolfi et al., 2003; Zhu et al., 2013). The challenge is that cell debris as well organics excreted by the algae (including, fatty acids, rhamnose-rich polysaccharides, and uronic acids) can accumulate in the medium to modify its rheological properties and also inhibit subsequent algae growth (Depraetere et al., 2014).

Optimisation procedures are also possible for the second cultivation step, that of the biopolymer-producing *Bacillus,* grown on hydrolysed algal biomass. The Design of Experiment (DOE) framework allows the investigation of the impacts of multiple factors simultaneously. Various crucial fermentation parameters such as carbon-to-nitrogen (C:N) ratio, agitation, pH and harvesting time can be investigated for their effects on the final *Bacillus* spp. biomass (g/L), polymer yield (g/L) and productivity (g/g) (Vu et al., 2022). Mathematical modelling, such as the Taguchi orthogonal array method, creates a factorial design with several parameters while minimising the experimentation runs required (Mohan & Reddy, 2013).

The PHB extraction method selected here was chosen due to the straightforward nature of the methodology and the high purity levels (>90%) of PHA recovered (Pagliano et al., 2021). However, on the downside, this solvant-based extraction of PHAs is associated with numerous drawbacks, as summarized by Pagliano et al., 2021. One such disadvantage involves using chloroform or other halogenated compounds as solvents, known for being toxic, flammable, and sometimes volatile and therefore associated with toxicity posing a risk to humans and the

environment (Pagliano et al., 2021). Forthcoming efforts should evaluate other types of solvents (e.g., alkanes and carbonates) or different recovery systems, such as cellular lysis with enzymes or alkaline compounds (Pagliano et al., 2021). As introduced in Chapter 3, a quick two-hour method can also be used for PHB extraction. Alternative and expeditious protocols should be evaluated by Gas Chromatography/Mass Spectrometry (GC-MS) analysis to determine the differences in purity content among different extraction methods and assess the presence of contaminants.

This study attempted to use the Golden Gate technique to create a *Chlamydomonas* transformant with a thermophilic amylase enzyme bound to the starch granules, in order to greatly simplify the harvesting and break-down of the produced starch for feedstock. This attempt was ultimately not fully successful, and with more time the efforts to trouble-shoot the problems encountered at the Level 2 stage would be continued and the final stages of the protocol detailed in Chapter 4 completed. The power of the Golden Gate technique as a modular, one-pot approach is that multiple inserts can be achieved simultaneously in parallel, and so a second (or indeed, several other) amylase could be genetically inserted to avoid the need to add a hydrolysing enzyme required for complete self-liquefaction of starch (Kim et al., 2000; Wang et al., 2014). The thermostable α-amylase obtained from *Bacillus stearothermophilu*s, mentioned, and recommended by Wang and colleagues (2014), would be an excellent candidate. This enzyme has successfully facilitated self-hydrolysis in transgenic rice seeds and its enzymatic activity is optimum at a pH (5.0 – 5.5) and temperature range (60 – 70 °C) compatible with the amylase (arAmyBH) used in this study (Wang et al., 2015; Xu et al., 2008).

In addition to the medical field, PHB can also be used as concrete in construction. Therefore, future work can include the production of composites of PHB and Martian regolith simulant and subsequently, 3D filaments with different ratios of each material and evaluation and optimization of printing parameters. A composite of recycled PLA and lunar stimulant was successfully 3D printed by extrusion (Li et al., 2020). The authors reported accelerated crystallization of PLA and printed components with satisfactory mechanical properties (Li et al., 2020). Moreover, 3D structures made from PHB/stimulant composites should be

investigated in terms of morphology, structural properties, crystallinity, thermal stability, tensile properties, and impact strength with the help of techniques such as FTIR, X-ray computed tomography and scanning electron microscopy as described by Li et al., 2020 and Zainuddin et al., 2023.

Finally, a better understanding of the level of risk of dispersal of human-associated microbes is required for future missions to Mars. Contamination risk assessments in analogue terrains are still in their infancy. Improvements to current protocols, including the one from this thesis, are therefore necessary. Ideally, monitoring protocols should be standardized and shared among the scientific community to obtain comparable results from all the different analogues locations. Comparison of the results of this study with the findings obtained in other locations can help validate and evaluate further the current protocol. Comparable indoor and external samples from another Mars analogue, the Hawai'i Space Exploration Analog and Simulation (HI-SEAS), have already been collected by a collaborator. Future work would involve the molecular characterisation of these samples and comparisons with the MDRS ones. An improvement made to the HI-SEAS procedure was using individual single-use sterile PBS tubes to moisturise each swab to address contamination risks.

Identification of contamination by reagents is particularly important in low biomass samples such as desert soils (Stinson et al., 2019). Specific to this area of research, Hornung et al., 2019 and de Goffau et al., 2019 discussed and outlined recommendations that include appeals for increased bioinformatic identification resolution, and reproductivity assays by isolating targeted DNA by more than one extraction kit. Based on their suggestions and on the knowledge acquired during this project, future studies focusing on the contamination of Martian-like soils should include the following:

- The presence and sequencing of negative controls in every step, including sampling solutions (e.g., PBS, deionized, ultrapure water);
- Identification of the kitome;
- Analysis of the researchers' microbiome through sampling and sequencing of their hands;
- Presence of positive controls representing Bacteria, Archaea and Fungi;

- Inclusion of dilution series with positive controls to access the methodology's detection limit;
- Sequencing of Archaeal species with Archaea-specific primers;
- Collection of temporal samples;
- Definition and expansion of the spectrum of microbial indicators of human contamination;
- Microbial profiling with molecular techniques instead of traditional methods;
- Better understanding and improved informatics tools for eliminating contaminants in sequencing data.
- Extraction of DNA by different kits for comparison;
- Monitoring of pathogens inside habitational facilities.

Bibliography

List of references

Abdallah, A. Q., Nixon, B.T., Fortwendel, J.R., 2016. The enzymatic conversion of major algal and cyanobacterial carbohydrates to bioethanol. Front. Energy Res. 4, 1–15. https://doi.org/10.3389/fenrg.2016.00036

Abdullah, A.H.D., Chalimah, S., Primadona, I., Hanantyo, M.H.G., 2018. Physical and chemical properties of corn, cassava, and potato starchs. IOP Conf. Ser. Earth Environ. Sci. 160. https://doi.org/10.1088/1755-1315/160/1/012003

Abu-Ghosh, S., Fixler, D., Dubinsky, Z., Iluz, D., 2015. Flashing light in microalgae biotechnology. Bioresour. Technol. 203. https://doi.org/10.1016/j.biortech.2015.12.057

Adams, R.I., Bateman, A.C., Bik, H.M., Meadow, J.F., 2015. Microbiota of the indoor environment: a meta-analysis. Microbiome 3, 49. https://doi.org/10.1186/s40168-015-0108-3

Adem, M., Beyene, D., Feyissa, T., 2017. Recent achievements obtained by chloroplast transformation. Plant Methods 13, 30. https://doi.org/10.1186/s13007-017-0179-1

Additive Manufacturing Facility (AMF) User's Guide. 2016. Made in Space. 2016. http://madeinspace.us/wp-content/uploads/AMF-User-Guide.pdf

Afreen, R., Tyagi, S., Singh, G.P., Singh, M., 2021. Challenges and Perspectives of Polyhydroxyalkanoate Production From Microalgae/Cyanobacteria and Bacteria as Microbial Factories: An Assessment of Hybrid Biological System. Front. Bioeng. Biotechnol. 9, 1–14. https://doi.org/10.3389/fbioe.2021.624885

Aikawa, S., Joseph, A., Yamada, R., Izumi, Y., Yamagishi, T., Matsuda, F., Kawai, H., Chang, J.-S., Hasunuma, T., Kondo, A., 2013. Direct conversion of Spirulina to ethanol without pretreatment or enzymatic hydrolysis process. Energy Environ. Sci. 6, 1844. https://doi.org/10.1039/c3ee40305j

Alexandrov, S., 2016. Algal Research in Space : History, Current Status, and Future Prospects. Innovare J. Life Sci. 4, 1–4.

Ali, I., Basit, M.A., 1993. Significance of hydrogen content in fuel combustion. Int. J. Hydrogen Energy 18, 1009–1011. https://doi.org/https://doi.org/10.1016/0360-3199(93)90083-M

Aller, J.Y., Kemp, P.F., 2008. Are Archaea inherently less diverse than Bacteria in the same environments? FEMS Microbiol. Ecol. 65, 74–87. https://doi.org/10.1111/j.1574-6941.2008.00498.x

Almaraz-Delgado, A.L., Flores-Uribe, J., Pérez-España, V.H., Salgado-Manjarrez, E., Badillo-Corona, J.A., 2014. Production of therapeutic proteins in the chloroplast of Chlamydomonas reinhardtii. AMB Express 4, 57. https://doi.org/10.1186/s13568-014-0057-4

Alsoufi, M., El-Sayed, A., 2017. Warping Deformation of Desktop 3D Printed Parts Manufactured by Open Source Fused Deposition Modeling (FDM) System. Int. J. Mech. Mechatronics Eng. 17, 7–16.

Ambekar, R., Kandasubramanian, B., 2019. Progress in the Advancement of Porous Biopolymer Scaffold: Tissue Engineering Application. Ind. Eng. Chem. Res. 58, 6163–6194. https://doi.org/10.1021/acs.iecr.8b05334

Anbukarasu, P., Sauvageau, D., & Elias, A., 2015. Tuning the properties of polyhydroxybutyrate films using acetic acid via solvent casting. Scientific Reports. 5. 17884. 10.1038/srep17884

Anderson, I.C., Parkin, P.I., 2007. Detection of active soil fungi by RT-PCR amplification of precursor rRNA molecules. J. Microbiol. Methods 68, 248–253. https://doi.org/10.1016/j.mimet.2006.08.005

Andrew, D.R., Fitak, R.R., Munguia-Vega, A., Racolta, A., Martinson, V.G., Dontsova, K., 2012. Abiotic factors shape microbial diversity in Sonoran desert soils. Appl. Environ. Microbiol. 78, 7527–7537. https://doi.org/10.1128/AEM.01459-12

Arnold, N.S., Butcher, F.E.G., Conway, S.J., Gallagher, C., Balme, M.R., 2022. Surface topographic impact of subglacial water beneath the south polar ice cap of Mars. Nat. Astron. 6, 1256–1262. https://doi.org/10.1038/s41550-022-01782-0

Arshad, M.A., Coen, G.M., 1992. Characterization of soil quality : Physical and chemical criteria 7, 25–31.

Ashter, S., 2016. Types of Biodegradable Polymers. pp. 81–151. https://doi.org/10.1016/B978-0-323-39396-6.00005-1

Auchtung, T.A., Fofanova, T.Y., Stewart, C.J., Nash, A.K., Wong, M.C., Gesell, J.R., Auchtung, J.M., Ajami, N.J., Petrosino, J.F., 2018. Investigating Colonization of the Healthy Adult Gastrointestinal Tract by Fungi. mSphere 3, 1–16. https://doi.org/10.1128/msphere.00092-18

Ausejo, J.G., Rydz, J., Musioł, M., Sikorska, W., Sobota, M., Włodarczyk, J., Adamus, G., Janeczek, H., Kwiecień, I., Hercog, A., Johnston, B., Khan, H., Kannappan, V., Jones, K., Morris, M., Jiang, G., Radecka, I., Kowalczuk, M., 2018. A comparative study of three-dimensional printing directions: The degradation and toxicological profile of a PLA/PHA blend. Polymer Degradation and Stability 152. https://doi.org/10.1016/j.polymdegradstab.2018.04.024

Averesch, N.J.H., Berliner, A.J., Nangle, S.N., Zezulka, S., Vengerova, G.L., Ho, D., Casale, C.A., Lehner, B.A.E., Snyder, J.E., Clark, K.B., Dartnell, L.R., Criddle, C.S., Arkin, A.P., 2023. Microbial biomanufacturing for space-exploration-what to take and when to make. Nat. Commun. 14, 2311. https://doi.org/10.1038/s41467-023-37910-1

Gatamaneni Loganathan, B., Valerie, O., Mark, L., 2018. Review on valuable bioproducts obtained from microalgal biomass and their commercial applications. Environ. Eng. Res. 23. https://doi.org/10.4491/eer.2017.22

Bahram, M., Anslan, S., Hildebrand, F., Bork, P., Tedersoo, L., 2019. Newly designed 16S rRNA metabarcoding primers amplify diverse and novel archaeal taxa from the environment. Environ. Microbiol. Rep. 11, 487–494. https://doi.org/10.1111/1758-2229.12684

Baker, G.C., Tow, L.A., Cowan, D.A., 2003. PCR-based detection of non-indigenous microorganisms in “pristine” environments. J. Microbiol. Methods 53, 157–164. https://doi.org/10.1016/s0167-7012(03)00021-6

Baker, M.J., Trevisan, J., Bassan, P., Bhargava, R., Butler, H.J., Dorling, K.M., Fielden, P.R., Fogarty, S.W., Fullwood, N.J., Heys, K.A., Hughes, C., Lasch, P., Martin-Hirsch, P.L., Obinaju, B., Sockalingum, G.D., Sulé-Suso, J., Strong, R.J., Walsh, M.J., Wood, B.R., Gardner, P., Martin, F.L., 2014. Using Fourier transform IR spectroscopy to analyze biological materials. Nat. Protoc. 9, 1771–1791. https://doi.org/10.1038/nprot.2014.110

Bakri, Y., Ammouneh, H., El-Khouri, S., Muhanad, M., 2012. Isolation and identification of a new Bacillus strain for amylase production. Res. Biotechnol. 3, 51–58.

Balaji, S., Gopi, K., Muthuvelan, B., 2013. A review on production of poly β hydroxybutyrates from cyanobacteria for the production of bio plastics. Algal Res. 2, 278–285. https://doi.org/10.1016/j.algal.2013.03.002

Balakrishnan, K., 2011. Isolation and recovery of microbial polyhydroxyalkanoates. Express Polym. Lett. 5, 620–634. https://doi.org/10.3144/expresspolymlett.2011.60

Barth, A., 2007. Infrared spectroscopy of proteins. Biochim. Biophys. Acta - Bioenerg. 1767, 1073–1101. https://doi.org/https://doi.org/10.1016/j.bbabio.2007.06.004

Barrett, J., Girr, P., Mackinder, L.C.M., 2021. Pyrenoids: CO2-fixing phase separated liquid organelles. Biochim. Biophys. Acta - Mol. Cell Res. 1868, 118949. https://doi.org/https://doi.org/10.1016/j.bbamcr.2021.118949

Bashir, K., Aggarwal, M., 2019. Physicochemical, structural and functional properties of native and irradiated starch: a review. J. Food Sci. Technol. 56, 513–523. https://doi.org/10.1007/s13197-018-3530-2

Ben Said, S., Or, D., 2017. Synthetic Microbial Ecology: Engineering Habitats for Modular Consortia. Front. Microbiol. 8, 1125. https://doi.org/10.3389/fmicb.2017.01125

Berliner, A., Hilzinger, J., Abel, A., McNulty, M., Makrygiorgos, G., Averesch, N., Gupta, S., Benvenuti, A., Caddell, D., Cestellos-Blanco, S., Doloman, A., Friedline, S., Ho, D., Gu, W., Hill, A., Kusuma, P., Lipsky, I., Mirkovic, M., Meraz, J., Arkin, A., 2021. Towards a Biomanufactory on Mars. Front. Astron. Sp. Sci. 8. https://doi.org/10.3389/fspas.2021.711550

Bertoft, E., 2017. Understanding starch structure: Recent progress. Agronomy 7. https://doi.org/10.3390/agronomy7030056

Bharti, R., Grimm, D.G., 2019. Current challenges and best-practice protocols for microbiome analysis. Brief. Bioinform. 22, 178–193.

Bhatnagar, A., Bhatnagar, M., 2005. Microbial diversity in desert ecosystems. Curr. Sci. 89, 91–100.

Bhushan, S., Singh, S., Maiti, T.K., Sharma, C., Dutt, D., Sharma, S., Li, C., Tag Eldin, E.M., 2022. Scaffold Fabrication Techniques of Biomaterials for Bone Tissue Engineering: A Critical Review. Bioengineering 9. https://doi.org/10.3390/bioengineering9120728

Billi, D., Baqué, M., Smith, H.D., Mckay, C.P., 2013. Cyanobacteria from Extreme Deserts to Space *. Adv. Microbiol. 3, 80–86. https://doi.org/10.4236/aim.2013.36A010

Blachowicz, A., Mayer, T., Bashir, M., Pieber, T.R., De León, P., Venkateswaran, K., 2017. Human presence impacts fungal diversity of inflated lunar/Mars analog habitat. Microbiome 5, 62. https://doi.org/10.1186/s40168-017-0280-8

Boguraev, A.-S., Christensen, H.C., Bonneau, A.R., Pezza, J.A., Nichols, N.M., Giraldez, A.J., Gray, M.M., Wagner, B.M., Aken, J.T., Foley, K.D., Copeland, D.S., Kraves, S., Alvarez Saavedra, E., 2017. Successful amplification of DNA aboard the International Space Station. npj Microgravity 3, 26. https://doi.org/10.1038/s41526-017-0033-9

Bolyen, E., Rideout, J.R., Dillon, M.R., Bokulich, N.A., Abnet, C.C., Al-Ghalith, G.A., Alexander, H., Alm, E.J., Arumugam, M., Asnicar, F., Bai, Y., Bisanz, J.E., Bittinger, K., Brejnrod, A., Brislawn, C.J., Brown, C.T., Callahan, B.J., Caraballo-Rodríguez, A.M., Chase, J., Cope, E.K., Da Silva, R., Diener, C., Dorrestein, P.C., Douglas, G.M., Durall, D.M., Duvallet, C., Edwardson, C.F., Ernst, M., Estaki, M., Fouquier, J., Gauglitz, J.M., Gibbons, S.M., Gibson, D.L., Gonzalez, A., Gorlick, K., Guo, J., Hillmann, B., Holmes, S., Holste, H., Huttenhower, C., Huttley, G.A., Janssen, S., Jarmusch, A.K., Jiang, L., Kaehler, B.D., Kang, K. Bin, Keefe, C.R., Keim, P., Kelley, S.T., Knights, D., Koester, I., Kosciolek, T., Kreps, J., Langille, M.G.I., Lee, J., Ley, R., Liu, Y.X., Loftfield, E., Lozupone, C., Maher, M., Marotz, C., Martin, B.D., McDonald, D., McIver, L.J., Melnik, A. V., Metcalf, J.L., Morgan, S.C., Morton, J.T., Naimey, A.T., Navas-Molina, J.A., Nothias, L.F., Orchanian, S.B., Pearson, T., Peoples, S.L., Petras, D., Preuss, M.L., Pruesse, E., Rasmussen, L.B., Rivers, A., Robeson, M.S., Rosenthal, P., Segata, N., Shaffer, M., Shiffer, A., Sinha, R., Song, S.J., Spear, J.R., Swafford, A.D., Thompson, L.R., Torres, P.J., Trinh, P., Tripathi, A., Turnbaugh, P.J., Ul-Hasan, S., van der Hooft, J.J.J., Vargas, F., Vázquez-Baeza, Y., Vogtmann, E., von Hippel, M., Walters, W., Wan, Y., Wang, M., Warren, J., Weber, K.C., Williamson, C.H.D., Willis, A.D., Xu, Z.Z., Zaneveld, J.R., Zhang, Y., Zhu, Q., Knight, R., Caporaso, J.G., 2019. Reproducible, interactive, scalable and extensible microbiome data science using QIIME 2. Nat. Biotechnol. 37, 852–857. https://doi.org/10.1038/s41587-019-0209-9

Bonartsev, A., Bonartseva, G.A., Reshetov, I., Kirpichnikov, M., Shaitan, K., 2019. Application of Polyhydroxyalkanoates in Medicine and the Biological Activity of Natural Poly(3-Hydroxybutyrate). Acta Naturae 11, 4–16. https://doi.org/10.32607/20758251-2019-11-2-4-16

Borowitzka, M., Vonshak, A., 2017. Scaling up microalgal cultures to commercial scale. Eur. J. Phycol. 52, 407–418. https://doi.org/10.1080/09670262.2017.1365177

Brar, A., Kumar, M., Vivekanand, V., Pareek, N., 2017. Photoautotrophic microorganisms and bioremediation of industrial effluents: current status and future prospects. 3 Biotech 7, 1–8. https://doi.org/10.1007/s13205-017-0600-5

Brodhagen, M., Peyron, M., Miles, C., Inglis, D., 2014. Biodegradable plastic agricultural mulches and key features of microbial degradation. Appl. Microbiol. Biotechnol. 99. https://doi.org/10.1007/s00253-014-6267-5

Broquet, A., Andrews-Hanna, J.C., 2023. Geophysical evidence for an active mantle plume underneath Elysium Planitia on Mars. Nat. Astron. 7, 160–169. https://doi.org/10.1038/s41550-022-01836-3

Bures, S., Fishbain, J.T., Uyehara, C.F., Parker, J.M., Berg, B.W., 2000. Computer keyboards and faucet handles as reservoirs of nosocomial pathogens in the intensive care unit. Am. J. Infect. Control 28, 465–471. https://doi.org/10.1067/mic.2000.107267

Burton, A.S., Stahl, S.E., John, K.K., Jain, M., Juul, S., Turner, D.J., Harrington, E.D., Stoddart, D., Paten, B., Akeson, M., Castro-Wallace, S.L., 2020. Off Earth Identification of Bacterial Populations Using 16S rDNA Nanopore Sequencing. Genes (Basel). 11. https://doi.org/10.3390/genes11010076

Busi, M., Barchiesi, J., Martin, M., Gomez-Casati, D., 2014. Starch metabolism in green algae. Starch/Staerke 66. https://doi.org/10.1002/star.201200211

Bussa, M., Eisen, A., Zollfrank, C., Röder, H., 2019. Life cycle assessment of microalgae products: State of the art and their potential for the production of polylactid acid. J. Clean. Prod. 213, 1299–1312. https://doi.org/10.1016/j.jclepro.2018.12.048

Byun, Y., Whiteside, S., Thomas, R.L., Dharman, M., Hughes, J., Kim, Y., 2012. The effect of solvent mixture on the properties of solvent cast polylactic acid (PLA) film. J. Appl. Polym. Sci. 124. https://doi.org/10.1002/app.34071

Capuano, L., Berenschot, J.W., Tiggelaar, R.M., Feinaeugle, M., Tas, N.R., Gardeniers, J.G.E., Römer, G.R.B.E., 2022. Fabrication of microstructures in the bulk and on the surface of sapphire by anisotropic selective wet etching of laser-affected volumes. J. Micromechanics Microengineering 32. https://doi.org/10.1088/1361-6439/ac9911

Carneiro, M., Maia, I.B., Cunha, P., Guerra, I., Magina, T., Santos, T., Schulze, P.S.C., Pereira, H., Malcata, F.X., Navalho, J., Silva, J., Otero, A., Varela, J., 2022. Effects of LED lighting on Nannochloropsis oceanica grown in outdoor raceway ponds. Algal Res. 64, 102685. https://doi.org/https://doi.org/10.1016/j.algal.2022.102685

Carpine, R., Raganati, F., Olivieri, G., Hellingwerf, K.J., Pollio, A., Salatino, P., Marzocchella, A., 2018. Poly-β-hydroxybutyrate (PHB) production by Synechocystis PCC6803 from CO2: Model development. Algal Res. 29, 49–60. https://doi.org/10.1016/j.algal.2017.11.011

Carrier, B., Beaty, D., Hutzler, A., Smith, A., Kminek, G., Meyer, M., Haltigin, T., Hays, L., Agee, C., Busemann, H., Cavalazzi, B., Cockell, C., Vinciane, D., Glavin, D., Grady, M., Hauber, E., Marty, B., Mccubbin, F., Pratt, L., Zorzano, M.-P., 2021. Science and Curation Considerations for the Design of a Mars Sample Return (MSR) Sample Receiving Facility. Astrobiology 22. https://doi.org/10.1089/AST.2021.0110

Carter, L., Wilson, L. L. and Orozco, N. (2011) 'Status of ISS water management and recovery', in 41st International Conference on Environmental Systems 2011, ICES 2011. American Institute of Aeronautics and Astronautics Inc. doi: 10.2514/6.2011-5223.

Castro-Wallace, S.L., Chiu, C.Y., John, K.K., Stahl, S.E., Rubins, K.H., McIntyre, A.B.R., Dworkin, J.P., Lupisella, M.L., Smith, D.J., Botkin, D.J., Stephenson, T.A., Juul, S., Turner, D.J., Izquierdo, F., Federman, S., Stryke, D., Somasekar, S., Alexander, N., Yu, G., Mason, C.E.,

Burton, A.S., 2017. Nanopore DNA Sequencing and Genome Assembly on the International Space Station. Sci. Rep. 7, 18022. https://doi.org/10.1038/s41598-017-18364-0

Castro, C., Velez Justiniano, Y.-A., Stahl-Rommel, S., Nguyen, H., Almengor, A., Dunbar, B., McLean, R., Sysoeva, T., Castro-Wallace, S., 2023. Genome Sequences of Bacteria Isolated from the International Space Station Water Systems. Microbiol. Resour. Announc. 12, e0015823. https://doi.org/10.1128/mra.00158-23

Chan, Q.H.S., Stroud, R., Martins, Z., Yabuta, H., 2020. Concerns of Organic Contamination for Sample Return Space Missions. Space Sci. Rev. 216, 56. https://doi.org/10.1007/s11214-020-00678-7

Chang, C.-K., Wang, H.-M.D., Lan, J.C.-W., 2018. Investigation and Characterization of Plasma-Treated Poly(3-hydroxybutyrate) and Poly(3-hydroxybutyrate-co-3-hydroxyvalerate) Biopolymers for an In Vitro Cellular Study of Mouse Adipose-Derived Stem Cells. Polymers (Basel). 10. https://doi.org/10.3390/polym10040355

Changela, H., Chatzitheodoridis, E., Antunes, A., Beaty, D., Bouw, K., Bridges, J., Capova, K.A., Cockell, C., Conley, C., Dadachova, E., Mey, T., Dong, C., Ferus, M., Foing, B., Fu, X., Fujita, K., Lin, Y., Jheeta, S., Hicks, L., Hallsworth, J., 2021. Mars: new insights and unresolved questions.

Chaogang, W., Zhangli, H., Anping, L., Baohui, J., 2010. Biosynthesis of Poly-3-hydroxybutyrate (PHB) in the transgenic green alga Chlamydomonas reinhardtii. J. Phycol. 46, 396–402. https://doi.org/10.1111/j.1529-8817.2009.00789.x

Chen, G.-Q., Wu, Q., 2005. Microbial production and applications of chiral hydroxyalkanoates. Appl. Microbiol. Biotechnol. 67, 592–599. https://doi.org/10.1007/s00253-005-1917-2

Chen, C.-Y., Zhao, X.-Q., Yen, H.-W., Ho, S.-H., Cheng, C.-L., Lee, D.-J., Bai, F.-W., Chang, J.-S., 2013. Microalgae-based carbohydrates for biofuel production. Biochem. Eng. J. 78, 1–10. https://doi.org/https://doi.org/10.1016/j.bej.2013.03.006

Chen, X., Ibrahim, S., Kunitskaya, A., Schaaf, K., Wang, Z.F., Gopalakrishan, P., Noor, M., Wilton-Clark, H., Grainger, J., Ivanova, A., Lim, P., Olsakova, M., Bharadwaj, L., Sher, B., Feehan, D., Varga, R., Arcellana-Panlilio, M., 2018. Astroplastic: A start-to-finish process for polyhydroxybutyrate production from solid human waste using genetically engineered bacteria to address the challenges for future manned Mars missions. bioRxiv.

Chiarello, M., McCauley, M., Villéger, S., Jackson, C.R., 2022. Ranking the biases: The choice of OTUs vs. ASVs in 16S rRNA amplicon data analysis has stronger effects on diversity measures than rarefaction and OTU identity threshold. PLoS One 17, e0264443. https://doi.org/10.1371/journal.pone.0264443

Chioccioli, M., Hankamer, B., Ross, I., 2014. Flow Cytometry Pulse Width Data Enables Rapid and Sensitive Estimation of Biomass Dry Weight in the Microalgae Chlamydomonas reinhardtii and Chlorella vulgaris. PLoS One 9, e97269. https://doi.org/10.1371/journal.pone.0097269

Choi, S.P., Nguyen, M.T., Sim, S.J., 2010. Enzymatic pretreatment of Chlamydomonas reinhardtii biomass for ethanol production. Bioresour. Technol. 101, 5330–5336. https://doi.org/10.1016/j.biortech.2010.02.026

Christine Butterwick, S.I.H., Talling, J.F., 1982. A comparison of eight methods for estimating the biomass and growth of planktonic algae. Br. Phycol. J. 17, 69–79. https://doi.org/10.1080/00071618200650091

Cinar, S., Chong, Z.K., Kucuker, M.A., Wieczorek, N., Cengiz, U., Kuchta, K., 2020. Bioplastic Production from Microalgae: A Review. Int. J. Environ. Res. Public Health 17. https://doi.org/10.3390/ijerph17113842

Cockell, C.S., 2010. Geomicrobiology beyond Earth: Microbe-mineral interactions in space exploration and settlement. Trends Microbiol. 18, 308–314. https://doi.org/10.1016/j.tim.2010.03.005

Cockell, C.S., 2004. Martian Expedition Planning, Science and Technology Series, Vol 107. American Astronautical Society.

Coelho, L.F., Blais, M.-A., Matveev, A., Keller-Costa, T., Vincent, W.F., Costa, R., Martins, Z., Canário, J., 2022. Contamination analysis of Arctic ice samples as planetary field analogs and implications for future life-detection missions to Europa and Enceladus. Sci. Rep. 12, 12379. https://doi.org/10.1038/s41598-022-16370-5

Cogen, A.L., Nizet, V., Gallo, R.L., 2008. Skin microbiota: a source of disease or defence? Br. J. Dermatol. 158, 442–455. https://doi.org/10.1111/j.1365-2133.2008.08437.x

Cortesão, M., Fuchs, F., Commichau, F., Eichenberger, P., Schuerger, A., Nicholson, W., Setlow, P., Moeller, R., 2019. Bacillus subtilis Spore Resistance to Simulated Mars Surface Conditions. Front. Microbiol. 10. https://doi.org/10.3389/fmicb.2019.00333

Cosseau, C., Romano-Bertrand, S., Duplan, H., Lucas, O., Ingrassia, I., Pigasse, C., Roques, C., Jumas-Bilak, E., 2016. Proteobacteria from the human skin microbiota: Species-level diversity and hypotheses. One Health (Amsterdam, Netherlands), 2, 33–41. https://doi.org/10.1016/j.onehlt.2016.02.002

Costa, O.Y.A., Raaijmakers, J.M., Kuramae, E.E., 2018. Microbial extracellular polymeric substances: Ecological function and impact on soil aggregation. Front. Microbiol. 9, 1–14. https://doi.org/10.3389/fmicb.2018.01636

Cruz, A.T., Cazacu, A.C., Allen, C.H., 2007. Pantoea agglomerans, a plant pathogen causing human disease. J. Clin. Microbiol. 45, 1989–1992. https://doi.org/10.1128/JCM.00632-07

Cuesta-Seijo, J.A. file:///Users/maraleite/Downloads/1-s2. .-S. pd., Ruzanski, C., Krucewicz, K., Meier, S., Hägglund, P., Svensson, B., Palcic, M.M., 2017. Functional and structural characterization of plastidic starch phosphorylase during barley endosperm development. PLoS One 12, 1–25. https://doi.org/10.1371/journal.pone.0175488

da Silva, T., Reis, A., 2015. Scale-up Problems for the Large Scale Production of Algae. pp. 125–149. https://doi.org/10.1007/978-3-319-22813-6_

Dalton, B., Bhagabati, P., Micco, J. De, Padamati, R.B., O'Connor, K.E., 2022. A Review on Biological Synthesis of the Biodegradable Polymers Polyhydroxyalkanoates and the Development of Multiple Applications. Catalysts.

Damrow, R., Maldener, I., Zilliges, Y., 2016. The multiple functions of common microbial carbon polymers, glycogen and PHB, during stress responses in the non-diazotrophic cyanobacterium synechocystis sp. PCC 6803. Front. Microbiol. 7, 1–10. https://doi.org/10.3389/fmicb.2016.00966

Dartnell, L., 2011. Biological constraints on habitability. Astron. Geophys. 52, 1.25-1.28. https://doi.org/10.1111/j.1468-4004.2011.52125.x

Darwish, R., Gedi, M., Akepach, P., Assaye, H., Zaky, A., Gray, D., 2020. Chlamydomonas reinhardtii Is a Potential Food Supplement with the Capacity to Outperform Chlorella and Spirulina. Appl. Sci. 10. https://doi.org/10.3390/app10196736

Dassey, A.J., Theegala, C.S., 2013. Harvesting economics and strategies using centrifugation for cost effective separation of microalgae cells for biodiesel applications. Bioresour. Technol. 128, 241–245. https://doi.org/https://doi.org/10.1016/j.biortech.2012.10.061

Dauvillée, D., Delhaye, S., Gruyer, S., Slomianny, C., Moretz, S.E., d'Hulst, C., Long, C.A., Ball, S.G., Tomavo, S., 2010. Engineering the Chloroplast Targeted Malarial Vaccine Antigens in Chlamydomonas Starch Granules. PLoS One 5, 1–8. https://doi.org/10.1371/journal.pone.0015424

de Goffau, M.C., Lager, S., Sovio, U., Gaccioli, F., Cook, E., Peacock, S.J., Parkhill, J., Charnock-Jones, D.S., Smith, G.C.S., 2019. Human placenta has no microbiome but can contain potential pathogens. Nature 572, 329–334. https://doi.org/10.1038/s41586-019-1451-5

de la Higuera, I., Lázaro, E., 2022. Viruses in astrobiology. Front. Microbiol. 13, 1032918. https://doi.org/10.3389/fmicb.2022.1032918

de Micco, V., Aronne, G., Colla, G., Fortezza, R., de Pascale, S., 2009. Agro-biology for bioregenerative life support systems in long-term space missions: General constraints and the Italian efforts. J. Plant Interact. 4, 241–252. https://doi.org/10.1080/17429140903161348

de Souza, P.M., de Oliveira Magalhães, P., 2010. Application of microbial α-amylase in industry - A review. Brazilian J. Microbiol. [publication Brazilian Soc. Microbiol. 41, 850–861. https://doi.org/10.1590/S1517-83822010000400004

Dehghani, J., Adibkia, K., Movafeghi, A., Barzegari, A., Pourseif, M.M., Maleki Kakelar, H., Golchin, A., Omidi, Y., 2018. Stable transformation of Spirulina (Arthrospira) platensis: a promising microalga for production of edible vaccines. Appl. Microbiol. Biotechnol. 9267–9278. https://doi.org/10.1007/s00253-018-9296-7

Demain, A., Fang, A., 2000. The natural functions of secondary metabolites. Adv. Biochem. Eng. Biotechnol. 69, 1–39.

Denine, A., Siegfried, P., 2022. The assessment of the Filament Extruder Equipment for 3D printing method. STED J. 4, 32–38. https://doi.org/10.7251/STED2201032D

Depraetere, O., Pierre, G., Noppe, W., Vandamme, D., Foubert, I., Michaud, P., Muylaert, K., 2015. Influence of culture medium recycling on the performance of Arthrospira platensis cultures. Algal Res. 10, 48–54. https://doi.org/10.1016/j.algal.2015.04.014

Direito, S.O.L., Ehrenfreund, P., Marees, A., Staats, M., Foing, B., Röling, W.F.M., 2011. A wide variety of putative extremophiles and large beta-diversity at the Mars Desert Research Station (Utah). Int. J. Astrobiol. 10, 191–207. https://doi.org/10.1017/S1473550411000012

Driver, T., Bajhaiya, A.K., Allwood, J.W., Goodacre, R., Pittman, J.K., Dean, A.P., 2015. Metabolic responses of eukaryotic microalgae to environmental stress limit the ability of FT-IR spectroscopy for species identification. Algal Res. 11, 148–155. https://doi.org/10.1016/j.algal.2015.06.009

Dogan Subasi, E., Demirer, G., 2016. Anaerobic digestion of microalgal (Chlorella vulgaris) biomass as a source of biogas and biofertilizer. Environ. Prog. Sustain. Energy 35, n/a-n/a. https://doi.org/10.1002/ep.12294

Du, B., Daniels, V.R., Vaksman, Z., Boyd, J.L., Crady, C., Putcha, L., 2011. Evaluation of physical and chemical changes in pharmaceuticals flown on space missions. AAPS J. 13, 299–308. https://doi.org/10.1208/s12248-011-9270-0

Dutta, D., De, D., Chaudhuri, S., Bhattacharya, S.K., 2005. Hydrogen production by Cyanobacteria. Microb. Cell Fact. 4, 1–11. https://doi.org/10.1186/1475-2859-4-36

Edmonds, K., Williams, L., 2017. The Role of the Negative Control in Microbiome Analyses. FASEB J. 31, 940.3-940.3. https://doi.org/https://doi.org/10.1096/fasebj.31.1_supplement.940.3

El-Kadi, S.M., Elbagory, M., EL-Zawawy, H.A.H., EL-Shaer, H.F.A., Shoukry, A.A., El-Nahrawy, S., Omara, A.E.-D., Ali, D.F.I., 2021. Biosynthesis of Poly-ß-Hydroxybutyrate (PHB) from Different Bacterial Strains Grown on Alternative Cheap Carbon Sources. Polymers (Basel). 13. https://doi.org/10.3390/polym1321380

Errington, J., Aart, L.T. van der, 2020. Microbe Profile: Bacillus subtilis: model organism for cellular development, and industrial workhorse. Microbiology 166, 425–427. https://doi.org/10.1099/mic.0.00092

European Space Agency. 2018. "MELT_3D_printer." ESA Multimedia. October 18. https://www.esa.int/ESA_Multimedia/Images/2018/10/MELT_3D_printer.

Lopez-Exposito, P., Suarez, A.B., Negro, C., 2016. Estimation of Chlamydomonas reinhardtii biomass concentration from chord length distribution data. J. Appl. Phycol. 28, 2315–2322. https://doi.org/10.1007/s10811-015-0749-4

López-Expósito, P., Blanco Suárez, A., Negro Álvarez, C., 2017. Laser reflectance measurement for the online monitoring of Chlorella sorokiniana biomass concentration. J. Biotechnol. 243, 10–15. https://doi.org/https://doi.org/10.1016/j.jbiotec.2016.12.020

Fadeev, E., Cardozo-Mino, M.G., Rapp, J.Z., Bienhold, C., Salter, I., Salman-Carvalho, VMolari, M., Tegetmeyer, H.E., Buttigieg, P.L., Boetius, A., 2021. Comparison of Two 16S rRNA Primers (V3-V4 and V4-V5) for Studies of Arctic Microbial Communities. Front. Microbiol. 12, 637526. https://doi.org/10.3389/fmicb.2021.637526

Fahrion, J., Mastroleo, F., Dussap, C.-G., Leys, N., 2021. Use of Photobioreactors in Regenerative Life Support Systems for Human Space Exploration. Front. Microbiol. 12. https://doi.org/10.3389/fmicb.2021.699525

Fairén, A.G., Parro, V., Schulze-Makuch, D., Whyte, L., 2017. Searching for Life on Mars Before It Is Too Late. Astrobiology 17, 962–970. https://doi.org/10.1089/ast.2017.1703

Fan, J., Zheng, L., Bai, Y., Saroussi, S., Grossman, A.R., 2017. Flocculation of Chlamydomonas reinhardtii with Different Phenotypic Traits by Metal Cations and High pH. Front. Plant Sci. 8, 1997. https://doi.org/10.3389/fpls.2017.01997

Favero, M.S., 1971. Microbiologic assay of space hardware. Environ. Biol. Med. 1, 27–36.

Favero, M.S., Puleo, J.R., Marshall, J.H., Oxborrow, G.S., 1966. Comparative levels and types of microbial contamination detected in industrial clean rooms. Appl. Microbiol. 14, 539–551. https://doi.org/10.1128/am.14.4.539-551.1966

Ferreira, E.A., Pacheco, C.C., Pinto, F., Pereira, J., Lamosa, P., Oliveira, P., Kirov, B., Jaramillo, A., Tamagnini, P., 2018. Expanding the toolbox for Synechocystis sp. PCC 6803: validation of replicative vectors and characterization of a novel set of promoters. Synth. Biol. (Oxford, England) 3, ysy014. https://doi.org/10.1093/synbio/ysy014

Fierer, N., Jackson, R.B., 2006. The diversity and biogeography of soil bacterial communities. Proc. Natl. Acad. Sci. U. S. A. 103, 626–631. https://doi.org/10.1073/pnas.0507535103

Filip, Z., Herrmann, S., Kubat, J., 2004. FT-IR spectroscopic characteristics of differently cultivated Bacillus subtilis. Microbiol. Res. 159, 257–262. https://doi.org/https://doi.org/10.1016/j.micres.2004.05.002

Findinier, J., Laurent, S., Duchêne, T., Roussel, X., Lancelon-Pin, C., Cuiné, S., Putaux, J.-L., Li-Beisson, Y., D'Hulst, C., Wattebled, F., Dauvillée, D., 2019. Deletion of BSG1 in Chlamydomonas reinhardtii leads to abnormal starch granule size and morphology. Sci. Rep. 9, 1990. https://doi.org/10.1038/s41598-019-39506-6

Franzetti, L., Scarpeluni, M., 2007. Characterisation of Pseudomonas spp. isolated from foods. Ann. Microbiol. 57, 39–47. https://doi.org/10.1007/BF03175048

Frone, A.N., Batalu, D., Chiulan, I., Oprea, M., Gabor, A.R., Nicolae, C.-A., Raditoiu, V., Trusca, R., Panaitescu, D.M., 2019. Morpho-Structural, Thermal and Mechanical Properties of PLA/PHB/Cellulose Biodegradable Nanocomposites Obtained by Compression Molding, Extrusion, and 3D Printing. Nanomater. (Basel, Switzerland) 10. https://doi.org/10.3390/nano10010051

Fu, N., Peiris, P., Markham, J., Bavor, J., 2009. A novel co-culture process with Zymomonas mobilis and Pichia stipitis for efficient ethanol production on glucose/xylose mixtures. Enzyme and Microbial Technology 45, 210–217. https://doi.org/10.1016/j.enzmictec.2009.04.006

Gajda, I., Greenman, J., Melhuish, C., Ieropoulos, I., 2015. Simultaneous electricity generation and microbially-assisted electrosynthesis in ceramic MFCs. Bioelectrochemistry 104, 58–64. https://doi.org/10.1016/j.bioelechem.2015.03.001

Gámez-Arjona, F.M., Li, J., Raynaud, S., Baroja-Fernández, E., Muñoz, F.J., Ovecka, M., Ragel, P., Bahaji, A., Pozueta-Romero, J., Mérida, Á., 2011. Enhancing the expression of starch synthase class IV results in increased levels of both transitory and long-term storage starch. Plant Biotechnol. J. 9, 1049–1060. https://doi.org/10.1111/j.1467-7652.2011.00626.x

Gauvry, E., Mathot, A.-G., Couvert, O., Leguérinel, I., Coroller, L., 2021. Effects of temperature, pH and water activity on the growth and the sporulation abilities of Bacillus subtilis BSB1. Int. J. Food Microbiol. 337, 108915. https://doi.org/10.1016/j.ijfoodmicro.2020.108915

Geigenberger, P., 2011. Regulation of starch biosynthesis in response to a fluctuating environment. Plant Physiol. 155, 1566–1577. https://doi.org/10.1104/pp.110.170399

Geminale, A., Formisano, V., Sindoni, G., 2011. Mapping methane in Martian atmosphere with PFS-MEX data. Planet. Space Sci. 59, 137–148. https://doi.org/https://doi.org/10.1016/j.pss.2010.07.011

Gifuni, I., Olivieri, G., Pollio, A., Franco, T.T., Marzocchella, A., 2017. Autotrophic starch production by Chlamydomonas species. J. Appl. Phycol. 29, 105–114. https://doi.org/10.1007/s10811-016-0932-2

Gimpel, J.A., Specht, E.A., Georgianna, D.R., Mayfield, S.P., 2013. Advances in microalgae engineering and synthetic biology applications for biofuel production. Curr. Opin. Chem. Biol. 17, 489–495. https://doi.org/10.1016/j.cbpa.2013.03.038

Giubilini, A., Siqueira, G., Clemens, F., Sciancalepore, C., Messori, M., Nyström, G., Bondioli, F., 2020. 3D Printing Nanocellulose-Poly(3-hydroxybutyrate-co-3-hydroxyhexanoate) Biodegradable Composites by Fused Deposition Modeling. ACS Sustain. Chem. Eng. XXXX. https://doi.org/10.1021/acssuschemeng.0c03385

Giuranna, M., Viscardy, S., Daerden, F., Neary, L., Etiope, G., Oehler, D., Formisano, V., Aronica, A., Wolkenberg, P., Aoki, S., Cardesín-Moinelo, A., Marín-Yaseli de la Parra, J., Merritt, D., Amoroso, M., 2019. Independent confirmation of a methane spike on Mars and a source region east of Gale Crater. Nat. Geosci. 12, 326–332. https://doi.org/10.1038/s41561-019-0331-9

Glavin, D.P., Bada, J.L., Brinton, K.L., McDonald, G.D., 1999. Amino acids in the Martian meteorite Nakhla. Proc. Natl. Acad. Sci. U. S. A. 96, 8835–8838. https://doi.org/10.1073/pnas.96.16.8835

Gòdia, F., Albiol, J., Montesinos, J.L., Pérez, J., Creus, N., Cabello, F., Mengual, X., Montras, A., Lasseur, C., 2002. MELISSA: A loop of interconnected bioreactors to develop life support in Space. file///Users/maraleite/Downloads/47-9-575(4).pdfJournal Biotechnol. 99, 319–330. https://doi.org/10.1016/S0168-1656(02)00222-5

Goh Escolar, G., Kazeminejad, B., n.d. Mars through the looking glass: An interdisciplinary analysis of forward and backward contamination. Space Policy 20, 217–225. https://doi.org/10.1016/j.spacepol.2004.06.008

Gonzalez-Menendez, V., Martin, J., Siles, J.A., Gonzalez-Tejero, M.R., Reyes, F., Platas, G., Tormo, J.R., Genilloud, O., 2017. Biodiversity and chemotaxonomy of Preussia isolates from the Iberian Peninsula. Mycol. Prog. 16, 713–728. https://doi.org/10.1007/s11557-017-1305-1

Grace, C.E.E., Lakshmi, P.K., Meenakshi, S., Vaidyanathan, S., Srisudha, S., Mary, M.B., 2020. Biomolecular transitions and lipid accumulation in green microalgae monitored by FTIR and Raman analysis. Spectrochim. Acta. A. Mol. Biomol. Spectrosc. 224, 117382. https://doi.org/10.1016/j.saa.2019.117382

Granath, B., 2017. Lunar, "Martian Greenhouses Designed to Mimic Those on Earth [WWW

Document]. NASA's Kennedy Sp. Center, Florida. URL url:https://www.nasa.gov/feature/lunar-martian-greenhouses-designed-to-feature/lunar-martian-greenhouses-designed-to-mimic-those-on-earth

Grossi, E., Berliner, A., Cumbers, J., Kagawa, H., Modarressi, B., Hogan, J., Flynn, M., 2013. Potential Applications for Bioelectrochemical Systems for Space Exploration, 43rd International Conference on Environmental Systems. https://doi.org/10.2514/6.2013-3331

Hadj-Romdhane, F., Zheng, X., Jaouen, P., Pruvost, J., Grizeau, D., Croué, J.P., Bourseau, P., 2013. The culture of Chlorella vulgaris in a recycled supernatant: Effects on biomass production and medium quality. Bioresour. Technol. 132, 285–292. https://doi.org/https://doi.org/10.1016/j.biortech.2013.01.025

Hahn, S.K., Chang, Y.K., Lee, S.Y., 1995. Recovery and characterization of poly(3-hydroxybutyric acid) synthesized in Alcaligenes eutrophus and recombinant Escherichia coli. Appl. Environ. Microbiol. 61, 34–39. https://doi.org/10.1128/aem.61.1.34-39.1995

Hakobyan, L., Gabrielyan, L., Trchounian, A., 2012. Bio-hydrogen production and the F0F1-ATPase activity of Rhodobacter sphaeroides: Effects of various heavy metal ions. Int. J. Hydrogen Energy 37, 17794–17800. https://doi.org/https://doi.org/10.1016/j.ijhydene.2012.09.091

Harris, E.H., Stern, D.B., Witman, G.B., 2009. The Chlamydomonas Sourcebook 3-Vol set. Chlamydomonas Sourceb. 3-Vol set 1

Hashimoto, K., Badarla, V., Kawai, A., Ideguchi, T., 2019. Complementary vibrational spectroscopy. Nat. Commun. 10. https://doi.org/10.1038/s41467-019-12442-9

Hashuel, R., Ben-Yehuda, S., 2019. Aging of a Bacterial Colony Enforces the Evolvement of Nondifferentiating Mutants. MBio 10. https://doi.org/10.1128/mBio.01414-19

Hauslage, J., Strauch, S.M., Eßmann, O., Haag, F.W.M., Richter, P., Kr, J., Stoltze, J., Becker, I., Nasir, A., Bornemann, G., Hartmut, M., Delovski, T., Berger, T., Rutczynska, A., Marsalek, K., Lebert, M., 2018. Eu : CROPIS – " Euglena gracilis : Combined Regenerative Organic-food Production in Space " - A Space Experiment Testing Biological Life. Microgravity Sci. Technol. 30, 933–942.

Hecht, M., Hoffman, J., Rapp, D., McClean, J., SooHoo, J., Schaefer, R., Aboobaker, A., Mellstrom, J., Hartvigsen, J., Meyen, F., Hinterman, E., Voecks, G., Liu, A., Nasr, M., Lewis, J., Johnson, J., Guernsey, C., Swoboda, J., Eckert, C., Alcalde, C., Poirier, M., Khopkar, P., Elangovan, S., Madsen, M., Smith, P., Graves, C., Sanders, G., Araghi, K., de la Torre Juarez, M., Larsen, D., Agui, J., Burns, A., Lackner, K., Nielsen, R., Pike, T., Tata, B., Wilson, K., Brown, T., Disarro, T., Morris, R., Schaefer, R., Steinkraus, R., Surampudi, R., Werne, T., Ponce, A., 2021. Mars Oxygen ISRU Experiment (MOXIE). Space Sci. Rev. https://doi.org/10.1007/s11214-020-00782-8

Hempel, F., Lau, J., Klingl, A., Maier, U.G., 2011. Algae as protein factories: expression of a human antibody and the respective antigen in the diatom Phaeodactylum tricornutum. PLoS One 6, e28424. https://doi.org/10.1371/journal.pone.0028424

Hicks, M., Tran-Dao, T.K., Mulroney, L., Bernick, D.L., 2021. De-novo Assembly of Limnospira fusiformis Using Ultra-Long Reads. Front. Microbiol. 12, 1–12. https://doi.org/10.3389/fmicb.2021.657995

Hirai, K., Nojo, M., Sato, Y., Tsuzuki, M., Sato, N., 2019. Contribution of protein synthesis depression to poly-β-hydroxybutyrate accumulation in Synechocystis sp. PCC 6803 under nutrient-starved conditions. Sci. Rep. 9, 1–10. https://doi.org/10.1038/s41598-019-56520-w

Horneck, G., Facius, R., Reichert, M., Rettberg, P., Seboldt, W., Manzey, D., Comet, B., Maillet, A., Preiss, H., Schauer, L., Dussap, C.G., Poughon, L., Belyavin, A., Reitz, G., Baumstark-Khan, C., Gerzer, R., 2003. Humex, a study on the survivability and adaptation of humans to long-duration exploratory missions, part I: Lunar missions. Adv. Sp. Res. 31, 2389–2401. https://doi.org/10.1016/S0273-1177(03)00568-4

Horneck, G., Klaus, D.M., Mancinelli, R.L., 2010. Space Microbiology. Microbiol. Mol. Biol. Rev. 74, 121–156. https://doi.org/10.1128/mmbr.00016-09

Hornung, B.V.H., Zwittink, R.D., Kuijper, E.J., 2019. Issues and current standards of controls in microbiome research. FEMS Microbiol. Ecol. 95, 1–7. https://doi.org/10.1093/femsec/fiz045

Huang, B., Li, D.-G., Huang, Y., Liu, C.-T., 2018. Effects of spaceflight and simulated microgravity on microbial growth and secondary metabolism. Mil. Med. Res. 5, 18. https://doi.org/10.1186/s40779-018-0162-9

Huang, Q., Jiang, F., Wang, L., Yang, C., 2017. Design of Photobioreactors for Mass Cultivation of Photosynthetic Organisms. Engineering 3, 318–329. https://doi.org/https://doi.org/10.1016/J.ENG.2017.03.020

Ichijo, T., Yamaguchi, N., Tanigaki, F., Shirakawa, M., Nasu, M., 2016. Four-year bacterial monitoring in the International Space Station—Japanese Experiment Module “Kibo” with culture-independent approach. npj Microgravity 2, 16007. https://doi.org/10.1038/npjmgrav.2016.7

Ivanov, I.N., Zachleder, V., Vítová, M., Barbosa, M.J., Bišová, K., 2021. Starch Production in Chlamydomonas reinhardtii through Supraoptimal Temperature in a Pilot-Scale Photobioreactor. Cells 10. https://doi.org/10.3390/cells10051084

Jackson, H.O., Taunt, H.N., Mordaka, P.M., Smith, A.G., Purton, S., 2021. The Algal Chloroplast as a Testbed for Synthetic Biology Designs Aimed at Radically Rewiring Plant Metabolism. Front. Plant Sci. 12, 708370. https://doi.org/10.3389/fpls.2021.708370

Jacquel, N., Lo, C.-W., Wei, Y.-H., Wu, H.-S., Wang, S.S., 2008. Isolation and purification of bacterial poly(3-hydroxyalkanoates). Biochem. Eng. J. 39, 15–27. https://doi.org/https://doi.org/10.1016/j.bej.2007.11.029

Janssen, Paul J. D., Lambreva, M.D., PlumerÃ©, N., Bartolucci, C., Antonacci, A., Buonasera, K., Frese, R.N., Scognamiglio, V., Rea, G., 2014. Photosynthesis at the forefront of a sustainable life. Front. Chem. 2, 1–22. https://doi.org/10.3389/fchem.2014.00036

Jiang, G., Hill, D.J., Kowalczuk, M., Johnston, B., Adamus, G., Irorere, V., Radecka, I., 2016. Carbon Sources for Polyhydroxyalkanoates and an Integrated Biorefinery. Int. J. Mol. Sci. 17. https://doi.org/10.3390/ijms17071157

Jiang, T., Duan, Q., Zhu, J., Liu, H., Yu, L., 2020. Starch-based biodegradable materials: Challenges and opportunities. Adv. Ind. Eng. Polym. Res. 3, 8–18. https://doi.org/https://doi.org/10.1016/j.aiepr.2019.11.003

Jie, L., Yu, Y., Cai, Z., Bartlam, M., Wang, Y., 2015. Comparison of ITS and 18S rDNA for estimating fungal diversity using PCR–DGGE. World J. Microbiol. Biotechnol. 31. https://doi.org/10.1007/s11274-015-1890-6

Kamravamanesh, D., Kovacs, T., Pflügl, S., Druzhinina, I., Kroll, P., Lackner, M., Herwig, C., 2018. Increased poly-β-hydroxybutyrate production from carbon dioxide in randomly mutated cells of cyanobacterial strain Synechocystis sp. PCC 6714: Mutant generation and characterization. Bioresour. Technol. 266, 34–44. https://doi.org/https://doi.org/10.1016/j.biortech.2018.06.057

Kannan, L. V, Rehacek, Z., 1970. Formation of poly-beta-hydroxybutyrate by Actinomycetes. Indian J. Biochem. 7, 126–129.

Kann, Y., Shurgalin, M., Krishnaswamy, R.K., 2014. FTIR spectroscopy for analysis of crystallinity of poly(3-hydroxybutyrate-co-4 -hydroxybutyrate) polymers and its utilization in evaluation of aging, orientation and composition. Polym. Test. 40. https://doi.org/10.1016/j.polymertesting.2014.09.009

Karatay, S.E., Erdoğan, M., Dönmez, S., Dönmez, G., 2016. Experimental investigations on bioethanol production from halophilic microalgal biomass. Ecol. Eng. 95, 266–270. https://doi.org/https://doi.org/10.1016/j.ecoleng.2016.06.058

Kast, J., Yu, Y., Seubert, C.N., Wotring, V.E., Derendorf, H., 2017. Drugs in space: Pharmacokinetics and pharmacodynamics in astronauts. Eur. J. Pharm. Sci. 109, S2–S8. https://doi.org/10.1016/j.ejps.2017.05.025

Katoh, K., Standley, D.M., 2013. MAFFT multiple sequence alignment software version 7: Improvements in performance and usability. Mol. Biol. Evol. 30, 772–780. https://doi.org/10.1093/molbev/mst010

Kaygusuz, B., Özerinç, S., 2019. Improving the ductility of polylactic acid parts produced by fused deposition modeling through polyhydroxyalkanoate additions. J. Appl. Polym. Sci. 136, 48154. https://doi.org/10.1002/app.4815

Keshavarz, T., Roy, I., 2010. Polyhydroxyalkanoates: bioplastics with a green agenda. Curr. Opin. Microbiol. 13, 321–326. https://doi.org/10.1016/j.mib.2010.02.006

Kim, D.-G., La, H.-J., Ahn, C.-Y., Park, Y.-H., Oh, H.-M., 2011. Harvest of Scenedesmus sp. with bioflocculant and reuse of culture medium for subsequent high-density cultures. Bioresour. Technol. 102, 3163–3168. https://doi.org/10.1016/j.biortech.2010.10.108

Kirchman, D.L., Yu, L., Cottrell, M.T., 2003. Diversity and Abundance of Uncultured Cytophaga-Like Bacteria in the Delaware Estuary. Appl. Environ. Microbiol. 69, 6587–6596. https://doi.org/10.1128/AEM.69.11.6587-6596.2003

Kwon, D.Y., Park, J.Y., Lee, B.Y., Kim, M.S., 2020. Comparison of Scaffolds Fabricated via 3D Printing and Salt Leaching: In Vivo Imaging, Biodegradation, and Inflammation. Polymers (Basel). 12. https://doi.org/10.3390/polym12102210

Koch, M., Bruckmoser, J., Scholl, J., Hauf, W., Rieger, B., Forchhammer, K., 2020. Maximizing PHB content in Synechocystis sp. PCC 6803: a new metabolic engineering strategy based on the regulator PirC. Microb. Cell Fact. 19, 231. https://doi.org/10.1186/s12934-020-01491-1

Koch, M., Forchhammer, K., 2021. Polyhydroxybutyrate: A Useful Product of Chlorotic Cyanobacteria. Microb. Physiol. 31, 67–77. https://doi.org/10.1159/000515617

Koim-Puchowska, B., Kłosowski, G., Dróżdż-Afelt, J.M., Mikulski, D., Zielińska, A., 2021. Influence of the Medium Composition and the Culture Conditions on Surfactin Biosynthesis by a Native Bacillus subtilis natto BS19 Strain. Molecules 26. https://doi.org/10.3390/molecules26102985

Kök, KF.N.; Hasirci, V. Polyhydroxybutyrate and its copolymers: Applications in the medical field. In Tissue Engineering and Novel Delivery Systems; Yaszemski, M.J., Trantolo, D.J., Lewandrowski, K.-U., Hasirci, V., Altobelli, D.E., Wise, D.L., Eds.; Marcel Dekker Inc.: New York, NY, USA, 2004; pp. 543–561.

Kõljalg, U., Nilsson, H.R., Schigel, D., Tedersoo, L., Larsson, K.H., May, T.W., Taylor, A.F.S., Jeppesen, T.S., Frøslev, T.G., Lindahl, B.D., Põldmaa, K., Saar, I., Suija, A., Savchenko, A., Yatsiuk, I., Adojaan, K., Ivanov, F., Piirmann, T., Pöhönen, R., Zirk, A., Abarenkov, K., 2020. The taxon hypothesis paradigm—On the unambiguous detection and communication of taxa. Microorganisms 8, 1–24. https://doi.org/10.3390/microorganisms8121910

Kominek, L.A., Halvorson, H.O., 1965. Metabolism of poly-beta-hydroxybutyrate and acetoin in Bacillus cereus. J. Bacteriol. 90, 1251–1259. https://doi.org/10.1128/jb.90.5.1251-1259.1965

Kontárová, S., Přikryl, R., Melčová, V., Menčík, P., Horálek, M., Figalla, S., Plavec, R., Feranc, J., Sadílek, J., Pospíšilová, A., 2020. Printability, Mechanical and Thermal Properties of Poly(3-Hydroxybutyrate)-Poly(Lactic Acid)-Plasticizer Blends for Three-Dimensional (3D) Printing. Mater. (Basel, Switzerland) 13. https://doi.org/10.3390/ma13214736

Koo, K.M., Jung, S., Lee, B.S., Kim, J.-B., Jo, Y.D., Choi, H.-I., Kang, S.-Y., Chung, G.-H., Jeong, W.-J., Ahn, J.-W., 2017. The Mechanism of Starch Over-Accumulation in Chlamydomonas reinhardtii High-Starch Mutants Identified by Comparative Transcriptome Analysis. Front. Microbiol. 8, 858. https://doi.org/10.3389/fmicb.2017.00858

Kosiewicz, M.M., Zirnheld, A.L., Alard, P., 2011. Gut microbiota, immunity, and disease: A complex relationship. Front. Microbiol. 2, 1–11. https://doi.org/10.3389/fmicb.2011.00180

Kulakov, L.A., McAlister, M.B., Ogden, K.L., Larkin, M.J., O'Hanlon, J.F., 2002. Analysis of bacteria contaminating ultrapure water in industrial systems. Appl. Environ. Microbiol. 68, 1548–1555. https://doi.org/10.1128/AEM.68.4.1548-1555.2002

Kumagai, S., 2007. Influence of Algal Fouling on Hydrophobicity and Leakage Current on Silicone Rubber. Dielectr. Electr. Insul. IEEE Trans. 14, 1201–1206. https://doi.org/10.1109/TDEI.2007.4339480

Kumari, P., Kiran, B., Venkata Mohan, S., 2022. Polyhydroxybutyrate production by Chlorella Sorokiniana SVMIICT8 under Nutrient-deprived Mixotrophy. Bioresour. Technol. 354, 127135. https://doi.org/10.1016/j.biortech.2022.127135

La Duc, M.T., Vaishampayan, P., Nilsson, H.R., Torok, T., Venkateswaran, K., 2012. Pyrosequencing-derived bacterial, archaeal, and fungal diversity of spacecraft hardware destined for mars. Appl. Environ. Microbiol. 78, 5912–5922. https://doi.org/10.1128/AEM.01435-12

Lang, J.M., Coil, D.A., Neches, R.Y., Brown, W.E., Cavalier, D., Severance, M., Hampton-Marcell, J.T., Gilbert, J.A., Eisen, J.A., 2017. A microbial survey of the International Space Station (ISS). PeerJ 5, e4029. https://doi.org/10.7717/peerj.4029

Larrea-Álvarez, M., Purton, S., 2021. The Chloroplast of Chlamydomonas reinhardtii as a Testbed for Engineering Nitrogen Fixation into Plants. Int. J. Mol. Sci. 22. https://doi.org/10.3390/ijms22168806

Laurence, M., Hatzis, C., Brash, D.E., 2014. Common contaminants in next-generation sequencing that hinder discovery of low-abundance microbes. PLoS One 9, 1–8. https://doi.org/10.1371/journal.pone.0097876

Lavens, P., Sorgeloos, P., 2000. The history, present status and prospects of the availability of Artemia cysts for aquaculture. Aquaculture 181, 397–403. https://doi.org/https://doi.org/10.1016/S0044-8486(99)00233-1

Law, J.H., Slepecky, R.A., 1961. Assay of poly-beta-hydroxybutyric acid. J. Bacteriol. 82, 33–36. https://doi.org/10.1128/jb.82.1.33-36.1961

Lehto, K.M., Lehto, H.J., Kanervo, E.A., 2006. Suitability of different photosynthetic organisms for an extraterrestrial biological life support system. Res. Microbiol. 157, 69–76. https://doi.org/10.1016/j.resmic.2005.07.011

Lemoigne M. Produit de déshydratation et de polymérisation de l'acide b-oxybutyrique. Bull Soc Chim Biol. 1926;8:770–82.

Li, H., Zhao, W., Wu, X., Tang, H., Li, Q., Tan, J., Wang, G., 2020. 3D Printing and Solvent Dissolution Recycling of Polylactide-Lunar Regolith Composites by Material Extrusion Approach. Polymers (Basel). 12. https://doi.org/10.3390/polym12081724

Li, M., Hu, D., Liu, H., Hu, E., Xie, B., Tong, L., 2013. Chlorella vulgaris culture as a regulator of CO2 in a bioregenerative life support system. Adv. Sp. Res. 52, 773–779. https://doi.org/10.1016/j.asr.2013.04.014

Li, Z., Wang, J., Li, D., 2016. Applications of Raman spectroscopy in detection of water quality. Appl. Spectrosc. Rev. 51, 313–337. https://doi.org/10.1080/05704928.2015.1131711

Li, C.Y., Zhang, R.Q., Fu, K.Y., Li, Chao, Li, Cheng, 2017. Effects of high temperature on starch morphology and the expression of genes related to starch biosynthesis and degradation. J. Cereal Sci. 73, 25–32. https://doi.org/https://doi.org/10.1016/j.jcs.2016.11.005

Limon, J.J., Skalski, J.H., Underhill, D.M., 2017. Commensal Fungi in Health and Disease. Cell Host Microbe 22, 156–165. https://doi.org/10.1016/j.chom.2017.07.002

Linne, D., Palaszewski, B., Gokoglu, S., Balasubramaniam, B., Hegde, U., Gallo, C., 2014. Waste Management Options for Long-Duration Space Missions: When to Reject, Reuse, or Recycle, 7th Symposium on Space Resource Utilization. https://doi.org/10.2514/6.2014-0497

Liu, J., Zhu, Y., Tao, Y., Zhang, Y., Li, A., Li, T., Sang, M., Zhang, C., 2013. Freshwater microalgae harvested via flocculation induced by pH decrease. Biotechnol. Biofuels 6, 98. https://doi.org/10.1186/1754-6834-6-98

Liu, L.G., 2022. Water on/in Mars and the Moon. Terr. Atmos. Ocean. Sci. 33, 1–6. https://doi.org/10.1007/s44195-022-00001-7

Liu, Y., Wu, X., Zhao, Y.-Y.S., Pan, L., Wang, C., Liu, J., Zhao, Z., Zhou, X., Zhang, C., Wu, Y., Wan, W., Zou, Y., 2022. Zhurong reveals recent aqueous activities in Utopia Planitia, Mars. Sci. Adv. 8, eabn8555. https://doi.org/10.1126/sciadv.abn8555

Llop, P., 2015. Genetic islands in pome fruit pathogenic and non-pathogenic Erwinia species and related plasmids. Front. Microbiol. 6, 1–8. https://doi.org/10.3389/fmicb.2015.00874

López Expósito, P., Blanco Suárez, A., Negro Álvarez, C., 2017. Laser reflectance measurement for the online monitoring of Chlorella sorokiniana biomass concentration. J. Biotechnol. 243, 10–15. https://doi.org/https://doi.org/10.1016/j.jbiotec.2016.12.020

Löwe, H., Hobmeier, K., Moos, M., Kremling, A., Pflüger-Grau, K., 2017. Photoautotrophic production of polyhydroxyalkanoates in a synthetic mixed culture of Synechococcus elongatus cscB and Pseudomonas putida cscAB. Biotechnol. Biofuels 10, 190. https://doi.org/10.1186/s13068-017-0875-0

Lukasiewicz, B., Basnett, P., Nigmatullin, R., Matharu, R., Knowles, J., Roy, I., 2018. Binary Polyhydroxyalkanoate Systems for Soft Tissue Engineering. Acta Biomater. 71. https://doi.org/10.1016/j.actbio.2018.02.027

Macrae, R.M., Wilkinson, J.F., 1958. Poly-beta-hyroxybutyrate metabolism in washed suspensions of Bacillus cereus and Bacillus megaterium. J. Gen. Microbiol. 19, 210–222. https://doi.org/10.1099/00221287-19-1-210

Madison, L.L., Huisman, G.W., 1999. Metabolic Engineering of Poly(3-Hydroxyalkanoates): From DNA to Plastic. Microbiol. Mol. Biol. Rev. 63, 21–53. https://doi.org/10.1128/mmbr.63.1.21-53.1999

Mahnert, A., Moissl-Eichinger, C., Zojer, M., Bogumil, D., Mizrahi, I., Rattei, T., Martinez, J.L., Berg, G., 2019. Man-made microbial resistances in built environments. Nat. Commun. 10, 1–12. https://doi.org/10.1038/s41467-019-08864-0

Mahnert, A., Verseux, C., Schwendner, P., Koskinen, K., Kumpitsch, C., Blohs, M., Wink, L., Brunner, D., Goessler, T., Billi, D., Moissl-Eichinger, C., 2021. Microbiome dynamics during the HI-SEAS IV mission, and implications for future crewed missions beyond Earth. Microbiome 9, 1–21. https://doi.org/10.1186/s40168-020-00959-x

Maia, J.L. da, Cardoso, J.S., Mastrantonio, D.J. da S., Bierhals, C.K., Moreira, J.B., Costa, J.A.V., Morais, M.G. de, 2020. Microalgae starch: A promising raw material for the bioethanol production. Int. J. Biol. Macromol. 165, 2739–2749. https://doi.org/10.1016/j.ijbiomac.2020.10.159

Malinova, I., Qasim, H.M., Brust, H., Fettke, J., 2018. Parameters of Starch Granule Genesis in Chloroplasts of Arabidopsis thaliana. Front. Plant Sci. 9, 761. https://doi.org/10.3389/fpls.2018.00761

Manuell, A.L., Mayfield, S.P., 2006. A bright future for Chlamydomonas. Genome Biol. https://doi.org/10.1186/gb-2006-7-9-327

Mapstone, L.J., Leite, M.N., Purton, S., Crawford, I.A., Dartnell, L., 2022. Cyanobacteria and microalgae in supporting human habitation on Mars. Biotechnol. Adv. 59, 107946. https://doi.org/https://doi.org/10.1016/j.biotechadv.2022.107946

Marcello, E., 2020. Antibiotic-free PHA-based antibacterial materials for bone regeneration. University of Westminster.

Marino, A., 2023. Astroenvironmentalism as SF. Environ. Humanit. 15, 25–43. https://doi.org/10.1215/22011919-10216140

Martins, Z., Sephton, M.A., Foing, B.H., Ehrenfreund, P., 2011. Extraction of amino acids from soils close to the Mars Desert Research Station (MDRS), Utah. Int. J. Astrobiol. 10, 231–238. https://doi.org/10.1017/S1473550410000431

Masojídek, J., Torzillo, G., 2008. Mass Cultivation of Freshwater Microalgae, in: Encyclopedia of Ecology, Five-Volume Set. Elsevier Inc., pp. 2226–2235. https://doi.org/10.1016/B978-008045405-4.00830-2

Massa, G.D., Emmerich, J.C., Morrow, R.C., Bourget, C.M., Mitchell, C. a, 2006. Plant growth lighting for space life support: a review. Gravitational Sp. Biol. 19, 19–30.

Mathiot, C., Ponge, P., Gallard, B., Sassi, J.-F., Delrue, F., Le Moigne, N., 2019. Microalgae starch-based bioplastics: Screening of ten strains and plasticization of unfractionated microalgae by extrusion. Carbohydr. Polym. 208, 142–151. https://doi.org/10.1016/j.carbpol.2018.12.057

Mattei, V., Murugesan, S., al hashmi, M., Mathew, R., James, N., Singh, P., Kumar, M., Lakshmanan, A.P., Terranegra, A., Khodor, S., Tomei, S., 2019. Evaluation of Methods for the Extraction of Microbial DNA From Vaginal Swabs Used for Microbiome Studies. Front. Cell. Infect. Microbiol. 9, 197. https://doi.org/10.3389/fcimb.2019.00197

Maul, J.E., Lilly, J.W., Cui, L., dePamphilis, C.W., Miller, W., Harris, E.H., Stern, D.B., 2002. The Chlamydomonas reinhardtii plastid chromosome: islands of genes in a sea of repeats. Plant Cell 14, 2659–2679. https://doi.org/10.1105/tpc.006155

Maule, J., Wainwright, N., Steele, A., Monaco, L., Morris, H., Gunter, D., Damon, M., Wells, M., 2009. Rapid culture-independent microbial analysis aboard the International Space Station (ISS). Astrobiology 9, 759–775. https://doi.org/10.1089/ast.2008.0319

Mayer, T., Blachowicz, A., Probst, A.J., Vaishampayan, P., Checinska, A., Swarmer, T., Leon, P. de, Venkateswaran, K., 2016. Microbial succession in an inflated lunar/Mars analog habitat during a 30-day human occupation. Microbiome 4, 1–17. https://doi.org/10.1186/s40168-016-0167-0

Mayfield, S. P., Manuell, A. L., Chen, S., Wu, J., Tran, M., Siefker, D., Muto, M., & Marin-Navarro, J. (2007). Chlamydomonas reinhardtii chloroplasts as protein factories. Current opinion in biotechnology, 18(2), 126–133. https://doi.org/10.1016/j.copbio.2007.02.001

McKay, C., 2014. Requirements and limits for life in the context of exoplanets. Proc. Natl. Acad. Sci. U. S. A. 111. https://doi.org/10.1073/pnas.1304212111

Mehrpouya, M., Vahabi, H., Barletta, M., Laheurte, P., Langlois, V., 2021. Additive manufacturing of polyhydroxyalkanoates (PHAs) biopolymers: Materials, printing techniques, and applications. Mater. Sci. Eng. C 127, 112216. https://doi.org/https://doi.org/10.1016/j.msec.2021.112216

Menčík, P., Přikryl, R., Krobot, Š., Melčová, V., Kontárová, S., Plavec, R., Bočkaj, J., Horváth, V., Alexy, P., 2022. Evaluation of the Properties of PHB Composite Filled with Kaolin Particles for 3D Printing Applications Using the Design of Experiment. Int. J. Mol. Sci. 23. https://doi.org/10.3390/ijms232214409

Menezes, A.A., Cumbers, J., Hogan, J.A., Arkin, A.P., 2015. Towards synthetic biological approaches to resource utilization on space missions. J. R. Soc. Interface 12. https://doi.org/10.1098/rsif.2014.0715

Merilä, P., Malmivaara-Lämsä, M., Spetz, P., Stark, S., Vierikko, K., Derome, J., Fritze, H., 2010. Soil organic matter quality as a link between microbial community structure and vegetation composition along a successional gradient in a boreal forest. Appl. Soil Ecol. 46, 259–267. https://doi.org/10.1016/j.apsoil.2010.08.003

Merino, N., Aronson, H.S., Bojanova, D.P., Feyhl-Buska, J., Wong, M.L., Zhang, S., Giovannelli, D., 2019. Living at the extremes: Extremophiles and the limits of life in a planetary context. Front. Microbiol. 10. https://doi.org/10.3389/fmicb.2019.00780

Metsalu, T., Vilo, J., 2015. ClustVis: a web tool for visualizing clustering of multivariate data using Principal Component Analysis and heatmap. Nucleic Acids Res. 43, W566-70. https://doi.org/10.1093/nar/gkv468

Meyen, F., Hecht, M., Hoffman, J., 2016. Thermodynamic model of Mars Oxygen ISRU Experiment (MOXIE). Acta Astronaut. 129. https://doi.org/10.1016/j.actaastro.2016.06.005

Meyer, F.M., Jules, M., Mehne, F.M.P., Le Coq, D., Landmann, J.J., Görke, B., Aymerich, S., Stülke, J., 2011. Malate-mediated carbon catabolite repression in Bacillus subtilis involves the HPrK/CcpA pathway. J. Bacteriol. 193, 6939–6949. https://doi.org/10.1128/JB.06197-11

Mezzomo, N., Ferreira, S.R.S., 2016. Carotenoids functionality, sources, and processing by supercritical technology: A review. J. Chem. 2016. https://doi.org/10.1155/2016/3164312

Mikos, A.G., Thorsen, A.J., Czerwonka, L.A., Bao, Y., Langer, R., Winslow, D.N., Vacanti, J.P., 1994. Preparation and characterization of poly(l-lactic acid) foams. Polymer (Guildf). 35, 1068–1077. https://doi.org/https://doi.org/10.1016/0032-3861(94)90953-9

Mikos, A. G., Sarakinos, G., Leite, S. M., Vacanti, J. P. and Langer, R. 1993. Laminated three-dimensional biodegradable foams for use in tissue engineering. Biomaterials 14:323-330.

Mills, W., 2003. Growth and Metabolism of the Green Alga, Chlorella Pyrenoidosa, in Simulated Microgravity. National Aeronautics and Space Administration (NASA). Retrieved n.d. from https://ntrs.nasa.gov/citations/20030064067

Mishra, A., Singh, L., Singh, D., 2022. Unboxing the black box—one step forward to understand the soil microbiome: A systematic review. Microb. Ecol. https://doi.org/10.1007/s00248-022-01962-5

Mitchell, C.A., 1994. Bioregenerative life-support systems. Am. J. Clin. Nutr. 60. https://doi.org/10.1093/ajcn/60.5.820S

Mohan, A., Antony, A R.., Greeshma, K., Yun, J.-H., Ramanan, R., Kim, H.-S., 2022. Algal biopolymers as sustainable resources for a net-zero carbon bioeconomy. Bioresour. Technol. 344, 126397. https://doi.org/https://doi.org/10.1016/j.biortech.2021.126397

Mohapatra, S., Sarkar, B., Samantaray, D.P., Daware, A., Maity, S., Pattnaik, S., Bhattacharjee, S., 2017. Bioconversion of fish solid waste into PHB using Bacillus

Moissl-Eichinger, C., 2011. Archaea in artificial environments: their presence in global spacecraft clean rooms and impact on planetary protection. ISME J. 5, 209–219. https://doi.org/10.1038/ismej.2010.124

Moissl, C., Bruckner, J.C., Venkateswaran, K., 2008. Archaeal diversity analysis of spacecraft assembly clean rooms. ISME J. 2, 115–119. https://doi.org/10.1038/ismej.2007.98

Monshupanee, T., Chairattanawat, C., Incharoensakdi, A., 2019. Disruption of cyanobacterial γ-aminobutyric acid shunt pathway reduces metabolites levels in tricarboxylic acid cycle, but enhances pyruvate and poly(3-hydroxybutyrate) accumulation. Sci. Rep. 9. https://doi.org/10.1038/s41598-019-44729-8

Mora, M., Mahnert, A., Koskinen, K., Pausan, M.R., Oberauner-Wappis, L., Krause, R., Perras, A.K., Gorkiewicz, G., Berg, G., Moissl-Eichinger, C., 2016. Microorganisms in confined habitats: Microbial monitoring and control of intensive care units, operating rooms, cleanrooms and the international space station. Front. Microbiol. 7, 1–20. https://doi.org/10.3389/fmicb.2016.01573

Morse, A., Jackson, A., Rainwater, K., & Pickering, K., 2002. Membrane Bioreactor for the Treatment of Simulated Wastewater. Proceedings of the Water Environment Federation, 2002(10), 474–484. https://doi.org/10.2175/193864702784164541

Mothes, G., Rivera, I.S., Babel, W., 1996. Competition between β-ketothiolase and citrate synthase during poly(β-hydroxybutyrate) synthesis inMethylobacterium rhodesianum. Arch. Microbiol. 166, 405–410. https://doi.org/10.1007/BF01682987

Mozejko-Ciesielska, J., Dabrowska, D., Szalewska-Palasz, A., Ciesielski, S., 2017. Medium-chain-length polyhydroxyalkanoates synthesis by Pseudomonas putida KT2440 relA/spoT mutant: bioprocess characterization and transcriptome analysis. AMB Express 7, 92. https://doi.org/10.1186/s13568-017-0396-z

Musa, H., Bolanle, B.B., Kasim, F.H., Arbain, D., 2016. Screening and production of Polyhydroxybutyrate (PHB) by bacterial strains isolated from rhizosphere soil of groundnut plants. Sains Malaysiana 45, 1469–1476.

Nangle, S.N., Wolfson, M.Y., Hartsough, L., Ma, N.J., Mason, C.E., Merighi, M., Nathan, V., Silver, P.A., Simon, M., Swett, J., Thompson, D.B., Ziesack, M., 2020. The case for biotech on Mars. Nat. Biotechnol. 38, 401–407. https://doi.org/10.1038/s41587-020-0485-4

Narala, R.R., Garg, S., Sharma, K.K., Thomas-Hall, S.R., Deme, M., Li, Y., Schenk, P.M., 2016. Comparison of microalgae cultivation in photobioreactor, open raceway pond, and a two-stage hybrid system. Front. Energy Res. 4, 1–10. https://doi.org/10.3389/fenrg.2016.00029

Navarro, A.K., Farrera, R.R., López, R., Pérez-Guevara, F., 2006. Relationship between poly-beta-hydroxybutyrate production and delta-endotoxin for Bacillus thuringiensis var. kurstaki. Biotechnol. Lett. 28, 641–644. https://doi.org/10.1007/s10529-006-0029-0

Nelson, M., Pechurkin, N.S., Allen, J.P., Somova, L.A., Gitelson, J.I., 2010. Closed Ecological Systems, Space Life Support and Biospherics. Environ. Biotechnol. 517–565. https://doi.org/10.1007/978-1-60327-140-0_11

Neoh, S., Fey Chek, M., Tiang Tan, H., Linares-Pastén, J.A., Nandakumar, A., Hakoshima, T., Sudesh, K., 2022. Polyhydroxyalkanoate synthase (PhaC): The key enzyme for biopolyester synthesis. Curr. Res. Biotechnol. 4, 87–101. https://doi.org/https://doi.org/10.1016/j.crbiot.2022.01.002

Nguyen, M.A., Hoang, A.L., 2016. A review on microalgae and cyanobacteria in biofuel production. Economics and Finance. 2016. ⟨hal-01383026⟩

Niederwieser, T., Kociolek, P., Klaus, D., 2018. A review of algal research in space. Acta Astronaut. 146, 359–367. https://doi.org/10.1016/j.actaastro.2018.03.026

Nilsson, R.H., Larsson, K.H., Taylor, A.F.S., Bengtsson-Palme, J., Jeppesen, T.S., Schigel, D., Kennedy, P., Picard, K., Glöckner, F.O., Tedersoo, L., Saar, I., Kõljalg, U., Abarenkov, K., 2019. The UNITE database for molecular identification of fungi: Handling dark taxa and parallel taxonomic classifications. Nucleic Acids Res. 47, D259–D264. https://doi.org/10.1093/nar/gky1022

Nishioka, M., Nakai, K., Miyake, M., Asada, Y., Taya, M., 2001. Production of poly-β-hydroxybutyrate by thermophilic cyanobacterium, Synechococcus sp. MA19, under phosphate-limited conditions. Biotechnol. Lett. 23, 1095–1099. https://doi.org/10.1023/A:1010551614648

Nishanth, S., Bharti, A., Gupta, H., Gupta, K., Gulia, U., Prasanna, R., 2021. Chapter 14 - Cyanobacterial extracellular polymeric substances (EPS): Biosynthesis and their potential applications, in: Das, S., Dash, H.R.B.T.-M. and N.M. (Eds.), . Academic Press, pp. 349–369. https://doi.org/https://doi.org/10.1016/B978-0-12-820084-1.00015-6

Novikova, N., De Boever, P., Poddubko, S., Deshevaya, E., Polikarpov, N., Rakova, N., Coninx, I., Mergeay, M., 2006. Survey of environmental biocontamination on board the International Space Station. Res. Microbiol. 157, 5–12. https://doi.org/10.1016/j.resmic.2005.07.010

Nowicka-Krawczyk, P., Mühlsteinová, R., Hauer, T., 2019. Detailed characterization of the Arthrospira type species separating commercially grown taxa into the new genus Limnospira (Cyanobacteria). Sci. Rep. 9, 1–12. https://doi.org/10.1038/s41598-018-36831-0

Nozzi, N.E., Oliver, J.W.K., Atsumi, S., 2013. Cyanobacteria as a Platform for Biofuel Production. Front. Bioeng. Biotechnol. 1, 1–6. https://doi.org/10.3389/fbioe.2013.00007

Oba, Y., Takano, Y., Furukawa, Y., Koga, T., Glavin, D.P., Dworkin, J.P., Naraoka, H., 2022. Identifying the wide diversity of extraterrestrial purine and pyrimidine nucleobases in carbonaceous meteorites. Nat. Commun. 13, 2008. https://doi.org/10.1038/s41467-022-29612-x

Oeding, V., Schlegel, H.G., 1973. Beta-ketothiolase from Hydrogenomonas eutropha H16 and its significance in the regulation of poly-beta-hydroxybutyrate metabolism. Biochem. J. 134, 239–248. https://doi.org/10.1042/bj1340239

National Academies of Science, Engineering, Medicine, 2017. Microbiomes of the Built Environment: A Research Agenda for Indoor Microbiology, Human Health, and Buildings. The National Academies Press, Washington, DC. https://doi.org/10.17226/23647

Ozyigit, I.I., Yucebilgili Kurtoglu, K., 2020. Particle bombardment technology and its applications in plants. Mol. Biol. Rep. 47, 9831–9847. https://doi.org/10.1007/s11033-020-06001-5

Pagliano, G., Galletti, P., Samorì, C., Zaghini, A., Torri, C., 2021. Recovery of Polyhydroxyalkanoates From Single and Mixed Microbial Cultures: A Review. Front. Bioeng. Biotechnol. 9, 1–28. https://doi.org/10.3389/fbioe.2021.624021

Pagliano, G., Gugliucci, W., Torrieri, E., Piccolo, A., Cangemi, S., Di Giuseppe, F.A., Robertiello, A., Faraco, V., Pepe, O., Ventorino, V., 2020. Polyhydroxyalkanoates (PHAs) from dairy wastewater effluent: bacterial accumulation, structural characterization and physical properties. Chem. Biol. Technol. Agric. 7, 29. https://doi.org/10.1186/s40538-020-00197-1

Pedregosa, F., Varoquaux, G., Gramfort, A., Michel, V., Thirion, B., Grisel, O., Blondel, M., Prettenhofer, P., Weiss, R., Dubourg, V., Vanderplas, J., Passos, A., Cournapeau, D., Brucher, M., Perrot, M., Duchesnay, É., 2011. Scikit-Learn: Machine Learning in Python. J. Mach. Learn. Res. 12, 2825–2830

Pereira, T., Oliveira, M., Maia, I., Silva, J., Costa, M., Thiré, R., 2012. 3D Printing of Poly(3-hydroxybutyrate) Porous Structures Using Selective Laser Sintering. Macromol. Symp. 319. https://doi.org/10.1002/masy.201100237

Pfister, B., Lu, K.-J., Eicke, S., Feil, R., Lunn, J.E., Streb, S., Zeeman, S.C., 2014. Genetic Evidence That Chain Length and Branch Point Distributions Are Linked Determinants of Starch Granule Formation in Arabidopsis . Plant Physiol. 165, 1457–1474. https://doi.org/10.1104/pp.114.241455

Plancke, C., Colleoni, C., Deschamps, P., Dauvillée, D., Nakamura, Y., Haebel, S., Ritte, G., Steup, M., Buléon, A., Putaux, J.-L., Dupeyre, D., d'Hulst, C., Ral, J.-P., Löffelhardt, W., Ball, S.G., 2008. Pathway of cytosolic starch synthesis in the model glaucophyte Cyanophora paradoxa. Eukaryot. Cell 7, 247–257. https://doi.org/10.1128/EC.00373-07

Plavec, R., Hlaváčiková, S., Omaníková, L., Feranc, J., Vanovčanová, Z., Tomanová, K., Bočkaj, J., Kruželák, J., Medlenová, E., Gálisová, I., Danišová, L., Přikryl, R., Figalla, S., Melčová, V., Alexy, P., 2020. Recycling possibilities of bioplastics based on PLA/PHB blends. Polymer Testing 92, 106880. https://doi.org/https://doi.org/10.1016/j.polymertesting.2020.106880

Plavec, R., Horvath, V., Hlaváčiková, S., Omaníková, L., Repiská, M., Medlenová, E., Feranc, J., Kruželák, J., Přikryl, R., Figalla, S., Kontárová, S., Baco, A., Danisova, L., Vanovčanová, Z., Alexy, P., 2022. Influence of Multiple Thermomechanical Processing of 3D Filaments Based on Polylactic Acid and Polyhydroxybutyrate on Their Rheological and Utility Properties. Polymers (Basel). 14, 1947. https://doi.org/10.3390/polym14101947

Prasad, A., Fotou, G., li, S., 2013. The Effect of Polymer Hardness, Pore Size and Porosity on the Performance of Thermoplastic Polyurethane-Based Chemical Mechanical Polishing Pads. J. Mater. Res. 28, 2380–2393. https://doi.org/10.1557/jmr.2013.173

Prater T, Bean QA, Werkheiser N, et al. "A Ground-Based Study on Extruder Standoff Distance for the 3D Printing in Zero Gravity Technology Demonstration Mission." NASA Technical Publication —2017–219631. NASA Marshall Space Flight Center, Huntsville, AL, 94 pp., 6 2017.

Prater, T., Werkheiser, N., Ledbetter, F., Timucin, D., Wheeler, K., Snyder, M., 2019. 3D Printing in Zero G Technology Demonstration Mission: complete experimental results and summary of related material modeling efforts. Int. J. Adv. Manuf. Technol. 101, 391–417. https://doi.org/10.1007/s00170-018-2827-7

Preston, L.J., Dartnell, L.R., 2014. Planetary habitability: Lessons learned from terrestrial analogues. Int. J. Astrobiol. 13, 81–98. https://doi.org/10.1017/S1473550413000396

Puleo, J.R., Fields, N.D., Bergstrom, S.L., Oxborrow, G.S., Stabekis, P.D., Koukol, R., 1977. Microbiological profiles of the Viking spacecraft. Appl. Environ. Microbiol. 33, 379–384. https://doi.org/10.1128/aem.33.2.379-384.1977

Purkan, P., Baktir, A., Puspaningsih, N.N.T., Ni'Mah, M., 2017. Direct conversion of starch to ethanol using recomblnant Saccharomyces cerevisiae containing glucoamylase gene. AIP Conf. Proc. 1888. https://doi.org/10.1063/1.5004318

Quast, C., Pruesse, E., Yilmaz, P., Gerken, J., Schweer, T., Yarza, P., Peplies, J., Glöckner, F.O., 2013. The SILVA ribosomal RNA gene database project: Improved data processing and web-based tools. Nucleic Acids Res. 41, 590–596. https://doi.org/10.1093/nar/gks1219

Race, M., Denning, K., Bertka, C.M., Dick, S.J., Harrison, A.A., Impey, C., Mancinelli, R., 2012. Astrobiology and society: building an interdisciplinary research community. Astrobiology 12, 958–965. https://doi.org/10.1089/ast.2011.0723

Radakovits, R., Jinkerson, R.E., Darzins, A., Posewitz, M.C., 2010. Genetic engineering of algae for enhanced biofuel production. Eukaryot. Cell 9, 486–501. https://doi.org/10.1128/EC.00364-09

Rahman, A., Linton, E., Hatch, A.D., Sims, R.C., Miller, C.D., 2013. Secretion of polyhydroxybutyrate in Escherichia coli using a synthetic biological engineering approach. J. Biol. Eng. 7, 24. https://doi.org/10.1186/1754-1611-7-24

Rai, R., Keshavarz, T., Roether, J.A., Boccaccini, A.R., Roy, I., 2011. Medium chain length polyhydroxyalkanoates, promising new biomedical materials for the future. Mater. Sci. Eng. R Reports 72, 29–47. https://doi.org/https://doi.org/10.1016/j.mser.2010.11.002

Rapp, D., 2008. Human missions to Mars. Springer, Berlin.

Raza, Z.A., Tariq, M.R., Majeed, M.I., Banat, I.M., 2019. Recent developments in bioreactor scale production of bacterial polyhydroxyalkanoates. Bioprocess Biosyst. Eng. 42, 901–919. https://doi.org/10.1007/s00449-019-02093-x

Rios, P., Dodiuk, H., Kenig, S., Mccarthy, S., Dotan, A., 2012. The effect of polymer surface on the wetting and adhesion of liquid systems. J. Adhes. Sci. Technol. 21, 227–241. https://doi.org/10.1163/156856107780684567

Rodolfi, L., Zittelli, G.C., Barsanti, L., Rosati, G., Tredici, M.R., 2003. Growth medium recycling in Nannochloropsis sp. mass cultivation. Biomol. Eng. 20, 243–248. https://doi.org/https://doi.org/10.1016/S1389-0344(03)00063-7

Rohman, A., Man, Y.B.C., 2010. Fourier transform infrared (FTIR) spectroscopy for analysis of

extra virgin olive oil adulterated with palm oil. Food Res. Int. 43, 886–892. https://doi.org/https://doi.org/10.1016/j.foodres.2009.12.006

Roiko, M., May, M., Relich, R.F., 2017. Characterization of Pontibacter altruii, sp. nov., isolated from a human blood culture. New Microbes New Infect. 19, 71–77. https://doi.org/10.1016/j.nmni.2017.05.016

Roldán, D.M., Kyrpides, N., Woyke, T., Shapiro, N., Whitman, W.B., Králová, S., Sedláček, I., Busse, H.-J., Menes, R.J., 2020. Hymenobacter artigasi sp. nov., isolated from air sampling in maritime Antarctica. Int. J. Syst. Evol. Microbiol. 70, 4935–4941. https://doi.org/10.1099/ijsem.0.004362

Rummel, J.D., 2001. Planetary exploration in the time of astrobiology: Protecting against biological contamination. Proc. Natl. Acad. Sci. U. S. A. 98, 2128–2131. https://doi.org/10.1073/pnas.061021398

Rummel, J.D., Beaty, D.W., Jones, M.A., Bakermans, C., Barlow, N.G., Boston, P.J., Chevrier, V.F., Clark, B.C., De Vera, J.P.P., Gough, R. V., Hallsworth, J.E., Head, J.W., Hipkin, V.J., Kieft, T.L., Mcewen, A.S., Mellon, M.T., Mikucki, J.A., Nicholson, W.L., Omelon, C.R., Peterson, R., Roden, E.E., Sherwood Lollar, B., Tanaka, K.L., Viola, D., Wray, J.J., 2014. A new analysis of mars “Special Regions”: Findings of the second MEPAG special regions science analysis group (SR-SAG2). Astrobiology 14, 887–968. https://doi.org/10.1089/ast.2014.1227

Rydz, J., Ausejo, J.G., Musioł, M., Sikorska, W., Włodarczyk, J., Janeczek, H., 2018. Forensic Engineering of Advanced Polymeric Materials . Part VI – Degradation of Polyester-based Materials Obtained by Different Processing Methods – Comparative Studies. Mathews J. Forensic Res. 1, 1–8.

Saei, A.A., Omidi, A.A., Barzegari, A., 2013. Screening and genetic manipulation of green organisms for establishment of biological life support systems in space. Bioengineered 4, 65–71. https://doi.org/10.4161/bioe.22286

Sah, R.N., Brown, P.H., 1997. Techniques for boron determination and their application to the analysis of plant and soil samples. Plant Soil 193, 15–33. https://doi.org/10.1007/978-94-011-5580-9_2

Salisbury, F.B., Gitelson, J.I., Lisovsky, G.M., 1997. Bios-3: Siberian experiments in bioregenerative life support. Bioscience 47, 575–585. https://doi.org/10.2307/1313164

Salomé, P.A., Merchant, S.S., 2019. A Series of Fortunate Events: Introducing Chlamydomonas as a Reference Organism. Plant Cell 31, 1682–1707. https://doi.org/10.1105/tpc.18.00952

Salter, S.J., Cox, M.J., Turek, E.M., Calus, S.T., Cookson, W.O., Moffatt, M.F., Turner, P., Parkhill, J., Loman, N.J., Walker, A.W., 2014. Reagent and laboratory contamination can critically impact sequence-based microbiome analyses. BMC Biol. 12, 1–12. https://doi.org/10.1186/s12915-014-0087-z

Samson, R., LeDuyt, A., 1986. Detailed study of anaerobic digestion of Spirulina maxima algal biomass. Biotechnol. Bioeng. 28, 1014–1023. https://doi.org/10.1002/bit.260280712

Sankhla, I.S., Bhati, R., Singh, A.K., Mallick, N., 2010. Poly(3-hydroxybutyrate-co-3-hydroxyvalerate) co-polymer production from a local isolate, Brevibacillus invocatus MTCC 9039. Bioresour. Technol. 101, 1947–1953. https://doi.org/https://doi.org/10.1016/j.biortech.2009.10.006

Santomartino, R., Averesch, N.J.H., Bhuiyan, M., Cockell, C.S., Colangelo, J., Gumulya, Y., Lehner, B., Lopez-Ayala, I., McMahon, S., Mohanty, A., Santa Maria, S.R., Urbaniak, C., Volger, R., Yang, J., Zea, L., 2023. Toward sustainable space exploration: a roadmap for harnessing the power of microorganisms. Nat. Commun. 14, 1–11. https://doi.org/10.1038/s41467-023-37070-2

Santomartino, R., Waajen, A.C., de Wit, W., Nicholson, N., Parmitano, L., Loudon, C.M., Moeller, R., Rettberg, P., Fuchs, F.M., Van Houdt, R., Finster, K., Coninx, I., Krause, J., Koehler, A., Caplin, N., Zuijderduijn, L., Zolesi, V., Balsamo, M., Mariani, A., Pellari, S.S., Carubia, F., Luciani, G., Leys, N., Doswald-Winkler, J., Herová, M., Wadsworth, J., Everroad, R.C., Rattenbacher, B., Demets, R., Cockell, C.S., 2020. No Effect of Microgravity and Simulated Mars Gravity on Final Bacterial Cell Concentrations on the International Space Station: Applications to Space Bioproductionfile:///Users/maraleite/Downloads/0016-09.pdf. Front. Microbiol. 11, 1–15. https://doi.org/10.3389/fmicb.2020.579156

Sasso, S., Stibor, H., Mittag, M., Grossman, A.R., 2018. From molecular manipulation of domesticated Chlamydomonas reinhardtii to survival in nature. Elife 7. https://doi.org/10.7554/eLife.39233

Sarsekeyeva, F., Zayadan, B.K., Usserbaeva, A., Bedbenov, V.S., Sinetova, M.A., Los, D.A., 2015. Cyanofuels: biofuels from cyanobacteria. Reality and perspectives. Photosynth. Res. 125, 329–340. https://doi.org/10.1007/s11120-015-0103-3

Sathish, A., Glaittli, K., Sims, R., Miller, C., 2014. Algae Biomass Based Media for Poly(3-hydroxybutyrate) (PHB) Production by Escherichia coli. J. Polym. Environ. 22. https://doi.org/10.1007/s10924-014-0647-x

Scaife, M.A., Nguyen, G.T.D.T., Rico, J., Lambert, D., Helliwell, K.E., Smith, A.G., 2015. Establishing Chlamydomonas reinhardtii as an industrial biotechnology host. Plant J. 82, 532–546. https://doi.org/10.1111/tpj.12781

Schirrmeister, B.E., Gugger, M., Donoghue, P.C.J., 2015. Cyanobacteria and the Great Oxidation Event: Evidence from genes and fossils. Palaeontology 58, 769–785. https://doi.org/10.1111/pala.12178

Scholz, M., Hoshino, T., Johnson, D., Riley, M.R., Cuello, J., 2011. Flocculation of wall-deficient cells of Chlamydomonas reinhardtii mutant cw15 by calcium and methanol. Biomass and Bioenergy 35, 4835–4840. https://doi.org/https://doi.org/10.1016/j.biombioe.2011.08.020

Schönert, S., Seitz, S., Krafft, H., Feuerbaum, E.A., Andernach, I., Witz, G., Dahl, M.K., 2006. Maltose and maltodextrin utilization by Bacillus subtilis. J. Bacteriol. 188, 3911–3922. https://doi.org/10.1128/JB.00213-06

Schuerger, A.C., Lee, P., 2015. Microbial ecology of a crewed rover traverse in the arctic: Low microbial dispersal and implications for planetary protection on human mars missions. Astrobiology 15, 478–491. https://doi.org/10.1089/ast.2015.1289

Schwendner, P., Mahnert, A., Koskinen, K., Moissl-Eichinger, C., Barczyk, S., Wirth, R., Berg, G., Rettberg, P., 2017. Preparing for the crewed Mars journey: microbiota dynamics in the confined Mars500 habitat during simulated Mars flight and landing. Microbiome 5, 129. https://doi.org/10.1186/s40168-017-0345-8

Scranton, M.A., Ostrand, J.T., Fields, F.J., Mayfield, S.P., 2015. Chlamydomonas as a model for biofuels and bio-products production. Plant J. 82, 523–531. https://doi.org/10.1111/tpj.12780

Sender, R., Fuchs, S., Milo, R., 2016. Revised Estimates for the Number of Human and Bacteria Cells in the Body. PLoS Biol. 14, e1002533. https://doi.org/10.1371/journal.pbio.1002533

Sephton, M.A., Botta, O., 2005. Recognizing life in the Solar System: guidance from meteoritic organic matter. Int. J. Astrobiol. 4, 269–276. https://doi.org/10.1017/S1473550405002806

Severinghaus, J.P., Broecker, W.S. pd., Dempster, W.F., MacCallum, T., Wahlen, M., 1994. Oxygen loss in biosphere 2. Eos, Trans. Am. Geophys. Union 75, 33–37. https://doi.org/https://doi.org/10.1029/94EO00285

Shigesada, N., Okubo, A., 1981. Analysis of the self-shading effect on algal vertical distribution in natural waters. J. Math. Biol. 12, 311–326. https://doi.org/10.1007/BF00276919

Shlosberg, Y., Schuster, G., Adir, N., 2022. Harnessing photosynthesis to produce electricity using cyanobacteria, green algae, seaweeds and plants. Front. Plant Sci. 13, 1–15. https://doi.org/10.3389/fpls.2022.955843

Showstack, R., 2023. Planetary Protection: Enabling Space Exploration While Safeguarding Against Biological Contamination. Bioscience 73, 161–167. https://doi.org/10.1093/biosci/biad006

Sibille, L., Dominguez, J., 2012. Joule-heated Molten Regolith Electrolysis Reactor Concepts for Oxygen and Metals Production on the Moon and Mars, in: 50th AIAA Aerospace Sciences Meeting Including the New Horizons Forum and Aerospace Exposition.

Sielaff, A.C., Urbaniak, C., Babu, G., Mohan, M., Stepanov, V.G., Tran, Q., Wood, J.M., Minich, J., Mcdonald, D., Mayer, T., Knight, R., Karouia, F., Fox, G.E., Venkateswaran, K., 2019. Characterization of the total and viable bacterial and fungal communities associated with the International Space Station surfaces. Microbiome 7, 50.

Siddiki, S.Y., Rahman, M.M., Kumar, P., Ahmed, S., Inayat, A., Kusumo, F., Badruddin, I., T.M., Y.K., Nghiem, L., Ong, H.C., Mahlia, T.M.I., 2022. Microalgae biomass as a sustainable source for biofuel, biochemical and biobased value-added products: An integrated biorefinery concept. Fuel 307, 121782. https://doi.org/10.1016/j.fuel.2021.121782

Singh, M., Patel, S.K., Kalia, V.C., 2009. Bacillus subtilis as potential producer for polyhydroxyalkanoates. Microb. Cell Fact. 8, 38. https://doi.org/10.1186/1475-2859-8-38

Singh, A., Olsen, S.I., 2011. A critical review of biochemical conversion, sustainability and life cycle assessment of algal biofuels. Appl. Energy 88, 3548–3555. https://doi.org/10.1016/j.apenergy.2010.12.012

Singh, A.K., Mallick, N., 2017. Advances in cyanobacterial polyhydroxyalkanoates production. FEMS Microbiol. Lett. 364. https://doi.org/10.1093/femsle/fnx189

Singh, J.S., Kumar, A., Rai, A.N., Singh, D.P., 2016. Cyanobacteria: A Precious Bio-resource in Agriculture, Ecosystem, and Environmental Sustainability. Front. Microbiol. 7, 529. https://doi.org/10.3389/fmicb.2016.00529

Singh, J.S., Kumar, A., Singh, M., 2019. Cyanobacteria: A sustainable and commercial bio-resource in production of bio-fertilizer and bio-fuel from waste waters. Environ. Sustain. Indic. 3–4, 100008. https://doi.org/10.1016/j.indic.2019.100008

Singh, U.B., Ahluwalia, A.S., 2013. Microalgae: A promising tool for carbon sequestration. Mitig. Adapt. Strateg. Glob. Chang. 18, 73–95. https://doi.org/10.1007/s11027-012-9393-3

Sjöling, S., Cowan, D.A., 2000. Detecting human bacterial contamination in Antarctic soils. Polar Biol. 23, 644–650. https://doi.org/10.1007/s003000000137

Snyder, M., Dunn, J., Gonzalez, E., 2013. The Effects of Microgravity on Extrusion Based Additive Manufacturing. https://doi.org/10.2514/6.2013-5439

Socci, M.C., Rodríguez, G., Oliva, E., Fushimi, S., Takabatake, K., Nagatsuka, H., Felice, C.J., Rodríguez, A.P., 2023. Polymeric Materials, Advances and Applications in Tissue Engineering: A Review. Bioeng. (Basel, Switzerland) 10. https://doi.org/10.3390/bioengineering10020218

Soutar, C.D., Stavrinides, J., 2019. Molecular validation of clinical Pantoea isolates identified by MALDI-TOF. PLoS One 14, 1–16. https://doi.org/10.1371/journal.pone.0224731

Spiegelman, D., Whissell, G., Greer, C.W., 2005. A survey of the methods for the characterization of microbial consortia and communities. Can. J. Microbiol. 51, 355–386. https://doi.org/10.1139/w05-003

Stahl-rommel, S., Jain, M., Nguyen, H.N., Arnold, R.R., Aunon-chancellor, S.M., Sharp, G.M., Castro, C.L., John, K.K., Juul, S., Turner, D.J., Stoddart, D., Paten, B., Akeson, M., Burton, A.S., Castro-wallace, S.L., 2021. the International Space Station Using Nanopore Sequencing. Genes (Basel)

Stahl-Rommel, S., Jain, M., Nguyen, H.N., Arnold, R.R., Aunon-Chancellor, S.M., Sharp, G.M., Castro, C.L., John, K.K., Juul, S., Turner, D.J., Stoddart, D., Paten, B., Akeson, M., Burton, A.S., Castro-Wallace, S.L., 2021. Real-Time Culture-Independent Microbial Profiling Onboard the International Space Station Using Nanopore Sequencing. Genes (Basel). 12. https://doi.org/10.3390/genes12010106

Stark, J.M., Firestone, M.K., 1995. Mechanisms for soil moisture effects on activity of nitrifying bacteria. Appl. Environ. Microbiol. 61, 218–221. https://doi.org/10.1128/aem.61.1.218-221.1995

Stinson, L., Keelan, J., Payne, M., 2019. Profiling bacterial communities in low biomass samples: Pitfalls and considerations. Microbiol. Aust. 40. https://doi.org/10.1071/MA19053

Stoker, C.R., Clarke, J., Direito, S.O. ~L., Blake, D., Martin, K.R., Zavaleta, J., Foing, B., 2011. Mineralogical, chemical, organic and microbial properties of subsurface soil cores from Mars Desert Research Station (Utah, USA): Phyllosilicate and sulfate analogues to Mars mission landing sites. Int. J. Astrobiol. 10, 269–289. https://doi.org/10.1017/S1473550411000115

Sun, J., Xing, M., Wang, W., Dai, F., Liu, J., Hao, J., 2018. Hymenobacter profundi sp. nov., isolated from deep-sea water. Int. J. Syst. Evol. Microbiol. 68, 947–950. https://doi.org/10.1099/IJSEM.0.002621

Sun, L., Guo, J., Chen, H., Zhang, D., Shang, L., Zhang, B., Zhao, Y., 2021. Tailoring Materials with Specific Wettability in Biomedical Engineering. Adv. Sci. 8, 1–34. https://doi.org/10.1002/advs.202100126

Sultanpuram, V., Mothe, T., Mahmood, S., 2008. Production of PHB and P (3HB-co-3HV) biopolymers by Bacillus megaterium strain OU303A isolated from municipal sewage sludge. World J. Microbiol. Biotechnol. 25. https://doi.org/10.1007/s11274-008-9903-3

Sychev, V., Levinskikh, M., Gostimsky, S., Bingham, G., Podolskiy, I., 2007. Spaceflight effects on consecutive generations of peas grown onboard the Russian segment of the International Space Station. Acta Astronaut. 60, 426–432. https://doi.org/10.1016/j.actaastro.2006.09.009

Talan, A., Kaur, R., Tyagi, R.D., Drogui, P., 2020. Bioconversion of oily waste to polyhydroxyalkanoates: Sustainable technology with circular bioeconomy approach and multidimensional impacts. Bioresour. Technol. Reports 11, 100496. https://doi.org/https://doi.org/10.1016/j.biteb.2020.100496

Tan, F., Nadir, N., Sudesh, K., 2022. Microalgal Biomass as Feedstock for Bacterial Production of PHA: Advances and Future Prospects. Front. Bioeng. Biotechnol. 10, 879476. https://doi.org/10.3389/fbioe.2022.879476

Tan, G.Y.A., Chen, C.L., Li, L., Ge, L., Wang, L., Razaad, I.M.N., Li, Y., Zhao, L., Mo, Y., Wang, J.Y., 2014. Start a research on biopolymer polyhydroxyalkanoate (PHA): A review. Polymers (Basel). 6, 706–754. https://doi.org/10.3390/polym6030706

Tang, Y., Rosenberg, J.N., Bohutskyi, P., Yu, G., Betenbaugh, M.J., Wang, F., 2016. Microalgae as a Feedstock for Biofuel Precursors and Value-Added Products: Green Fuels and Golden Opportunities. BioResources 11, 2850-2885. https://doi.org/10.15376/BIORES.11.1.2850-2885

Taunt, H.N., Stoffels, L., Purton, S., 2018. Green biologics: The algal chloroplast as a platform for making biopharmaceuticals. Bioengineered 9, 48–54. https://doi.org/10.1080/21655979.2017.1377867

Taylor, G.M., Mordaka, P.M., Heap, J.T., 2018. Start-Stop Assembly: a functionally scarless DNA assembly system optimized for metabolic engineering. Nucleic Acids Res. 47, e17–e17. https://doi.org/10.1093/nar/gky1182

Tessmar, J.K., Göpferich, A.M., 2007. Matrices and scaffolds for protein delivery in tissue engineering. Adv. Drug Deliv. Rev. 59, 274–291. https://doi.org/https://doi.org/10.1016/j.addr.2007.03.020

Thiruvenkatam, R., Scholz, C., 2000. Synthesis of Poly(β-hydroxybutyrate) in Simulated Microgravity: An Investigation of Aeration Profiles in Shake Flask and Bioreactor. J. Polym. Environ. 8, 155–159. https://doi.org/10.1023/A:1015246125427

Thomma, B.P.H.J., 2003. Alternaria spp.: From general saprophyte to specific parasite. Mol. Plant Pathol. 4, 225–236. https://doi.org/10.1046/j.1364-3703.2003.00173.x

Thompson, K., Summers, R., Cook, S., 2017. Development and Experimental Validation of the Composition and Treatability of a New Synthetic Bathroom Greywater (SynGrey). Environ. Sci. Water Res. Technol. 3. https://doi.org/10.1039/C7EW00304H

Titus, T., Kieffer, H., Christensen, P., 2003. Exposed Water Ice Discovered near the South Pole of Mars. Science 299, 1048–1051. https://doi.org/10.1126/science.1080497

Tofail, S.A.M., Koumoulos, E.P., Bandyopadhyay, A., Bose, S., O'Donoghue, L., Charitidis, C., 2018. Additive manufacturing: scientific and technological challenges, market uptake and opportunities. Mater. Today 21, 22–37. https://doi.org/https://doi.org/10.1016/j.mattod.2017.07.001

Trakunjae, C., Boondaeng, A., Apiwatanapiwat, W., Kosugi, A., Arai, T., Sudesh, K., Vaithanomsat, P., 2021. Enhanced polyhydroxybutyrate (PHB) production by newly isolated rare actinomycetes Rhodococcus sp. strain BSRT1-1 using response surface methodology. Sci. Rep. 11. https://doi.org/10.1038/s41598-021-81386-2

Tran, N.T., Kaldenhoff, R., 2020. Metabolic engineering of ketocarotenoids biosynthetic pathway in Chlamydomonas reinhardtii strain CC-4102. Sci. Rep. 10, 10688. https://doi.org/10.1038/s41598-020-67756-2

Tran, R.T., Naseri, E., Kolasnikov, A., Bai, X., Yang, J., 2011. A new generation of sodium chloride porogen for tissue engineering. Biotechnol. Appl. Biochem. 58, 335–344. https://doi.org/10.1002/bab.44

Troschl, C., Meixner, K., Drosg, B., 2017. Cyanobacterial PHA Production—Review of Recent Advances and a Summary of Three Years' Working Experience Running a Pilot Plant. Bioengineering 4, 26. https://doi.org/10.3390/bioengineering4020026

Tschörtner, J., Lai, B., Krömer, J.O., 2019. Biophotovoltaics: Green power generation from sunlight and water. Front. Microbiol. 10. https://doi.org/10.3389/fmicb.2019.00866

Turco, R., Santagata, G., Corrado, I., Pezzella, C., Di Serio, M., 2020. In vivo and Post-synthesis Strategies to Enhance the Properties of PHB-Based Materials: A Review. Front. Bioeng. Biotechnol. 8, 619266. https://doi.org/10.3389/fbioe.2020.619266

Ubalua, A., 2014. Production and optimization of extracellular alpha-amylase productivity from Bacillus subtilis.

Underhill, D.M., Iliev, I.D., 2014. The mycobiota: interactions between commensal fungi and the host immune system. Nat. Rev. Immunol. 14, 405–416. https://doi.org/10.1038/nri3684

Upton, M., Pennington, T.H., Haston, W., Forbes, K.J., 1997. Detection of human commensals in the area around an Antarctic research station. Antarct. Sci. 9, 156–161. https://doi.org/10.1017/S0954102097000205

Urbaniak, C., Mhatre, S., Grams, T., Parker, C., Venkateswaran, K., 2020. Validation of the International Space Station Smart Sample Concentrator for Microbial Monitoring of Low Biomass Water Samples. J. Biomol. Tech. https://doi.org/10.7171/jbt.20-3104-005

Utharn, S., Yodsang, P., Incharoensakdi, A., Jantaro, S., 2021. Cyanobacterium Synechocystis sp. PCC 6803 lacking adc1 gene produces higher polyhydroxybutyrate accumulation under modified nutrients of acetate supplementation and nitrogen-phosphorus starvation. Biotechnol. reports (Amsterdam, Netherlands) 31, e00661. https://doi.org/10.1016/j.btre.2021.e00661

Uysal, Onder, Uysal, Ozge, Ek, K., 2016. Determination of fertilizing characteristics of three different microalgae cultivated in raceways in greenhouse conditions could increase soil fertility and product yield . At the same time , it has been reported to be environmentally friendly approach (. Ser. Agron. 59, 15–18.

Vaidya, A.A., Collet, C., Gaugler, M., Lloyd-Jones, G., 2019. Integrating softwood biorefinery lignin into polyhydroxybutyrate composites and application in 3D printing. Mater. Today Commun. 19, 286–296. https://doi.org/https://doi.org/10.1016/j.mtcomm.2019.02.008

Valappil, S., Peiris, D., Langley, G., Herniman, J., Boccaccini, A., Bucke, C., Roy, I., 2007. Polyhydroxyalkanoate (PHA) biosynthesis from structurally unrelated carbon sources by a newly characterized Bacillus spp. J. Biotechnol. 127, 475–487. https://doi.org/10.1016/j.jbiotec.2006.07.015

Valappil, S.P., Rai, R., Bucke, C., Roy, I., 2008. Polyhydroxyalkanoate biosynthesis in Bacillus cereus SPV under varied limiting conditions and an insight into the biosynthetic genes involved. J. Appl. Microbiol. 104, 1624–1635. https://doi.org/10.1111/j.1365-2672.2007.03678.x

Van Houdt, R., Mijnendonckx, K., Leys, N., 2012. Microbial contamination monitoring and control during human space missions. Planet. Space Sci. 60, 115–120. https://doi.org/10.1016/j.pss.2011.09.001

Varol, A., Ugurlu, A., 2017. Comparative evaluation of biogas production from dairy manure and co-digestion with maize silage by CSTR and new anaerobic hybrid reactor. Eng. Life Sci. 17, 402–412. https://doi.org/10.1002/elsc.201500187

Velásquez-Mejía, E.P., de la Cuesta-Zuluaga, J., Escobar, J.S., 2018. Impact of DNA extraction, sample dilution, and reagent contamination on 16S rRNA gene sequencing of human feces. Appl. Microbiol. Biotechnol. 102, 403–411. https://doi.org/10.1007/s00253-017-8583-z

Velazquez, J., Rodriguez-Jasso, R., Colla, L., Galindo, A., Cervantes, D., Aguilar, C., Fernandes, B., Ruiz, H., 2018. Microalgal biomass pretreatment for bioethanol production: A review. Biofuel Res. J. 5. https://doi.org/10.18331/BRJ2018.5.1.5

Venkata Mohan, S., Venkateswar Reddy, M., 2013. Optimization of critical factors to enhance polyhydroxyalkanoates (PHA) synthesis by mixed culture using Taguchi design of experimental methodology. Bioresour. Technol. 128, 409–416. https://doi.org/10.1016/j.biortech.2012.10.037

Venkateswaran, K., La Duc, M.T., Horneck, G., 2014. Microbial Existence in Controlled Habitats and Their Resistance to Space Conditions. Microbes Environ. 29, 243–249. https://doi.org/10.1264/jsme2.ME14032

Verlinden, R.A., Hill, D.J., Kenward, M.A., Williams, C.D., Piotrowska-Seget, Z., Radecka, I.K., 2011. Production of polyhydroxyalkanoates from waste frying oil by Cupriavidus necator. AMB Express 1, 11. https://doi.org/10.1186/2191-0855-1-11

Verseux, C., Baqué, M., 2014. Towards cyanobacterial-based life support systems on Mars 11, 50–56.

Verseux, C., Baqué, M., Lehto, K., De Vera, J.P.P., Rothschild, L.J., Billi, D., 2016. Sustainable life support on Mars - The potential roles of cyanobacteria. Int. J. Astrobiol. 15, 65–92. https://doi.org/10.1017/S147355041500021X

Vesper, S.J., Wong, W., Kuo, C.M., Pierson, D.L., 2008. Mold species in dust from the International Space Station identified and quantified by mold-specific quantitative PCR. Res. Microbiol. 159, 432–435. https://doi.org/10.1016/j.resmic.2008.06.001

Vikram, S., Guerrero, L.D., Makhalanyane, T.P., Le, P.T., Seely, M., Cowan, D.A., 2016. Metagenomic analysis provides insights into functional capacity in a hyperarid desert soil niche community. Environ. Microbiol. 18, 1875–1888. https://doi.org/10.1111/1462-2920.13088

Viola, R., Nyvall, P., Pedersén, M., 2001. The unique features of starch metabolism in red algae. Proceedings. Biol. Sci. 268, 1417–1422. https://doi.org/10.1098/rspb.2001.1644

Vishwanathan, A.S., 2021. Microbial fuel cells: a comprehensive review for beginners. 3 Biotech 11, 248. https://doi.org/10.1007/s13205-021-02802-y

Voloshin, R., Rodionova, M., Zharmukhamedov, S., Veziroglu, T., Allakhverdiev, S., 2019. Review: Biofuel Production from Plant and Algal Biomass. Altern. Energy Ecol. 12–31. https://doi.org/10.15518/isjaee.2019.07-09.012-031

Vu, D.H., Wainaina, S., Taherzadeh, M.J., Åkesson, D., Ferreira, J.A., 2021. Production of polyhydroxyalkanoates (PHAs) by Bacillus megaterium using food waste acidogenic fermentation-derived volatile fatty acids. Bioengineered 12, 2480–2498. https://doi.org/10.1080/21655979.2021.1935524

Vu, D., Mahboubi Soufiani, A., Root, A., Heinmaa, I., Taherzadeh, M., Åkesson, D., 2022. Thorough Investigation of the Effects of Cultivation Factors on Polyhydroalkanoates (PHAs) Production by Cupriavidus necator from Food Waste-Derived Volatile Fatty Acids. Fermentation 8, 605. https://doi.org/10.3390/fermentation8110605

Wade, W., 2002. Unculturable Bacteria—The Uncharacterized organisms that Cause Oral Infections. J. R. Soc. Med. 95, 81–83. https://doi.org/10.1177/014107680209500207

Wahadoszamen, M., Rahaman, A., Hoque, N.M.R., Talukder, A., Abedin, K.M., Haider, A., 2015. Laser Raman Spectroscopy with Different Excitation Sources and Extension to Surface Enhanced Raman Spectroscopy. J. Spectrosc. 2015. https://doi.org/10.1155/2015/895317

Walterson, A.M., Stavrinides, J., 2015. Pantoea: insights into a highly versatile and diverse genus within the Enterobacteriaceae. FEMS Microbiol. Rev. 39, 968–984. https://doi.org/10.1093/femsre/fuv027

Wang, Y., Lu, L., Zheng, Y., Chen, X., 2006. Improvement in hydrophilicity of PHBV films by plasma treatment. J. Biomed. Mater. Res. A 76, 589–595. https://doi.org/10.1002/jbm.a.30575

Wang, C. yu, Zhou, X., Guo, D., Zhao, J. hua, Yan, L., Feng, G. zhong, Gao, Q., Yu, H., Zhao, L. po, 2019. Soil pH is the primary factor driving the distribution and function of microorganisms in farmland soils in northeastern China. Ann. Microbiol. 69, 1461–1473. https://doi.org/10.1007/s13213-019-01529-9

Wang, G., Liu, Y., Li, G., Hu, C., Zhang, D., Li, X., 2008. A simple closed aquatic ecosystem (CAES) for space. Adv. Sp. Res. 41, 684–690. https://doi.org/10.1016/j.asr.2007.09.020

Wang, G.H., Li, G.B., Li, D.H., Liu, Y.D., Song, L.R., Tong, G.H., Liu, X.M., Cheng, E.T., 2004. Real-time studies on microalgae under microgravity. Acta Astronaut. 55, 131–137. https://doi.org/https://doi.org/10.1016/j.actaastro.2004.02.005

Wang, X., Ruan, Z., Boileau, D., Sears, B.B., Liu, Y., Liao, W., 2015. Transgenic Expression of a Bacterial Thermophilic Amylase in the Chlamydomonas reinhardtii Chloroplast to Facilitate Algal Biofuel Production. Bioenergy Res. 8, 527–536. https://doi.org/10.1007/s12155-014-9538-1

Wannathong, T., Waterhouse, J.C., Young, R.E.B., Economou, C.K., Purton, S., 2016. New tools for chloroplast genetic engineering allow the synthesis of human growth hormone in the green alga Chlamydomonas reinhardtii. Appl. Microbiol. Biotechnol. 100, 5467–5477. https://doi.org/10.1007/s00253-016-7354-6

Wang, X., Li, Z., Li, Xin, Qian, H., Cai, X., Li, Xinfeng, He, J., 2016. Poly-β-hydroxybutyrate Metabolism Is Unrelated to the Sporulation and Parasporal Crystal Protein Formation in Bacillus thuringiensis. Front. Microbiol. 7, 836. https://doi.org/10.3389/fmicb.2016.00836

Webster, C., Mahaffy, P., Atreya, S., Flesch, G., Mischna, M., Meslin, P.-Y., Farley, K., Conrad, P., Christensen, L., Pavlov, A., Martín-Torres, F.J., Zorzano, M.-P., McConnochie, T., Owen, T., Eigenbrode, J., Glavin, D., Steele, A., Malespin, C., Archer, P., Team, R., 2014. Mars methane detection and variability at Gale crater. Science (80-)

Webster, C.R., Mahaffy, P.R., Atreya, S.K., Moores, J.E., Flesch, G.J., Malespin, C., McKay, C.P., Martinez, G., Smith, C.L., Martin-Torres, J., Gomez-Elvira, J., Zorzano, M.-P., Wong, M.H., Trainer, M.G., Steele, A., Archer, D.J., Sutter, B., Coll, P.J., Freissinet, C., Meslin, P.-Y., Gough, R. V, House, C.H., Pavlov, A., Eigenbrode, J.L., Glavin, D.P., Pearson, J.C., Keymeulen, D., Christensen, L.E., Schwenzer, S.P., Navarro-Gonzalez, R., Pla-García, J., Rafkin, S.C.R., Vicente-Retortillo, Á., Kahanpää, H., Viudez-Moreiras, D., Smith, M.D., Harri, A.-M., Genzer, M., Hassler, D.M., Lemmon, M., Crisp, J., Sander, S.P., Zurek, R.W., Vasavada, A.R., 2018. Background levels of methane in Mars' atmosphere show strong seasonal variations. Science 360, 1093–1096. https://doi.org/10.1126/science.aaq0131

Wei, Y.H., Chen, W.C., Huang, C.K., Wu, H.S., Sun, Y.M., Lo, C.W., Janarthanan, O.M., 2011. Screening and evaluation of polyhydroxybutyrate-producing strains from indigenous isolate Cupriavidus taiwanensis strains. Int. J. Mol. Sci. 12, 252–265. https://doi.org/10.3390/ijms12010252

Werlang, E., Moraes, L., Muller, M., Julich, J., Corbellini, V.A., de Farias Neves, F., Souza, D., Benitez, L., Schneider, R., 2020. Polyhydroxybutyrate (PHB) Production via Bioconversion Using Bacillus pumilus in Liquid Phase Cultivation of the Biomass of Arthrospira platensis Hydrolysate as a Carbon Source. Waste and Biomass Valorization 12. https://doi.org/10.1007/s12649-020-01213-z

Wu, Z., Zhu, Y., Huang, W., Zhang, C., Li, T., Zhang, Y., Li, A., 2012. Evaluation of flocculation induced by pH increase for harvesting microalgae and reuse of flocculated medium. Bioresour. Technol. 110, 496–502. https://doi.org/10.1016/j.biortech.2012.01.101

Xu, X., Fang, J., Wang, W., Guo, J., Chen, P., Cheng, J., Shen, Z., 2008. Expression of a bacterial alpha-amylase gene in transgenic rice seeds. Transgenic Res. 17, 645–650. https://doi.org/10.1007/s11248-007-9144-5

Xu, Y., Zhang, R., Jiao, N., 2015. Complete genome sequence of Paracoccus marcusii phage vB_PmaS-R3 isolated from the South China Sea. Stand. Genomic Sci. 10, 2–7. https://doi.org/10.1186/s40793-015-0089-7

Yagi, H., Ninomiya, F., Funabashi, M., Kunioka, M., 2014. Mesophilic anaerobic biodegradation test and analysis of eubacteria and archaea involved in anaerobic biodegradation of four specified biodegradable polyesters. Polym. Degrad. Stab. 110, 278–283. https://doi.org/10.1016/j.polymdegradstab.2014.08.031

Yair, Y., Reshef, L., Shopen-Gochev, C., Yoffe, G., Azulay, G., Aharonson, O., Sorek-Abramovich, R., 2021. Temporal and Spatial Analysis of Forward and Backward Microbial Contamination in a Mars Analog Mission. Front. Astron. Sp. Sci. 8, 1–11. https://doi.org/10.3389/fspas.2021.589147

Yang, J., Hao, Z., Zhang, L., Fu, Y., Liu, H., 2022. Surface fungal diversity and several mycotoxin-related genes' expression profiles during the Lunar Palace 365 experiment. Microbiome 10, 1–17. https://doi.org/10.1186/s40168-022-01350-8

Yang, Z., Pei, H., Han, F., Wang, Y., Hou, Q., Chen, Y., 2018. Effects of air bubble size on algal growth rate and lipid accumulation using fine-pore diffuser photobioreactors. Algal Res. 32, 293–299. https://doi.org/https://doi.org/10.1016/j.algal.2018.04.016

Yang, S., Jia, Z., Ouyang, X., 2019. Effects of algae contamination on the hydrophobicity of high voltage composite insulators. High Volt. 4. https://doi.org/10.1049/hve.2019.0073

Yao, C., Ai, J., Cao, X., Xue, S., Zhang, W., 2012. Enhancing starch production of a marine green microalga Tetraselmis subcordiformis through nutrient limitation. Bioresour. Technol. 118, 438–444. https://doi.org/10.1016/j.biortech.2012.05.030

Yeates, C., Gillings, M.R., Davison, A.D., Altavilla, N., Veal, D.A., 1998. Methods for microbial DNA extraction from soil for PCR amplification. Biol. Proced. Online 1, 40–47. https://doi.org/10.1251/bpo6

Yilmaz, P., Parfrey, L.W., Yarza, P., Gerken, J., Pruesse, E., Quast, C., Schweer, T., Peplies, J., Ludwig, W., Glöckner, F.O., 2014. The SILVA and "All-species Living Tree Project (LTP)" taxonomic frameworks. Nucleic Acids Res. 42, D643-8. https://doi.org/10.1093/nar/gkt1209

Zachleder, V., Kselíková, V., Ivanov, I.N., Bialevich, V., Vítová, M., Ota, S., Takeshita, T., Kawano, S., Bišová, K., 2021. Supra-Optimal Temperature: An Efficient Approach for Overaccumulation of Starch in the Green Alga Parachlorella kessleri. Cells 10. https://doi.org/10.3390/cells10071806

Zainuddin, M.Z., Abu Bakar, A.A., Adam, A.N., Abdullah, S.M., Tamchek, N., Alauddin, M.S., Mahat, M.M., Wiwatcharagoses, N., Alforidi, A., Ghazali, M.I.M., 2023. Mechanical and Structural Properties of Polyhydroxybutyrate as Additive in Blend Material in Additive Manufacturing for Medical Applications. Polymers (Basel). 15. https://doi.org/10.3390/polym15081849

Zannini, E., Lynch, K., Nyhan, L., Sahin, A., Riordan, P., Luk, D., Arendt, E., 2022. Influence of Substrate on the Fermentation Characteristics and Culture-Dependent Microbial Composition of Water Kefir. Fermentation 9, 28. https://doi.org/10.3390/fermentation9010028

Zavřel, T., Očenášová, P., Sinetova, M., Červený, J., 2018. Determination of Storage (Starch/Glycogen) and Total Saccharides Content in Algae and Cyanobacteria by a Phenol-Sulfuric Acid Method. BIO-PROTOCOL 8. https://doi.org/10.21769/BioProtoc.2966

Zhang, J., Müller, B.S.F., Tyre, K.N., Hersh, H.L., Bai, F., Hu, Y., Resende, M.F.R.J., Rathinasabapathi, B., Settles, A.M., 2020. Competitive Growth Assay of Mutagenized Chlamydomonas reinhardtii Compatible With the International Space Station Veggie Plant Growth Chamber. Front. Plant Sci. 11, 631. https://doi.org/10.3389/fpls.2020.00631

Zhang, L., Jiang, Z., Tsui, T.-H., Loh, K.-C., Dai, Y., Tong, Y.W., 2022. A Review on Enhancing Cupriavidus necator Fermentation for Poly(3-hydroxybutyrate) (PHB) Production From Low-Cost Carbon Sources. Front. Bioeng. Biotechnol. 10, 946085. https://doi.org/10.3389/fbioe.2022.946085

Zhang, N., Pazouki, L., Nguyen, H., Jacobshagen, S., Bigge, B.M., Xia, M., Mattoon, E.M., Klebanovych, A., Sorkin, M., Nusinow, D.A., Avasthi, P., Czymmek, K.J., Zhang, R., 2022. Comparative Phenotyping of Two Commonly Used Chlamydomonas reinhardtii Background Strains: CC-1690 (21gr) and CC-5325 (The CLiP Mutant Library Background). Plants (Basel, Switzerland) 11. https://doi.org/10.3390/plants11050585

Zhao, T., Jiang, L., 2018. Contact angle measurement of natural materials. Colloids Surf. B. Biointerfaces 161, 324–330. https://doi.org/10.1016/j.colsurfb.2017.10.056

Zhang, Y.Y., Wu, W., Liu, H., 2019. Factors affecting variations of soil pH in different horizons in hilly regions. PLoS One 14, 1–13. https://doi.org/10.1371/journal.pone.0218563

Zhao, X.H., Niu, Y.N., Mi, C.H., Gong, H.L., Yang, X.Y., Cheng, J.S.Y., Zhou, Z.Q., Liu, J.X., Peng, X.L., Wei, D.X., 2021. Electrospinning nanofibers of microbial polyhydroxyalkanoates for applications in medical tissue engineering. J. Polym. Sci. 59, 1994–2013. https://doi.org/10.1002/pol.20210418

Zhu, L.D., Takala, J., Hiltunen, E., Wang, Z.M., 2013. Recycling harvest water to cultivate Chlorella zofingiensis under nutrient limitation for biodiesel production. Bioresour. Technol. 144, 14–20. https://doi.org/https://doi.org/10.1016/j.biortech.2013.06.061

Zielińska, S., Radkowski, P., Blendowska, A., Ludwig-Gałęzowska, A., Łoś, J.M., Łoś, M., 2017. The choice of the DNA extraction method may influence the outcome of the soil microbial community structure analysis. Microbiologyopen 6. https://doi.org/10.1002/mbo3.453

Appendix

Appendix A. Elements with concentrations above MaDL (maximum detection limit) in all six soil samples.

Concentration (mg/kg)	Ba	Ca	K	Mg	Na	S	Si	Sr	V
S1	0.0399	46.95	15.14	13.56	389.8	506.0	6.2	1.42	0.0178
S2	0.0401	2.33	5.13	0.85	168.8	147.6	13.21	0.06	0.1002
S3	0.0594	6.46	8.87	0.37	265.1	259.2	8.22	0.15	0.0785
S4	0.274	7.20	12.23	8.40	97.03	46.39	85.68	0.12	0.0616
S5	2.0961	49.27	0.89	2.72	14.43	13.16	2.22	0.55	0.0016
S6	0.2015	13.97	2.44	0.99	35.29	11.69	5.39	0.22	0.0043
MaDL	0.0003	0.01	0.02	0.01	0.17	0.01	0.01	0.001	0.0007
Dilution Factor	x10	x10	x10	x10	x100	x100	x100	x10	x10

Appendix B. Number of Reads for Bacteria, Archaea, and Fungi per Sample (Including Control)

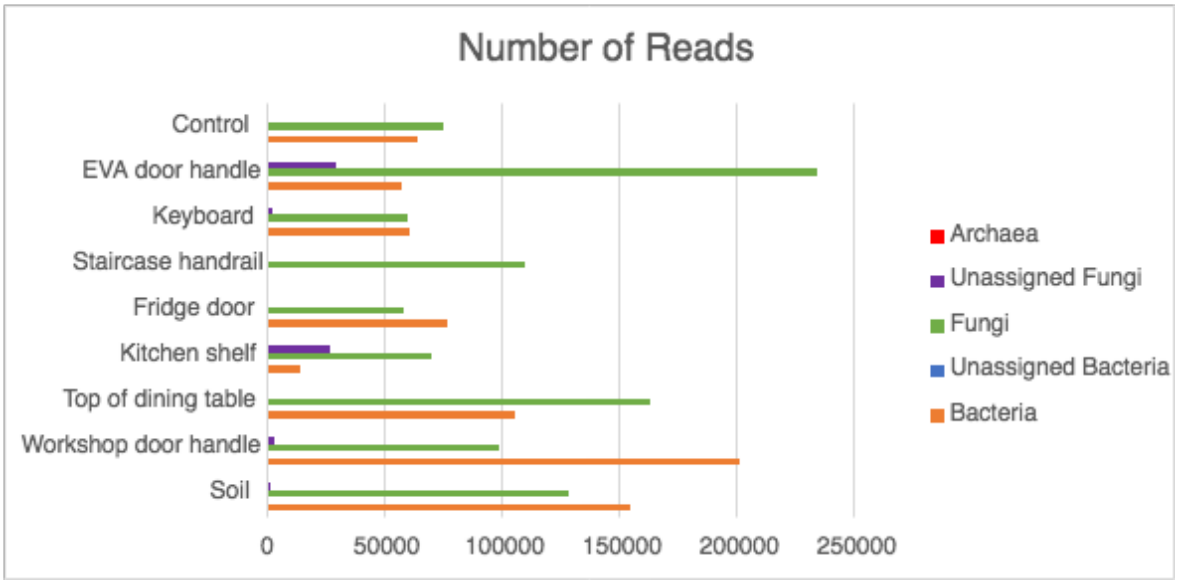

Appendix C: Bacterial and Fungal Diversity in Control Phosphate-Buffered Saline (PBS)

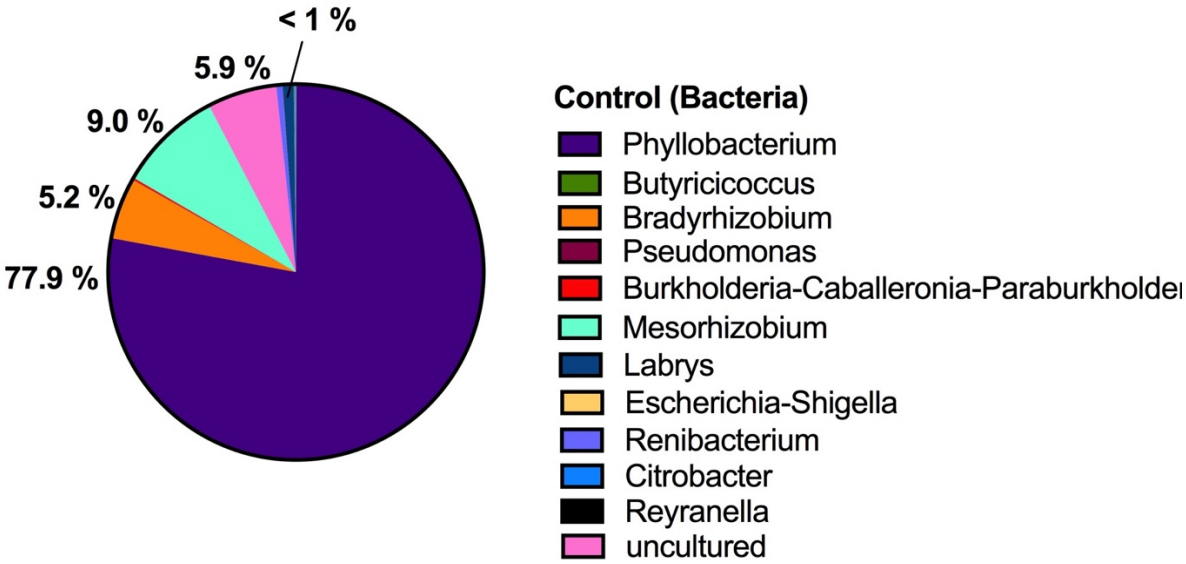

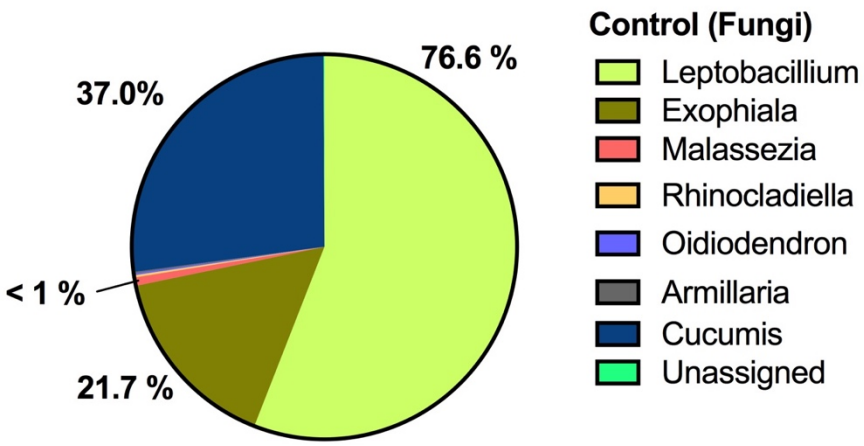

Appendix D: Bacterial Phylum-Level Composition of Each Indoor Sample

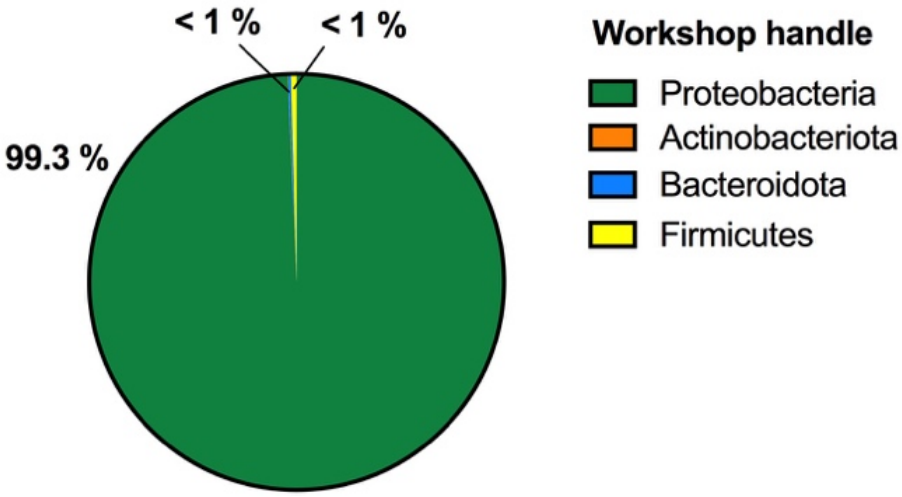

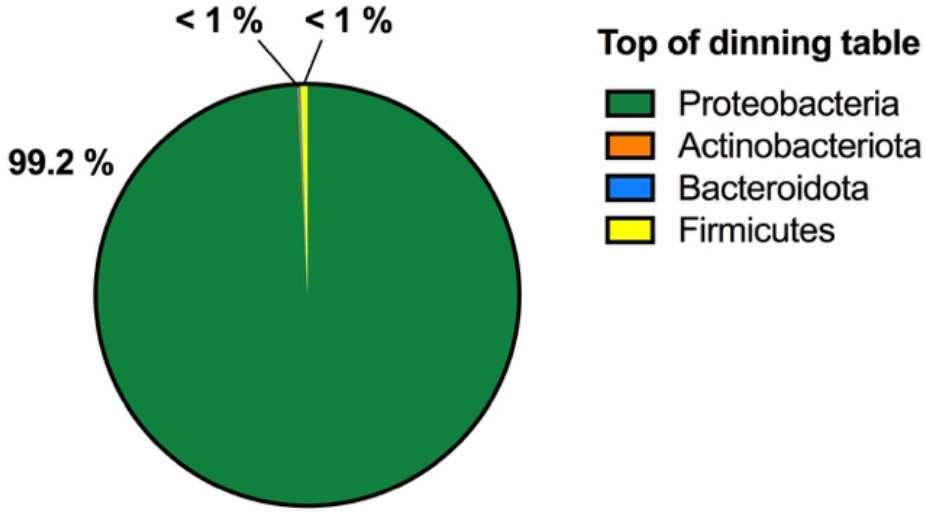
< 1 %
< 1 %
99.2 %
Top of dinning table
Proteobacteria
Actinobacteriota
Bacteroidota
Firmicutes

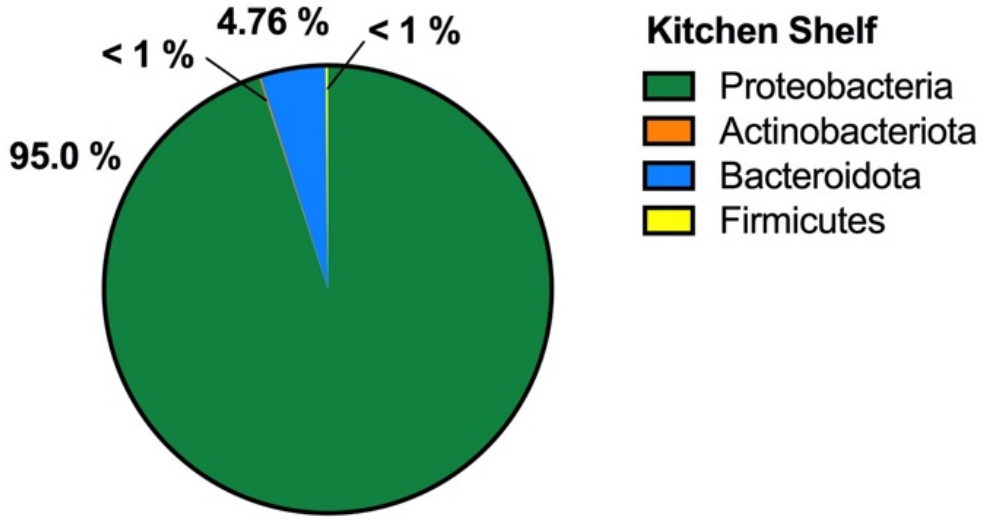
4.76 %
< 1 %
< 1 %
95.0 %
Kitchen Shelf
Proteobacteria
Actinobacteriota
Bacteroidota
Firmicutes

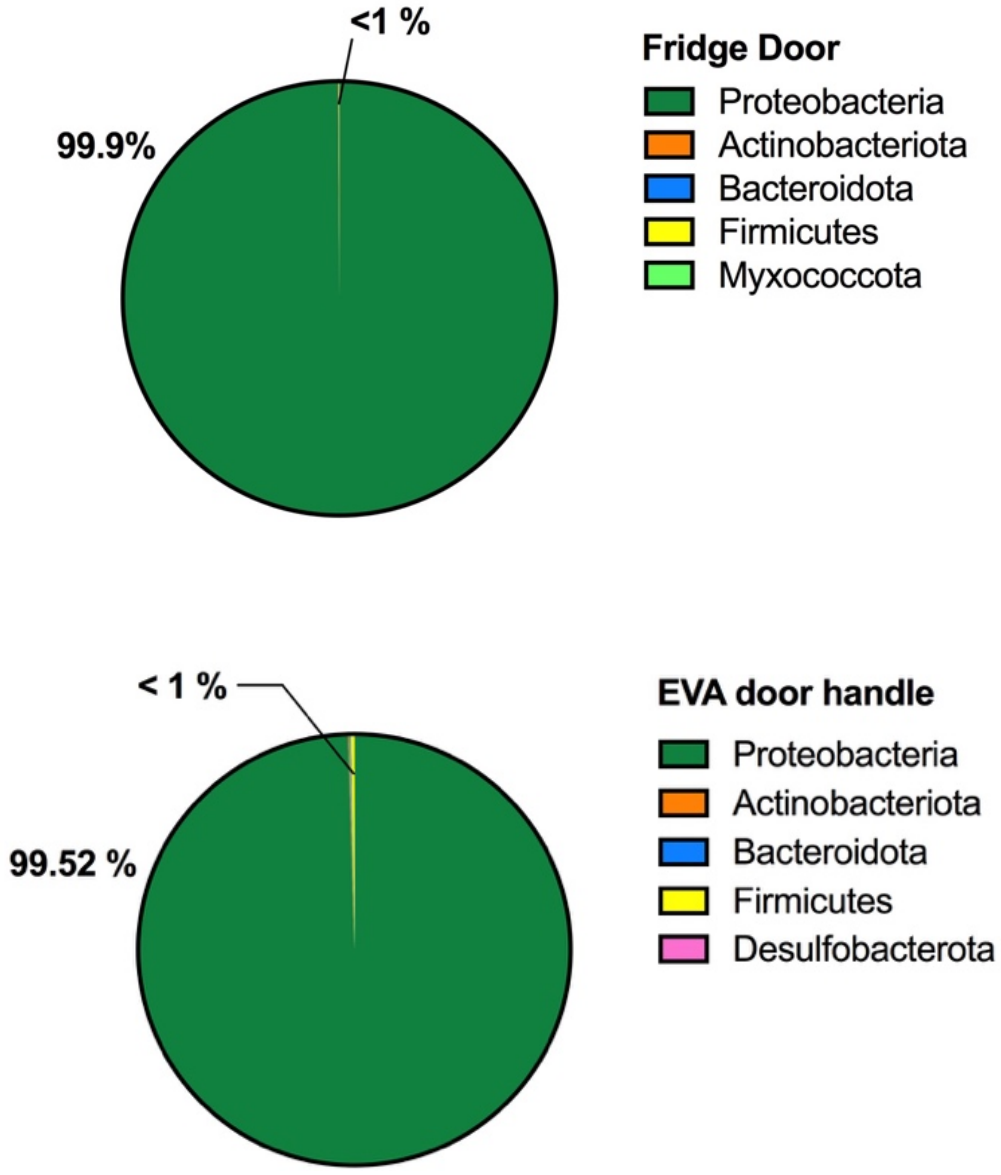
<1 %
99.9%
Fridge Door
Proteobacteria
Actinobacteriota
Bacteroidota
Firmicutes
Myxococcota
< 1 %
99.52 %
EVA door handle
Proteobacteria
Actinobacteriota
Bacteroidota
Firmicutes
Desulfobacterota

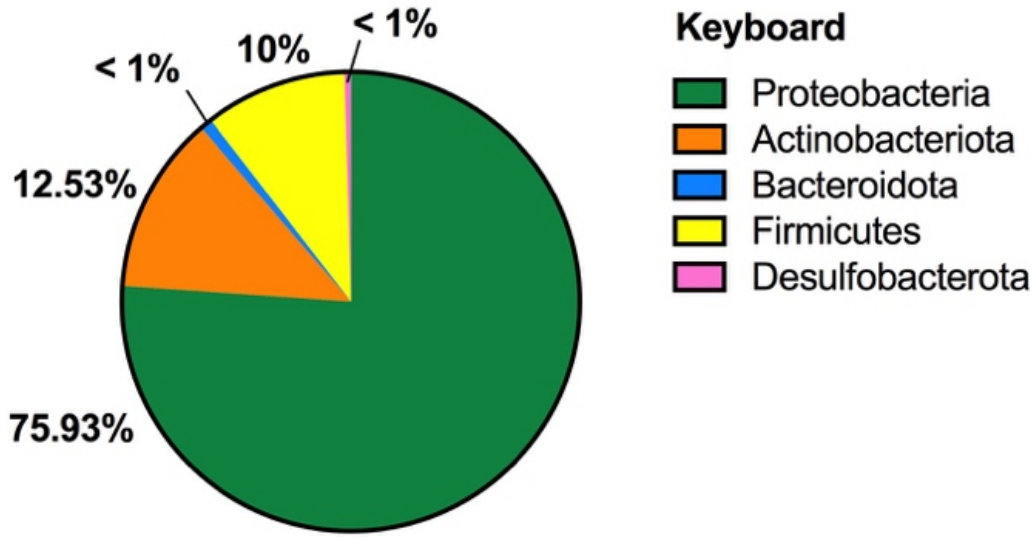

Appendix E: Fungal Phylum-Level Composition of Each Indoor Sample

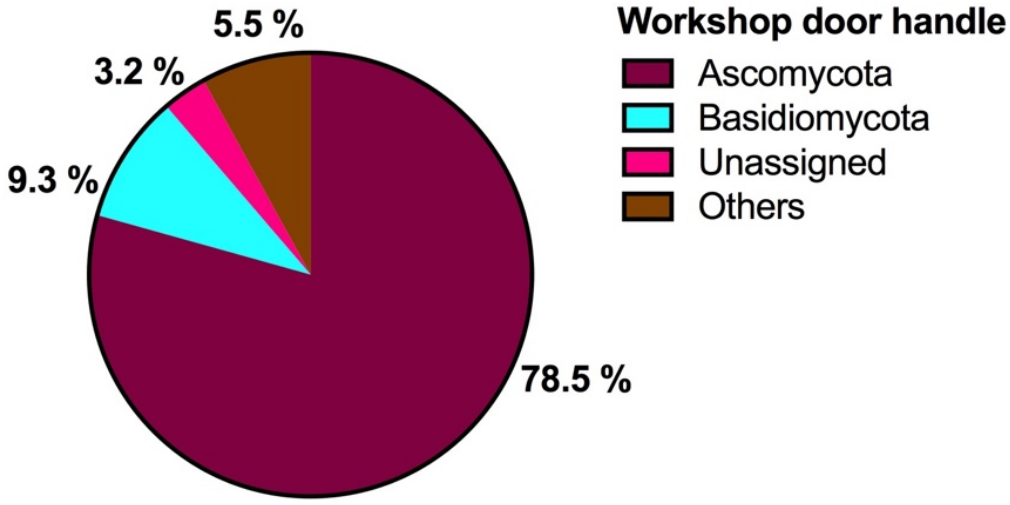

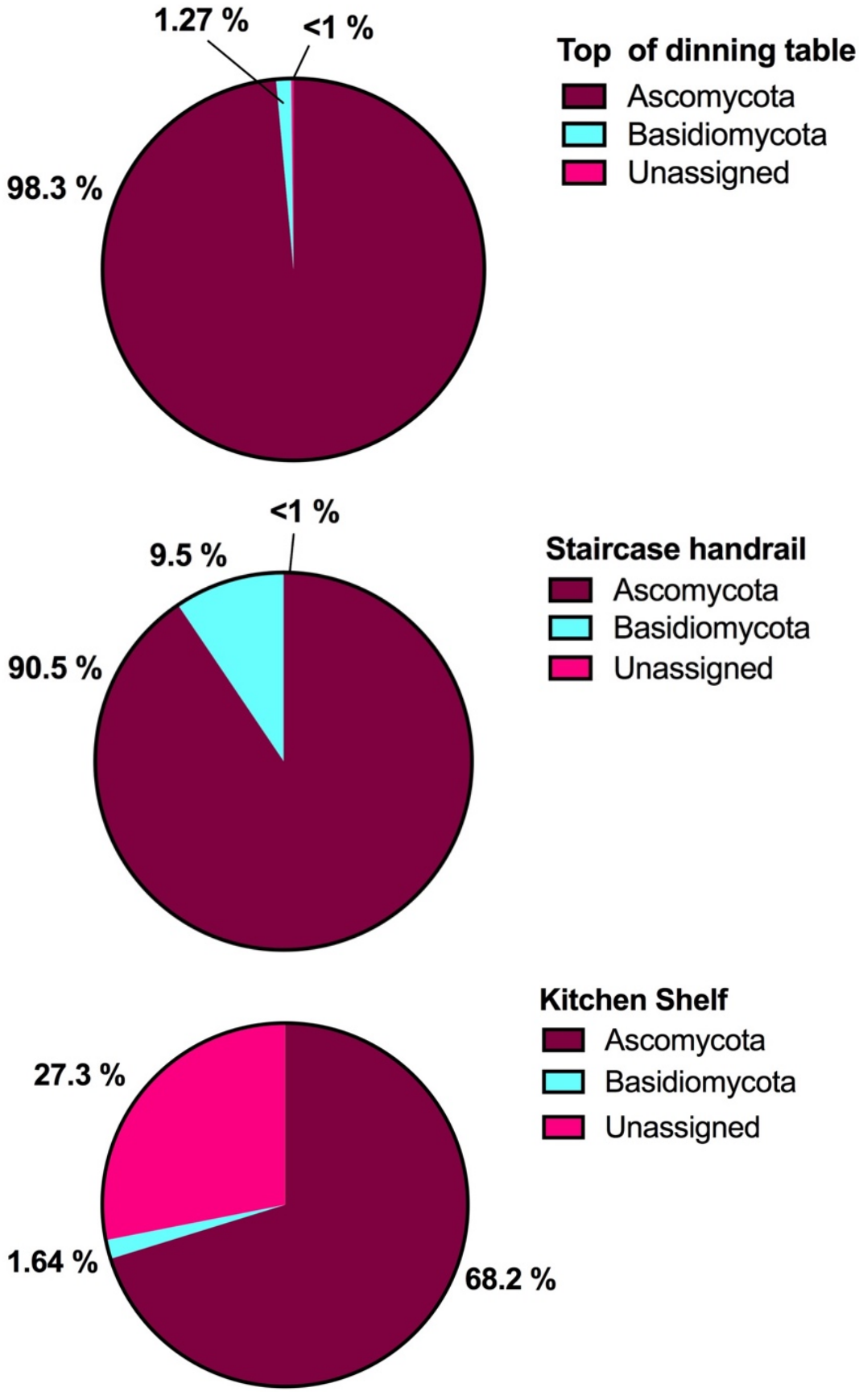
1.27 %
<1 %
98.3 %
Top of dinning table
Ascomycota
Basidiomycota
Unassigned
<1 %
9.5 %
90.5 %
Staircase handrail
Ascomycota
Basidiomycota
Unassigned
Kitchen Shelf
Ascomycota
Basidiomycota
Unassigned
27.3 %
1.64 %
68.2 %

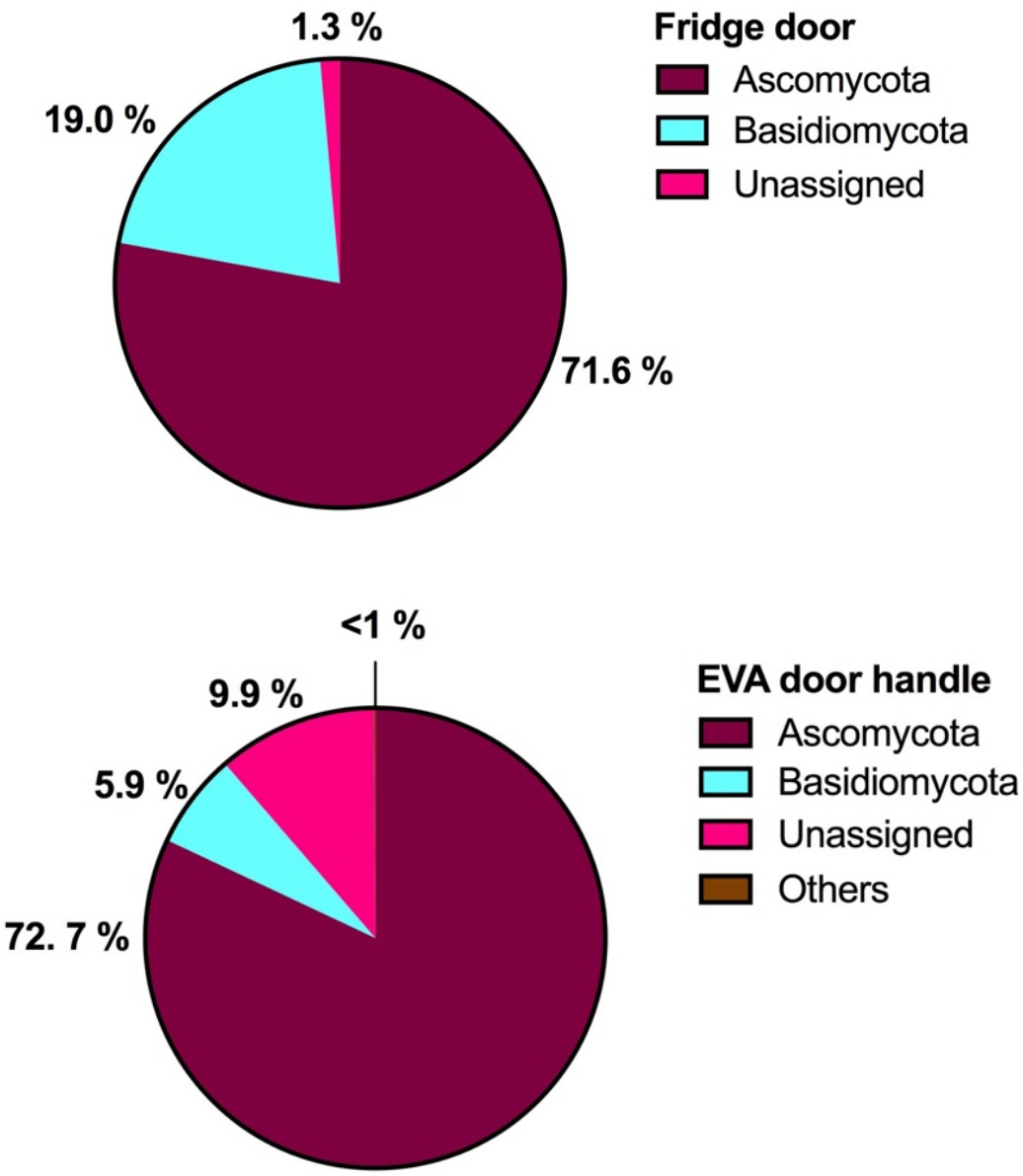
1.3 %
19.0 %
71.6 %
Fridge door
Ascomycota
Basidiomycota
Unassigned
<1 %
9.9 %
5.9 %
72. 7 %
EVA door handle
Ascomycota
Basidiomycota
Unassigned
Others

Appendix F: Bacterial Phylum-Level Composition of the Soil Sample

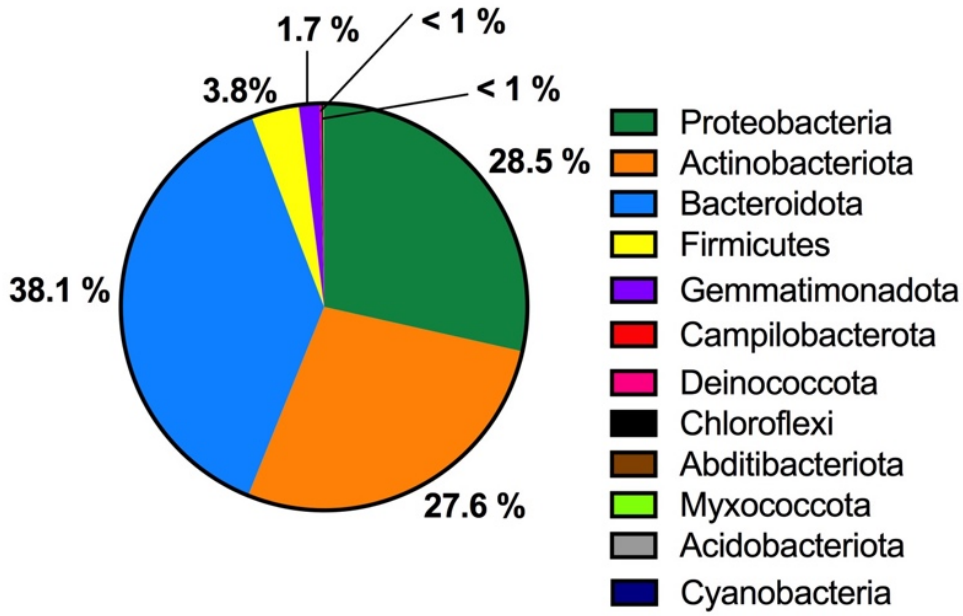

Appendix G: Fungal Phylum-Level Composition of the Soil Sample